THE PROPAGATION OF THE ACTION POTENTIAL IN CARDIAC TISSUE

by

David Alan Israel
M.D., B.Sc.(Med.), University of Manitoba (1977)
S.M., Massachusetts Institute of Technology (1982)

Submitted to the Department of Aeronautics and Astronautics
and the Interdepartmental Committee on Biomedical Engineering
in partial fulfillment of the requirements for the degree of
Doctor of Philosophy
at the
Massachusetts Institute of Technology
February 1988

Signature of Author_____
Department of Aeronautics and Astronautics
December 1st, 1987

Certified by_____
Roger G. Mark
Thesis Supervisor, Associate Professor of Electrical Engineering

Certified by_____
David J. Edell
Assistant Professor of Electrical Engineering

Certified by_____
Raphael C. Lee
Assistant Professor of Electrical Engineering

Certified by_____
Kathleen G. Morgan
Associate Professor of Physiology in Medicine, Harvard Medical School

Accepted by_____
Alan J. Grodzinsky
Professor and Chairman, Interdepartmental Committee on Biomedical Engineering

Accepted by_____
Harold Y. Wachman
Professor and Chairman, Aeronautics and Astronautics Departmental Graduate Committee

THE PROPAGATION OF THE ACTION POTENTIAL IN CARDIAC TISSUE

by

David Alan Israel

Submitted to the Interdepartmental Committee on Biomedical Engineering on December 1, 1987 in partial fulfillment of the requirements for the degree of Doctor of Philosophy.

Abstract

The cardiac action potential must propagate from cell to cell every one to two-hundred micrometers. Intercellular connections enable propagation by allowing the flow of current from cell to cell. The effects of intercellular connections on the details of action potential propagation are not fully known. Cardiac conduction has classically been analyzed using the cable theory models first developed for nerve axons. This approach implicitly ignores any possible effect of the discontinuous structure of cardiac muscle on propagation. Recent work has suggested that the coupling between cells affects cardiac conduction. Decreased coupling between cells in various pathological states may underly slow conduction or block and therefore might be involved in the genesis of a variety of arrhythmias. Simulations have suggested that discrete time delays between cells could occur under physiological conditions.

To investigate the existence of such time delays, monolayers of 10-day chick-embryo ventricular myocytes were grown in cell culture on arrays of extracellular microelectrodes fabricated using microelectronics technology. The arrays contained 28 planar recording electrodes, each 10 μm square, 16 of which could be recorded from simultaneously. The most closely spaced recording electrodes were on 20 μm centers. Some pairs of electrodes recorded from different points on the same cell while other pairs straddled intercellular junctions. The preparation was electrically paced to obtain a repeatable propagation pathway. Arrival times of extracellular activity at each microelectrode were measured, using the maximum negative derivative of the extracellular action potential as the fiducial point. After a series of beats was recorded under control conditions, the preparation was exposed to medium containing 20 mM NH_4Cl for 15 minutes, and then returned to normal medium. This intervention produces transient intracellular acidification which decreases intercellular coupling. After acidification, the average (multicellular) conduction velocity decreased to about 2/3 of the control value. Propagation velocity measured between most electrode pairs decreased proportionately. However, disproportionately long propagation delays of up to 410 μSec were observed between some pairs of electrodes in various experiments. The delays recovered as pH returned to normal. The localized long delays were thought to be due to decreased intercellular coupling at gap junctions. These data suggest that decreasing intercellular coupling does cause propagation to be "discontinuous" in this preparation, and that this may be a significant mechanism for pathologic slowing of conduction in myocardium.

Thesis Supervisor: Roger G. Mark
Title: Matsushita Associate Professor of Electrical Engineering in Medicine

Acknowledgements

Over the course of this work, many people gave of their time and resources to help me. I would like to thank them all.

Fellowship support was received from the Medical Research Council of Canada during the early part of this work. The Whitaker Health Sciences Fund provided operating funds. The assistance of these organizations is gratefully acknowledged.

The principals of the Cardiovascular Research Laboratory, Brigham & Women's Hospital, graciously provided laboratory resources and cultured cells which would have been difficult to obtain otherwise. Bill Barry introduced me to the cardiac cell-culture preparation and pointed me in the direction which led to this project. Special thanks are also due to David Clapham for friendly criticism, and to Jim Marsh and Donghee Kim for their continued interest and material support. Thanks also to all the technicians who cheerfully cultured cells for me over the years, especially to Jim Greaney and Kathy Sweeney.

I thank the members of my thesis committee for reviewing this work and suggesting improvements to this manuscript. I am grateful to David Edell for all his advice on the fabrication of microelectrode arrays and on other useful techniques. Roger Mark has been the driving force behind this project since its inception. His realistic assessment of goals saved me from attempting the impossible more than once. He has added perspective to my view of this problem and its place in the scheme of things. I am thankful for his continued support.

The greatest thanks are due my family, who have spent many lonely evenings and weekends while I pursued this research. It is a debt I hope I can more than repay.

To my family.

Table of Contents

List of Figures

Chapter 1: INTRODUCTION

There is general agreement that the conduction of excitation in cardiac tissue is by an electrical mechanism. However, there is still uncertainty about the details of cell-to-cell propagation. In the heart, excitation must spread from cell to cell every one to two hundred micrometers. Most investigators believe that there are intercellular connections which enable propagation by allowing the flow of current from cell to cell. However, the effects of such connections on the details of action potential propagation have not been thoroughly studied. Cardiac conduction has classically been analyzed using the cable theory models first developed for nerve axons, which do not contain elements to account for the intercellular junctions in cardiac tissue. This approach implicitly ignores any possible effect of the discontinuous structure of cardiac muscle on propagation.

The conduction of excitation in the heart is of paramount importance to its normal functioning; abnormalities of conduction are responsible for much morbidity and mortality, including a large number of sudden deaths. Conduction abnormalities (rather than abnormalities of impulse generation) are thought to be responsible for many types of arrhythmias. Slow conduction is frequently cited as a major factor in arrhythmogenesis; the mechanisms of slow conduction most frequently considered, however, are those due to abnormalities of the generation of the action potential and not those which may be due to slow propagation of excitation from one cell to the next (Cranefield, 1975). Most of the proposed mechanisms of re-entrant arrhythmias have some slowing or block of conduction as a basis. For example, the classical description of re-entry around an anatomical obstacle requires both slow conduction and a transient or unidirectional block of conduction. The "leading circle" hypothesis of re-entry requires an area of slow conduction, which is supposedly due to the propagation of excitation in

partially refractory tissue (Wit and Cranefield, 1978). In discussions of these mechanisms, however, it has almost always been assumed that the slowing of conduction and/or block is the result of what could be called "membrane" factors rather than a "junctional" delay of conduction from one cell to the next.

Recently, the experimental work of Spach has suggested that the coupling between cells affects cardiac conduction (Spach et al., 1982b). The hypothesized effects of the intercellular junctions on conduction include both quantitative effects (e.g: changes in conduction velocity) as well as qualitative ones (e.g: changes in wave-shapes and pathways of conduction). Spach has proposed that the properties of intercellular coupling combined with specific geometries of cell-to-cell connections can give rise to unidirectional conduction block and re-entrant arrhythmias (Spach, 1982).

Furthermore, the usually well-coupled state of healthy muscle probably does not always prevail. Evidence exists to show that after various types of injury, the degree of coupling between cells decreases drastically (De Mello, 1982a). This type of change might be a factor in the development of slow conduction or block, and therefore could be involved in the genesis of arrhythmias associated with abnormal conduction. As the degree of coupling decreases in such situations, the effect of coupling on the nature of propagation should become more prominent, i.e. propagation should become more "discontinuous".

Diaz has simulated cardiac conduction with a computer model which contained elements to explicitly account for the intercellular connections in cardiac tissue (Diaz, 1983). This simulation showed some of the same properties found by Spach's group in their work with intact cardiac tissue. The simulation also displayed properties which were not apparent in the experiments of Spach and co-workers. These properties have not been looked for in vivo, but if present, would provide strong support for the

discontinuous propagation hypothesis.

The medical therapy of many arrhythmias is based upon a model of the effects of the drugs on cardiac conduction. An understanding of the details of conduction in health and the changes that occur in disease is essential to rational treatment. The actions of most anti-arrhythmic drugs now in use are explained on the basis of effects on membrane factors (Rosen and Wit, 1983). However, if further investigations show that the discontinuous propagation mechanism is indeed a factor in arrhythmogenesis, more work will be needed to investigate the effects of existing drugs on the propagation of excitation from cell to cell, and it is likely that an attempt will be made to find new drugs with such specific effects. The goal of the present work is to experimentally test some predictions of the Diaz model of discontinuous cardiac propagation in live tissue. specifically, the existence of discrete time delays in the conduction of activity between adjacent cells is of interest. If these experiments confirm the existence of such time delays in a preparation of living cardiac cells, serious consideration would have to be given to the possible implications in the pathogenesis and treatment of arrhythmias in humans.

Chapter 2: BACKGROUND

Historically, cardiac muscle was thought to be an anatomical syncytium because the cell boundaries were not discernible using the light microscope. From the standpoint of the spread of electrical activity in the heart, this syncytial structure implied that an action potential should propagate throughout the myocardium much as it would in a nerve axon. In 1954, electron microscopy proved that the heart is composed of separate cells (Sjostrand and Andersson, 1954). This finding raised the question of how excitation can spread from cell to cell. It is now generally believed that there are relatively low-resistance pathways between adjacent cells which allow the passage of local-circuit currents of sufficient magnitude for propagation. This theory is supported by anatomical evidence, measurements of diffusion of radioactive tracers, and measurements of electrotonic coupling. Because of such evidence, the heart has come to be considered as an "electrical" syncytium; that is, from the point of view of conduction of activity, the intercellular connections are generally thought to be so good that they have negligible effects on conduction. Cardiac conduction is therefore often modelled using the cable theory models first developed for conduction in nerve axons; this approach implicitly ignores any effects of intercellular junctions on cardiac conduction.

In the following sections, the current understanding of the structure of cardiac cells and tissue will be reviewed, with emphasis on the morphological details of intercellular connections. Then the functional properties of these connections will be discussed. This discussion is followed by a brief review of the classical view of action potential propagation in the heart, and some more recent literature regarding the discontinuous propagation hypothesis which calls this view into question. Finally, there is a review of literature pertaining to the experiments to be described, specifically, the properties of a cell culture preparation of chick embryo cardiac cells, the generation of extracellular

action potentials, and a technique for sensing such action potentials.

2.1 The Structure of Cardiac Tissue

In the heart, as in other organs, functional properties are closely related to morphology. In the case of the heart, a knowledge of structure is important to an understanding of the propagation of action potentials. This review will focus on the structure of working ventricular myocytes, which comprise the majority of cardiac tissue. The characteristics of atrial cells, nodal cells, and cells of the conduction system will not be discussed. The bulk of the myocardium is composed of striated myocytes within a framework of connective tissue. Individual myocytes are roughly cylindrical in shape. The ends of the cells are usually not simple planar surfaces, but rather have a step-like morphology with "terraces" at which adjacent cells are joined. This structure gives intact cardiac muscle the appearance of branching, although individual myocytes do not typically branch. In mammalian hearts, the length of single cells is approximately 30-160 μm and their width (the diameter of the cylinder) is approximately 10-20 μm (Sommer and Dolber, 1982). Each myocyte contains myofibrils which are oriented longitudinally and are anchored to the inner aspect of the cell membrane along their length at the Z-lines, and at each end of the cell. The myofibrils occupy approximately 50% of the cell by volume. The cell membrane is grooved at places corresponding to the Z-lines in the adjacent myofibrils. These grooves are the starting point for the transverse tubules, in myocytes which have them. The transverse tubules are tube-like invaginations of the cell membrane which run across the width of the cells, enclosing extracellular space. These channels have a variable diameter, with 200 nm being an approximate size. The ventricular cells of all adult mammals have transverse tubules, but those of several infant mammals and of birds of all ages (including the chick embryo myocytes used in the experiments to be described) do not (Sommer and Dolber, 1982).

The myofibrils are surrounded by a tubular network of membranes known as the sarcoplasmic reticulum (SR). This network moderates excitation-contraction coupling by the release and uptake of calcium. The smooth tubules of the SR which surround the myofibrils are known as "free SR"; they are continuous with the granular "junctional SR" (called terminal cisterna in skeletal muscle) which makes contact with the inside of the cell membrane both at the periphery of the cell and at the transverse tubules (Sommer and Johnson, 1979).

Other constituents of cardiac myocytes include a nucleus, endoplasmic reticulum, Golgi bodies, and lysosomes. Some glycogen is stored. Because of the large energy consumption of these cells, mitochondria are abundant, occupying roughly 35% of the cell volume (Sommer and Johnson, 1979).

2.2 The Morphology of Intercellular Connections

The cells are joined to one another end-to-end at regions known as the intercalated disks. The disks, which are visible under light microscopy only as dark bands running across cardiac muscle fibers, have been shown by electron microscopy to be highly organized, complex structures. By E.M., an intercalated disk is seen to consist of a pair of cell membranes separated by an extracellular space of variable width. The course of the disk is tortuous, with extensive interdigitation of membrane projections from the joined cells. These interdigitations of the two membranes lead to a distinction between the transverse segments of the disk (membranes parallel to the ends of the cells) and the longitudinal segments of the disk (membranes parallel to the long axis of the cells). The transverse segments are called the interfibrillar regions, and the longitudinal segments are known as the intersarcoplasmic regions (Berger, 1972). The connections of the ends of the myofibrils of a cell to its membrane occur in the interfibrillar regions of the disk. In these regions, the membranes of the adjacent cells are separated by a gap of about 25-30

nm which is filled with a filamentous material. These regions appear to provide mechanical adhesion between the two cells. In the intersarcoplasmic regions of the disk, which are parallel to the long axis of the cells, the gap between the adjacent membranes is smaller, only 10-25 nm wide. Two morphologically distinct types of structures are found distributed in the intersarcoplasmic regions. One of these, the desmosome, or macula adhaerens, is characterized by a prominent gap between the membranes filled with a mixture of carbohydrates and polypeptides. There is a dense-staining collection of filamentous material in the adjacent cytoplasm. The other of these structures is known as the nexus, gap junction, or macula communicans. In the nexus, the membranes are much closer together than in the desmosome, separated by a gap of 2-3 nm. It may seem curious that a junction in which the gap is very small would be given the name "gap junction"; the rationale was to distinguish it from yet another type of intercellular junction found in epithelial tissues, the "tight junction" or zonula occludens. The latter has no discernible gap, but the two were confused in early studies of intercellular junctions, primarily due to inadequate fixation and staining methods.

2.2.1 The Structure of Gap Junctions

The gap junction is characterized by the presence of aggregates of particles in each of the two adjoining membranes. In an electron micrograph of a cross-section, structures can be seen crossing the 2-3 nm gap from one membrane to the other, often at regularly-spaced intervals on the order of 10-12 nm. Electron microscopic views of freeze-fractured faces of nexi reveal arrays of particles, 7-8 nm in diameter, in arrangements which vary from crystal-like hexagonal regularity to the absence of any order whatsoever. Each particle has a 1.5-2 nm diameter central area of contrasting density. These particles are called protochannels. X-ray diffraction studies show that the particles on the two apposed membranes are paired. Each such pair of protochannels from the two adjoining membranes is called a connexon.

Chemical analysis of nexi isolated from various preparations has revealed that the particles are composed of protein. The number of different protein species in the connexon is small, at most only a few or perhaps only one major species as found in studies of rat hepatocytes (Hertzberg and Gilula 1979). X-ray diffraction evidence (Caspar et al. 1977) suggests that there are six sub-units surrounding a watery core which is about 2 nm in diameter. Although a direct channel through the center of the connexon joining the cytoplasm of one cell to that of its neighbor has not been directly visualized, there is much evidence which supports the existence of such a channel. Of the half-dozen morphologically distinct types of membrane specializations which are known to exist at intercellular junctions, it has been consistently shown that only the gap junction must be present for a permeable intercellular connection to be detected by functional means; absence of gap junctions is correlated with the lack of a permeable connection between cells. Thus, it seems likely that the nexus is indeed the morphological substrate of low-resistance cell-to-cell connections in the heart.

2.3 The Properties of Permeable Intercellular Junctions

The functional properties of such permeable intercellular connections can be considered regardless of whether the gap junction is the anatomical correlate of these connections. Indeed, the properties of permeable intercellular connections were studied well before anything was known about their morphology. In a study of rat atrial tissue in 1962, Woodbury observed that current injected via a microelectrode resulted in a voltage shift in a cell several cell-lengths distant (Woodbury, 1962). In 1964, it was discovered that a relatively large molecule, fluorescein (molecular weight 330), can pass from cell to cell in salivary gland epithelium (Kanno and Loewenstein, 1964). Since that time, most organized tissues, including myocardium, have been found to have connections which allow such molecules to pass between adjacent cells (Loewenstein, 1981). Weidmann demonstrated that radioactive $^{42}K^{+}$ ions diffused freely in bundles of sheep ventricular

fibers; he calculated a length constant of 1.55 mm, or 12 cell-lengths (Weidmann, 1966). Permeability to fluorescein has also been demonstrated in cardiac muscle (Pollack and Huntsman, 1973). The intercellular connections are highly permeable to ions and a variety of hydrophilic tracer molecules having molecular weights below 3000, including dyes, amino acids, small peptides, and sugars. Macromolecules do not permeate the connections. The tracer substances injected into cells in such experiments remain in the intracellular space; they do not permeate non-junctional cell membrane to the exterior, nor do they appear to leak to the exterior in traversing the intercellular junctions (Loewenstein, 1981). These findings suggest the presence of small, aqueous channels from cell to cell that are well-insulated from the extracellular space. The inner bore of the channels, as determined by the maximum size of permeant tracer molecule, is between 1.6 and 2 nm (Schwarzmann et al., 1981). The length of the channels, assuming that they pass through 2 thicknesses of cell membrane at a site where 2 cells are in intimate contact, is about 15 nm. A tube of these dimensions filled with fluid having a resistivity of 150 Ω-cm would have a resistance of about 10^{10} Ω (Loewenstein, 1975).

The tracer-flux experiments described above were important in establishing the existence of permeable intercellular connections and in giving some idea of their size. However, to monitor the permeability of the connections under a variety of experimental conditions, it is far more convenient to use one of a variety of techniques which measure their conductance electrically. All of the techniques measure the flow of current between two coupled cells, each of which is maintained at a controlled potential; the techniques differ in the number of microelectrodes required (one or two in each cell), and in the circuitry used to control the cell potentials. One recent method is the dual voltage-clamp technique, in which each cell of a coupled pair is penetrated by one glass microelectrode and clamped at a common potential (Spray et al., 1984). Then one of the cells is stepped to a different potential, causing the clamp circuitry to supply current to maintain

the potential in each cell; the resulting current flows through the intercellular junction. Given the junctional current flow and the transjunctional potential, the junctional conductance may be calculated. Using this technique, it is possible to measure the junctional conductance at different levels of transjunctional potential. It has been found that the conductance of the junctions in some cell types depends on the transjunctional potential, being maximum near zero and decreasing as the potential across the junction increases. However, in pairs of ventricular myocytes from adult rat heart, the conductance did not depend on voltage (Spray et al., 1984).

The permeability of the intercellular junctions is not a constant; in addition to the dependance on transjunctional potential exhibited by some types of junctions, a variety of changes in conditions, some physiological and some not, have been found to affect junctional conductance. Junctional permeability depends upon intracellular pH in many types of tissues, decreasing as cytoplasmic acidity increases. It also depends upon intracellular free Ca^{++} concentration in many preparations; there has been some debate about whether these two factors are independent, since many of the interventions which increase cytoplasmic free Ca^{++} also produce cytoplasmic acidification. Other interventions which have been found to decrease junctional conductance ("decouple" cells) are thought to act by decreasing the pH or increasing the free $[Ca^{++}]$.

Historically, the effect of $[Ca^{++}]$ on the degree of coupling between cells was investigated first. It had been observed when experimenting with the junctions of electrically excitable tissues that when a cell membrane was damaged so as to short-circuit its interior to the exterior, the cells to which it was connected did not become short-circuited to the exterior; it seemed as though the formerly conducting junctions between the cells had sealed. An apparent consequence of this sealing, the rapid disappearance of injury potentials in damaged heart muscle ("healing-over"), had been observed as early as 1877 by Engelmann (De Mello, 1982a). It has been found that

healing-over in cardiac tissue requires the presence of Ca^{++} to occur (Deleze, 1965).

Direct evidence of the regulation of junctional conductance by Ca^{++} was obtained by monitoring conductance with microelectrodes during the intracellular injection of Calcium ions into the cells of the salivary gland of the midge Chironomus (Rose and Loewenstein, 1976). In these experiments, the intracellular Ca^{++} concentration was monitored using intracellarly injected aqueorin. The Ca^{++}-dependant light emission of the aqueorin was measured using a photomultiplier system. The junctional conductance was observed to fall only when the cytoplasmic Calcium concentration at the junctions rose from the normal level of less than 0.5 μM to around 10 μM. This change was found to be reversible.

Intracellular Ca^{++} concentration has also been found to affect coupling between cardiac cells. Dahl and Isenberg treated sheep Purkinje fibers with dihydro-ouabain or alternately, dinitrophenol, both of which increase intracellular [Ca^{++}]. They monitored coupling electrically, and also monitored intracellular Ca^{++} activity using a Ca^{++}-sensitive microelectrode system; they also looked for changes in nexus ultrastructure in decoupled fibers by electron microscopy of freeze-fractured junctions. As the intracellular free [Ca^{++}] rose from its resting level of about 0.08 μM to 0.5 μM, detectable decoupling began to occur. Further increases in the intracellular [Ca^{++}] were accompanied by further decoupling. Significant changes in the size and shapes of the nexal particles were seen in the freeze-fractured junctions of decoupled fibers (Dahl and Isenberg, 1980). In experiments on bovine ventricular muscle, Weingart used ouabain to decouple cells while monitoring the internal longitudinal resistance of the fiber with microelectrodes. He observed an increase in the internal resistivity of fibers by a factor of 2.5, which was presumably attributable to increased resistivity of the intercellular junctions. Although intracellular [Ca^{++}] was not monitored in these experiments, it was presumably elevated, since it was observed that significant decoupling was accompanied

by contracture of the cells (Weingart, 1977).

Conflicting results were obtained in an investigation of the effects of elevating intracellular [Ca^{++}] in a preparation of cultured neonatal rat ventricular myocytes (Burt et al., 1982). These investigators used the calcium ionophore A23187 and alternately, monensin, to raise intracellular Calcium levels such that partial contracture of the myocytes was observed. They cited previous evidence to establish that such levels should be above the threshold for decoupling cells. Nevertheless, intercellular transfer of Lucifer Yellow was not abolished by these interventions. Actual Ca^{++} levels and junctional conductance were not measured in these experiments. The authors suggested that the cells in this preparation were resistant to decoupling by elevated intracellular Ca^{++}.

Soon after the demonstration of the regulation of intercellular conductance by [Ca^{++}] by Rose and Loewenstein in 1976, it was shown that acidification by exposure to 100% CO_2 decreases junctional conductance in coupled embryonic amphibian cells (Turin and Warner, 1977). Since that time a modulation of intercellular conductance by intracellular [H^+] has been shown in many types of coupled cells, including cardiac cells. Reber and Weingart investigated the effect of intracellular pH on cell-to-cell coupling in Purkinje fibers from sheep and calf hearts. They exposed the fibers to solutions equilibrated with varying amounts of CO_2 to acidify them; they alternately used a solution containing 15 mM NH_4Cl, which produces cytoplasmic alkalinization, followed by acidification upon return to normal medium. They monitored the intracellular [H^+] using pH-sensitive microelectrodes, and measured the intracellular resistance using one current-injecting and two voltage-measuring microelectrodes. They observed that cytoplasmic alkalinization by 0.26 pH units decreased the internal resistance of the fiber by 21%, and that cytoplasmic acidification by 0.48 pH units increased the internal resistance (decreased coupling) by 30%. Although they did not measure intracellular

$[Ca^{++}]$ in these experiments, they cited previous experiments that they had done in the same preparation in which intracellular acidosis gave rise to a decrease in $[Ca^{++}]$; thus, they argued, changes in pH were not affecting junctional conductance by changing intracellular $[Ca^{++}]$. They also pointed out that previous experiments with intracellular acidification had demonstrated a drop in cytoplasmic resistance with decreased pH, indicating that the increase in internal fiber resistance observed in these experiments must be due to an increase in junctional resistance (Reber and Weingart, 1982). It is of interest that the junctional conductance in cardiac tissues appears to be most sensitive to changes in pH near the normal level; cytoplasmic acidification sufficient to affect coupling is known to occur during ischemia (Spray et al., 1985).

In a recent review of the regulation of gap junctional conductance, the physiological significance of the effect of intracellular $[Ca^{++}]$ on gap junctional conductance has been called into question (Spray et al., 1985). Spray and co-workers argue that except for junctions in arthropods, decoupling of cells by high intracellular $[Ca^{++}]$ has required large, non-physiologic concentrations of the ion. They criticize other studies, including that of Dahl and Isenberg discussed above, because simultaneous increase of intracellular $[H^{+}]$ was not ruled out. They cite experiments of their own in which pairs of ventricular myocytes undergo irreversible contracture (indicating intracellular $[Ca^{++}]$ above 12 μM) without a detectable change in junctional conductance (White et al., in press). While they do not dispute the participation of Ca^{++} in the healing-over process in severely damaged cardiac tissue, they question its role in the regulation of conductance in undamaged heart.

How junctional permeability changes is still an open question. The closure of individual intercellular channels could be all-or-none, such that the conductivity change with various interventions is due to the proportion of open channels. Alternately, the channels could be capable of graded closure. Yet another possibility is rapid flickering

between open and closed states, with permeability being dependant upon the average time spent in each state. Spray and co-workers have reviewed the relevant evidence and conclude that while definitive experiments are still needed, the most likely mechanism is all-or-none closure of individual channels (Spray et al., 1984).

Permeable intercellular junctions can form within minutes after the membranes of two cells are brought into contact. This has been shown in many types of cells, including isolated cardiac myocytes (DeHaan and Hirakow, 1972). In large amphibian embryo cells, it has been shown by repeatedly pushing two cells together at different locations that conductive junctions form at random spots on the cell membrane (Ito and Loewenstein, 1969). The degree of coupling between newly apposed cardiac cells was investigated by Clapham and co-workers using spheroidal aggregates of chick-embryo ventricular myocytes. Two aggregates were held by suction pipettes and manipulated into contact. A recording micro-electrode was inserted into each aggregate, and another electrode was used to inject current into one of the aggregates. This configuration allowed the measurement of input and coupling resistances, and the delay of action potential propagation between aggregates. Immediately after being brought into contact, the aggregates continued to beat at their own intrinsic rates. After a few minutes, the beating rates synchronized, with initial action potential propagation delays of 50 mSec or more. The propagation delay decreased progressively during the first two hours; the shortest delay observed in any experiment was 0.5 mSec. Coupling resistance became low enough to be measurable between 5 and 60 minutes minutes after contact, and decreased along with propagation delay. Initial coupling resistivities ranged from 0.8 to 1.8 $k\Omega\text{-}cm^2$; final coupling resistivities were almost all below 0.2 $k\Omega\text{-}cm^2$. The contact area used to normalize these resistivities was estimated using a dissecting microscope, and the true contact area was thought to be 1 to 2 orders of magnitude lower, which would imply a junctional resistivity on the order of 2 to 20 $\Omega\text{-}cm^2$ (Clapham et al., 1980).

2.4 Classical Electrophysiology -- The Conduction of the Action Potential

The conduction of the action potential in excitable tissues involves the interaction of two distinguishable sets of properties of the cells and their connections to one another. On the one hand are the non-linear, time-varying ionic conductances of the cell membrane and the energy-requiring ionic pumps which maintain a potential gradient across the membrane, which together allow the generation of action potentials. On the other hand are the passive electrical properties of the tissue, which are important in governing the way in which action potentials spread from an excited area of tissue to neighboring regions. We will be mainly concerned with the passive properties since the effects of the intercellular connections on conduction fall into this category.

The potential across the cell membrane in the resting state is typically between 50 and 100 mV, interior negative; this resting potential is determined chiefly by the equilibrium potential for K^+, to which the resting membrane is most permeable. When a region of the membrane is depolarized by some stimulus beyond a threshold level, the permeability of that region to Na^+ ions increases. This results in an influx of positive charge in the region in the form of Na^+ ions, which further depolarizes the membrane and regeneratively increases the Na^+ permeability. The membrane potential approaches the equilibrium potential for sodium as the Na^+ permeability exceeds the K^+ permeability. As the membrane potential rises, however, inactivation of the Na^+ conductance begins and the sodium permeability begins to fall. In addition, other ionic permeabilities of the membrane change from their resting values, triggered by the change in membrane potential. All of these changes in combination produce the time-course of the action potential. A complete discussion of the ionic basis of cardiac action potentials is given by Noble (Noble, 1979, Noble, 1984).

For the study of propagation of the action potential, the depolarization phase is of

primary importance. The action potential described above does not remain confined to the original stimulated region of membrane. Since the depolarization produces intra- and extra-cellular potential differences between the active region and the adjacent resting regions, currents flow in the intra- and extra-cellular media. The intracellular current flow is from the active region to adjacent resting regions; the extracellular current flows from the resting regions to the active region. Current flows outward across the resting membrane, discharging the membrane capacitance in these areas; current flow across the membrane is inward in the active region. These currents are known as "local circuit" currents. As the capacitance of the resting membrane regions discharges, those areas become depolarized to the threshold for initiation of an action potential and the leading edge of the active region propagates.

The velocity of propagation of the action potential is determined by many factors. These include: geometric factors, such as the size and shape of the excitable cells; membrane factors, such as the properties of the ionic conductances (which differ between cell types) and the state of polarization of the membrane; and the passive electrical properties of the tissue, such as intra- and extra-cellular resistivities and membrane capacitance. There is a wide range of conduction velocities in cardiac tissue under normal conditions, and an even wider range if pathophysiologic conditions are considered. Conduction velocities as low as 0.01 M/sec and as high as 4 M/sec have been measured in cardiac tissue under various conditions (Cranefield, 1975).

The cell membrane of cardiac myocytes is a relatively good insulator in the quiescent state, separating the low-resistivity cytoplasm from the low-resistivity extracellular fluid. Since cardiac myocytes have a roughly cylindrical shape, and since they are most frequently coupled to one another by low-resistance connections at either end (although there is also side-to-side coupling), a model that is frequently used to describe the passive electrical properties of heart tissue is the cable model. The cable

model had been used to describe the electrical properties of neurons, and was first applied to cardiac Purkinje fibers by Weidmann (Weidmann, 1952). In this model, a fiber of heart muscle or other excitable tissue is treated as a long, cylindrical cable; an inner, core conductor, homogeneous along its length, is separated from an outer, homogeneous conductor by an imperfect cylindrical insulator (see figure 2-1). Current is assumed to flow in the inner and outer conductors only in the longitudinal axis, and through the boundary only radially. A further simplification which is often made is to assume that the outer conductor has negligible resistivity; the potential of the outer conductor is the zero reference. Let $V(x,t)$ be the potential on the inner conductor at point x and time t. Define $i_a(x,t)$ as the current flowing axially along the core conductor in the positive x direction [Amps], and $i_m(x,t)$ as the current flowing radially outward across the membrane per unit length of the cable [Amps/cm]. Let r_i be the resistance of the inner conductor per unit length [Ω/cm]. By Ohm's law, the voltage drop across r_i due to i_a is

$$\frac{\partial V}{\partial x} = -r_i i_a \tag{2.1}$$

By Kirchoff's current law, the outward transmembrane current flow must result in a reduction of axial current flow, so

$$i_m = -\frac{\partial i_a}{\partial x} \tag{2.2}$$

The relationship between membrane voltage and membrane current can be obtained by eliminating the axial current variable from these equations; differentiating the first expression with respect to x gives

$$\frac{\partial^2 V}{\partial x^2} = -r_i \frac{\partial i_a}{\partial x} \tag{2.3}$$

Since the right-hand side of this expression equals the membrane current

$$\frac{\partial^2 V}{\partial x^2} = r_i i_m \tag{2.4}$$

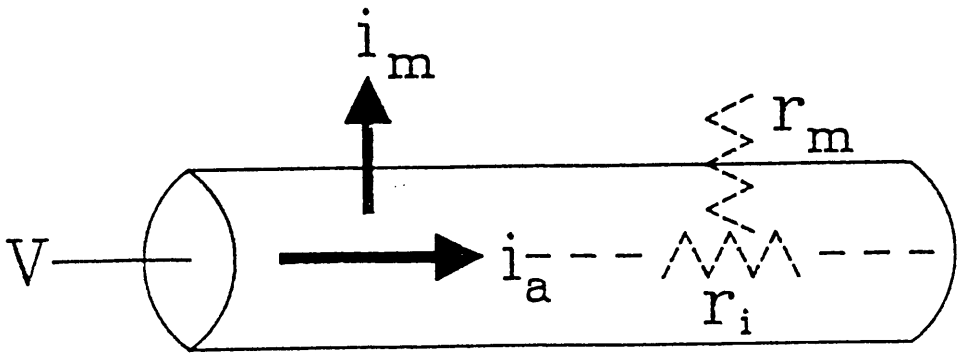

Figure 2-1: Classical cable theory model

This equation, known as the "core conductor" equation, relates the potential across the boundary layer of this model to the current flowing through it. No knowledge about the electrical properties of the boundary layer were used in deriving it, so it is valid regardless of those properties. However, it cannot be used, say, to learn the form of the potential across the boundary without specifying the form of the current across it. This restriction can be removed if the V-I characteristic of the boundary is incorporated into the core conductor equation. In the case of excitable cells, the boundary is the cell membrane, which behaves electrically as a capacitance in parallel with a resistance. This provides another constraint on the relationship between V and i_m

$$i_m = \frac{V}{r_m} + c_m \frac{\partial V}{\partial t} \tag{2.5}$$

where r_m is the resistance of a unit length of membrane [Ω-cm] and c_m is its capacitance [F/cm]. Substituting this constraint for i_m into the core conductor equation yields the "cable equation"

$$\frac{r_m}{r_i} \frac{\partial^2 V}{\partial x^2} = V + c_m r_m \frac{\partial V}{\partial t} \tag{2.6}$$

If the space constant λ and the time constant τ are defined as

$$\lambda = \sqrt{r_m / r_i} \quad , \quad \tau = c_m r_m \tag{2.7,2.8}$$

the cable equation can be written as

$$-\lambda^2 \frac{\partial^2 V}{\partial x^2} + \tau \frac{\partial V}{\partial t} + V = 0 \tag{2.9}$$

The cable equation is a second-order partial differential equation for membrane potential as a function of both space and time. Given a potential function at some initial time, it describes the potential for subsequent times at all locations along the cable. In the case of a cell which has an excitable membrane, the membrane displays increasing non-linearity as its potential depolarizes from the resting value, since the ionic conductances which comprise r_m depend upon membrane potential. Equation (2.5) is not valid under these conditions, so the cable equation does not describe the membrane potential of

excited membrane; the voltage- and time-dependant characteristics of the ionic conductances must be taken into account to describe action potentials. Nevertheless, for a region of membrane that has not been excited, for example the membrane just ahead of a propagating action potential, the cable equation applies and can be used to describe the course of the membrane potential. Thus, the cable properties are an important determinant of the initial part of the action potential (the action potential "foot") as it propagates from excited regions to adjacent quiescent ones.

To allow a simple analytical solution of the cable equation in the linear region, it is convenient to consider action potential propagation at constant velocity, θ. At a constant velocity, the shape of a propagating wave is the same whether considered as a function of position or as a function of time; given a particular potential function of position moving at a constant speed, the potential seen at any one point as a function of time has the same wave-shape. Since the wave-shape is the same as a function of time and space, its derivatives with respect to time and space must also have the same shape as one another; for the first and second derivatives

$$\frac{\partial V}{\partial x} = \frac{-1}{\theta}\frac{\partial V}{\partial t} \quad , \quad \frac{\partial^2 V}{\partial x^2} = \frac{1}{\theta^2}\frac{\partial^2 V}{\partial t^2} \tag{2.10}$$

This allows the elimination of either the space derivative or the time derivative from the cable equation. Eliminating the space derivative and considering only the time derivative gives the ordinary differential equation

$$-\frac{\lambda^2}{\theta^2}\frac{d^2V}{dt^2} + \tau\frac{dV}{dt} + V = 0 \tag{2.11}$$

The solution of this second-order differential equation contains the sum of two exponentials having time constants determined by the roots of the characteristic equation

$$-\frac{\lambda^2}{\theta^2}s^2 + \tau s + 1 = 0 \tag{2.12}$$

Measurements of the parameters λ, θ, and τ in cardiac tissue reveals that

$$\tau^2 \gg \frac{4\lambda^2}{\theta^2} \tag{2.13}$$

so that the time constant of this system is

$$\frac{1}{s} = \frac{\frac{2\lambda^2}{\theta^2}}{\tau + \sqrt{\tau^2}} = \frac{\lambda^2}{\tau\theta^2} = \tau_{foot} \tag{2.14}$$

The greater this time constant, the slower the initial depolarization of the membrane leading to the action potential. By substituting into this expression the definitions of space constant and membrane time constant (Eq. 2.7 and 2.8), we arrive at

$$\tau_{foot} = \frac{1}{r_i c_m \theta^2} \tag{2.15}$$

It would be convenient to be able to use this expression to directly infer the effect of changes in internal resistance and membrane capacitance upon the time constant of the action potential foot; however this is not possible. The reason is that the expression for τ_{foot} contains a dependance on the conduction velocity, θ. We have assumed that conduction velocity is constant, but the value has not been constrained. The actual conduction velocity obtained in excitable tissue depends upon multiple factors which include both the active and the passive properties of the tissue (r_i and c_m included). There is no known analytical method of deriving the conduction velocity given the parameters of the excitable tissue; the usual method is to reach the result numerically by simulation. With regard to (Eq. 2.15), it may be noted that if r_i and c_m remain fixed in a particular tissue, an increase in τ_{foot} implies a decrease in conduction velocity. We cannot, however, consider conduction velocity to be fixed and conclude that an increase in c_m should result in a smaller (faster) time constant for the foot; the increase in c_m will in fact result in a decreased conduction velocity and, very likely, a greater τ_{foot}.

2.5 The Discontinuous Propagation Hypothesis

A recent investigation of action potential propagation in cardiac tissue revealed properties which cannot be explained by the continuous cable theory model (Spach et al., 1981). The experiments were done using isolated, intact atrial and ventricular muscle preparations from dogs. The propagation velocity at various sites was altered in two different ways. One method of slowing the velocity was to drive the tissue with stimuli of controlled prematurity; the rationale for this intervention was to cause a change in "membrane" factors by modulating the fast sodium-current mechanism. Alternately, the propagation velocity at a given site was changed by changing the location of the applied stimulus; due to the anisotropy of intact cardiac muscle, activity travels along the longitudinal axis of a fiber more quickly than in the transverse direction. This intervention was used to provide a "non-membrane" change in conduction velocity, since the membrane properties are the same in the longitudinal and transverse axes. Intracellular and extracellular potentials were monitored at the recording site.

When the prematurity of the stimulus was increased to decrease conduction velocity via a change in membrane properties, the maximum rate of rise of the action potential decreased, and the time-constant of the foot of the action potential was seen to increase. These results are consistent with the predictions of cable theory. However, when the direction of wavefront propagation relative to the orientation of the muscle fibers was altered, opposite changes were observed in the shape of the action potential. Specifically, in the transverse axis, where propagation velocity was lower, the action potentials had a greater maximum upstroke velocity, greater amplitude, and a faster-rising foot than they did when propagation was in the longitudinal axis. In addition, the transmembrane potentials recorded during transverse propagation frequently had irregular notches just after the upstroke. The proposed explanation for these observations was that they resulted from the non-uniform distribution of effective axial resistivity due to the relatively large

resistivity at the intercellular junctions. It was postulated that the unexpected results in the case of transverse propagation were attributable to the relatively sparse distribution of intercellular connections that is found anatomically in the transverse axis. It was noted that a given patch of membrane has its fastest upstroke velocity when it is an isopotential patch; when it is closely coupled to adjacent areas of membrane, it must supply depolarizing current to them, slowing its own depolarization. If the path along the transverse axis consisted of relatively poorly coupled areas of membrane, transverse propagation could produce action potentials with faster upstrokes. The notch following the peak of the transmembrane potential might be due to the prolonged current flow needed to discharge the adjacent cell, with recovery occurring when it fired. It was proposed that "during transverse propagation, then, activity would seem to halt momentarily or to hesitate before moving on to the next unit along the path."

This "discontinuous propagation" hypothesis was advanced for propagation in the transverse axis, based on comparisons between the waveforms obtained during transverse and longitudinal propagation. It must be noted, however, that the same basic structure is thought to couple cells in both axes; thus, the difference between propagation in the two axes should be one of degree, rather than a fundamental one. If propagation is indeed discontinuous in the transverse axis, it should also be discontinuous in the longitudinal axis, although to the extent that the cells are better coupled and the junctions more widely separated in the longitudinal axis, the phenomenon will be less obvious. In pathological states in which coupling between cells is impaired, it might become more significant.

In a subsequent study using the same preparation and recording techniques, variations in longitudinal and transverse conduction velocities were examined as the stimulus rate was varied or as ouabain was applied to the preparation (Spach et al., 1982a). A numerical model based upon cable theory was used to predict the effects of

separate changes in cytoplasmic and junctional resistivities on propagation velocity in the longitudinal and transverse axes. This model predicted opposite effects of such changes on the ratio between the longitudinal and transverse velocities; the ratio decreased with increasing cytoplasmic resistance, but increased as junctional resistance was increased. Experimentally, it was found that the ratio increased with increasing stimulation rate over the range of 60 to 200 BPM; the possibility that such changes were due to modulation of the sodium mechanism by rapid stimulation was excluded by demonstrating that the shape of the transmembrane potential remained unchanged throughout the procedure. Ouabain exposure also increased the ratio of longitudinal to transverse velocities. The results were interpreted as showing increased coupling resistance between cells associated with ouabain exposure and increased stimulation rates.

Another study using combined intracellular and extracellular recordings from canine atrium focussed on the effects of structural complexities, such as branch sites and connective-tissue septa, on the patterns of propagation through small areas of cardiac muscle (Spach et al., 1982b). It was experimentally demonstrated, given only the normal types of complex geometric arrangements of cells found in vivo, that by manipulating the site, and in some instances, the timing, of stimulation, conduction disturbances such as unidirectional block and reentry could be elicited. These findings were explained in terms of discontinuities of the axial resistivity of the preparations occurring at the sites of anatomic discontinuities; changes in membrane properties were not found. This hypothesis is more general than that of discontinuous propagation discussed above, since it includes the effects of the macroscopic anatomical complexities of the tissue. Such anatomical complexities are more common in cardiac tissue than once thought, however. For example, recent histological studies have shown that ventricular cells are organized by connective tissue into so-called "unit bundles" which are about 200 μm in diameter (Sommer and Dolber, 1982). Connections between cells in adjacent bundles do occur, but are less numerous than those between cells in the same bundle.

2.5.1 Simulations of Discontinuous Propagation

The experimental data discussed above contradict the classical cable-theory model of action potential propagation in cardiac tissue. It was hypothesized that the discrepancy is due to the nature of the coupling between cardiac cells. Diaz developed a computer simulation of action potential propagation which explicitly modelled the intercellular connections (Diaz et al., 1982, Diaz, 1983, Diaz et al., 1983). The "discontinuous cable model" designed by Diaz consisted of a computer simulation of an electric network representation of a one-dimensional fiber consisting of 35 to 50 "cells", each 100 μm long and 15 μm in diameter. Each cell in the fiber was modelled by 10 membrane patches, which were implemented using the ventricular action potential model of Beeler and Reuter (Beeler and Reuter, 1977). These patches were connected to one another by a resistance representing the myoplasmic resistance. Adjacent cells in the fiber were connected by a resistive "T" network, which modelled the intercellular connections; this configuration was chosen based on theoretical work by Heppner and Plonsey (Heppner and Plonsey 1970). It contained two axial resistances and a leakage resistance connected to the extracellular space. Parameter values for the membrane model and for the various resistances were assigned based on measurements made in cardiac muscle. The action potential at all points along the fiber and the extracellular potential at selected external points were calculated.

The model was used to study the effects of the intercellular connections on various aspects of action potential propagation. It was found that as the leakage to the extracellular space at the junctions was increased, conduction velocity slowed and conduction eventually failed. Changes in the two components of the axial resistivity of the fiber (myoplasm resistivity and junctional resistivity) had different effects on the conduction velocity. Increases in either one slowed conduction, as would be expected; however, increases in the intracellular (myoplasm) resistivity alone were found to slow

conduction less than would be predicted on the basis of continuous cable theory; on the other hand, increases in the intercellular (junctional) resistivity alone slowed conduction by much more than continuous cable theory would predict. When junctional resistivity was increased and myoplasm resistivity held constant, the upstroke velocity of the action potential increased even though the conduction velocity decreased. This result is similar to that found experimentally by Spach et al., and is contrary to the relationship between conduction velocity and upstroke velocity in a continuous cable. It was also found, with model parameters adjusted to "normal", that the conduction velocity within a cell was 10 times higher that the average conduction velocity over many cells. This was due to a time delay in crossing the intercellular junction. The time delay predicted by the model was 0.45 mSec when the junctional resistivity was set to 1 Ω-cm^2. The extracellular potential predicted by the Diaz model was of interest; it was predicted that at the surface of the fiber, the extracellular waveform would change from having a large positive phase at the proximal end of the cell, through a biphasic shape at the center of the cell, to having a large negative phase at the distal end of the cell. However, it was later realized (Diaz, personal communication) that the extracellular field calculations contained a methodological error. A subsequent publication (Plonsey and Barr, 1985) demonstrated that the relative sizes of the junctional and cellular regions must be taken into account in making such calculations. Thus, the extracellular waveforms that would be predicted by the discontinuous cable model have not been established.

Another simulation of action potential propagation which modelled the effects of resistive intercellular junctions was developed by Joyner (Joyner, 1982). The modelling details were somewhat different from those of the Diaz study. A one-dimensional strand of cells was modelled. Each membrane element was considered to represent a single, isopotential, "cell". Cells were grouped into "islands", each containing the same number of tightly-coupled cells, and each loosely coupled (by a relatively high resistance) to two neighboring islands. The number of cells per island was varied while the overall

longitudinal resistance was held fixed by increasing the coupling resistance between islands as the number of cells in each island increased (increasing the number of cells in each island implied a decrease in the number of islands, and hence fewer high-resistance couplings in a fixed length of strand). This allowed a semi-quantitative comparison of various "packaging" arrangements of cells. As the number of cells per island increased from the "control" value of one, (and as the coupling resistance concomitantly increased), the maximum velocity of the action potential upstroke increased at first, and then decreased as the number of cells per island went above some value. The foot of the action potential showed progressive slowing, and notches appeared following the peak of the action potential. As the coupling resistance increased beyond some point, conduction became decremental and then failed completely.

The simulation results show some of the behavior observed by Spach et al., but not all of it. The simulations of discontinuous propagation do show the increase in maximum upstroke velocity with decreasing conduction velocity that has been observed experimentally; they also show the notches following the peak of the action potential. However, they show a slower-rising action potential foot (increase in time constant), which contradicts the experimental results obtained by Spach (Diaz, 1983, Spach, 1983). These simulations treated one-dimensional linear arrays of cells only. The number of cells simulated was small, about 50 to 100. Spach has suggested that the discrepancies between the experimental results and these simulations are due to the simplified nature of the simulations; he believes that a simulation having a dimensionality of at least two will be necessary for agreement with the experimental results (Spach, 1983).

2.6 The Chick-Embryo Ventricle Cell-Culture Preparation

The experiments to be described were carried out on a preparation of cultured ventricular cells from chick embryo; this preparation is commonly used in the study of

cellular cardiac physiology. The cells are harvested from the ventricles of 10-day White Leghorn chick embryos; they are dissociated from the tissue by a combined enzymatic and mechanical technique. The properties of this preparation will be reviewed here; for details of the method used to obtain the cells, see the methods section.

The dissociation of chick embryo ventricular tissue yields a mixture of cell types. The majority of the cells are myocytes (technically, many of these are myoblasts, since some mitotic activity is still observed; however, they are referred to as myocytes in most of the literature on this subject). The rest are mostly fibroblasts; some endothelial cells and cells of the conduction system are also present. The proportions of the two major cell types depend upon the culture techniques used, and control of the proportions is possible by selecting the trypsinization fraction to be cultured and by exploiting the difference in time taken by the two cell types to attach to the surface of the culture vessel. The histology of the myocytes in this preparation is not the same as that of myocytes from adult hearts. The myofibrils are not as regularly arranged as they are in adult cells, nor are they as abundant. At stage 29 in embryonic development, after approximately 6.5 days of incubation (Hamburger and Hamilton, 1951), myofibrils occupy about 18%, and mitochondria about 11%, of the cell volume (Clark et al., 1986). In comparison, myofibrils account for 50% of the volume of adult cells, and mitochondria occupy about 35% of cell volume. (Corresponding data for the 10-day embryonic cells that are used in these experiments are not available, but they presumably lie between the 6.5-day and the adult values.)

The organization of the cells in culture depends upon the density at which they are plated. At low plating densities (less than 100,000 cells/ml), the cells are scattered over the surface of the plate; most have no contact with their neighbors. At the usual plating density (around 500,000 cells/ml), a monolayer of cells results, with most cells being in physical contact with their surrounding neighbors; such monolayers do have some 'holes'

which have no cells, as well as small patches which are more than one cell thick. At higher plating densities, the multilayer areas become larger and thicker.

The dissociation procedure separates the tissue into a suspension of single, isolated cells, yet it is invariably observed, after some time in culture, that the spontaneous contraction of neighboring cells becomes synchronized. This synchronization was studied by Jongsma and co-workers in a similar preparation of cultured neonatal rat myocytes (Jongsma et al., 1982). The motion of neighboring cells was monitored using a video system. In most cases, synchronization of beating occurred within seconds to hours after 2 cells had visibly made contact. In a minority of cases, cells which were visibly in contact did not synchronize. In other cases, cells between which there was no visible connection by light microscopy nevertheless developed synchronization; this observation was explained by the existence of thin processes between cells which could not be seen using the light microscope. At different times following synchronization, the cell pairs were fixed for electron microscopy; gap junctions were found to be present between the cells within a few minutes of synchronization.

In an earlier study of junctions in cultured chick embryo heart cells, junction morphology and electrical coupling were examined in three types of junction: myoblast-myoblast, myoblast-fibroblast, and fibroblast-fibroblast (Hyde et al., 1969). Myoblast-myoblast junctions were found to contain both desmosomes and nexi, and were said to closely resemble the intercalated discs of adult heart tissue. Myoblast-fibroblast junctions contained desmosomes, but no nexi were found. Fibroblast-fibroblast junctions had neither desmosomes nor nexi, although regions of close contact with no intercellular gap were found. Electrical coupling was also measured in these experiments by injecting current using one microelectrode and measuring the electrotonic response with another microelectrode at a variable distance from the first. As expected, predominantly myoblastic cultures had the greatest degree of coupling, with a space constant of 1100

μm. The space constant in mixed myoblast-fibroblast cultures was 400 μm, and in predominantly fibroblastic cultures it was 200 μm.

The first recordings of action potentials from cultured embryonic heart cells (from rats) were made by Cole's group in 1934 (Hogg, Goss, and Cole, 1934). The electrophysiology of cultured chick embryo heart cells has been studied since the mid 1950's (Fange et al., 1956). A large variability of properties has been reported, attributable to the range of age of embryos studied (from 3 to 18 days in ovo), the variety of culture preparations (e.g: monolayer, spherical aggregates, linear strands, isolated cells), and perhaps to local variations in culture technique. The properties of intact chick embryo heart are not subject to variability due to culture techniques, and so will serve as a reference point for the discussion of properties of cultured cells. In intact chick embryo heart, there is an ontogenetic progression of membrane electrical properties. In young hearts (2-4 days in ovo) the resting potential is low (-40 mV), due to low K^+ permeability (P_K). The permeability ratio P_{Na}/P_K is 0.2, resulting in a resting potential closer than usual to the Na^+ equilibrium potential in these cells. By day 15, P_{Na}/P_K has dropped to 0.01, and the resting potential has increased to around -70 mV (Sperelakis and Shigenobu, 1972).

Cells in 2-4 day hearts exhibit slowly-rising action potentials (dV/dt_{max} of 10 - 20 V/sec) with an amplitude of about 55 mV. Lowering the take-off potential by injecting hyperpolarizing current does not greatly increase the upstroke velocity, which would be expected if the sodium channels in this tissue were the same as those in adult hearts (which will generate slow action potentials when the resting potential is low). Tetrodotoxin (TTX) does not abolish these action potentials, which again would be expected of the sodium channels in adult cells. However, changing the Na^+ equilibrium potential by changing the extracellular $[Na^+]$ changes the reversal potential in a way which is consistent with a sodium channel. Therefore, it is thought that the action

potentials in these hearts are generated by "slow", TTX-insensitive Na^+ channels (Sperelakis and McLean 1978). On about the 5th day in ovo the maximum upstroke velocity of the action potential rises to 50-70 V/sec, and exhibits slowing on exposure to TTX. After about the 8th day, the action potential is completely abolished by exposure to TTX; the maximum upstroke velocity continues to rise until reaching the adult value of 150 V/sec on about the 18th day in ovo. Sperelakis and McLean explain these results by a gradual replacement of a population of TTX-insensitive "slow" sodium channels with a population of TTX-sensitive "fast" sodium channels. At the same time, the membrane P_k increases (see above), and the amplitude of the action potential rises to about 100 mV. The duration of the action potential remains about 125 mSec throughout embryonic development (Yeh and Hoffman, 1968). The propagation velocity in intact chick embryo atrium is 0.4-0.5 m/Sec (Lieberman and Paes de Carvalho, 1965).

Some of the properties of cultured chick embryo myocardial cells are essentially the same as those in-situ, while others are somewhat different. Morphologically, for example, cultured cells look "younger" than the corresponding cells in an embryo of the same age; there are fewer myofibrils, and those that are present are less well-organized. The resting potential and action potential amplitude are roughly the same as are found in intact hearts. However, the maximum rate of rise of the action potential in monolayer cultures of cells from 7 to 16 day hearts has been reported by some investigators to be in the range of 2-20 V/sec, which is about the same as in intact hearts at 2-4 days in ovo. Furthermore, the same studies showed a lack of sensitivity of these slow action potentials to TTX (Sperelakis and Lehmkuhl, 1965, McLean and Sperelakis, 1974). These results, along with the immature morphology found in monolayer cultures, led to the hypothesis that cardiac cells in monolayer culture partially de-differentiate to an early embryonic state. Other workers, however, using both embryonic chick (Lompre et al., 1979) and rat (Robinson and Legato, 1980) cardiac cells in monolayer culture, have found fast, TTX-sensitive action potentials. More recently, McLean and Sperelakis have reported on

variations on their original culture techniques which result in cells which retain their fast, TTX-sensitive action potentials. Thus, it appears that the chick embryo myocyte preparation will exhibit action potentials like those in adult cardiac tissue given appropriate culture preparation.

The cable parameters of cardiac cells in culture are of interest in the study of action potential propagation. These have been studied by several investigators using cultured chick embryo cells prepared in different ways. Sachs studied myocytes prepared from 6 to 9-day chick embryos, and grown on agar coated glass slides having 10 μ wide slits which resulted in the formation of long strands of cells (Sachs, 1976). The strands were penetrated using two intracellular microelectrodes at variable distances. One of these electrodes was used to apply a stimulus, the other recorded the amplitude of the response. Since the cells were spontaneously active and demonstrated the phase 4 depolarization that is seen in pacemaking cardiac cells, the cable properties could not be measured on a completely quiescent membrane. Instead, test stimuli were timed to arrive during diastole, i.e: in phase 4. It was found that the membrane conductance continually changed during phase 4, so that the value measured depended upon the timing of the measurement with respect to the action potential. Light and electron microscopy were performed on the strands to measure cell width, cross-sectional area, and surface area. The cable parameters of this preparation were: core resistivity (cytoplasmic plus junctional), 245 Ω-cm; membrane capacitance, 1.46 $\mu F/cm^2$. Parameters whose values depended upon the time of measurement in phase 4 were: membrane resistance, 16 to 136 $k\Omega\text{-}cm^2$; space constant, 0.95 to 3.2 mm; time constant, 29 to 269 mSec; and input resistance, 1.1 to 3.8 MΩ.

The passive electrical properties of cultured neonatal rat myocytes have been measured in a monolayer preparation using a two-microelectrode technique (Jongsma and van Rijn, 1972). In that study, the core resistivity (cytoplasmic plus junctional) was

estimated to be 502 Ω-cm; membrane capacitance was 1.3 $\mu F/cm^2$. Membrane resistance was estimated to be 1316 $\Omega\text{-}cm^2$; the space constant was 362 μm, and the time constant was 1.7 mSec. It will be noted that the agreement between some of the parameters obtained from the two experiments is only within orders of magnitude. The differences in the types of cells used and the culture preparations notwithstanding, it must be observed that the values of the parameters obtained from any given experiment are extremely dependant upon the physical model to which the data are fit. In the Sachs experiment on the linear strand of cells, the physical model was that of a continuous cable, whereas in the experiment on monolayer cultures, the physical model was a thin conducting sheet of infinite extent. Given the cellular nature of the preparations and the random distribution of intercellular connections in each preparation, the correspondence of either model to reality is open to speculation. From this point of view, the agreement between the two sets of results is acceptable.

2.7 Extracellular Action Potentials

Excitable tissues generate potentials in the extracellular region by virtue of current flow through the membrane and in the extracellular space. These can be sensed by appropriate electrodes and used to monitor cellular activity. The generation of these potentials is discussed here since they are recorded in the experiments to be described.

The extracellular action potential waveform is quite different from the transmembrane action potential to which it is related. In cardiac tissue, the transmembrane potential is roughly a monophasic, positive-going pulse, about one hundred mV in amplitude and a few hundred mSec in duration, with a sharp rising edge and a slowly decaying falling edge. The extracellular potential in the same tissue is roughly a biphasic or triphasic wave, occurring at the beginning of the corresponding transmembrane action potential, and having an amplitude of less than a few mV and a

duration of a few mSec. The relationship between intracellular and extracellular potentials from cardiac muscle was examined experimentally by Vaughan Williams in a preparation of rabbit atrial tissue (Vaughan Williams, 1959). The recording electrode was a glass microelectrode which could be positioned either intracellularly or extracellularly on the endocardial surface by a micromanipulator. The preparation was paced externally and the recordings were made on a synchronously triggered oscilloscope. Vaughan Williams identified 4 phases of the extracellular action potential: (1) upward positive, (2) fast downward negative, (3) upward positive to just above the baseline, and (4) slow return to zero. The first three phases occurred during the upstroke of the membrane potential; the last phase occurred during repolarization. The fast downward negative phase was coincident with the fast portion of the membrane potential upstroke.

Simple models can account for the general features of the extracellular waveform. When an action potential propagates along an excitable fiber in a conducting medium, current flows outward through the membrane ahead of the active region, discharging the membrane capacitance. Within the active region, current flows inward through the membrane. Behind the active region, there is outward current flow as repolarization takes place. Now consider the potential that will be observed at a point near the fiber in the extracellular space relative to some distant reference electrode whose potential is defined to be zero. As excitation approaches the observation point, current flows away from the fiber; since this current must be flowing down a potential gradient, the potential must be decreasing with distance from the fiber. Since the potential at the distant reference electrode is zero, the potential at the observation point near the fiber must be positive. As the active region moves closer to the observation point, the net current away from the fiber decreases through zero to a negative value, i.e: net current flow is towards the fiber in the active region. This corresponds to the potential at the observation point decreasing through zero to negative values. Finally, as the excited region moves past the observation

point, a repolarizing region approaches; net current is again outward and a third, positive phase of potential is seen. Since the current in the repolarization phase is typically smaller than that in the preceding phases, the amplitude of the potential observed is also smaller, frequently negligible in comparison to the preceding phases.

Another simple model which accounts for the general features of the extracellular action potential is the travelling dipole model. The active region of the fiber is conceptualized as two potential dipoles separated by some distance and oriented "back-to-back", i.e: +-,-+. The central negative region represents the active region of tissue; the pair of dipoles travels along the length of the fiber. As in the previous model, the waveform seen at some extracellular observation point is triphasic, first positive, then negative, then positive again, as the potential field moves with respect to the observation point. As might be expected, these two simple models are related. This can be seen by considering the isopotential field lines in the double dipole model; current flows in the volume conductor orthogonally to these lines. The current flow that is implied by the potential field set up by the two dipoles in the second model is the same as that described in the first model above.

While these simple models explain the general features of the extracellular action potential, they are not nearly detailed enough to account for the extracellular potentials recorded experimentally. A detailed prediction of extracellular waveforms requires a far more quantitative model. Such a model was developed for isolated nerve fibers in the classical work of Lorente de No (Lorente de No, 1947). The goal of his work was to understand the variety of shapes and sizes of extracellular potentials that were recorded from nerve fibers experimentally. Lorente de No's work was carried out before the Hodgkin-Huxley theory of the nature of action potentials was developed, and so contains no reference to the nature of the sources of the measured potentials. Rather, the sources were defined empirically from the waveform recorded by extracellular electrodes placed

in the sciatic nerve of a bullfrog and therefore at the surface of the axons being investigated. Using the equations of the cable model and graphical integration and differentiation methods, Lorente de No reconstructed the potential field and the current flow field surrounding the nerve under the assumptions of uniform conduction velocity and an infinite volume conductor. Once the potential field in the volume conductor was known, it was used to predict the shape and magnitude of extracellular potentials measured at various distances from the nerve with reasonable success. An interesting insight into the reason for the change in shape of the waveform with distance from the fiber was obtained by plotting the instantaneous value of the potential field versus distance from the fiber along lines perpendicular to the fiber at various points along the travelling waveform. The decrease in potential along these lines was found to be a different function of the distance from the fiber for each line. Therefore, the waveform seen by a stationary electrode observing a travelling action potential depends upon the distance of the electrode from the fiber. The changes in shape that are due to this mechanism are subtle changes in curvature of various segments of the waveform -- the major characteristics such as the number of peaks, their polarity, and their time relationship to one another, are not significantly affected.

The amplitude of the extracellular potential decreases with increasing distance from the tissue that generates it, as would be expected. However, there is no simple relationship for the decrement of potential with distance, even in the case of a single cable in an infinite volume conductor. Hakansson measured the extracellular potential amplitudes versus distance from frog muscle fibers and attempted to empirically obtain an expression for the peak-to-peak amplitude as a function of distance (Hakansson, 1957). He concluded that close to the fiber, the decrease in potential was linear with the logarithm of the distance r, whereas further away, the decrease was proportional to $r^{-1.3}$. An understanding of these results was provided by Krakau, who calculated the Fourier transform of Lorente de No's expression for the spread of potentials in a volume

conductor (Krakau, 1959). In the frequency domain representation, a factor in each frequency component is a Bessel function having the frequency in its argument; in other words, the attenuation of each component of the extracellular waveform with distance is a function of its frequency. The greater the frequency of the component, the more it is attenuated with distance from the fiber. This accounts for the lack of a simple amplitude versus distance relationship for the action potential as a whole, and also provides another insight into the change of shape of the waveform with distance from the tissue.

The Lorente de No model of extracellular action potential generation deals only with the case of constant velocity propagation along a single linear cable in an infinite conducting medium. Whereas a single axon or even a nerve containing multiple axons all conducting synchronously can conform to such a model well, cardiac tissue is less well-described by this model. The introduction of variations in the geometry and/or propagation velocity can be expected to affect the extracellular potentials.

The extracellular action potentials occurring in cardiac tissue have been extensively investigated by Spach and co-workers (Spach et al., 1972). The preparation used was isolated canine left ventricle which was pinned to the floor of a perfusion bath. Both intracellular potentials and extracellular potentials were recorded from "functionally single" Purkinje strands on the septal surface; functionally single strands had a single biphasic extracellular deflection along their entire length, with the delay from the time of stimulation monotonically increasing along the strand. Photographs were taken to document the geometry, and conduction velocity was calculated. The conduction of action potentials was perturbed in different experiments by applying progressively premature stimuli, by raising the $[K^+]_o$, and by lowering the temperature. The recorded intracellular potentials were used to calculate the expected extracellular potentials using a model which assumed a cylindrical geometry for the strand. Reasonable agreement was obtained between the measured and predicted extracellular waveforms under all

experimental conditions. The extracellular waveforms were superficially similar in shape to the second temporal derivative of the intracellular potentials; however, the leading and trailing edges of the latter approached the baseline more quickly than those of the former. Changes in conduction due to interventions revealed that the amplitude of the extracellular potential was highly correlated with the maximum rate of rise of the intracellular potential (r=0.98), and the duration of the extracellular potential was highly correlated with the duration of the upstroke (r=0.98).

In another, related study, the shape of extracellular action potentials was examined as a function of distance from the source, and the origin of the polyphasic waveforms typically found in the cardiac conduction system of the dog was explored (Spach et al., 1973). The preparation used was isolated canine left ventricle as described above. Measurements were made as described above, and in addition, extracellular potentials were recorded at several distances from the Purkinje strands. The interventions used were elevation of the $[K^+]_o$, and lowering of the temperature.

Functionally single Purkinje strands were stimulated. The amplitude of the extracellular deflection decreased as the electrode was withdrawn from the surface, markedly at first and then more gradually; the time between the positive and negative peaks of the waveform also increased with distance. The recorded intracellular action potential was used to compute the expected extracellular action potentials at various distances from the fiber using the expression for volume conduction outside a cable in an infinite volume conductor. Good agreement was obtained between the measured and predicted extracellular amplitudes; however, the time between the positive and negative peaks was overestimated by this expression. It was shown that even though the temperature and $[K^+]_o$ interventions could decrease conduction velocity by similar (in one case identical) amounts, the extracellular amplitudes and waveforms were different in the two cases, and were predicted well on the basis of volume conduction of the

associated intracellular action potentials. Extracellular recordings made from around the main branches of the conduction system were found to have a complex shape with multiple, separated peaks. By recording from multiple locations in the vicinity of such a polyphasic waveform, it was demonstrated (in one particular experiment, at least) that the complex shape was due to the superposition of signals from several adjacent sources rather than to a single cell undergoing a complex depolarization. Through trial and error, an arrangement of fibers whose depolarization combined to produce similar-looking waveforms was found.

Another mechanism for variability in the shape of extracellular action potentials recorded from cardiac tissue is the occurrence of "collisions" of two wavefronts travelling towards one another. In experiments with isolated dog ventricle Purkinje strands, Spach et al. demonstrated that the normal biphasic extracellular potential in a strand conducting in one direction became monophasic (positive-going) at the site of a collision induced by stimulating it at both ends simultaneously (Spach et al., 1971). This phenomenon has recently been explored in great detail using a computer simulation of cardiac conduction in a cable geometry (Spach and Kootsey, 1985). The goal was to understand alterations in the shape of the extracellular potential in terms of the corresponding transmembrane potential and the underlying sodium current and conductances. The model was a simplified Hodgkin-Huxley type, simulating only the sodium mechanism, and having a constant repolarizing conductance; this was permissible since the events of interest occurred during depolarization only, when other membrane conductances are negligible. Voltage-clamp data from heart muscle were used to assign parameters for the model. Four situations were compared: the uniformly propagating action potential, the action potential around the site where propagation is initiated, the action potential approaching the end of the cable, and the action potential in the vicinity of a collision (simulated by applying stimuli to both ends of the "cable"). The "measured" variables were: transmembrane potential, sodium current, sodium

conductance, and extracellular potential.

As expected, the extracellular waveform produced by the simulation during uniform propagation was biphasic, with the second (negative) phase having greater amplitude than the first, (positive) phase. This corresponded to the asymmetry in the membrane current waveform, in which the magnitude of the initial outward (capacitive) current is smaller than the magnitude of the subsequent inward (ionic) current. At the site of collision, the simulated extracellular potential was almost entirely positive, with a small negative phase. The membrane current in this case was found to be predominantly outward (capacitive), in spite of the fact that the sodium conductivity of the membrane rose to about the same level as in the case of uniform propagation. The small inward current in this situation occurred because the collision shifted the phase of the sodium conductivity with respect to the rise of the transmembrane potential, resulting in a lower influx of current for a shorter period of time. To see why the inward current should be smaller in this case, consider that the downstream membrane is already depolarized in the case of a collision, so the active area does not supply local circuit current to depolarize it. A complementary sequence of events occurs in the vicinity of action potential initiation, and results in the transmembrane current being predominantly inward, and the extracellular potential having a much greater negative phase than normal.

Extracellular action potentials are frequently used to determine the timing of activation of regions of an excitable tissue. Since extracellular potentials are a few mSec in duration, a fiducial point on the waveform must be chosen if the time of activation is to be determined to any greater accuracy than that. Such a fiducial point must be readily measurable. Moreover, it should ideally reflect some particular underlying membrane event or state that is the same regardless of variations in shape of the extracellular action potential. Obvious choices such as the time of zero-crossing or the time of the positive or negative peak are not well-suited for this purpose; the simulations done by Spach and

Kootsey show that their locations with respect to underlying membrane events vary when propagation is not uniform. Furthermore, in the case of monophasic waveforms it may be impossible to determine a meaningful zero-crossing or the peak of the opposite polarity. The practical question of a choice of fiducial point was addressed in this group of simulation experiments. It was found that regardless of the shape of the extracellular potential, the negative peak of its first derivative occurred at the same time as the maximum upstroke velocity of the transmembrane potential. Also, during uniform propagation, the peak sodium current and the peak sodium conductance occurred within 20 μSec of this time. During non-uniform propagation, the peak sodium current and conductance are less closely in phase with one another, but still occurred within 50 μSec of the negative peak dv/dt of the extracellular potential. Spach and Kootsey strongly suggested that the negative peak of the first derivative of the extracellular potential be used as a fiducial point for the time of activation in experiments on cardiac tissue.

2.8 Arrays of Extracellular Microelectrodes

Extracellular microelectrodes are used to sense the electrical activity of cells non-invasively. Their advantage over the other commonly used sensor of cellular electrical activity, the intracellular microelectrode, is that they leave the cell intact -- they do not require the puncture of a hole through the cell membrane. They are simpler to use, since they must only be positioned near the cell being studied, and are typically simpler to make and much more rugged than intracellular microelectrodes. Recordings can be made for longer periods of time, since there is no attendant cell damage. These characteristics make the extracellular microelectrode the sensor of choice when the requirement is to monitor the electrical activity of a tissue or a group of cells at many locations simultaneously or for extended periods.

The last 16 years have seen the development of arrays of extracellular

microelectrodes, which contain multiple electrodes that are used to record the activity at several locations in a single preparation. Since the experiments to be described in this work employ such an array, the development of these devices will be briefly reviewed here.

The first report of an array of extracellular microelectrodes fabricated using microelectronics techniques appeared in 1970 (Wise et al., 1970). This device was designed to be used as a probe for brain tissue. The electrodes were gold on a silicon dioxide-coated silicon substrate, and were insulated by a layer of silicon dioxide. Recording tip surface areas as small as 15 μm^2 were fabricated. The maximum number of electrodes fabricated on the prototype devices described was two, but larger numbers were thought to be feasible. Signals were successfully sensed from adult cat cortex by 18 of 40 devices tested.

Since the report of their first microelectrode array probes, Wise and co-workers have improved the signal-to-noise ratio of their devices and reduced problems with crosstalk between electrodes by incorporating microelectronic circuits into their designs. Their first such probe was a two-chip hybrid. One chip was a passive microelectrode array similar in design to that described above. The other chip, which was situated within 2 mm of the first and connected to it by wires, contained one junction field-effect transistor for each microelectrode, which served as a buffer amplifier for the high-impedance signals. The low-impedance output signals were then routed up the length of the probe to conventional external amplifying circuitry (Wise and Angell, 1975). A much more recent probe device, still being developed, shows a far greater degree of integration. In this design, a monolithic micro-machined silicon substrate contains up to 12 gold microelectrodes, connected via thin-film leads to a 12-channel on-chip signal processor. This circuit contains 12 buffer amplifiers having a gain of 100 and a bandwidth from 100 Hz to 6 kHz, a 12-channel analog multiplexer to multiplex all the

signals onto a single output line, a clock and shift register to drive the multiplexer, and a test waveform generator which can be switched on to drive all the electrodes with a square wave for testing purposes (Bement, Wise et al., 1986).

A variation on the probe-type microelectrode array was described by Edell (Edell, 1986). In contrast to the probes described above, this device was designed for long-term implantation in the peripheral nervous system, with the ultimate goal of development being medical use in humans. The array is a silicon wafer having 10 slots chemically machined through it, each 200 μm wide. Each slot contains a single metal microelectrode with a 17 x 37 μm exposed surface. Action potentials of up to 600 μv have been recorded from such devices up to 32 weeks post-implantation.

Other groups have developed probe-type microelectrode arrays as well (Pickard and Welberry, 1976, Kuperstein and Whittington, 1981). See Pickard (Pickard, 1979) for a survey of devices up until 1979. Probe-type microelectrode arrays are needed in working with intact tissues and organs, but they are not used to record from cells in culture. They have been mentioned here because many of the technical problems and fabrication techniques used are the same as for a second type of microelectrode array, the "culture-dish" device. In this type of array, the microelectrodes are fabricated on the surface of a substrate upon which excitable cells can be cultured. The first such microelectrode arrays for recording from cell cultures were described in 1972 (Thomas et al., 1972). These arrays had 30 electrodes arranged in 2 rows of 15. The spacing between the 2 rows was 50 μm, and between adjacent electrodes in a row, 100 μm. The recording surface of each microelectrode was a 7 x 7 μm square. The electrodes were made of gold-plated nickel on a 25 mm square glass substrate. They were electroplated with platinum-black to decrease the tip impedance; the magnitude of the platinized tip impedances was approximately 0.5 MΩ. The insulating material that covered the electrode leads was a photopolymer (photoresist) layer of unspecified type and thickness.

The cultured cells that were recorded from in experiments using these arrays were cardiac cells derived from 6-10 day chick embryos. Biphasic and triphasic action potentials were observed, ranging in amplitudes from 0.02 to 2.5 mV peak-to-peak. Attempts to stimulate the preparation by external pulses were not reported.

An array of 12 microelectrodes was used by Shtark and co-workers to record neural activity from explants of rat brain in tissue culture (Shtark et al., 1974). The electrodes were made of vacuum-deposited Ti-Au or Ti-Pt, and insulated with a layer of SiO_2. EEG-like electrical activity with amplitudes of up to 700 μv was recorded from this preparation.

Gross and co-workers have described the development and use of another culture-dish type of microelectrode array. Like its predecessors, the basic construction is a photolithographed gold metal film on a glass substrate. However, the material chosen to insulate the non-recording portions of the metal film was not patterned by photolithography; rather, a UV laser was used to remove a 10 μm diameter spot of insulator from over the electrode contact. A variety of insulating resins which could otherwise not be patterned were tried, and a methylpolysiloxane resin (Dow Corning DC648) was found to be most satisfactory. This design of array has been used to record signals from the brain ganglion of snails (Gross et al., 1977, Gross, 1979) and from dissociated neurons from embryonic mouse spinal cord in culture (Gross et al., 1982). An array of 32 microelectrodes for recording from cultured neurons was designed by Pine (Pine, 1980). The electrodes were of Cr-Au metal, 8 μm in width, and insulated with a 0.5 μm thick layer of SiO_2. The contact holes were rectangular, 8 μm by 10 μm, and the electrode tips were platinized. Dissociated neurons from the superior cervical ganglia of neonatal rats were plated on a layer of collagen 3 to 5 μm thick. Spikes with amplitudes of up to a few hundred μV and durations of less than 1 mSec were recorded. Stimulation of neuronal activity by application of short pulses (less than 1 mSec) to a

recording electrode was possible in this preparation. In one experiment, extracellular potentials were recorded from an apparently isolated single cell.

There has been one report of a culture-dish type of microelectrode array containing active semiconductor devices (Jobling et al., 1981). This array contained 9 microelectrodes arranged in a 3 by 3 matrix on a silicon substrate. Each microelectrode was a 20 μm square gold film which had been deposited atop the aluminum gate metal of a MOSFET. The MOSFETs were configured as source followers and transformed the high impedance input signals into low impedance signals which could then be utilized without external interference problems. The insulating materials used on this array were SiO_2 and positive photoresist. The array was successfully used to record neuronal activity from slices of rat hippocampus. The limiting noise in this system was said to be 50 μV P-P noise originating in the power supply.

The first steps in the development of a new fabrication technique for active microelectrode arrays were recently described by Kim and co-workers (Kim et al., 1985). The new technique addresses the problems of protecting semiconductor devices from the hostile biological environment, and of integrating switching circuitry such as multiplexers in close proximity to the sensing surfaces of microelectrodes, where the operation of the former would generate interfering signals for the latter. The method locates the microelectrodes on one face of the silicon substrate, and the active circuitry on the opposite surface. The electrodes are coupled to the amplifying circuitry via laser-induced trans-substrate conductive channels. The creation of electrodes and trans-substrate channels was demonstrated, and the electrodes were used to record extracellular activity from the medial giant nerve of a crayfish. So far, however, no active circuitry has been integrated into this device.

We described a passive microelectrode array designed for both stimulation and

recording from cardiac cells in cell culture (Israel et al., 1984). This array contained 25 recording electrodes in a 5 by 5 matrix and 6 stimulating electrodes. The recording electrodes had 15 μm square tips and the stimulating electrodes ranged in size from 40 to 120 μm square. The electrodes were made of platinized gold with a chromium adhesion layer. The substrate was glass and the insulating layer was negative photoresist (KTI 732). This device was used to make recordings from monolayers of ventricular cells isolated from 10-day White Leghorn chick embryos. The extracellular signals recorded had amplitudes in the range of 0.5 to 5 mV P-P, and durations of 2 to 3 mSec. It was possible to pace the preparation by applying either cathodal or anodal-break stimuli via the stimulating electrodes; the stimuli used were 0.2 to 1 mSec in duration and greater than 0.4 V in amplitude.

Chapter 3: METHODS and APPARATUS

The experimental work of Spach et al. and the simulations of Diaz have suggested that the fundamental nature of conduction of excitation in cardiac tissue is discontinuous. The goal of the present work was to directly measure the delay time of conduction between adjacent cells to see if the phenomena predicted by the Diaz simulations of discontinuous conduction could be observed in a living preparation.

3.1 Overview of the Method

Using microelectronics technology, we have developed techniques for the fabrication of arrays of extracellular microelectrodes to be used in the study of cardiac electrophysiology. Both recording and stimulating electrodes may be made on the same array using these techniques (Israel et al., 1984). The microelectrodes on these arrays may be arranged in almost any desired pattern, with minimum spacings smaller than the size of an individual cell, if needed. Ventricular myocardial cells from chick embryos may be cultured directly on the surface of these arrays. At the time of plating, the cells are dispersed as single units in suspension. Over a 2 to 3 day period, they settle on the surface of the array and form a confluent monolayer which exhibits spontaneous, rhythmic electrical and mechanical activity. The beat rate and conduction speed in this preparation range over values similar to those in intact cardiac tissue. The signals recorded from these microelectrodes are roughly biphasic pulses which are about 2 mSec in duration and up to 2 mV in amplitude (peak-to-peak). The electrical activity picked up by the microelectrodes demonstrates that the cells are coupled over large areas of the monolayer. That is, after the initial time of plating when they are totally isolated from one another, they develop a network of electrical connections sufficient for action potential propagation. The morphology of the connections that develop in embryonic

chick (Purdy et al., 1972) and neonatal rat (Hyde et al., 1969) heart cell tissue cultures is indistinguishable by electron microscopy from that in intact heart (although the distribution of connections is probably different).

This preparation has several characteristics which make it advantageous for experimentally testing the hypothesis of discontinuous propagation. The number of cells under study can be kept small by restricting the area in which cells can settle and attach. The dimensionality of the preparation is 2, rather than 3 as in isolated tissue preparations; all the cells are potentially visible at once. The spacing of the extracellular microelectrodes can be much closer and is far more precise than is possible with intracellular microelectrodes, and there is no possibility of tissue damage such as that caused by the insertion of such electrodes, or that caused by the insertion of conventional extracellular microelectrodes.

The predictions of the Diaz model of cardiac propagation were considered in designing the microelectrode array for these experiments. A simulation with a disc resistivity of 1 Ω–cm^2 and a cell length of 100 μm had an average overall conduction velocity of 0.13 m/Sec, which resulted from a single-cell conduction velocity of 0.25 m/Sec with a delay of 0.34 mSec at each disc (Diaz, 1983). Two electrodes spaced 20 μm apart on the same cell in this situation would see a passing wavefront with a delay of 80 μSec, whereas two electrodes the same distance apart but contacting two neighboring cells would exhibit a time delay of 340 + 80 = 420 μSec (5.25 times greater). In a similar simulation with a disc resistivity of 2 Ω–cm^2, the average overall conduction velocity was 0.10 m/Sec, while the single-cell conduction velocity was 0.26 m/Sec and the disc delay was 0.52 mSec. Electrodes spaced on 20 μm centers in this case should see delays of 77 μSec if on the same cell and 520 + 77 = 597 μSec if on opposite sides of a junction. In a simulation with a very low junctional resistivity of 0.1 Ω–cm^2, the junctional delay was only 0.046 mSec and the microscopic and macroscopic

conduction velocities were 0.216 and 0.193 m/Sec, respectively. Thus, the simulations done by Diaz predict behavior ranging from "almost continuous" propagation in the case of cells coupled with very low-resistance junctions, to very discontinuous in the case of poorly-coupled cells.

The behavior of the model as the coupling resistance between the cells was varied was of interest in the design of these experiments. As the disc resistivity was increased by one order of magnitude from 0.1 to 1.0 Ω-cm^2, the time delay between adjacent cells increased by almost an order of magnitude, from 0.046 to 0.34 mSec. However, the average conduction velocity exhibited a much smaller change, decreasing by a factor of 0.67. This was due to a concomitant rise in the intracellular velocity. Diaz explained this phenomenon by noting that increasing the intercellular resistance lowered the flow of longitudinal current, thus making more local circuit current available to discharge the membrane. This feature of the model predicts that velocities (or time delays) measured over long distances will be less sensitive indicators of discontinuous propagation than those measured over short distances. While a large separation between 2 electrodes will increase the chance of an intercellular junction being located somewhere between them, it will also "dilute" any time delay that is caused by that junction.

The Diaz model of discontinuous propagation predicts that conduction velocity should be faster within cells than it is between cells. This effect should be observable with microelectrodes spaced closely enough together. The difference in excitation arrival times at two electrodes contacting the same cell should be smaller than that of two electrodes contacting two adjacent cells. Within practical limits, the best spacing between microelectrodes to observe this effect should be the closest spacing.

In a given preparation of cardiac tissue, there are two fundamentally different ways to alter conduction velocity (Spach, 1983). One is to change membrane properties in

some way; the other is to alter the state of the intercellular connections. There are a variety of interventions that can be applied to cardiac tissue in order change conduction velocity. Some of these, such as changes in temperature and changes in $[K^+]_o$, should act primarily by affecting membrane properties; others, such as changing the intracellular pH, should act predominantly on the intercellular connections. Still others, such as treatment with ouabain, might act by both mechanisms. Interventions which slow conduction velocity by affecting only the membrane properties would be expected to increase the difference in excitation arrival times between electrodes in contact with the same cell; while they would also increase the time delay between electrodes on opposite sides of an intercellular junction, the amount of the increase should be proportional to the interelectrode distance. Conversely, interventions which slow conduction velocity by affecting only junctional properties would not be expected to change the difference in arrival times between electrodes contacting the same cell at all; however, the delay between electrodes on opposite sides of a junction should be increased. Thus, the application of such interventions to cardiac cell cultures on the microelectrode array should be useful both in determining whether discontinuous propagation occurs as well as locating electrode pairs which are on opposite sides of a junction.

3.2 Details of the Method

A pattern of microelectrodes was designed to allow the testing of the discontinuous propagation hypothesis (figure 3-1). The layout contained two central rows of six closely spaced microelectrodes. Each microelectrode was square, with 10 μm sides. Adjacent electrodes in each row were spaced on 20 μm centers; the two rows were spaced on 25 μm centers. This spacing was chosen with regard for typical sizes of myocytes in culture, to make it likely that the central strip of electrodes would usually be overlaid by several cells, and that each cell overlying the strip would contact one or more electrodes. (See appendix D for a discussion of the technical considerations

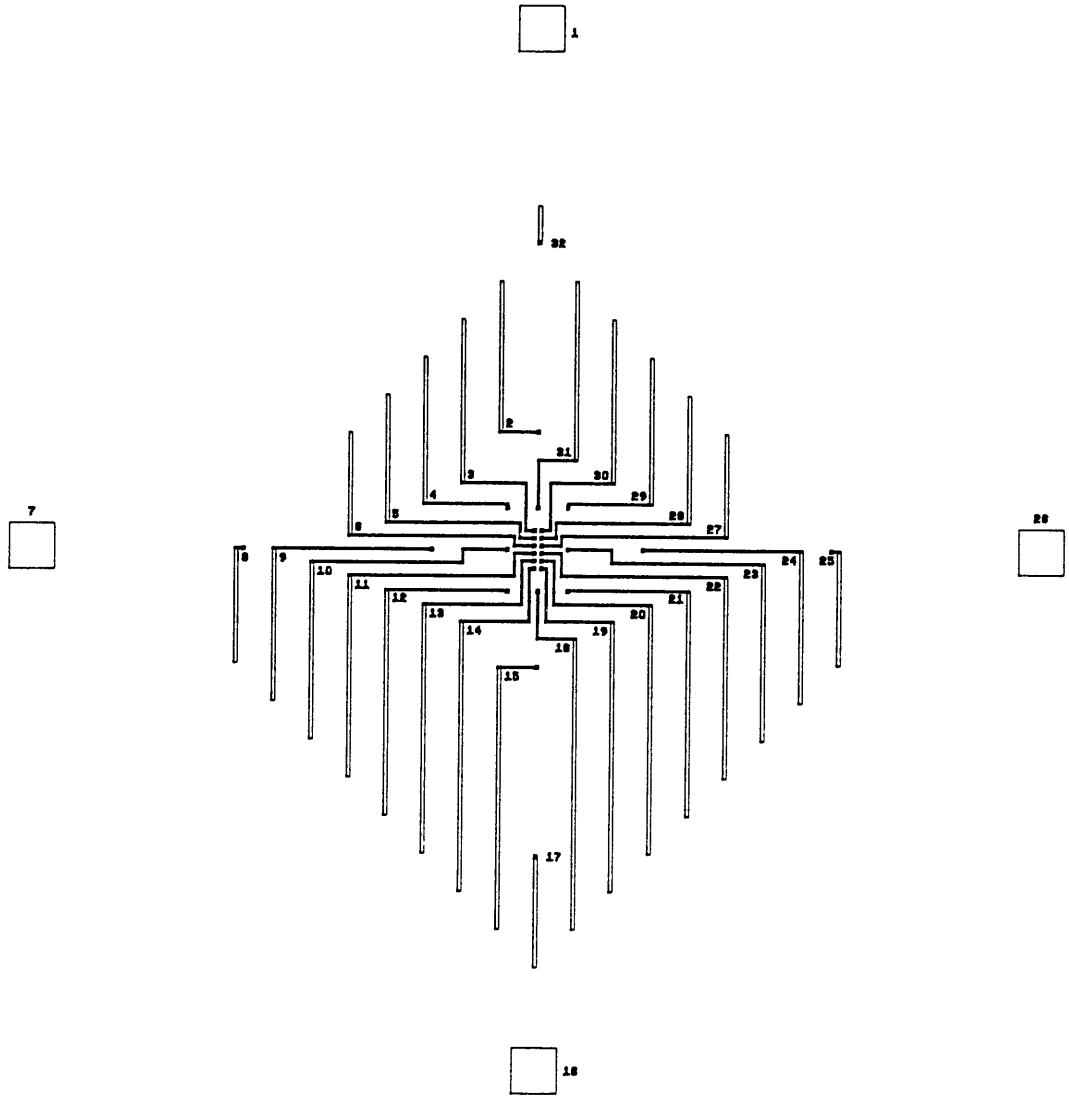

Figure 3-1: Layout of center of microelectrode array

underlying the choice of electrode size.) Surrounding the twelve central microelectrodes were fourteen additional recording electrodes to allow measurement of average conduction velocities and verification of propagation pathways. Peripheral to the recording electrodes were four stimulating electrodes for pacing the preparation. The stimulating electrodes were square, with 120 μm sides. The stimulating and recording electrode pattern was surrounded on 3 sides by a large electrode that served as a reference electrode for the recording electrodes. The reference electrode was 1 mm wide and a total of 30 mm long. Two complete identical patterns were fabricated on each substrate as described below, so that the better one of the two could be chosen for subsequent use. The reference electrode of the unused pattern was used as the reference electrode for the stimulating electrodes.

3.2.1 Fabrication of the Microelectrode Array

A glass cover-slip (round, 40 mm diameter, #2 thickness, Bellco) was cleaned to remove organic and ionic surface contaminants. In order to promote the subsequent adhesion of gold, a layer of chromium 10 nm thick was deposited on the glass surface by electron beam evaporation. A layer of gold about 400 nm in thickness was then deposited. The Au surface was coated with a 1 μm thick layer of positive photo-resist (Kodak 820), an organic compound which undergoes photochemical decomposition upon exposure to UV light. The photoresist was exposed to UV light through a photographic plate containing the image of the desired pattern of electrodes. After developing, a protective layer of photoresist having the electrode pattern was left on the metal surface. The metal was then removed from the unprotected areas by RF sputter-etching in an Argon plasma. A 3.5:1 mixture of H_2SO_4 : H_2O_2 was used to remove the photoresist from the surface of the remaining metal.

The electrode metal was insulated everywhere except at the tips and at the bonding

pads. The insulating material used was a negative photoresist (KTI 732, KTI Chemicals Inc, Sunnyvale CA). (Previous tests of three photoresists led to this choice. Shipley AZ1350J did not survive the saline environment as long as KTI 732; cells did not adhere as well to KTI 747 as they did to KTI 732.) A 1.5 μm layer was applied to the top of the electrode array, and was then exposed to UV light through a mask which defined the location of the holes through the insulation at the electrode tips and bonding pads. The photoresist was then chemically developed to remove the resist from these areas, and hardened by baking.

The array was fastened with epoxy glue to a circuit board, over a hole which allowed viewing from below using an inverted microscope. Gold wires (76 μm diameter) were ultrasonically welded to the bonding pads of each microelectrode; they were run to a miniature connector (Amphenol series 221) at the edge of the board and fastened to it with silver-epoxy (H20E, Epoxy Technology Inc.). A ring of pyrex glass, 4 mm high, 31 mm i.d., was fastened to the top of the array with medical-grade Silastic (Dow Corning MDX-4-4210 Clean-grade Elastomer) to form a culture dish whose bottom was the electrode array. The gold wires were insulated and mechanically protected with a layer of Silastic. The assembled microelectrode array is shown in figure 3-2.

The impedance at 1 kHz of each microelectrode was measured to check for open or short circuits. This measurement was made by connecting the microelectrode under test as the feedback impedance of an electrometer operational amplifier (AD515, Analog Devices). The feedback circuit was completed through normal saline solution and the large reference electrode on the array. A 1 kHz sine-wave current, 1 nA in amplitude, was injected through the electrode via the op-amp. The current through and voltage across the electrode were measured by a digital spectrum analyzer (Hewlett-Packard 3582A) in its transfer-function mode, which provided a direct readout of the magnitude and angle of the impedance. (A complete description of the impedance measurement

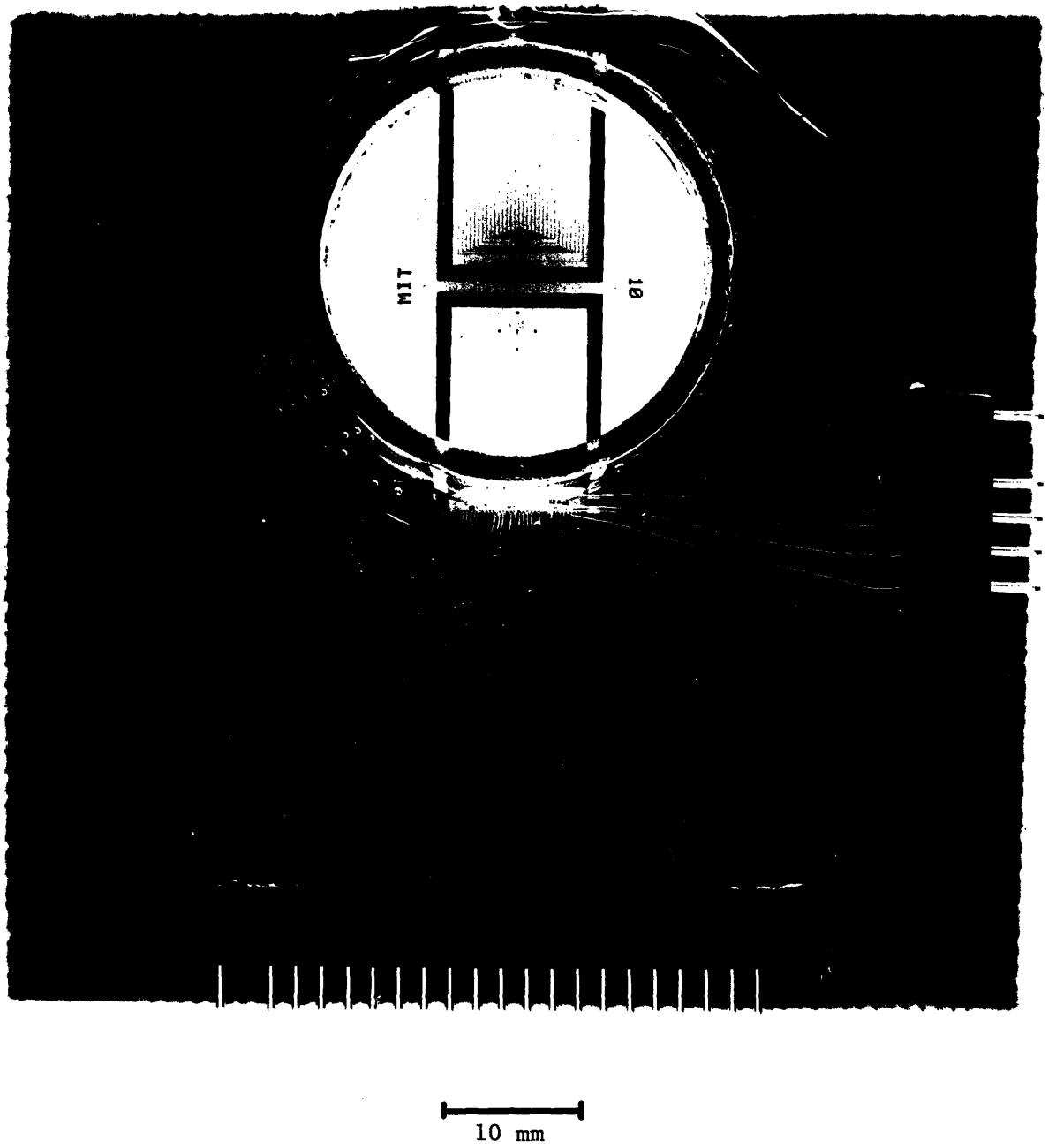

Figure 3-2: Photograph of assembled microelectrode array

technique is in Appendix A.) All electrodes were then platinized in a solution containing 3% platinum chloride and 0.025% lead acetate at a plating current density of 100 mA/cm^2 for 20 seconds. The platinizing solution was washed from the dish by soaking in distilled water for 30 minutes. The impedance at 1 kHz was again checked by the above method. Prior to use for tissue culture, the array was sterilized with dry heat at 155 °C for 2 hours.

3.2.2 Tissue Culture

Ventricular cells from 10-day chick embryos were cultured on the surface of the electrode arrays. The tissue culture technique has been described in detail elsewhere (Barry et al., 1980), and will only be outlined here. The ventricles of 8- to 10-day old chick embryos were aseptically removed into a bath of Ca^{++} - and Mg^{++} - free Hanks' solution. The tissue was separated into small fragments by sharp dissection, and then further dissociated by four cycles of trypsinization in a bath containing 0.025% (weight/volume) trypsin at 37 °C. Isolated cells were suspended in a trypsin-inhibitor solution containing 50% heat-inactivated fetal calf serum and 50% Ca^{++} - and Mg^{++} - free Hanks' solution, and then centrifuged for 10 minutes at 1000 RPM. The resulting pellet was resuspended in culture medium consisting of: 6% heat-inactivated fetal calf serum, 40% Medium 199 with Hanks' salts (GIBCO), 0.1% Penicillin-Streptomycin solution, and 54% balanced salt solution containing (mM concentrations): NaCl 116, NaH_2PO_4 1.0, $MgSO_4$ 0.8, KCl 1.18, $NaHCO_3$ 26.2, and glucose 5.5. Final ionic concentrations (millimolar) in the culture medium were: Na^+ 144, K^+ 4.0, Ca^{++} 0.97, HCO_3^- 18, Mg^{++} 0.8, Cl^- 131. The cell suspension was diluted to $5x10^5$ cells/cc. The culture dish of the sterilized electrode array was filled with 2 cc. of this suspension. The culture was incubated at 37 °C in a humidified atmosphere containing 5% CO_2. As has been well-described elsewhere, a confluent monolayer of cells which exhibit spontaneous rhythmic activity usually developed under these conditions. Cells were incubated for

three days following plating. At the end of the incubation period, the culture was inspected by phase contrast microscopy to ensure that a continuous region of spontaneously active cells was in place over the microelectrodes.

3.2.3 Recording of Electrical Activity

The preparation was transferred into the experimental chamber, which was a small culture incubator (Thermolyne I37925) which maintained a temperature of 37 °C. The metal walls of the incubator provided shielding from electrical noise in the environment. The culture medium was replaced with a Hepes-buffered medium to maintain an extracellular pH of 7.4 without the need for a 5% CO_2 atmosphere. The electrode array was connected to a specially-built 20-channel amplifier which was small enough to fit inside the incubator. This formed a rigid assembly which minimized motion-induced noise. Each of the 20 identical channels consisted of an FET-input operational amplifier (Burr-Brown OPA121) connected in a non-inverting, DC-coupled, gain-of-10 configuration; the input impedance was $10^{13}\Omega$ shunted by 1 pF. The preamplified signals were brought out of the chamber via shielded cables to a second stage of amplifiers and anti-aliasing lowpass filters.† From there, they were connected to the inputs of a multi-channel, 12-bit analog-to-digital converter system (Data Translation DT1711) under control of a laboratory minicomputer (Digital Equipment Corporation PDP-11/44). Up to 16 recording electrodes could be sampled simultaneously at a rate of 6 kHz each. The raw data were stored directly in digital form for later analysis. Individual channels could be monitored during experiments on a 4-channel storage oscilloscope (Tektronix 5113).

† See Appendix C for details of amplifiers and filters.

3.2.4 Electrical Stimulation

The output of a stimulus generator (Grass Instruments S88) was connected through a stimulus isolation unit (Grass Instruments SIU-5) to one of the four stimulating electrodes. The repetition rate of the stimulator was set approximately 25% higher than the spontaneous beat rate of the culture. Rectangular stimuli were capacitively coupled to the electrode. The amplitude, duration, and polarity of the stimuli were independently adjustable. Capture was verified by the appearance of a fixed latency between the stimulus and the action potentials recorded from nearby extracellular electrodes.

A digital output from the PDP-11/44 computer generated trigger pulses at programmable intervals to a specially-built synchronizing circuit.† This circuit in turn controlled the timing of the stimuli generated by the stimulus generator and the timing of the samples taken by the analog-to-digital converter. The synchronizing circuit ensured that sampling of the activity at the recording electrodes began approximately 1.5 mSec before the application of the stimulus and continued long enough for activity to traverse the region containing the recording electrodes. This was between 10 and 40 mSec, depending upon the conduction velocity in the particular preparation. The hardware was capable of delivering stimuli with any sequence of times at rates ranging from arbitrarily slow up to hundreds of stimuli per second. In practice, the lower bound on the rate of stimulation was set by the desire to exceed the spontaneous rate of the preparation; the upper bound was set by the maximum rate at which the preparation would respond, typically between 3 and 4 stimuli per second.

† See Appendix C for details of the synchronizing circuit.

3.2.5 Discontinuous propagation experiments

A microelectrode array containing a layer of cultured cells was transferred to the experiment chamber and connected to the 20-channel preamplifier as described above. Each of the preamplifier output signals was connected in turn to the storage oscilloscope and examined. Extracellular action potentials were identified on the basis of amplitude, waveform, and rhythmicity, and their peak-to-peak amplitudes were recorded. The spontaneous beat rate was recorded. Each channel was examined for the presence of extraneous, interfering signals or excessive noise levels. Since the digital recording system only allowed recording from 16 of the 20 channels, 4 were eliminated. The channels with the lowest signal to noise ratios based on the above inspection were eliminated first. If not enough channels were eliminated on this basis, additional ones were chosen, with channels outside of the central group of closely-spaced electrodes being eliminated first.

The channels to be used for recording were connected to the recording system and spontaneous activity was recorded from the preparation. Recordings were made of ten successive 100-mSec intervals initiated at random with respect to the spontaneous beating of the culture. This procedure usually resulted in the recording of one or more spontaneous beats. It was repeated until a few such beats were recorded. Plots were made of the signals from all sixteen channels to check for a pattern consistent with action potential propagation and to verify the setup and functionality of the recording equipment.

Next, the ability to pace the culture and the parameters of effective stimuli were determined. The stimulus generator was connected to stimulating electrode number 1, and stimuli were delivered as described above. One or two of the recording channels were connected to the storage oscilloscope to visually determine the occurrence of

capture; the oscilloscope horizontal sweep was triggered by the synchronization output of the stimulus generator at the leading edge of each stimulus. The length of the stimulating pulse was initially adjusted to 0.3 mSec, its amplitude to 0.5 Volt, and the stimulation rate to about 25% greater than the culture's spontaneous rate. These parameters were usually not adequate to stimulate the preparation. The amplitude and duration were adjusted until a point of adequate stimulation was found, as indicated by the appearance of a fixed latency between the stimulus and the action potential at the monitoring electrode; then the amplitude was increased by a further 10% to ensure reliable pacing. If capture could not be obtained by stimulating at electrode 1, electrode 16 was tried, followed by electrode 7 and 32 if necessary. (This order of preference for the stimulating electrodes reflects the desire to have the action potential propagate approximately along the axis of the central region of electrodes.) If the preparation could not be paced at all, the session was terminated.

Once the stimulation parameters were determined, recordings of paced activity could be made. In each experiment, activity was first recorded from the preparation under control conditions. In most experiments, an intervention (described below) was applied with the aim of affecting propagation by changing junctional properties; paced activity was then recorded under these conditions. When possible, control conditions were restored and further recordings were made. For each set of conditions, the responses to multiple stimuli were recorded. The number of responses that could be recorded was limited by digital storage space considerations. In preliminary experiments, up to 100 responses were recorded under each set of conditions. In later experiments, 10 or 20 responses were recorded for each set of conditions.

The intervention chosen to affect conduction in these experiments was cytoplasmic acidification. As reviewed in section 2.3, intracellular pH has been shown to modulate gap junctional resistivity in cardiac tissue. Several agents are known which alter the

intracellular pH; these include CO_2 and ammonium salts. Carbon dioxide dissolved in the medium rapidly crosses the cell membrane. Inside the cell, it combines with water in a reaction catalyzed by intracellular carbonic anhydrase to form H_2CO_3 (carbonic acid), which dissociates and lowers the pH.

Ammonium ions have been used in a number of investigations to change intracellular pH. The chloride salt has usually been used, although ammonium sulfate $(NH_4)_2SO_4$ has also been administered for the same purpose. The intervention has been applied to a variety of cell types ranging from snail neurons (Thomas, 1974) to mammalian cardiac cells (Deitmer and Ellis, 1980). Different techniques have been used to monitor the effects of this intervention on intracellular pH.

The effect of NH_4Cl on intracellular pH depends upon the existence of NH_3 in solution in equilibrium with the ammonium ion, NH_4^+. Ammonia diffuses across the cell membrane rapidly, while ammonium ions diffuse much more slowly. Upon the initial addition of ammonium chloride to the medium, ammonia enters the cells rapidly and there reacts with water to form NH_4^+ and OH^-, which alkalinizes the cytoplasm. Ammonium ions gradually enter, neutralizing the pH gradient across the membrane. Upon removal of the ammonium chloride from the medium, the reverse occurs; ammonia rapidly diffuses out of the cells, leaving behind an excess of ammonium, which gives up protons and acidifies the cytoplasm. This acidification is only transient, however, as the outward diffusion of ammonia and ammonium species proceeds and the membrane proton pump expels excess H^+ (Reber and Weingart, 1982).

Reber and Weingart acidified sheep Purkinje fibers with 15 mM ammonium chloride, monitoring the effect on intracellular pH using a pH-sensitive intracellular microelectrode. They measured a mean intracellular pH of 7.27 ± 0.03 in Tris-buffered control medium. They exposed the cells to ammonium chloride for periods of 10 to 15

minutes and observed an increase in intracellular pH (alkalinization) which ranged from 0.11 to 0.31 units (mean 0.19); the pH peaked within 2 to 5 minutes and then decreased towards normal as the exposure continued. Upon return to normal medium, they observed acidification ranging from 0.39 to 0.62 units (mean 0.50), peaking within 5.5 to 10 minutes and then exponentially returning towards normal within 30 to 40 minutes. The results were reported as deviations from control values; absolute measurements of the lowest pH achieved were not given.

Other investigators have applied NH_4Cl to cardiac tissues with basically similar results; however, the time course of the responses seen has been different in different reports. Deitmer and Ellis applied 20 mM ammonium chloride to sheep Purkinje fibers and monitored intracellular pH with pH-sensitive microelectrodes (Deitmer and Ellis, 1980). In one representative experiment, they recorded an intracellular acidification of 0.5 pH unit upon removal of ammonium chloride; the time to the development of peak acidification was 4 minutes. The pH then returned to control levels over about 40 minutes, with a time constant of about 10 minutes. The maximum rate of pH recovery, seen a few minutes after peak acidification, was 0.07 pH units/min.

Kim and Smith used 20 mM ammonium chloride to acidify cultured ventricular myocytes from 10-day chick embryos (the same as used in our experiments). They monitored intracellular pH using a pH-sensitive fluorescent dye, BCECF. In this technique, the culture was incubated for 20 minutes with the dye, washed, and placed into a fluorimeter which responded to the average fluorescence of all the cells. Calibration was done at the end of each experiment by treating the cells with nigericin to equilibrate intracellular and extracellular pH, and then varying the pH of the medium over the range of interest and measuring the fluorescence. There was a period of several seconds between a change of the bathing solution and the start of pH measurement during which the pH was unknown. The time course of intracellular pH measured using

this technique was different than that observed using pH-sensitive microelectrodes. Following addition of NH_4Cl, alkalinization was virtually immediate; the peak pH occurred within the few seconds of no measurement following a solution change. Following washout, acidification was slower, but still much faster than the results discussed above; acidification typically peaked within one minute of washout. After an 8 to 10 minute exposure to 20 mM NH_4Cl, the peak acidification achieved during washout was about pH 6.5 (D. Kim, personal communication).

The reason for the discrepancies in the time-courses of acidification and recovery among these studies is not clear. The most obvious possibilities are the differences in cell types and the differences in the methodology of applying the intervention and monitoring the pH. For example, the speed of response of pH-sensitive intracellular microelectrodes depends upon the pH and the buffering capacity of their environment; around pH 7, in weak buffer, the response time can be several minutes, and varies from electrode to electrode (Thomas, 1974). Some of the slow changes recorded may be partly attributable to this property.

The addition of ammonium ions to cardiac cells has been observed to have other effects besides changing intracellular pH. The membrane depolarizes slightly during the exposure to ammonium chloride. Deitmer and Ellis reported a depolarization of 10 mV upon exposure to 20 mM NH_4Cl; recovery began immediately upon return to control conditions and normal membrane potential was achieved within 5 minutes, followed by a slight transient hyperpolarization. Reber and Weingart recorded a depolarization of about 12 mV in one preparation upon exposure to 15 mM NH_4Cl; complete recovery appeared to take about 20 minutes and no hyperpolarization was seen. Another preparation depolarized only by about 4 mV during exposure, but did show a transient hyperpolarization during recovery. Reber and Weingart also measured the effect of ammonium chloride on the cable parameters of their Purkinje strands. They measured the

space constant, input resistance, and membrane time constant directly using a two-microelectrode technique; they calculated the internal longitudinal resistance r_i, and the membrane resistance r_m from these measurements. It was found that r_i decreased during alkalinization and increased during acidification as discussed earlier; these effects were attributed to a change in cell coupling due to intracellular pH. However, membrane effects were found as well; r_m decreased by 50% over the course of exposure to NH_4Cl, and subsequently recovered over a period of an hour.

The effects of the ammonium chloride intervention on membrane currents and on the resulting action potentials do not appear to have been measured. However, the effects of changing intracellular pH by other means have been studied in single ventricular cells, and are relevant to the extent that the effects we are interested in are due to the change in H^+ concentration. Kurachi investigated the effects of directly injecting acidic solutions ranging from pH 3.7 to 4.7 and basic solutions of pH 9.3 to 9.7 into isolated guinea-pig ventricular cells (Kurachi, 1982). Unfortunately, the actual amount of solution injected was not known and the resulting intracellular pH was not measured in these experiments. Intracellular acidification resulted in shortening of the duration of the action potential from over 200 mSec by as much as 100 mSec. The resting membrane potential sometimes changed by up to 5 mV, but not consistently. No changes were noted in the upstroke of the action potential. Membrane current recordings using a two-microelectrode voltage-clamp indicated a decreased slow-inward current during acidification, which was consistent with the observed shortening of the action potential plateau. The changes seen were observed during acidification using any one of 6 different acids, thus making it likely that they were related to the change in proton concentration rather than to the presence of the associated anion.

The results of such studies indicate that intracellular acidification, regardless of how it is achieved, will not affect intercellular coupling exclusively; changes in membrane

parameters which might affect conduction are bound to occur. However, such membrane effects should presumably be distributed uniformly throughout the preparation, whereas effects on intercellular coupling should produce localized changes in conduction that are present only at junctions.

Ammonium chloride was used to modify the intracellular pH in our experiments as follows. The experimental setup and control recordings were performed as described above. NH_4Cl was added to Hepes-buffered medium (pH 7.4) at a concentration of 20 mM. The prepared medium was warmed to 37 °C. The normal medium was removed as completely as possible by aspiration with a Pasteur pipette; only a thin film remained on the surface of the layer of cells. Two mL of the medium containing 20 mM NH_4Cl was immediately added to the dish using a second Pasteur pipette. The entire exchange required approximately 15 seconds. The electrical activity of the culture was monitored by observing 2 recording channels on the oscilloscope. Replacement of the medium invariably resulted in the appearance of baseline drift and excess noise in the electrode signals, which subsided over the course of several minutes. This intervention also usually made the preparation temporarily inexcitable. If the preparation could be stimulated, recordings of propagated activity were made as described previously. After a 15-minute wash-in period in NH_4Cl, the medium was again completely exchanged with fresh Hepes-buffered medium in order to acidify the cytoplasm. The culture was washed once with fresh medium during this exchange to remove as much of the NH_4Cl as possible. Electrical activity was monitored continuously, and recordings began as soon as the baseline drift subsided and the culture responded to stimulation. Recordings were made at varying intervals until 30 minutes after the return to normal medium, by which time intracellular pH should have returned to normal (Kim and Smith, in press).

3.2.6 Morphology of tissue cultures

It was desirable to determine which groups of electrodes were in contact with a single cell, and where intercellular boundaries were located with respect to the electrodes. Such information would be of great value in interpreting the recordings of electrical activity. In order to be of use, this determination would have to be made without disturbing the arrangement of the cells that existed during the recording. In view of the effort required to fabricate microelectrode arrays, and the need to re-use them, no procedure that would damage them (such as histological fixation techniques) could be tolerated. It was found to be impossible to obtain the needed morphological information by inspection with the unaided light microscope (phase or differential interference contrast). This was partly because of the low contrast of cell boundaries inherent in these techniques, and partly because in the central recording area of the microelectrode array, which is the region in which we are interested in locating cell boundaries, the microelectrodes themselves block the transmission of light over much of the area and obscure many of the visual cues which help to identify the locations of cell boundaries.

Attempts were made to determine the locations of cell boundaries using light microscopy assisted by fluorescent dyes. In preliminary experiments using cell cultures grown on plain glass cover-slips, it was found that one type of dye (FluoroBora-P, Polysciences) aided in visualization of the boundaries of these cells. This dye stains the cytoplasm of living cells, increasing the contrast between cytoplasm and boundary regions; no fixation is used. However, attempts to use this method on cultures grown on a microelectrode array failed, because the photoresist insulation layer used on the array also illuminated brightly under the UV light required to excite the fluorescent dye. The intensity of the background illumination nullified the gain in contrast provided by the dye.

No satisfactory method of determining the arrangement of cells on the microelectrode array in individual experiments was found. However, it was possible to collect data about the sizes and shapes of cells, and the distribution of boundaries in the culture preparation. Two types of studies were performed. The goal of the first was to characterize the sizes and shapes of cells. A confluent sheet of cells was not well-suited to this goal, since the outlines of individual cells are difficult to see in such a sheet. Cells were cultured as described above except that in the final dilution step before plating, the number of cells was decreased to 1×10^5 cells/mL. It has been found that at this plating density, a confluent layer of cells does not develop after 3 days of incubation; most areas of the plate contain isolated cells. Cover-slips plated at this density were examined using phase-contrast optics with a 40x objective. Photomicrographs were taken of several randomly chosen fields. A microscope stage calibrator (Olympus objective micrometer) with markings at 10 μm intervals was photographed using the same optics. Measurements of cell length and width were made on arbitrarily selected cells from each photograph; dividers were used to make the measurements, using the photograph of the calibrator as the length reference. Because of the irregularity of the shape of the cells, "length" and "width" could only be approximately measured.

The goal of the second morphological study was to characterize the distribution of cell boundaries in monolayers of the type from which electrical activity was recorded. Knowing this distribution would allow some prediction to be made about the number of boundaries to be expected in the central recording area of an array in any experiment. Cells were cultured on glass cover-slips using the technique described above for preparing cells for propagation experiments. Photomicrographs were taken of several randomly chosen microscope fields. A transparent overlay having a straight line scribed on it was aligned with each edge of each photomicrograph so as to define a randomly-oriented line through the culture. Proceeding from one end of this line to the other, distances from one cell boundary to the next were measured as before. The resulting

measurements were combined into a histogram which showed the relative frequency of boundary-to-boundary distances along a randomly oriented line bisecting the preparation.

3.3 Data Analysis

The extracellular action potentials recorded from cardiac cell cultures by the microelectrode array had a duration of approximately 2 mSec. The most closely-spaced electrodes on the array were located on 20 μm centers. Neglecting discontinuous propagation for the moment, and assuming a uniform conduction velocity of 1/3 m/Sec, activation would travel 20 μm in 60 μSec. If the direction of propagation was not along the axis of the two electrodes, the delay in the arrival time of activation between them would be even less than this, as low as zero for a wavefront approaching perpendicular to this axis. These delays are small compared to the duration of the extracellular event; 60 μSec is 3% of 2 mSec, and could be difficult to measure accurately. Now consider the delay between two electrodes on opposite sides of an intercellular junction if discontinuous propagation occurs; if the delay were on the order of 0.5 mSec (as predicted by the simulations of Diaz), it would be 25% of the duration of the extracellular waveform, and should be readily apparent even by visual inspection of the signals. Intermediate delays might be less obvious but could still be readily measured.

Several approaches were considered to measure the difference in arrival times between electrodes. One method which was used early in this study was cross-correlation of the signals from adjacent electrodes. Given recordings from two observation points of a signal emanating from a single source, possibly corrupted by independent random noise, this technique yields a maximum likelihood estimate of the delay between them. However, when the waveforms change shape from one observation point to another, as is the case for extracellular action potentials due to the distributed nature of the sources, the method cannot be used.

Other approaches to measuring the difference in arrival times between two electrodes require estimating the time of arrival of excitation at each electrode and calculating the difference between the two measurements. These approaches vary in the way that the arrival time is estimated. To estimate the arrival time, a fiducial point on the waveform may be chosen and the time that it occurs located. Examples of fiducial points are the time of zero-crossing and the time of occurrence of the positive or negative peak amplitude; these are not good choices because they do not have a fixed relationship to underlying membrane events. The choice of an appropriate fiducial point for extracellular waveforms has been demonstrated by simulation (Spach and Kootsey, 1985) (see section 2.8). It was shown that the negative peak of the first derivative of the extracellular action potential coincides closely with the time of peak sodium conductance of the underlying membrane, regardless of changes in the shape of the action potential due to structural discontinuities nearby. This point was chosen as the fiducial point for the present experiments.

3.3.1 Signal conditioning

The signals recorded during discontinuous propagation experiments were stored digitally as sequences of 12-bit samples. The time was not stored with the raw data since it was known implicitly from the sampling rate and the fixed time relationship between the start of sampling and the delivery of the stimulus. The sampling rate for each of the 16 channels was 6 kHz. Since all channels were multiplexed into the input of a single A-D converter, they were not sampled simultaneously; there was a fixed time offset between samples on different channels which had to be accounted for in subsequent calculations of arrival times. The integer sampled data were converted to floating-point representation for further processing. The mean value was computed for each channel and subtracted from the data. A time channel was added to the data at this stage to facilitate keeping track of time while examining selected intervals of the data.

The 6 kHz sampling rate for each channel resulted in a period of 167 μS between adjacent samples. Since the incoming signals were band-limited to the Nyquist rate of 3 kHz, these samples contained the information needed to uniquely reconstruct the waveform at times between the samples by interpolation, according to the sampling theorem. Interpolation was used in order to allow estimation of the location of the fiducial points with time resolution better than the the 167 μS sampling period. Interpolation also served to provide a smoothed time function to the numerical differentiation algorithm that subsequently located the fiducial point of the signal, thereby reducing the errors inherent in this procedure.

The resemblance of the interpolated sequence to the original waveform depends upon the interpolation algorithm used. In order to perfectly reproduce the original waveform, the sampled data would have to be convolved with a function of the form (sin x) / x, which is infinite in length. In the frequency domain, this corresponds to filtering the data with an ideal low-pass filter having its cutoff frequency at the Nyquist rate of the original samples; however, ideal low-pass filters are unrealizable (Oppenheim and Schafer, 1975). Practical interpolation methods are limited to finite data lengths and therefore involve some error.

The interpolator used for the experimental data was implemented digitally in software using an algorithm designed by R. E. Crochiere (Crochiere, 1979). The algorithm increases the sampling rate by a factor of L by inserting L-1 zero-valued samples between each pair of input samples. The resulting signal is then filtered using a finite impulse response lowpass filter having a cutoff frequency at the Nyquist rate of the original samples. The interpolation filter to be implemented had to be supplied as a set of coefficients. These coefficients were generated by means of an interpolation filter design program (Oetken et al., 1979). This program designed finite-impulse-response (FIR) interpolation filters which satisfied the criterion that the mean square error between the

interpolated points and the theoretically ideal points was minimized. In addition, the design of the filters was such that the original samples in the data being interpolated were unchanged by the interpolation process. The user specified the number of original data points to be used in the calculation of each interpolated datum; increasing this number decreased the amount of interpolation error at the expense of added computation time.

The interpolation filter designed for the present purpose was a 51-tap linear-phase filter. It increased the effective sampling rate of the data by a factor of 5. Each interpolated point was derived from a combination of 10 original sampled data. These parameters were chosen ad hoc. The performance of the interpolator is illustrated in figure 3-3. Panel (a) shows samples of an extracellular action potential recorded from a microelectrode at a sampling rate of 6 kHz over an interval of 10 mSec. Panel (b) shows an interpolated version of the same action potential at a sampling rate of 30 kHz generated using the interpolator described above. Panel (c) shows actual samples of the same action potential at a sampling rate of 32 kHz. All the features of the sampled data are present in the interpolated version except for the small amount of high-frequency noise which cannot be reproduced from the samples taken at the 6 kHz rate. Of course, this noise does contribute to the corruption of the samples, which causes the interpolated waveform to deviate from the actual waveform. At the signal and noise levels in this example, the errors are small. The location of the fiducial point (see below) calculated from the interpolated data was within 8 μSec of that calculated from the data sampled at 32 kHz.

A plot of all 16 raw signals during a representative stimulus and its associated response was made for each set of conditions in an experiment. This plot was used to select a time interval beginning after the end of the stimulus artifact and containing the responses from all channels. The selection of a sub-interval from the data was necessary

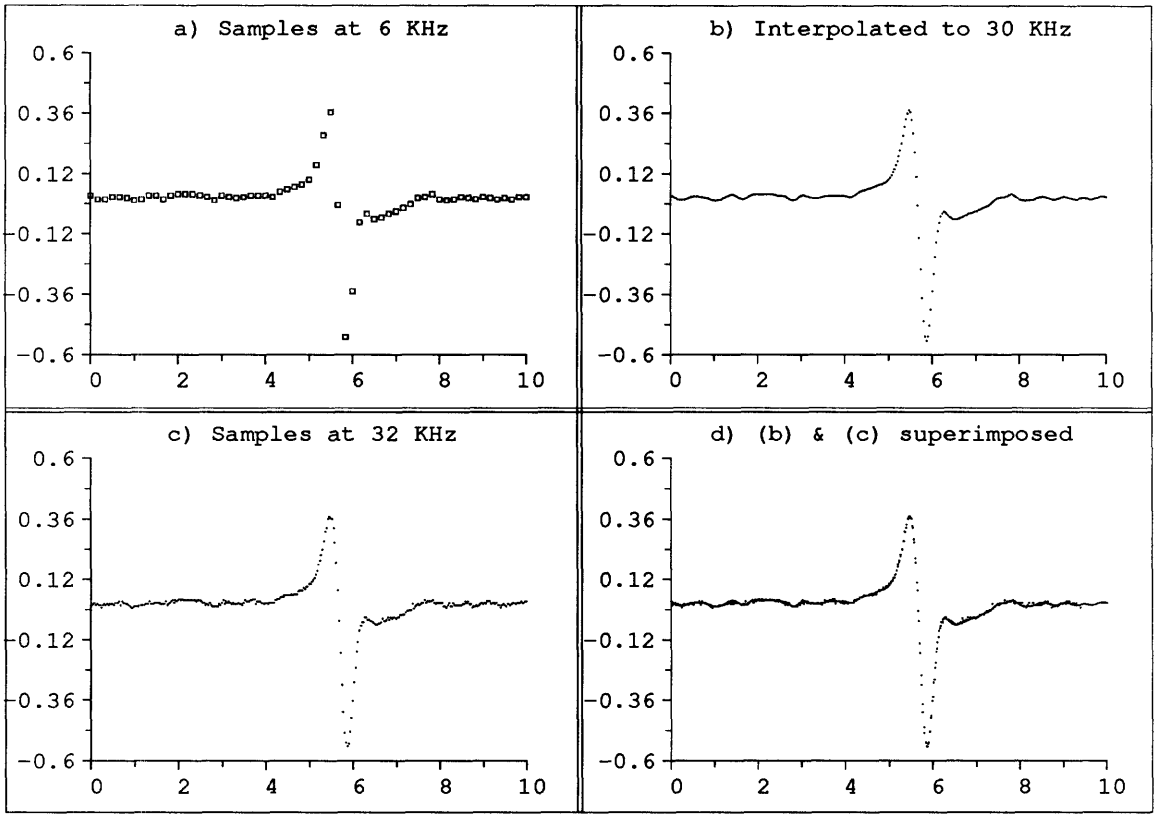

Figure 3-3: Interpolation of sampled data

to prevent the stimulus artifact from being detected subsequently as an arrival of excitation because of its fast rate of change; this procedure also helped to reduce computation time by processing only relevant portions of the signals. The selected interval was interpolated and stored. The interpolated version of the representative stimulus for each set of conditions was plotted and inspected visually for consistency with the raw data.

3.3.2 Estimation of arrival times

The interpolated data segments were processed by a program which computed the first central difference signal and located the maximum negative value for each channel. This computation is illustrated in figure 3-4 using the data of figure 3-3. The panels in the two figures correspond directly. In this example there was good agreement on the time of the maximum negative derivative between the interpolated waveform and the actual samples at 32 kHz; as noted above, the agreement was within 8 μSec. The time of the maximum negative derivative was the fiducial point chosen to indicate arrival of excitation at the electrode.

The arrival times (fiducial point times) for all stimuli under a given set of conditions were plotted together on a graph which had arrival time as the ordinate and "event number" on the abscissa. All points from each electrode were connected by straight lines. Each "event" was a single conducted beat. An example of such a plot is figure 4-j15.2 (which is discussed in detail in Chapter 4). These plots showed the order of arrival of activity at the electrodes for each beat, and the fluctuation, if any, from beat to beat. This presentation also clearly showed outlying fiducial points, which occurred occasionally due to noise. These plots were examined for the existence of gaps between lines indicating long delay times between the arrival of excitation at adjacent electrodes.

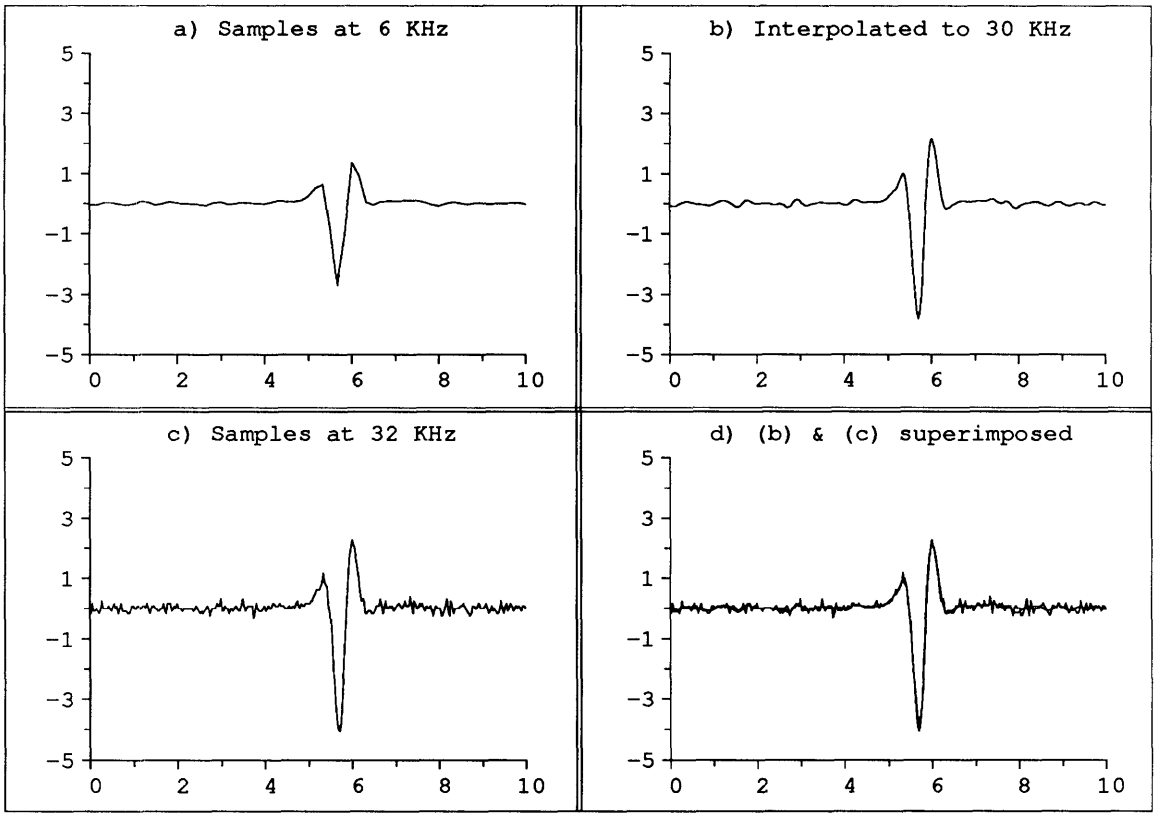

Figure 3-4: Differencing of sampled data

The accuracy to which the time of arrival of excitation at an electrode can be estimated is limited by the physical properties of the measurement system. In a real system, noise corrupts the recorded signal and limits the achievable accuracy; the signal to noise ratio (SNR) determines the accuracy to which a fiducial point can be located (assuming that the other properties of the signal and noise remain constant). In the case of recordings from extracellular electrodes, smaller electrodes are noisier and hence will result in lower-accuracy fiducial point determinations for a given signal amplitude.

The accuracy of estimation of arrival times using the microelectrode array with 10-μm electrodes was determined empirically as follows. Ten representative extracellular signal segments containing action potentials of the highest available SNR were selected from different experiments; the fiducial point was determined for each one. One hundred representative extracellular signal segments containing only electrode noise and no action potentials were randomly chosen from all experimental records. Each of the 10 action potential segments was scaled by multiplication by 15 arbitrarily chosen factors ranging from 1.4 to 0.07 and each result was added separately to each of the 100 noise segments, yielding a total of 15,000 different combinations of signal and noise; the SNR was computed for each combination. A fiducial point determination was made for each combination, and the value was subtracted from the fiducial point of the corresponding "noiseless" signal. A non-zero result was an error in the fiducial point determination due to noise. The results were separated into 9 groups on the basis of signal to noise ratio, and the standard deviation of the errors was computed for each group. Figure 3-5 shows the standard deviation of the error in arrival time estimation as a function of signal to noise ratio. As expected, as the SNR increased, the error in estimating the location of the fiducial point decreased.

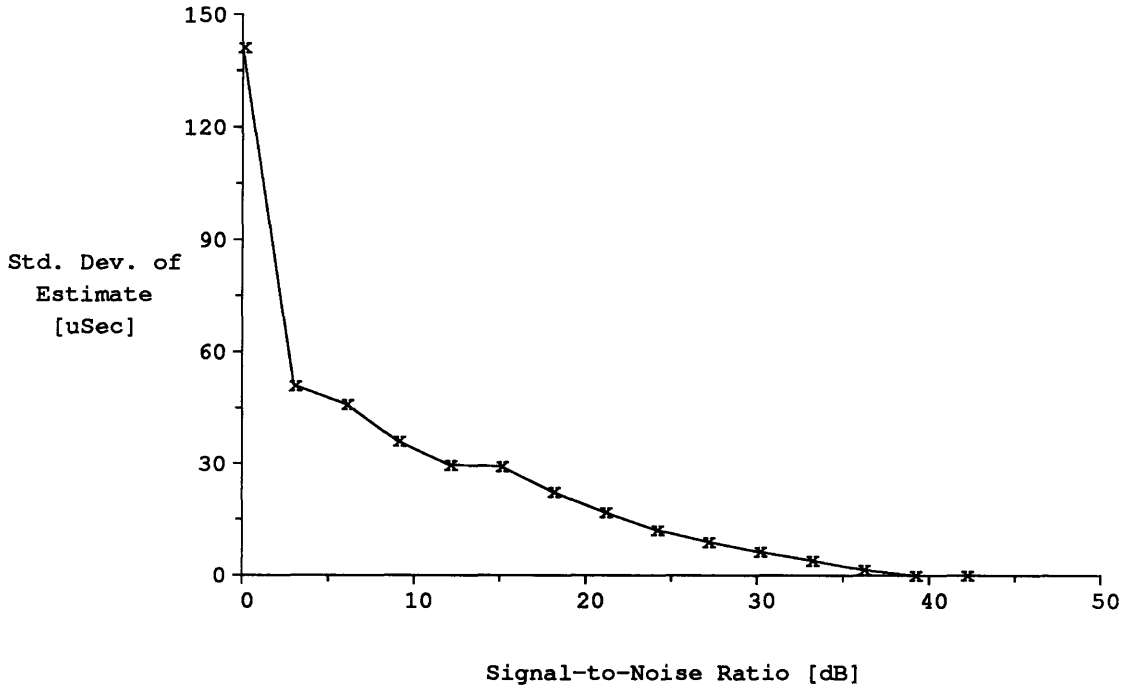

Figure 3-5: Error in arrival-time estimates due to noise

Chapter 4: EXPERIMENTAL RESULTS

4.1 Characteristics of the Microelectrode Array

The impedance of a typical 10 x 10 μm bright gold electrode (i.e: before platinization) was between 3.1 and 10 MΩ at 1 kHz (mean 5.8 MΩ ± s.d. 1.5, N=77), with a mean phase angle of -62 ± 12°. After platinization, the impedance ranged from 0.16 to 2.0 MΩ at 1 kHz (mean 620 kΩ ± 350, with a mean phase angle of -53 ± 11°.

The noise characteristics of several microelectrodes were measured as follows: a microelectrode array was filled with physiological saline solution, and the electrode to be tested was connected to the input of an OPA121 low-noise FET-input operational amplifier configured as a unity-gain buffer. The output of the buffer was connected to the input of a spectrum analyzer (Hewlett-Packard 3582A). The analyzer was set up to measure a time-averaged frequency spectrum. The noise of this measurement apparatus was tested by substituting a 1000 Ω low-noise metal-film resistor for the electrode under test; the noise output was 16 nV/$\sqrt{Hz}$ over the 0 to 10 kHz frequency range, which was significantly lower than the noise output measured during the subsequent testing of electrodes. The noise spectrum of a typical platinized 10 x 10 μm microelectrode is shown in figure 4-1.†

The major portion of the noise output was at the low frequency end of the spectrum, i.e. below about 500 Hz. The lowest-frequency peak in these figures also contained significant power due to interference from 60 and 120 Hz sources in the environment, so

† Amplitudes are charted in dBV; 1 volt RMS = 0 dBV. Each spectral bin was 60 Hz wide; the noise density is the quotient of the amplitude by the square-root of the bandwidth. For example, -120 dBV = $10^{(-120/20)}$ = 1 μV. The noise density is 1 μV / $\sqrt{60}$ = 0.129 μV/$\sqrt{Hz}$.

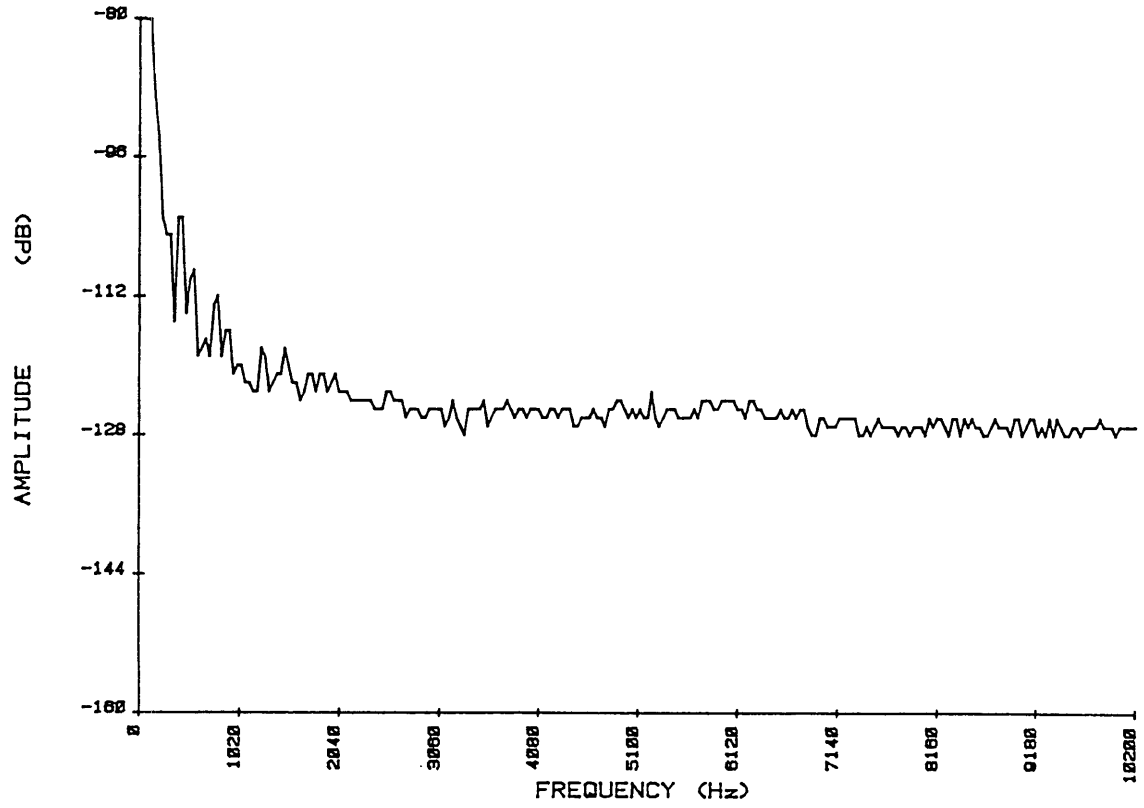

Figure 4-1: Noise spectrum of a typical platinized microelectrode

the amplitude shown at that frequency should be considered to be an upper bound on the actual value. The noise spectrum of a typical unplatinized electrode is shown for comparison in figure 4-2. It is qualitatively similar to that of the platinized electrode, but is noisier at all frequencies by 3-6 dB, reflecting the higher impedance of unplatinized electrodes.

The frequency response of several recording microelectrodes was measured as follows: a microelectrode array was filled with physiological saline solution, and the electrode to be tested was connected to the input of an OPA121 unity-gain buffer as described above. The output of the buffer was connected to one channel of a dual-channel spectrum analyzer (Hewlett-Packard 3582A). White noise at an amplitude of 3 mV RMS from the internal noise source of the spectrum analyzer was applied to the saline bath via a 2 x 10 mm platinum electrode. This noise source also drove the reference channel of the spectrum analyzer. The analyzer was set up to calculate the resulting transfer function, which in this case was the combined frequency response of the excitation electrode, the saline bath, the recording electrode, and the operational amplifier buffer. It was verified that when the recording microelectrode was replaced with an electrode of much larger area (i.e: one of the two large reference electrodes), the transfer function of this system was lossless from 0 to 10 kHz; therefore, any deviation from this with a microelectrode in the system must have been due to the frequency response of the microelectrode. The frequency response of a typical microelectrode from 0 to 10 kHz is shown in figure 4-3. The response gently decreased as the excitation frequency increased; at the maximum measured frequency of 10 kHz, the attenuation was 2.2 dB, which corresponds to a voltage ratio of 0.78.

4.1.1 Characteristics of the Recording system

The frequency response of the recording system, which consisted of the

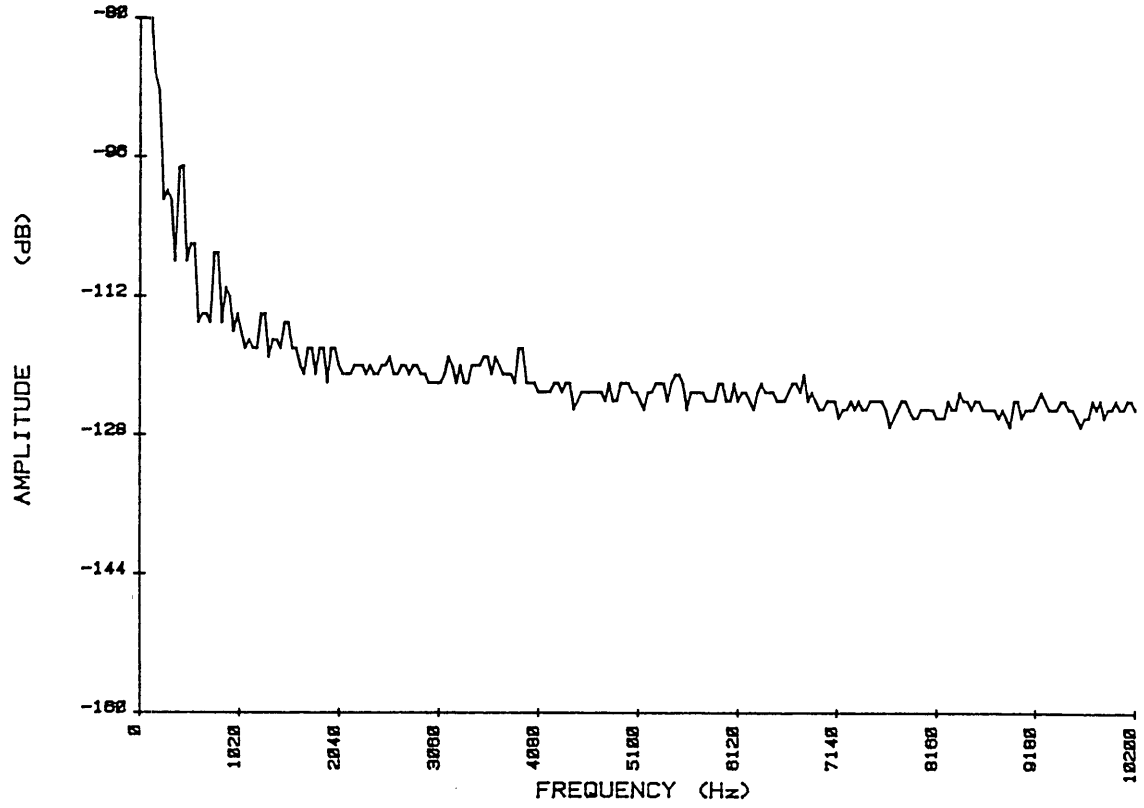

Figure 4-2: Noise spectrum of a typical unplatinized microelectrode

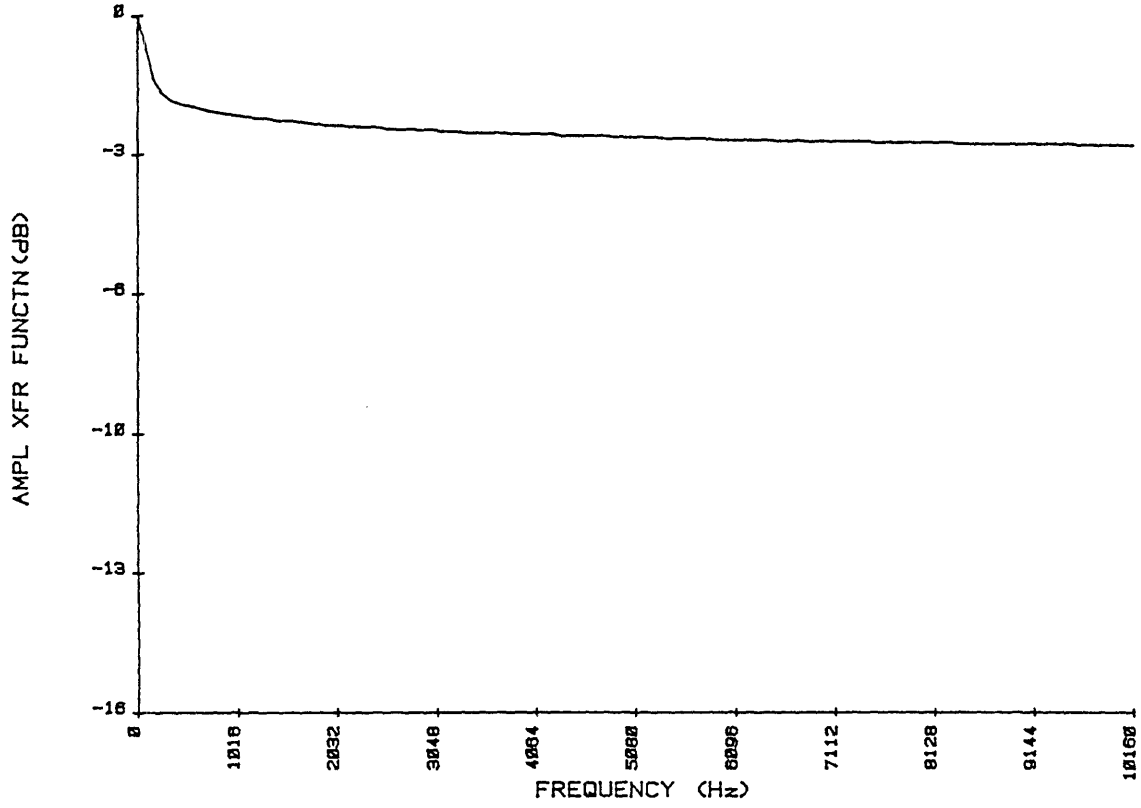

Figure 4-3: Frequency response of a typical microelectrode

preamplifier, the second-stage amplifier, and the anti-aliasing filter, is shown in figure 4-4. The overall gain was 1000, and the -3 dB corner frequency was 2000 Hz. The rolloff was 60 dB/decade. The noise output of the recording system with a 1000 Ω low-noise resistor to ground at the input is shown in figure 4-5. (The amplitudes shown in the figure were measured at the output; subtract 60 dB to refer them to the input.) The recording system noise was approximately 15 dB lower than the noise due to the signal source (typical platinized microelectrode noise) at all frequencies of interest.

4.2 Characteristics of the Tissue Cultures

Cultures of cardiac myocytes on microelectrode arrays examined on the third day after culturing almost invariably showed confluent growth and rhythmic mechanical activity. The rate of beating varied widely from culture to culture, ranging approximately from 1 to 6 beats per second. Cultures prepared from the same suspension of cells did not necessarily have similar rates, and individual cultures were sometimes observed to abruptly change rates in spite of apparently constant conditions. Culturing cells on the microelectrode array / culture dish exposed the cells to four types of surfaces: glass, KTI 732 photoresist, platinized gold, and Silastic. Examination of numerous monolayers growing on the photoresist surface and in the vicinity of the platinized gold using phase contrast microscopy revealed no morphological differences when compared with similar cells on plain glass. The mechanical activity of these cells was apparently normal. The Silastic did not appear to interfere with cell growth or function.

Figure 4-6 is a photomicrograph of cardiac ventricular myocytes cultured on the surface of a microelectrode array at half the usual density for clarity. Only the central region of the array is shown in this figure. The central microelectrodes are visible as opacities underlying the cells in this view. The same cells cultured at a density of 1 x 10^5 cells/mL on a glass cover-slip are shown in figure 4-7.

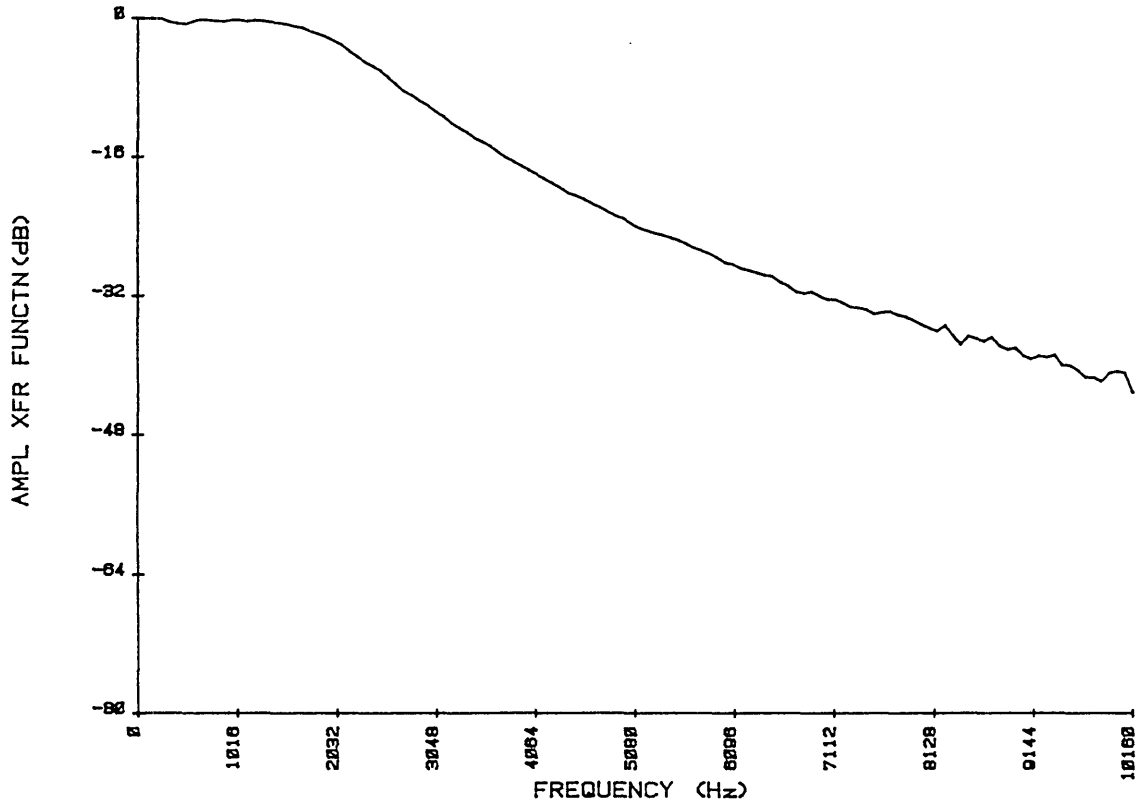

Figure 4-4: Frequency response of recording system

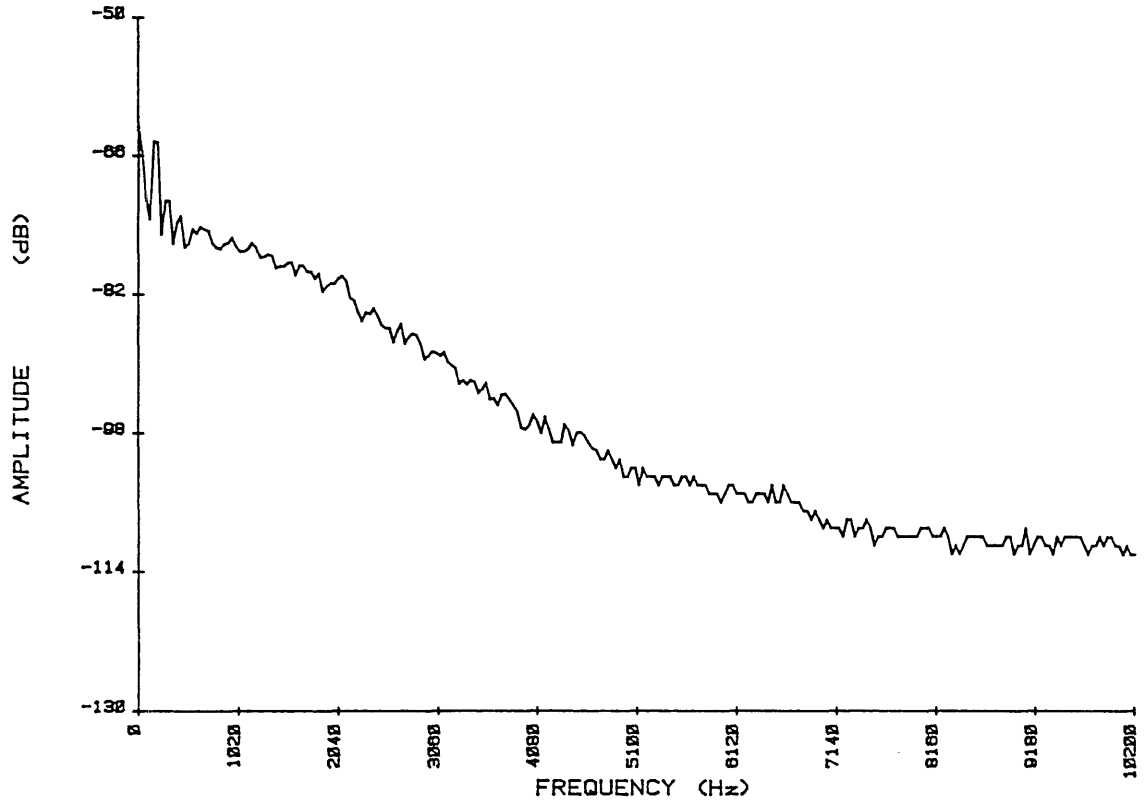

Figure 4-5: Noise spectrum of the recording system

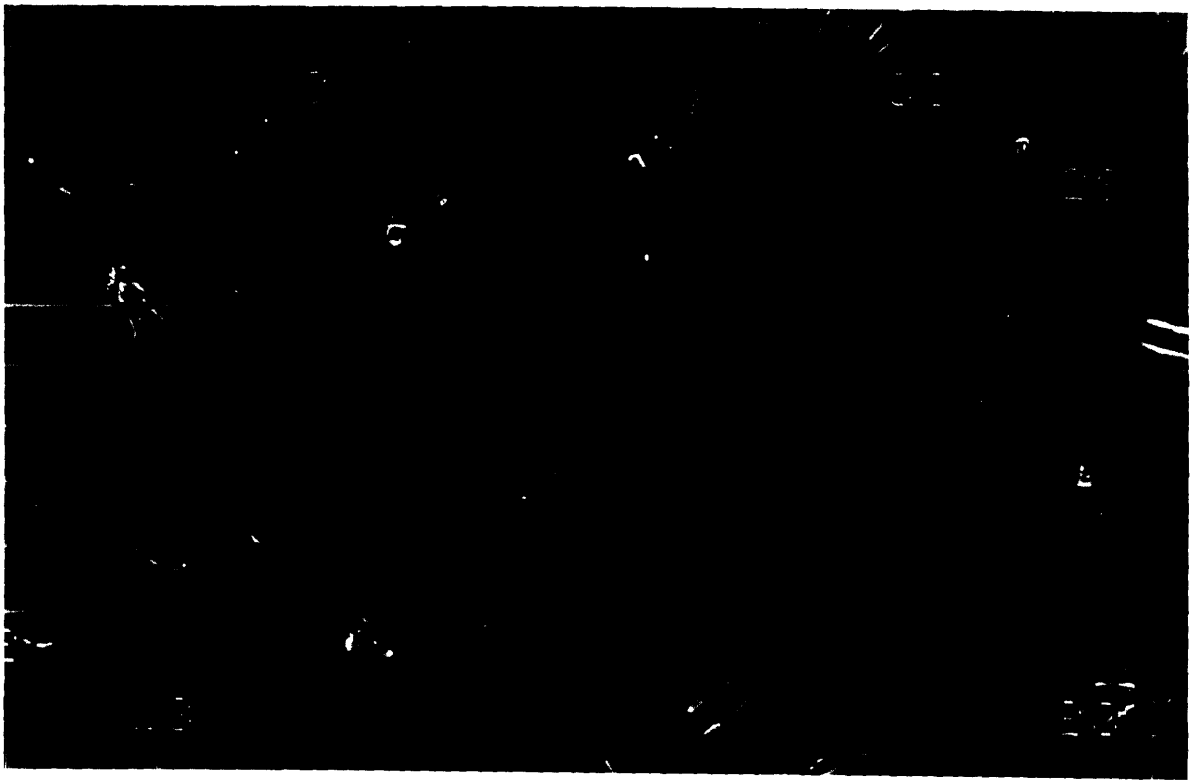

Figure 4-6: Ventricular myocytes cultured on a microelectrode array

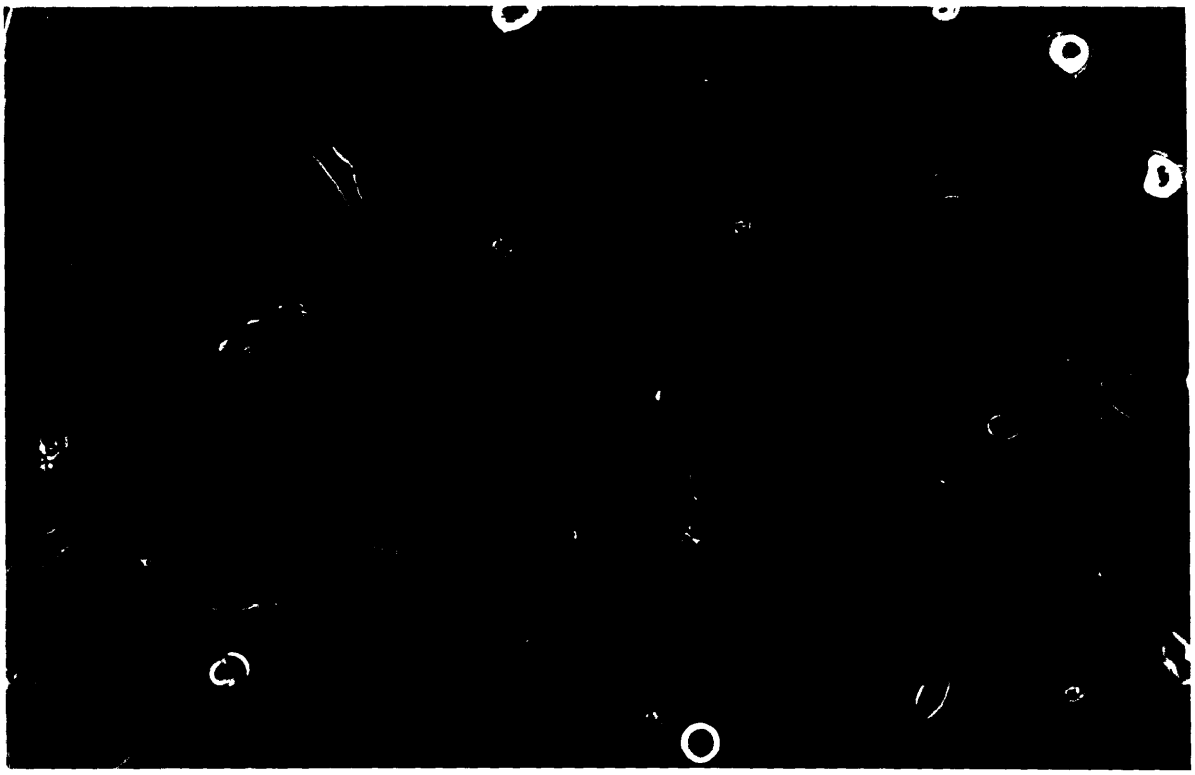

100 µm

Figure 4-7: Ventricular myocytes in cell culture at low density

The results of the size measurements of isolated cultured cells are shown in figures 4-8 and 4-9. Figure 4-8 shows the distribution of cell lengths and widths. These measurements were made from a series of photographs of cultures plated at low density, similar to figure 4-7. Cells were measured after the same incubation period used for the propagation experiments. Cell size as a function of incubation time was not studied. Cell lengths ranged from 41 through 185 μm with a mean length of 97.1 and a standard deviation of 28 (n=106). The widths of the same cells ranged from 7 through 40 μm, with a mean of 14.6 and a standard deviation of 5.9. Figure 4-9 shows the distribution of the product and the quotient of the length and width measurements of individual cells. The product is intended to give a rough appreciation of the range of areas spanned by single cells; it ranged from 500 to 3000 μm^2, with a mean of 1400 and a standard deviation of 570. The quotient is an index of the range of cell shapes, from more or less spherical to long and narrow; it ranged from 1.3 to 21, with a mean of 7.7 and a standard deviation of 3.5.

Figure 4-10 shows the distribution of distances between boundaries along randomly-oriented straight lines across a layer of cultured cells. Boundaries occurred as close together as 5 μm and as far apart as 130 μm. The mean distance along a randomly chosen straight line between boundaries was 22 μm with a standard deviation of 16 (n=214).

4.3 Spontaneous Electrical Activity

All cultures which subsequently responded to extrinsic stimulation exhibited spontaneous electrical activity. Such activity could be readily identified on the basis of its waveform and rhythmic nature, and its timing coincided with the mechanical activity of the culture when that was monitored simultaneously. The signals recorded from the extracellular microelectrodes were generally biphasic in shape (figure 4-11a), and

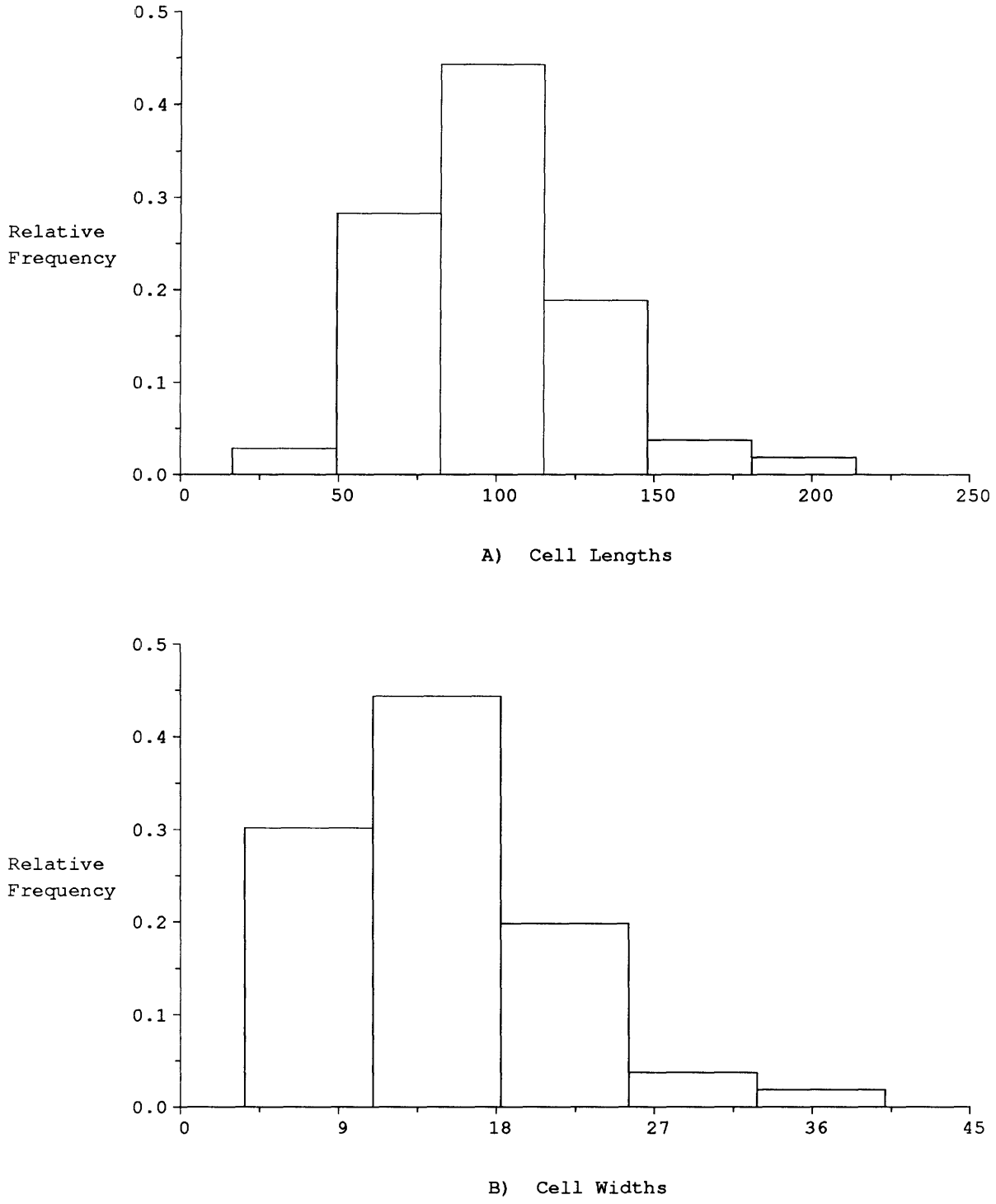

Figure 4-8: Distribution of cultured cell lengths and widths

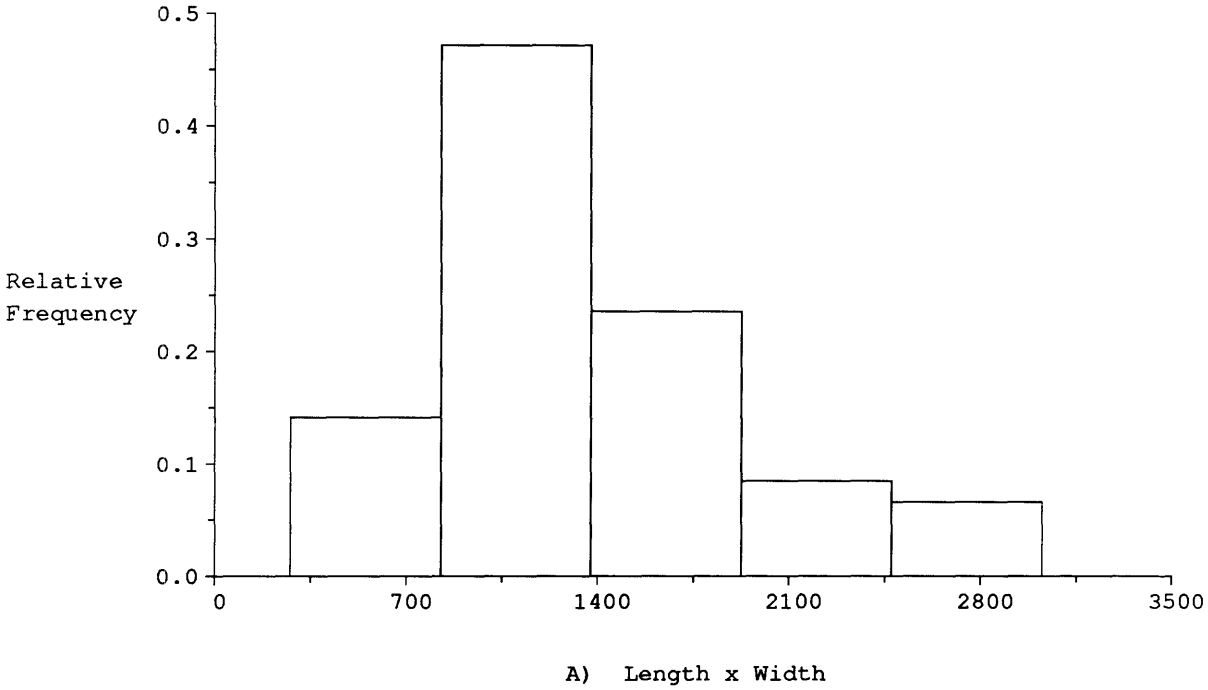

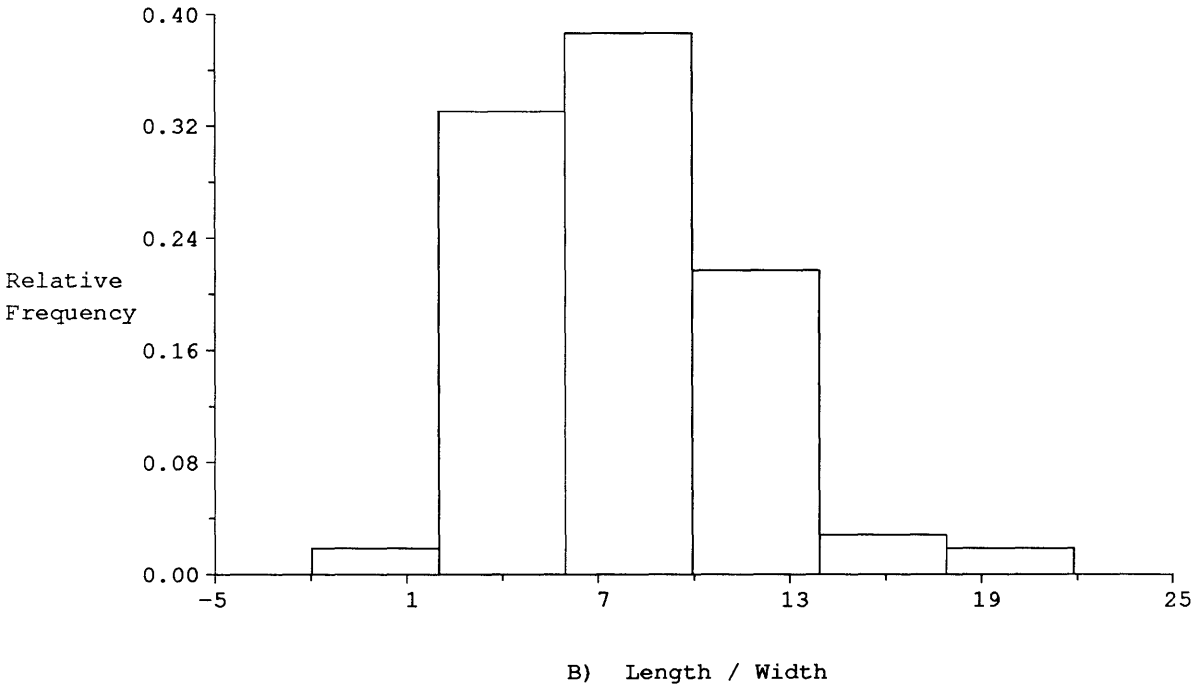

Figure 4-9: Distribution of cultured cell shape parameters

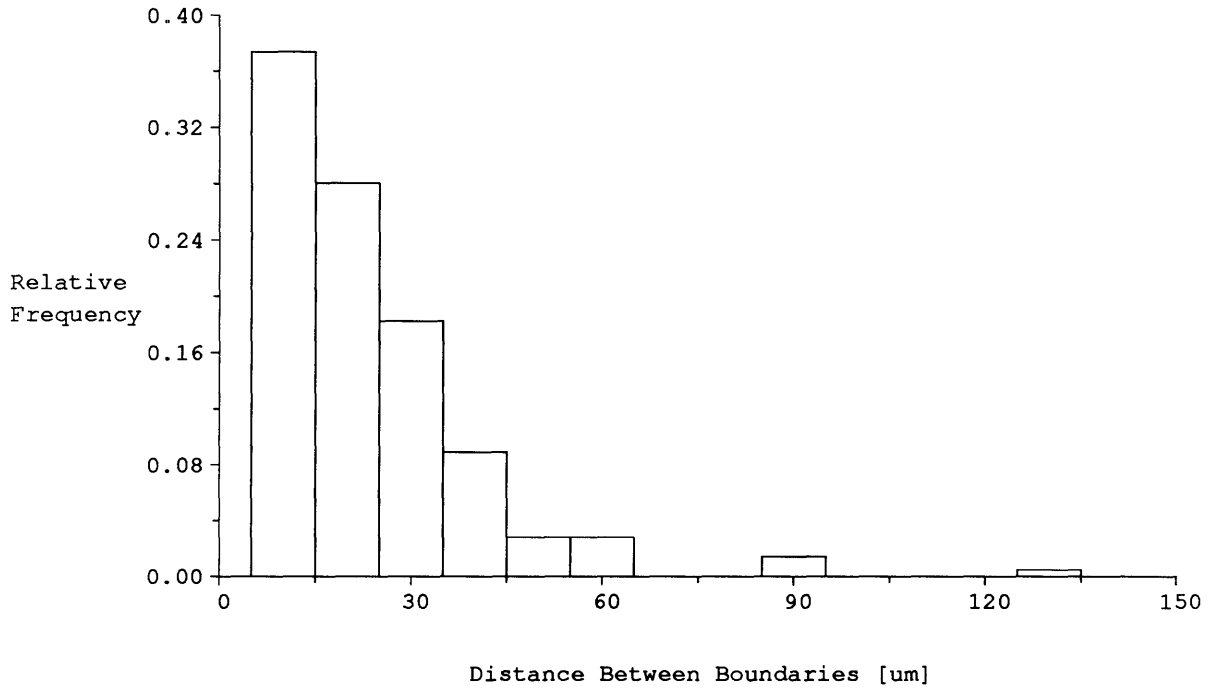

Figure 4-10 : Distribution of distances between cell boundaries

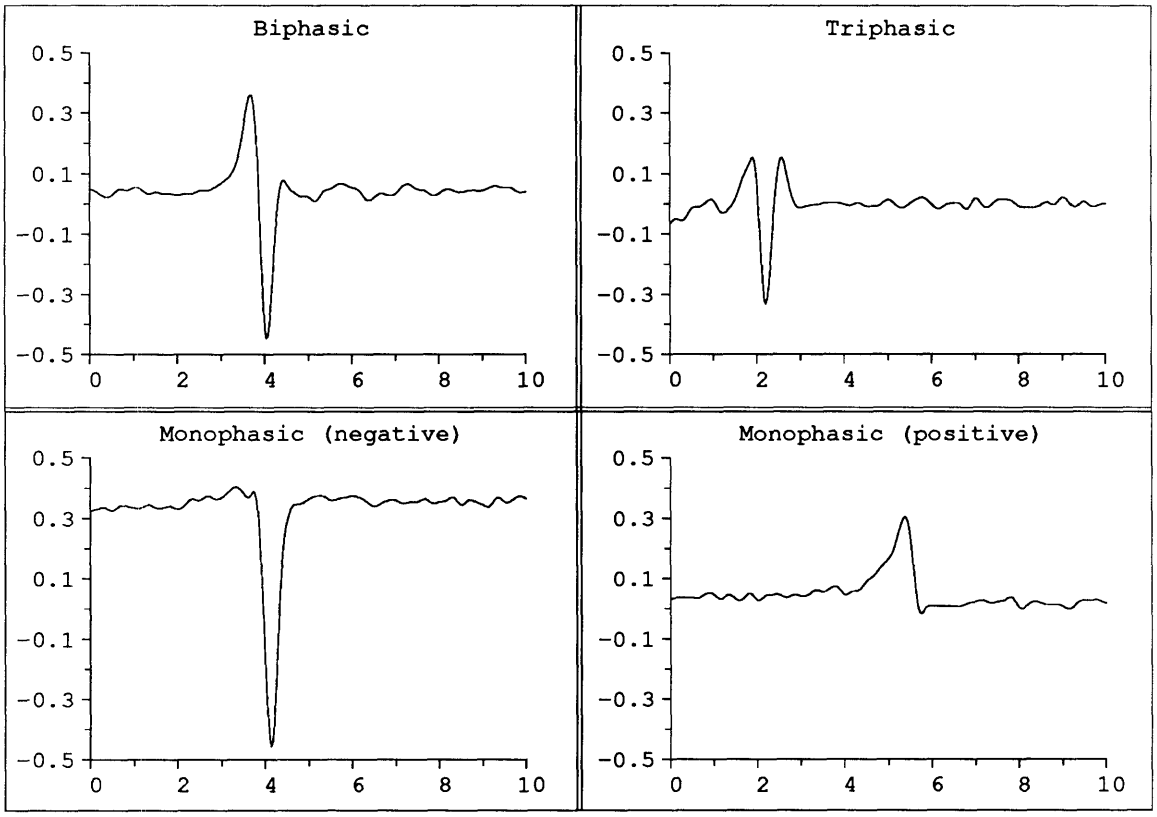

Figure 4-11: Examples of extracellular action potentials

asymmetric; most typically, the first, positive phase was of lower amplitude than the second, negative phase. Not infrequently, triphasic waveforms were seen, usually having a positive third phase that was smaller than the first positive phase. Occasionally, monophasic waveforms were seen; these were more often negative-going than positive-going. Typical spikes were 1 to 2 mSec in duration. The peak-to-peak amplitudes ranged from just barely discernible from the electrode noise, which corresponded to between 50 and 100 μV depending on the electrode, to a maximum of 2.8 mV.

The origin of the potentials recorded by the extracellular electrodes was investigated in early experiments by comparing them with intracellular potentials and mechanical activity of the preparation (Israel et al., 1984). Figure 4-12a is an oscilloscope photograph of extracellular and intracellular potentials recorded simultaneously from the same site. For intracellular recordings, glass microelectrodes were pulled, filled with 3M KCl, and mounted in a holder / head-stage (W-P Instruments MEH-1S / M-707) driven by a piezoelectric micro-positioner (Burleigh PZ-555). The micropipette was positioned in a cell adjacent to one of the extracellular microelectrodes under direct microscopic visualization. The head-stage signal was amplified by a standard micropipette amplifier (WPI M-707) and recorded. The extracellular spike occurred at the same time as the upstroke phase of the action potential, as expected.

Figure 4-12b shows a simultaneous recording of extracellular potentials and motion taken from sites separated by approximately 20 μm. The method of recording mechanical activity has been described in detail elsewhere (Barry et al., 1980). Briefly, cells were prepared as above except for the addition of latex microspheres (non-radioactive tracer microspheres, 3.2 μm diameter, 3M Company) to the cell suspension before plating. The electrode array was placed on the stage of an inverted phase contrast microscope (Leitz Diavert) with a 40x objective. A low-light-level television camera monitored the image

A.

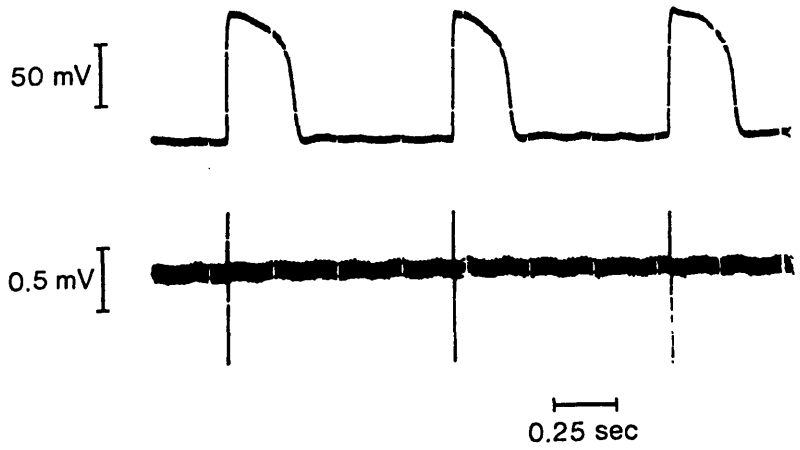

B.

Figure 4-12: Simultaneous EC and IC action potentials and membrane motion

of the moving cells. The signal from the camera was processed by a video motion detector (Colorado Video 633), which provided a voltage proportional to the displacement of a selected moving latex microsphere which was within 20 μm of one of the extracellular electrodes. The preparation of figure 4-12b was contracting at a rate of 75 beats per minute. The extracellular potential preceded contraction by about 70 mSec; thus, it could not have been a motion artifact. Furthermore, no activity was recorded at the extracellular microelectrode during the contraction of the overlying cell. The duration of each contraction was between 250 and 300 mSec, and the amplitude of contractions was about 2 μm.

The signals at adjacent closely-spaced electrodes were independent of one another. While it was usually the case that the waveforms from two adjacent microelectrodes on 20 μm centers had similar shapes and amplitudes, it was not always so. In one particular example of this, the signal from one central microelectrode had an amplitude of 0.16 mV while its immediate neighbors on three sides had signals of 1.6, 1.2, and 1.0 mV. In a subsequent recording session using the same microelectrode array but a different cell culture, the signal amplitude from the index electrode was 0.6 mV, while the same neighbors had amplitudes of 0.65, 0.65, and 0.5, respectively (thus establishing that the first result was not caused by a faulty electrode). This demonstrates that the central microelectrodes were electrically independent of one another, and that the similarities usually seen among their signals were due mainly to properties of the signal source rather than to properties of the microelectrode array.

4.4 Response to Electrical Stimulation

Most cultures could be paced using extrinsic electrical stimuli. Of 33 preparations in this series of experiments, 7 could not be paced in spite of attempts at all 4 stimulation electrodes. The minimum effective cathodal stimulus duration observed was 0.3 mSec.

The minimum effective stimulus amplitude ranged from 0.4 volts to 1.4 volts. The stimulus current delivered was not measured in these experiments.

4.5 Results of Discontinuous Propagation experiments

The results of all experiments in which the NH_4Cl intervention was applied will now be examined.

4.5.1 Experiment j15

Figure 4-j15.1 shows the electrical activity at all of the recording electrodes in response to a stimulus under control conditions. The inset diagram shows the relative locations of all the recording electrodes; each box represents a recording electrode. A number beside a box is the number of the recording channel to which the electrode was connected, and refers directly to the corresponding number on the chart of signals.† Un-numbered boxes represent unconnected electrodes. The distances between boxes in this schematic figure are approximately to scale. At the periphery, numbered arrows indicate electrodes which were too far from the center of the array to plot at this scale. Refer to figure 3-1 for an accurately scaled drawing of the electrode layout. The stimulating electrode that was used in this experiment is located beyond the bottom of this diagram (electrode 16 in figure 3-1).

The stimulus was delivered at time zero on the time axis; a stimulus artifact was recorded at this time on all channels. The electrical response of the culture was visible several milliseconds later in the recordings from each of the sixteen electrodes. Each electrode recorded an action potential of about 1 to 2 mSec in duration. Electrodes 12

† In the ensuing discussion, these numbers will be referred to as "electrode numbers" rather than as "channel numbers". However, the assignment of these numbers was different for each experiment and must be taken from the map prepared for that experiment.

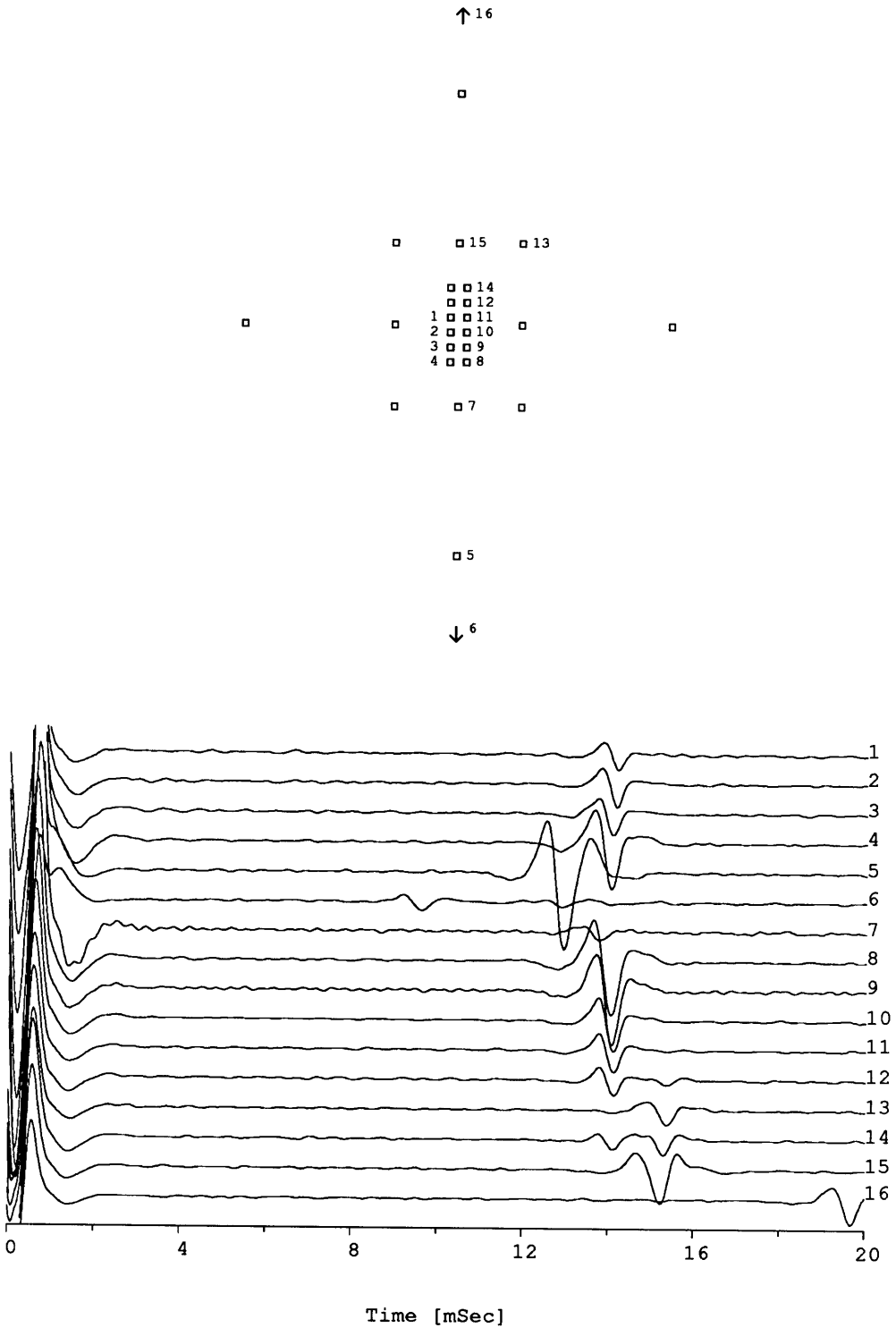

Figure 4-j15.1: A single beat under control conditions

and 14 each recorded two biphasic deflections. The second deflection on each of these electrodes occurred about 1 mSec after the first under control conditions, but this separation widened to about 3.5 mSec during the NH_4Cl intervention (figure 4-j15.3). This fact, and similar aberrant behavior of these two electrodes in another experiment with a different cell preparation, led to the the conclusion that these electrodes had fabrication defects in the photoresist insulation which resulted in the presence of two recording surfaces on each of these channels. The signals on these channels were therefore considered unusable.

The first electrode to record an action potential after the stimulus was electrode 6, which was the recording electrode closest to the stimulating electrode in this experiment. The distance from the stimulating electrode to electrode 6 was 500 μm. The arrival time at electrode 6 was 9.49 mSec for this beat. The apparent average conduction velocity in this region of the preparation was thus about 0.05 m/Sec. Activity next arrived at electrode 5, which was 500 μm from electrode 6, at 12.81 mSec. The apparent conduction velocity in this part of the preparation was 0.15 m/Sec, 3 times faster than in the adjacent region. This might reflect an actual difference in conduction velocity, or it might be because the wavefront of activation was further from being perpendicular to the axis of the electrodes in the region between electrodes 6 and 5 than it was in the region between the stimulating electrode and electrode 6.†

† The apparent conduction velocity of a planar wavefront based on arrival time measurements at two points will be equal to the actual conduction velocity only when the axis of wavefront travel is parallel to the axis of the two electrodes. At other angles, the apparent conduction velocity will be greater than the actual velocity:

$$V_{apparent} = \frac{V_{actual}}{\cos \theta}$$

where θ is the angle between the axis of travel and the axis of the electrodes. Note that when θ is 90°, the apparent velocity is infinite since the arrival times at the two electrodes are the same. In practice, since the arrival times are subject to random estimation errors, nearly simultaneous arrivals will result in nearly infinite apparent velocities which may appear to be oriented in either of two opposite directions. Thus, apparent conduction velocities calculated in this way must be interpreted with caution.

The arrival times of the action potential at the electrodes as determined by the fiducial point times for the beat shown in figure 4-j15.1 are given in ascending time order in the following table. The estimated signal-to-noise ratio at each electrode is also given to provide an index of the expected variability of the results (see figure 3-5).

Electrode	Arrival Time	SNR
6	9.49	20
5	12.81	37
7	13.70	18
4	13.93	36
8	13.97	36
3	13.99	28
9	14.02	32
10	14.06	36
1	14.07	26
2	14.08	31
11	14.10	29
12	14.12	27
14	14.14	20
15	15.25	31
13	15.36	26
16	19.72	28

The beat shown in figure 4-j15.1 is the fourth in a series of 10 beats which were recorded under identical conditions at a stimulus rate of 1.6 Hz. The timing of the fiducial points for this series of beats is shown in figure 4-j15.2. In this figure, each integer along the abscissa represents a single beat; the ordinate displays arrival time in milliseconds from the stimulus onset. Times for successive beats are connected by straight line segments to aid visualization, and each trace is labelled with its electrode number. Figure 4-j15.2b shows the arrival times at the central recording electrodes with greater time resolution than in 4-j15.2a. The arrival times in the above table for the beat of figure 4-j15.1 are plotted in figure 4-j15.2 as the ordinates of the fourth beat. The arrival times at each electrode varied slightly from beat to beat, but the variations were consistent from electrode to electrode. The arrival times at the central microelectrodes in this preparation were close together and spanned an interval of about 200 μSec. Since the distance from electrodes 8 to 14 was 100 μm, the apparent conduction velocity in the central region was about 0.5 m/Sec.

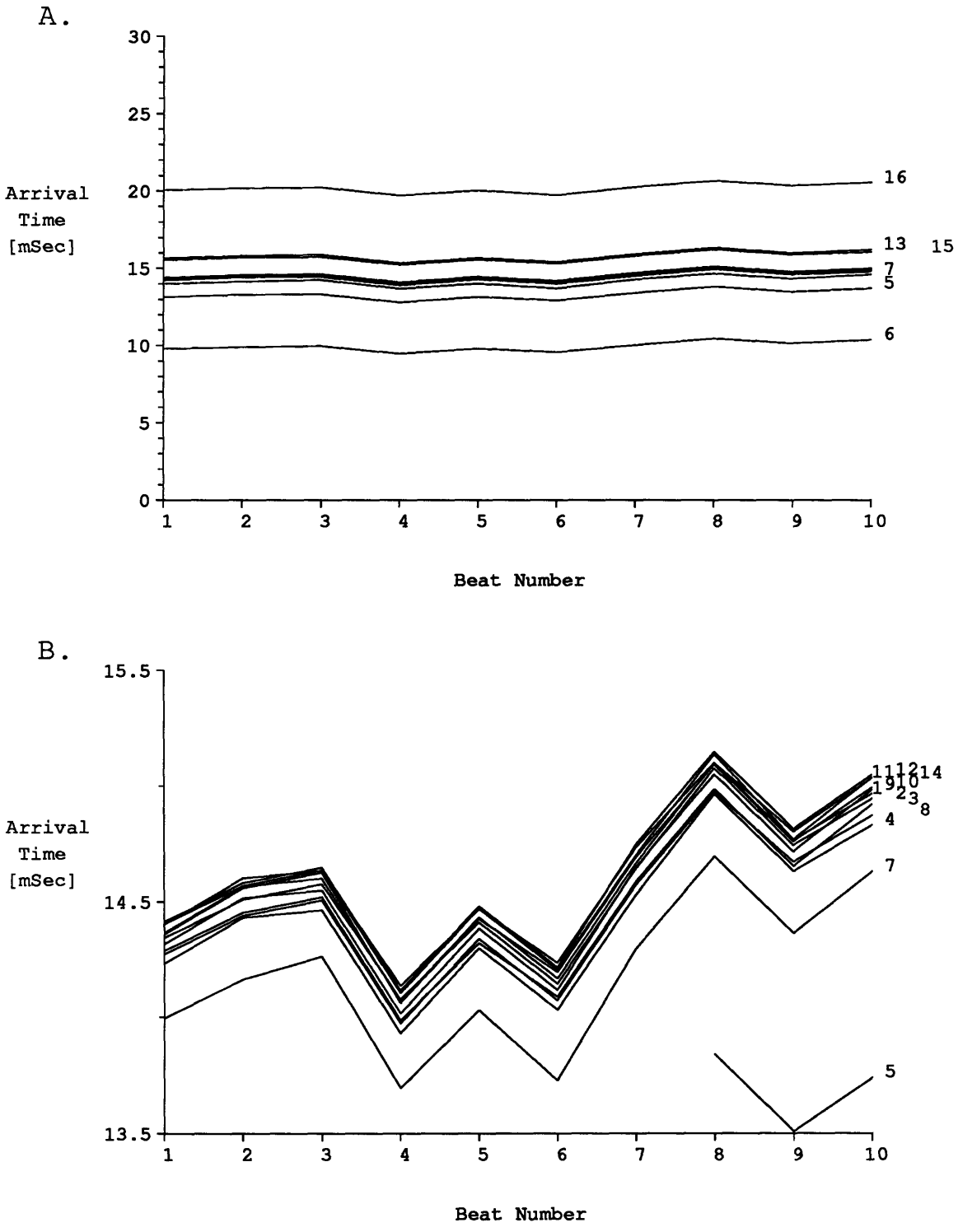

Figure 4-j15.2: Arrival times under control conditions in experiment j15

Figure 4-j15.3 shows the electrical activity at all of the recording electrodes in this preparation in response to a stimulus 3 minutes after cytoplasmic acidification by washout of ammonium chloride. The stimulus rate remained at 1.6 Hz. Under these conditions, the conduction velocity in this preparation was slower than it was under control conditions. The time taken for propagation from the stimulus electrode to electrode 6 was 14.65 mSec, and activity reached electrode 5 at 22.18 mSec, yielding apparent conduction velocities which were 68% and 60%, respectively, of those under control conditions. The waveform at each electrode changed somewhat from that in the control condition, but no major changes in morphology were noted. The amplitude at each electrode was lower than it was under control conditions. The signal from electrode 7, which was relatively small under control conditions, was small enough during acidification that automated detection of its fiducial point was confounded by noise for several of the beats; this was remedied by forcing the detector to look for the maximum negative slope within ± 0.67 mSec of 23.5 mSec post-stimulus (chosen by inspection of the remaining beats).

The activation arrival times for 10 beats under acidified conditions are shown in figure 4-j15.4. The beat of figure 4-j15.3 is the second beat in the series of figure 4-j15.4.

The pattern of activation at the recording electrodes during this series of beats was basically the same as it was under control conditions. Figure 4-j15.4b shows the order of arrival times at the central microelectrodes in greater detail. The sizes of the scales in figure 4-j15.4 are the same as those in figure 4-j15.2, so that the separations of the traces may be directly compared (note, however, that the ranges of the ordinates plotted are different). The estimated arrival times at most of the electrodes showed greater variability due to noise than the corresponding times under control conditions; this would be expected because of the decrease in signal amplitude that was seen at these electrodes

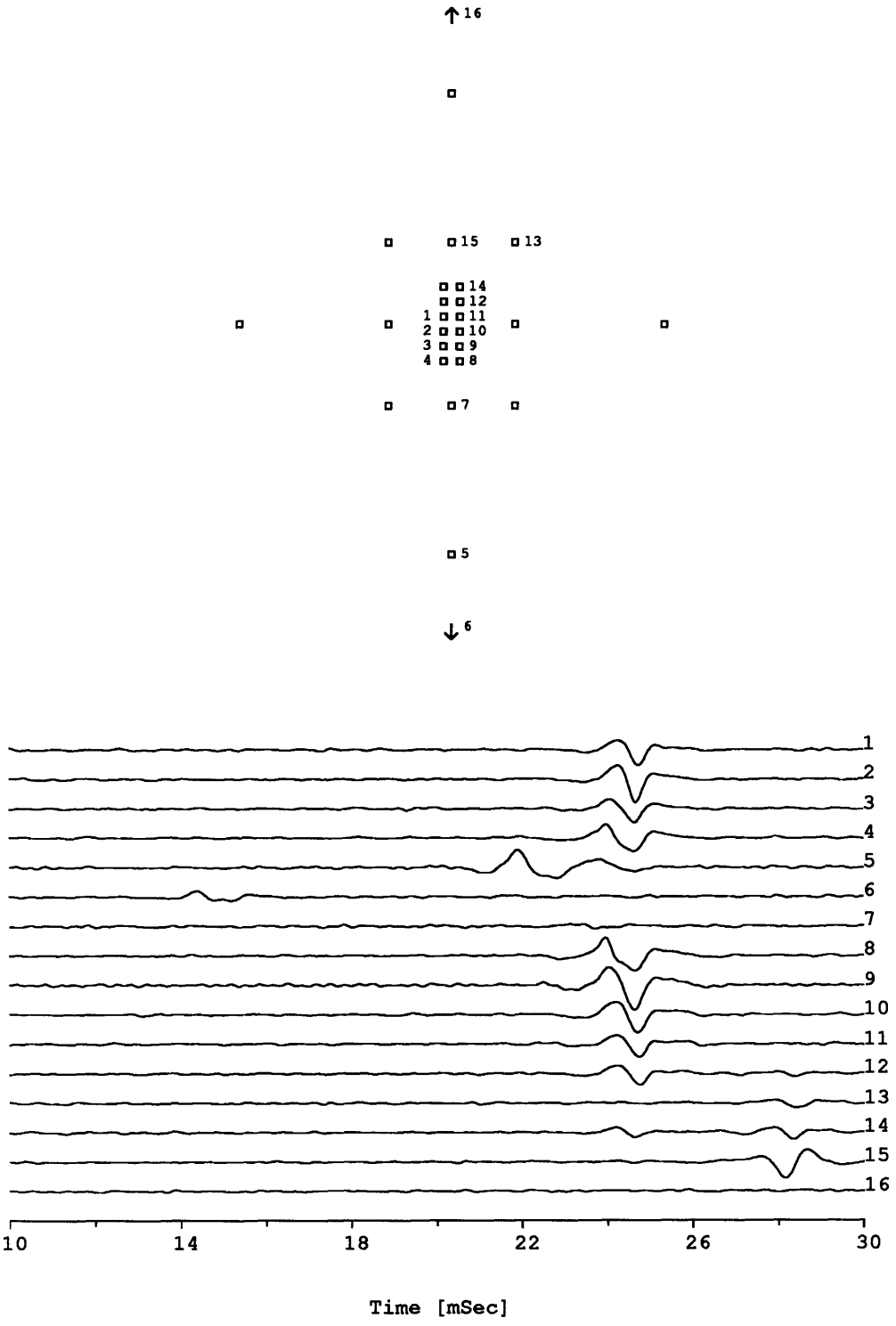

Figure 4-j15.3: A single beat under acidified conditions

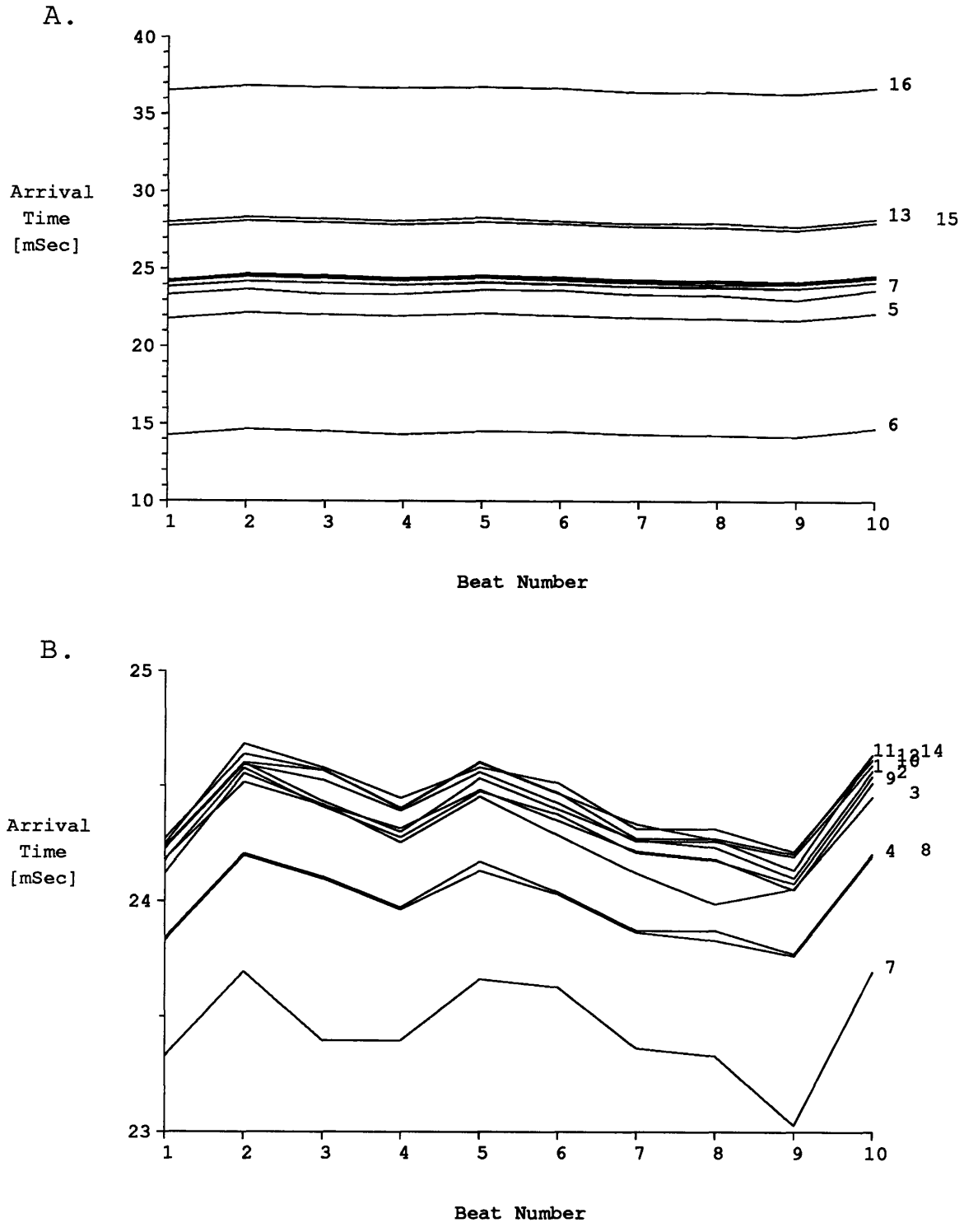

Figure 4-j15.4: Arrival times under acidified conditions in experiment j15

under acidified conditions. The mean difference in arrival time between electrodes 8 and 9 increased from 60 ± 7 μSec to 320 ± 7 in going from control to acidified conditions. Electrodes 8 and 9 were on 20 μm centers, so these time delays correspond to velocities of 0.33 and 0.063 m/Sec, respectively. Likewise, the delay at the adjacent pair of electrodes, 3 and 4, increased from 46 ± 7 to 280 ± 16 μSec. For comparison, consider the arrival times at electrodes 10 and 11, which were separated by the same distance as electrodes 8 and 9. The mean difference in arrival time between electrodes 10 and 11 went from 27 ± 5 μSec to 30 ± 5 in going from control to acidified conditions. These delays correspond to velocities of .74 and .67 m/Sec, respectively. As can be seen from Figure 4-j15.4b, the arrival times at the other central electrodes under acidification remained about as close together as they had been under control conditions.

The significance of the changes in the mean arrival time differences in going from control to acidified conditions was evaluated for selected electrode pairs using Student's t-test. The difference in means for electrode pair (8,9) was significant to p=0.000005 (two-sided test). In comparison, the p-value for electrode pair (10,11) was 0.69. Thus, the intervention is seen to have had a strong effect on the delay between electrodes 8 and 9, while in the case of the adjacent electrodes 10 and 11, the delay did not change significantly.

The delay between activation at the central electrodes and arrival of activity at electrodes 13 and 15 was relatively long; the mean difference in arrival times between electrodes 11 and 15 was 1.13 ± 7 mSec under control conditions, increasing to 3.44 ± 12 mSec during acidification. The apparent conduction velocities were 0.053 and 0.017 m/Sec, respectively. The change in mean delays was significant at the p=0.00037 level.

The behavior seen at the central microelectrodes can be explained by postulating that an intercellular junction was positioned with electrodes 4 and 8 on one side and

electrodes 3 and 9 on the other. Under control conditions, the junction had a high enough conductance that the action potential propagated from one cell to the next with a delay that was essentially unmeasurable using the present method; during acidification, a decrease in junctional conductance introduced an appreciable delay in propagation from one cell to the next, as predicted by the Diaz model. An alternate hypothesis is that the actual conduction velocity at any point in the culture did not change, but that the pathway of conduction between the electrodes changed. In this argument, the path of conduction changes because some cells have become inexcitable and stopped conducting completely due to the intervention, while others continue to conduct normally. This results in activity propagating from one electrode to the next at the same velocity, but following a longer, circuitous route. Yet another hypothesis to explain the changes in conduction velocity is to attribute them to uniform changes in membrane properties; in this case, pathways of conduction do not change, but conduction velocity changes everywhere by about the same amount.

Uniform changes in conduction velocity alone cannot account for the time delay changes seen in this experiment. The time delay between electrodes 8 and 9 increased by a factor of about five, whereas the delay between electrodes 10 and 11 increased by only about 1.3. Changes in propagation path are more difficult to rule out, since the detailed route of propagation is unknown in these experiments. These issues will be discussed in section 5.1 after the results of all experiments have been presented.

Several more recordings of propagated activity were made from this preparation to monitor the course of arrival times as the NH_4Cl was washed out and the intracellular pH returned to normal. Recordings were made at 5, 8, 10, 20, 30, and 64 minutes following acidification by removal of NH_4Cl. Throughout, the overall order of activation at the electrodes remained as described above. Figure 4-j15.5 shows the time course of the differences in arrival times at electrode pairs (8, 9) and (10, 11) during acidification

and return to normal pH. At 5 minutes post-acidification, the arrival time difference between electrodes 8 and 9 decreased from 320 to 110 μSec, while that between electrodes 10 and 11 went from 30 to 40 μSec. Three minutes later (8 minutes post-acidification), electrode pair (8, 9) and electrode pair (10, 11) both had arrival time differences of 40 μSec. At later times, the two diverged again, but both remained below 100 μSec. Thus, the apparent conduction velocities at two locations separated by a distance smaller than the length of most cells in the preparation showed very different behavior during the recovery from acidification.

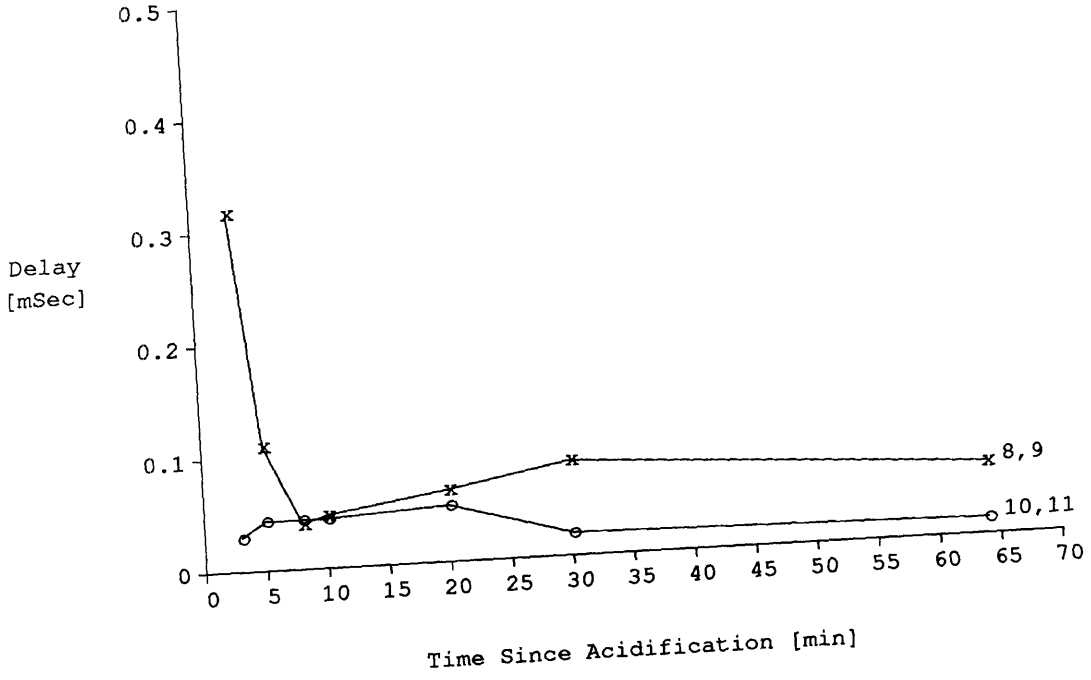

Figure 4-j15.5: Time-course of inter-electrode delays in experiment j15

4.5.2 Experiment a19

Figure 4-a19.1 shows the electrical activity under control conditions from experiment a19. The relative locations of the recording electrodes are shown in this figure. The stimulating electrode used in this experiment was located beyond the top of the diagram in figure 4-a19.1 (electrode 1 in figure 3-1). The electrode array used in this experiment had a fabrication defect which caused 6 of the microelectrodes to be shorted together (1, 2, 4, 5, 14, and 15). This defect was confirmed by the finding of low-resistance connections among these electrodes. It was also evident in the recordings from these electrodes. Two deflections were seen on each of these electrodes, the first apparently being due to arrival of activity at electrode 1, and the second being due to arrival of activity at the others, which were all physically close together. The first electrode to record an action potential after the stimulus was electrode 1, which was the recording electrode closest to the stimulating electrode in this experiment. The distance from the stimulating electrode to electrode 1 was 1000 μm. The arrival time (first deflection) at electrode 1 was 12.77 mSec for this beat. The apparent average conduction velocity in this region of the preparation was thus about .078 m/Sec. Activity next arrived at electrodes 3 and 16. The arrival time at electrode 16, which was 200 μm from electrode 1, was 13.59 mSec. The apparent conduction velocity in this part of the preparation was .24 m/Sec.

The beat shown in figure 4-a19.1 is the fourth in a series of 10 beats which were recorded under identical conditions at a stimulus rate of 1.0 Hz. The timing of the fiducial points for this series of beats is shown in figure 4-a19.2. The first beat, and to a lesser extent the second beat, were conducted slower than the remaining beats. This was probably due to the fact that each group of stimuli was initiated at a random time with respect to the spontaneous beating of the preparation, so that the first applied stimulus could easily be premature; premature stimuli may be conducted slower than usual. The

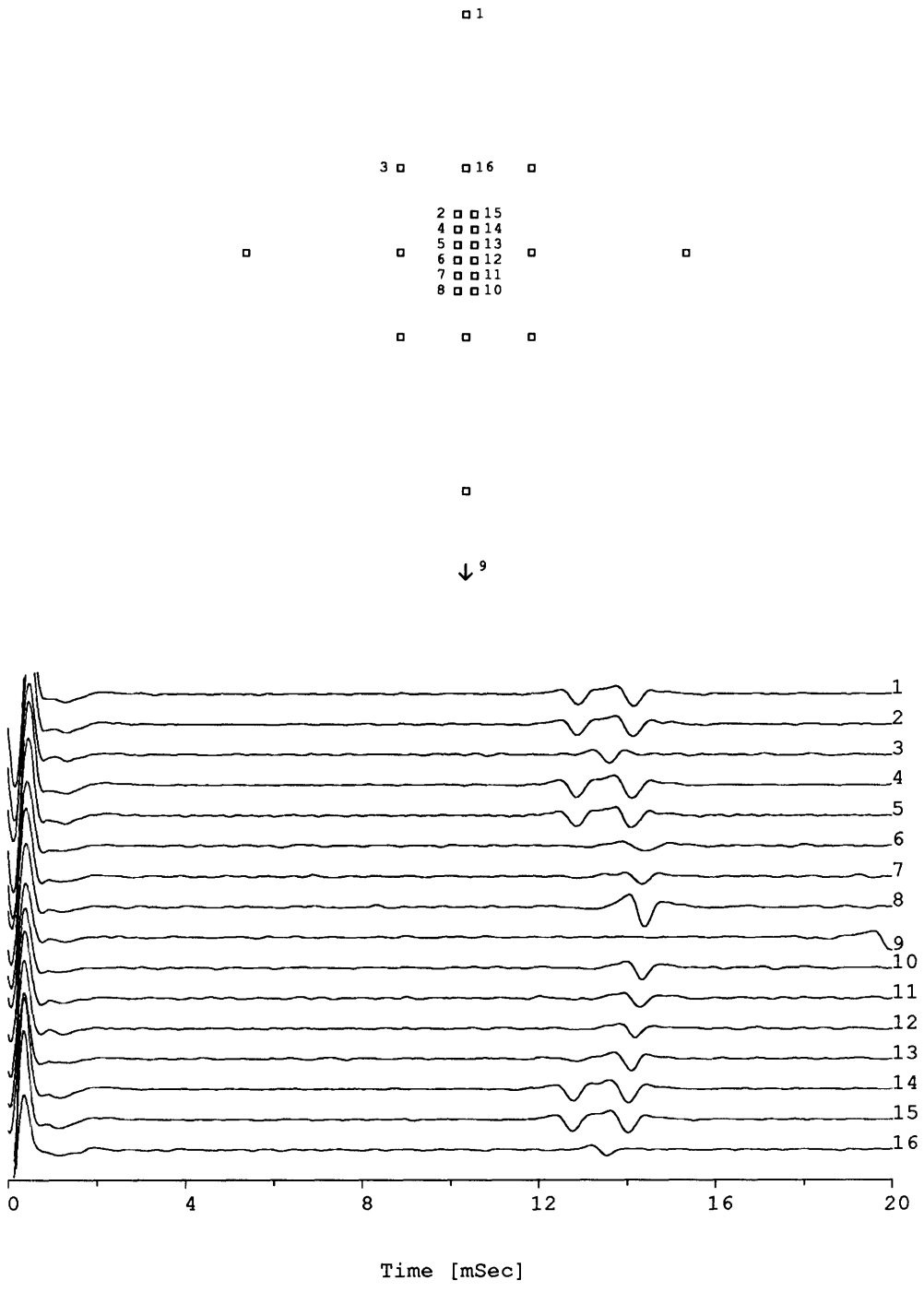

Figure 4-a19.1: A single beat under control conditions

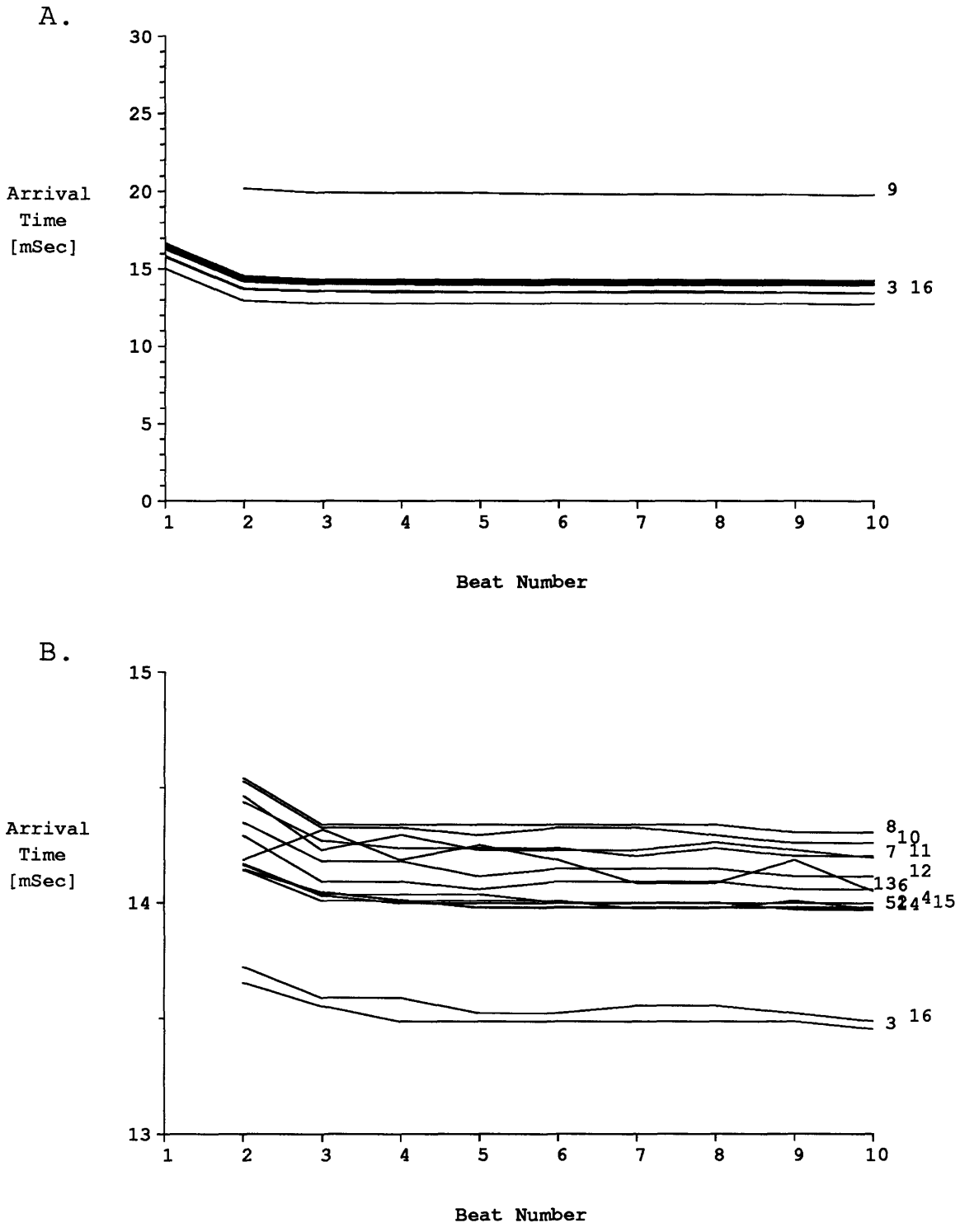

Figure 4-a19.2: Arrival times under control conditions in experiment a19

arrival times for the beat of figure 4-a19.1 are plotted in figure 4-a19.2 as the ordinates of the 4th beat. The arrival times at the central microelectrodes in this preparation spanned an interval of about 400 μSec. Since the length of the central region of microelectrodes was 100 μm, the conduction velocity in this region was approximately 0.25 m/Sec.

Figure 4-a19.3 shows the electrical activity at all of the recording electrodes in this preparation in response to a stimulus 4 minutes after cytoplasmic acidification by washout of ammonium chloride. The stimulus rate remained at 1.0 Hz. The conduction velocity in this preparation during acidification was less than it was under control conditions. The time taken for propagation from the stimulus electrode to electrode 1 was 18.87 mSec, corresponding to an apparent conduction velocity that was 68% of the velocity under control conditions. The arrival time at electrode 16 was 20.39 mSec, which corresponds to a reduction of apparent conduction velocity to about 54% of the control value in this region.

The activation arrival times for 20 beats under acidified conditions are shown in figure 4-a19.4. The beat of figure 4-a19.3 is the 8th beat in the series of figure 4-a19.4.

The sizes of the ordinate scales in figure 4-a19.4 are the same as those in figure 4-a19.2, so that the separations of the traces may be directly compared. The arrivals at the central groups of microelectrodes separated into two distinct populations, with the separation occurring in the vicinity of electrode pairs (12, 11) and (6, 7). The mean difference in arrival time between electrodes 12 and 11 increased from 90 ± 7 μSec to 370 ± 10 in going from control to acidified conditions. These time delays correspond to velocities of 0.22 and 0.054 m/Sec, respectively. The mean difference in arrival times between electrodes 6 and 7 increased from 97 ± 32 to 410 ± 15 μSec. On the two-sided t-test, this change was significant with a p-value of 0.00014. For comparison, consider

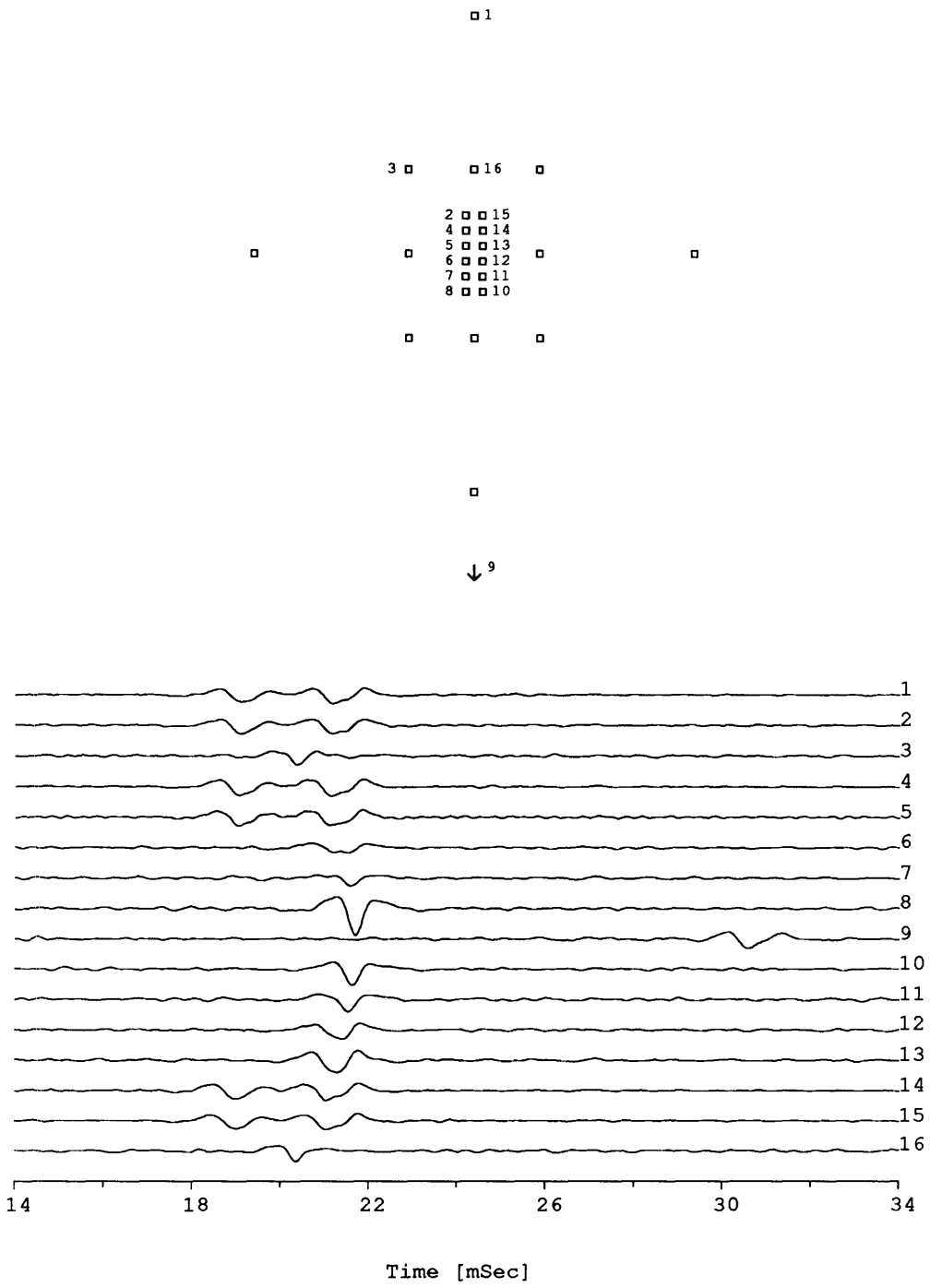

Figure 4-a19.3: A single beat under acidified conditions

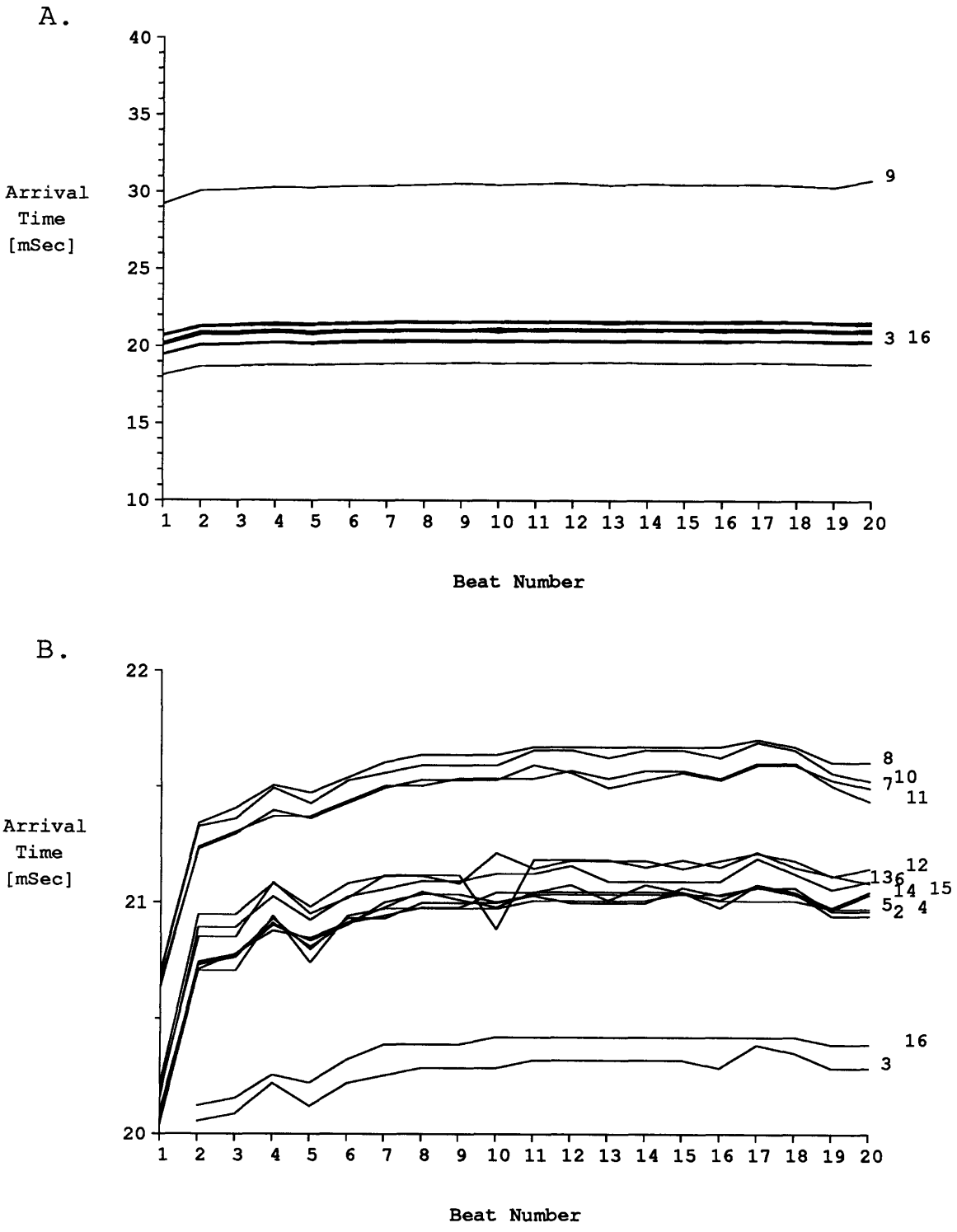

Figure 4-a19.4: Arrival times under acidified conditions in experiment a19

the arrival times at electrodes 11 and 10, which had the same separation as electrodes 12 and 11. The mean difference in arrival time between electrodes 11 and 10 went from 76 ± 7 μSec to 80 ± 5 in going from control to acidified conditions (p=0.72). These delays correspond to velocities of .26 and .25 m/Sec, respectively. Aside from the large delay that was noted in the central group of microelectrodes, other delays seem to have been in proportion to the overall decrease in conduction velocity in this preparation. The mean difference in arrival time between electrodes 16 and 2 increased from 440 ± 7 to 610 ± 8 μSec, corresponding to a 38% decrease in conduction velocity. While the difference in arrival times at electrodes 3 and 16 increased slightly, it is quite likely that given their locations and the direction of propagation, activity did not spread from electrode 3 to electrode 16 in any case.

Only one more series of recordings of propagated activity was obtained from this preparation, 30 minutes after washout of NH_4Cl. The arrival time differences during this series were 130 ± 24 μSec between electrodes 12 and 11, 150 ± 34 μSec between electrodes 6 and 7, and 100 ± 17 μSec between electrodes 11 and 10. Figure 4-a19.5 shows the time course of the differences in arrival times at electrode pairs (12, 11) and (11, 10) during acidification and return to normal pH.

Thus, as in the case of experiment j15, this preparation had one location in the central region of microelectrodes which had a normal conduction velocity under control conditions and developed a reversible long delay after acidification. This result could be explained by the existence of an intercellular junction at this location, or possibly by the development of circuitous paths of conduction with no change in velocity. However, it does not appear possible to account for the result by postulating a uniform decrease in conduction velocity throughout the preparation.

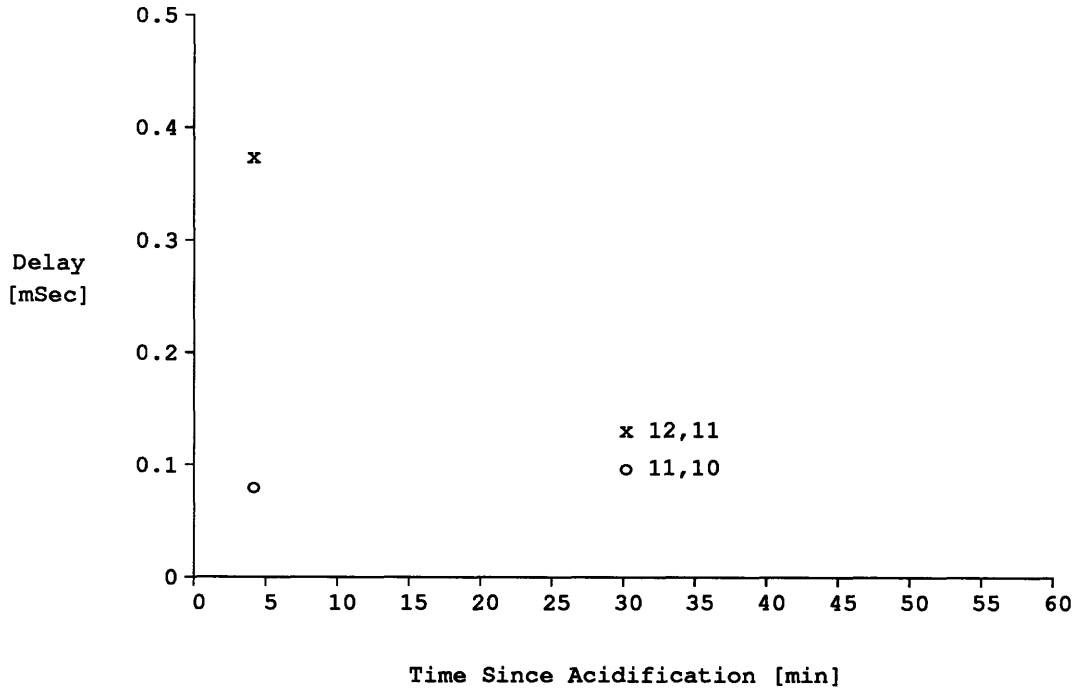

Figure 4-a19.5: Time-course of inter-electrode delays in experiment a19

4.5.3 Experiment s5

Figure 4-s5.1 shows the electrical activity under control conditions from experiment s5.

The stimulating electrode used in this experiment was located beyond the top of the diagram in figure 4-s5.1 (electrode 1 in figure 3-1). The stimulus was delivered at time zero on the time axis. The first electrode to record an action potential after the stimulus was electrode 16, which was located 500 μm from the stimulating electrode in this experiment. The arrival time at electrode 16 was 6.46 mSec for this beat. The apparent average conduction velocity in this region of the preparation was thus about .077 m/Sec. Activity next arrived at electrode 1, which was 500 μm from electrode 16, at 8.93 mSec. The apparent conduction velocity in this part of the preparation was 0.20 m/Sec.

The beat shown in figure 4-s5.1 is the fourth in a series of 20 beats which were recorded under control conditions at a stimulus rate of 2.6 Hz. The timing of the fiducial points for the first 10 of these beats is shown in figure 4-s5.2. The arrival times for the beat of figure 4-s5.1 are plotted in figure 4-s5.2 as the ordinates of the 4th beat. The distance from electrode 14 to electrode 7 was about 100 μm, and the mean difference in arrival times at these two electrodes was 300 μSec under control conditions, corresponding to an apparent conduction velocity of about 0.33 m/Sec.

Figure 4-s5.3 shows the electrical activity at all of the recording electrodes in this preparation in response to a stimulus 5 minutes after cytoplasmic acidification by washout of ammonium chloride. The stimulus rate was reduced to 1.3 Hz to obtain conduction on successive stimuli. Conduction was slower during acidification than it was under control conditions in this preparation. The time taken for propagation from the stimulus electrode to electrode 16 was 10.72 mSec, corresponding to an apparent conduction velocity that was 60% of the velocity under control conditions. There was no

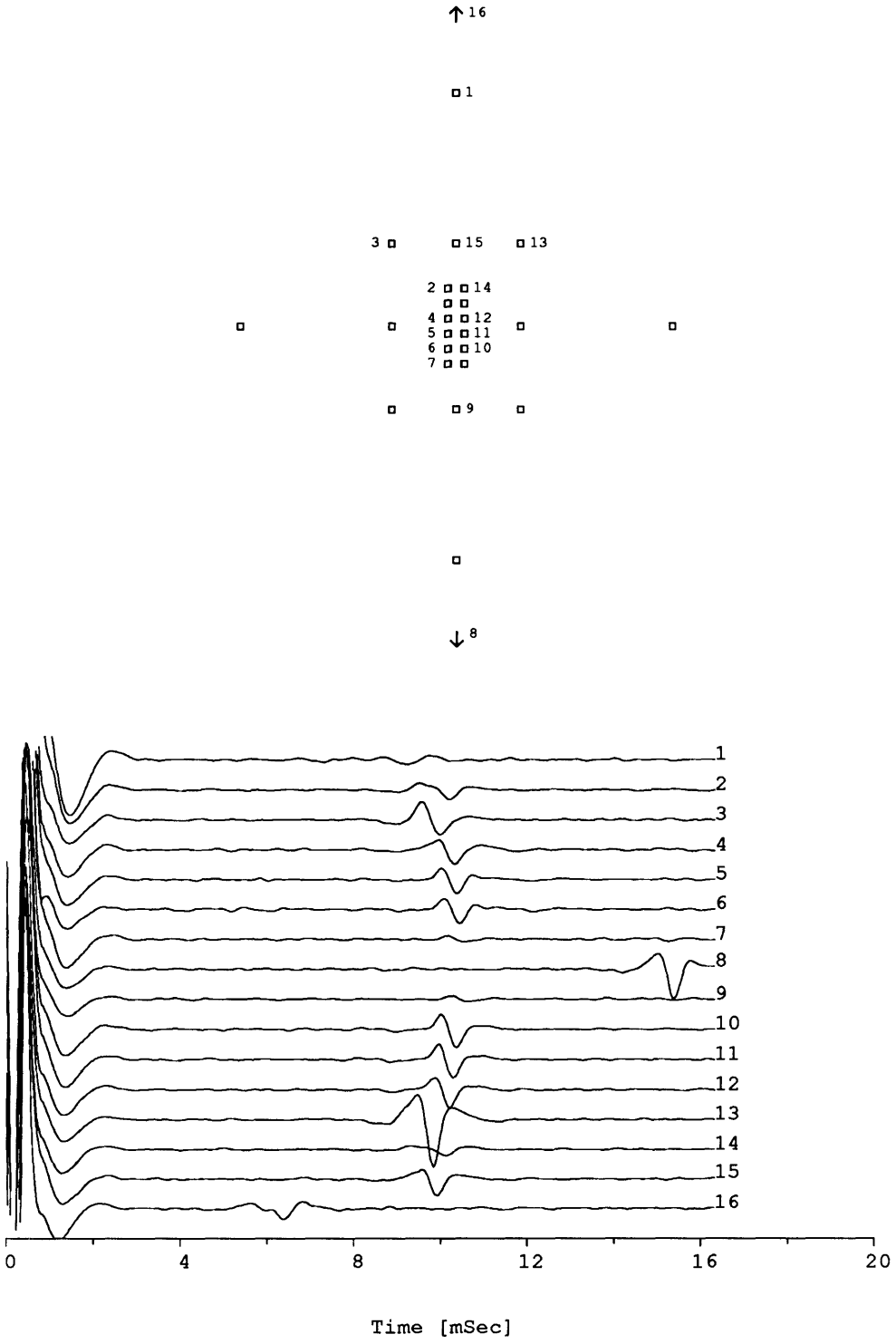

Figure 4-s5.1: A single beat under control conditions

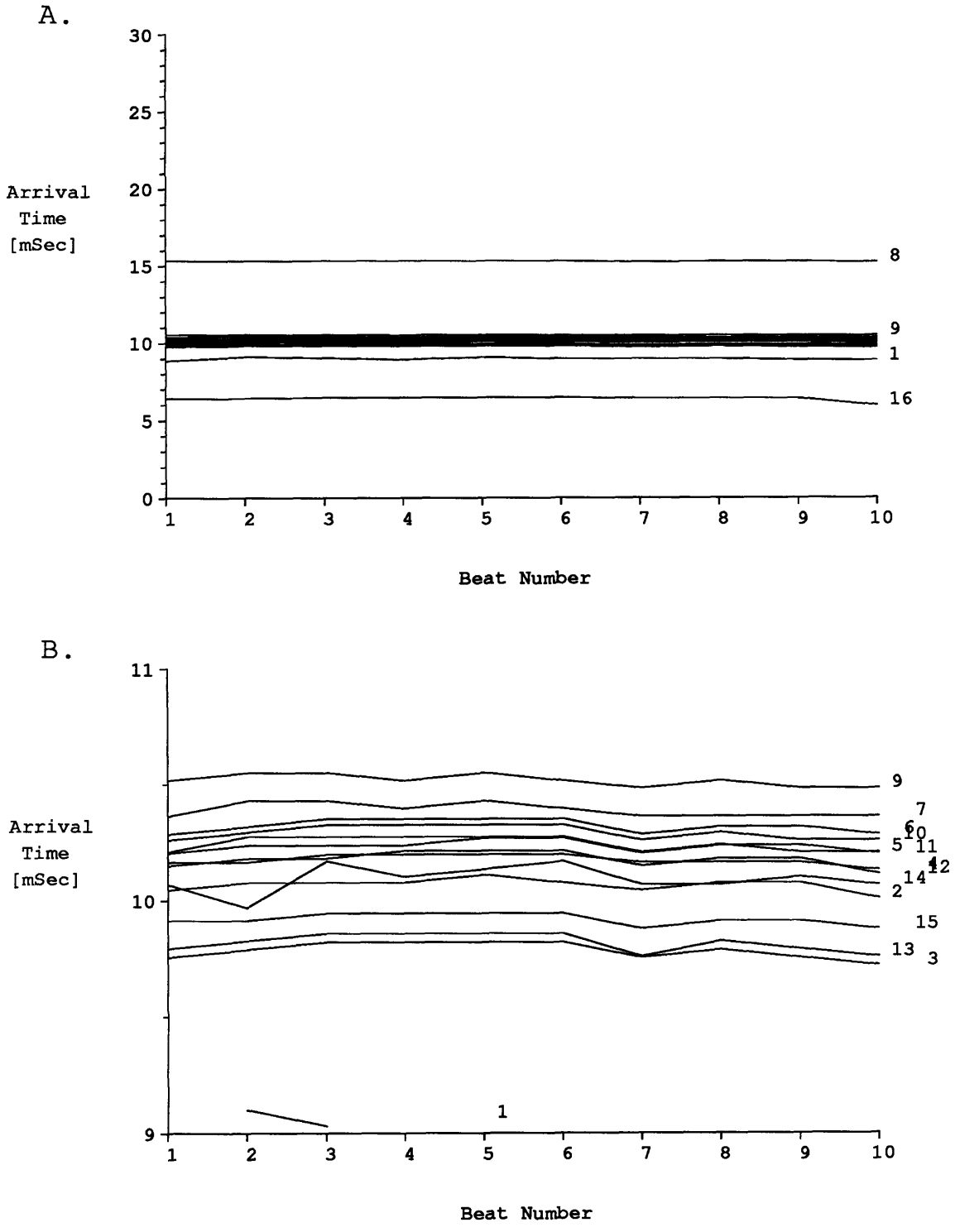

Figure 4-s5.2: Arrival times under control conditions in experiment s5

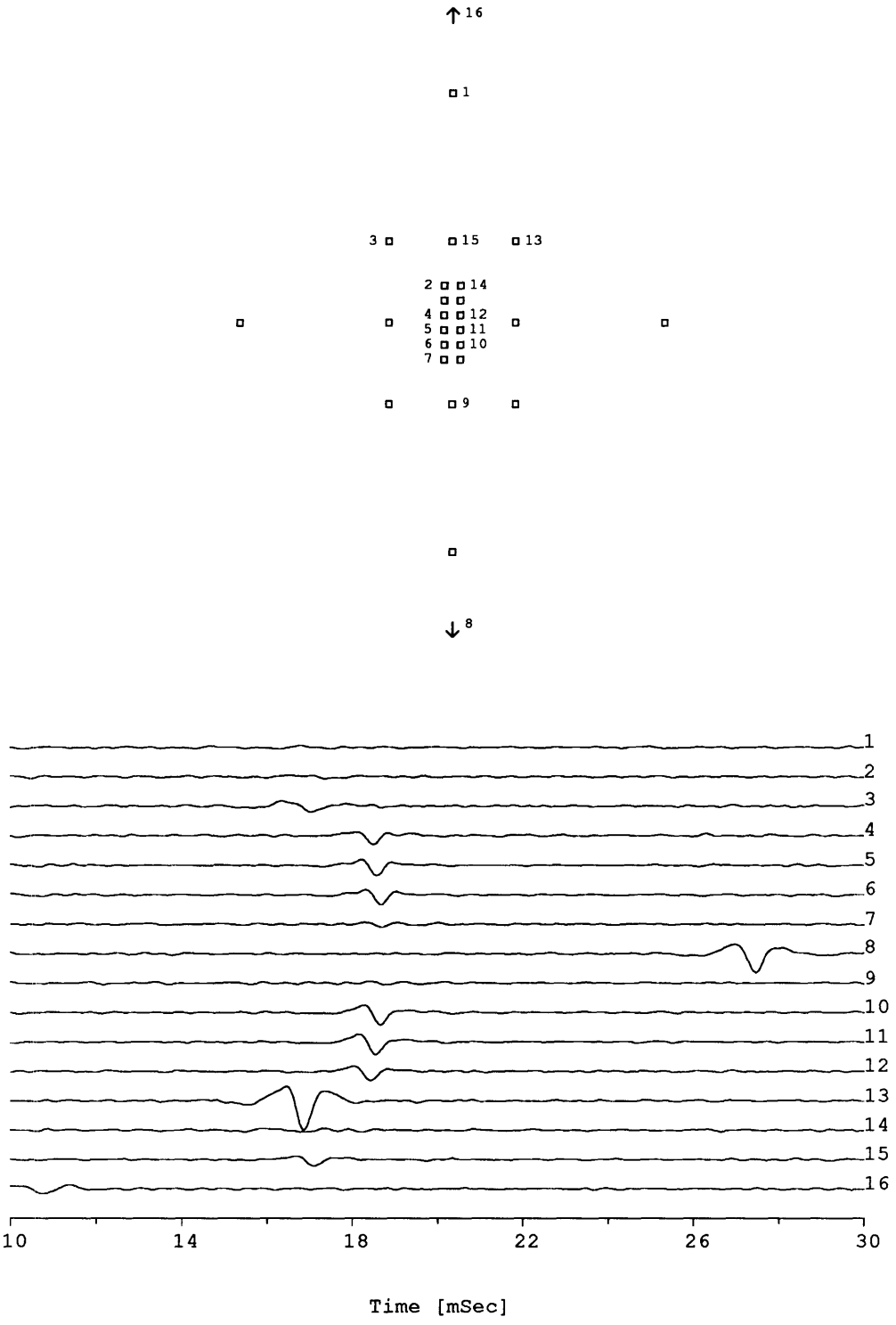

Figure 4-s5.3: A single beat under acidified conditions

visible activity at electrodes 1 and 2 under acidified conditions.

Only the first 7 of the 10 stimuli applied in this series initiated conducted action potentials. The activation arrival times are shown in figure 4-s5.4. The last conducted beat in this series was conducted more slowly than the first 6. This slowing of conduction may have been an indication of a developing conduction block which prevented the subsequent stimuli from being conducted. Note that conduction did not slow distal to electrode 16; the added delay occurred before this point. The beat of figure 4-s5.3 is the 6th beat in the series of figure 4-s5.4.

Figure 4-s5.4b shows the order of arrival times at the central microelectrodes under acidified conditions in detail. (The last beat is off-scale.) The arrivals at the central group of microelectrodes were only slightly more spread out than they were under control conditions. The mean difference between arrivals at electrodes 14 and 7 increased from 300 ± 10 μSec under control conditions to 410 ± 20 μSec, which was roughly proportional to the average overall decrease in conduction velocity. However, the delay between the arrivals at the central electrodes and the arrivals at electrodes 3, 13, and 15 dramatically increased. The mean difference between arrivals at electrodes 15 and 14 increased from 180 ± 9 μSec under control conditions to 1140 ± 15 μSec at 5 minutes following acidification ($p=1.67e-7$). The corresponding apparent conduction velocities were 0.33 and 0.053 m/Sec, respectively. This 6-fold decrease in conduction velocity is out of proportion to the average slowing seen in this preparation during acidification.

Two more series of recordings were obtained from this preparation. At 9 minutes following acidification, the mean difference between electrodes 15 and 14 was 860 ± 110 μSec. At 15 minutes following acidification it was 170 ± 43 μSec. No other disproportionate delays occurred at either of these times. Figure 4-s5.5 shows the time course of the differences in arrival times at electrode pair (14, 15) during acidification

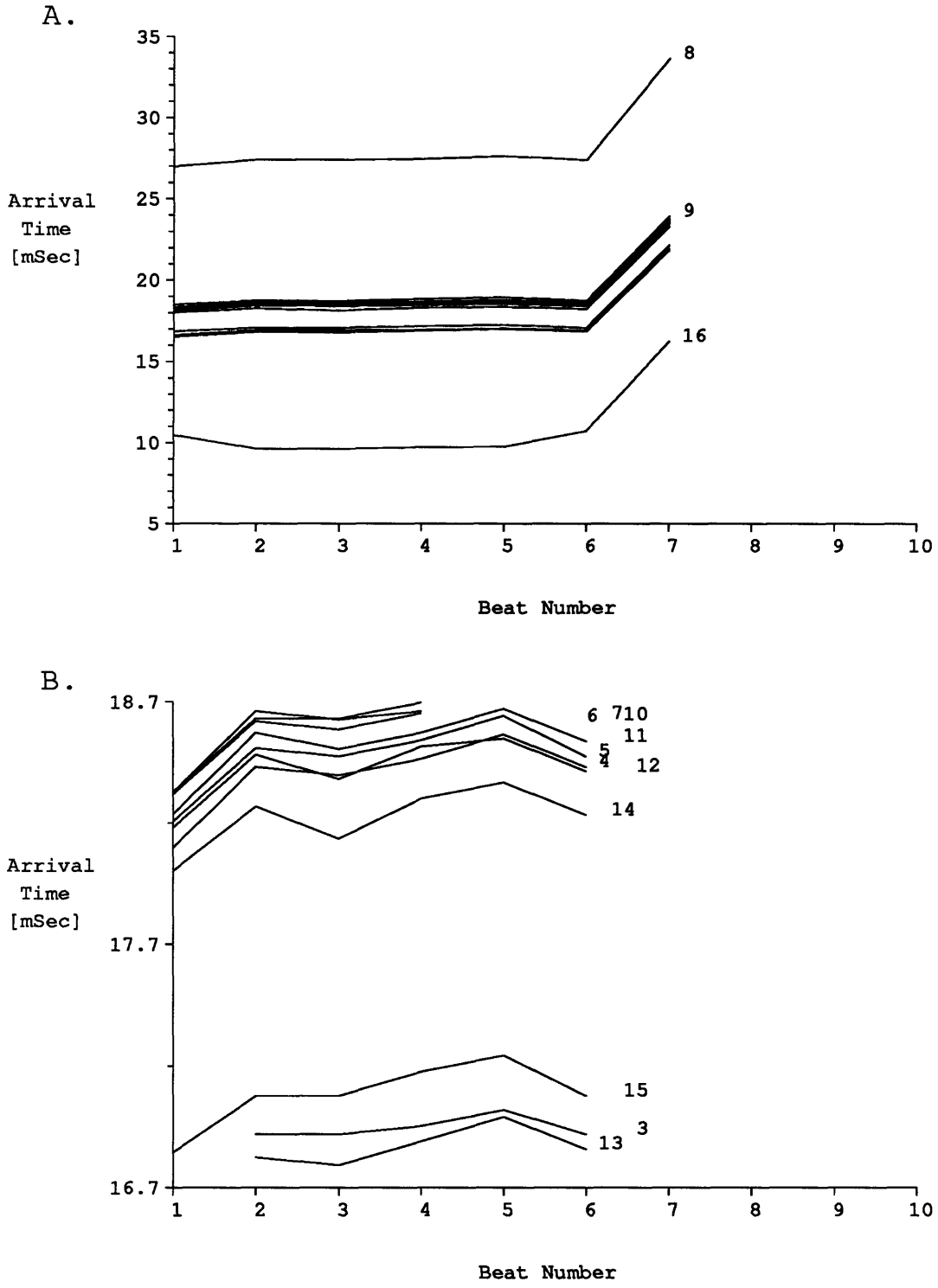

Figure 4-s5.4: Arrival times under acidified conditions in experiment s5

and return to normal pH. For comparison, the arrival time differences at electrodes (12, 11) are also shown. The latter showed no appreciable change with recovery from acidification.

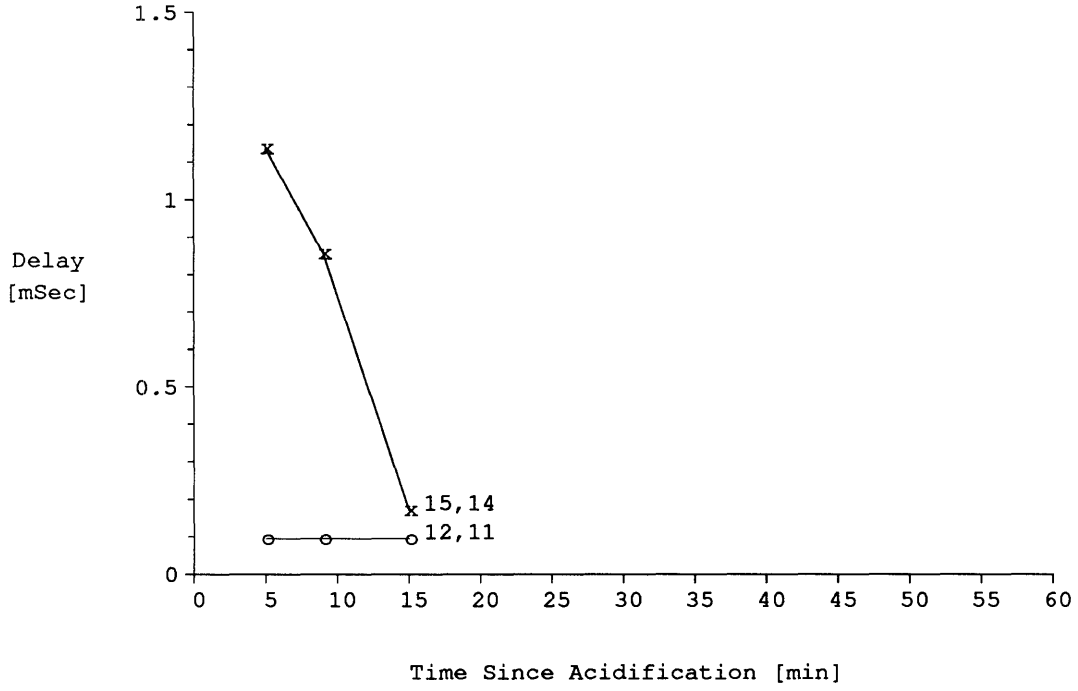

Figure 4-s5.5: Time-course of inter-electrode delays in experiment s5

4.5.4 Experiment d8

Figure 4-d8.1 shows the electrical activity under control conditions from experiment d8.

The stimulating electrode used in this experiment was located beyond the top of the diagram in figure 4-d8.1 (electrode 1 in figure 3-1). The first electrode to record an action potential after the stimulus was electrode 16, which was located 500 μm from the stimulating electrode in this experiment. The arrival time at electrode 16 was 2.86 mSec for this beat. The apparent average conduction velocity in this region of the preparation was thus about .17 m/Sec. Activity next arrived at electrode 15, which was 700 μm from electrode 16, at 5.15 mSec. The apparent conduction velocity in this part of the preparation was 0.31 m/Sec.

Twenty stimuli were applied to this preparation under control conditions, of which the last 15 were conducted. The beat shown in figure 4-d8.1 is the 11th in the series of 20 beats which were recorded under identical conditions at a stimulus rate of 2.0 Hz. The timing of the fiducial points for the last 10 beats of this series is shown in figure 4-d8.2. The signals on electrodes 5 and 8 were too small to allow reliable detection of the fiducial points and so were excluded from the analysis. The arrival times for the beat of figure 4-d8.1 are plotted in figure 4-d8.2 as the ordinates of the first beat. Under control conditions, the mean time for conduction across the central region of microelectrodes from electrode 14 to 9 was 170 ± 5 μSec, corresponding to a conduction velocity of 0.47 m/Sec. The propagation time from electrode 9 to 7 was 340 ± 13 μSec, corresponding to a conduction velocity of 0.24 m/Sec.

Figure 4-d8.3 shows the electrical activity at all of the recording electrodes in this preparation in response to a stimulus 5 minutes after cytoplasmic acidification by washout of ammonium chloride. The stimulus rate remained at 2.0 Hz. Conduction was

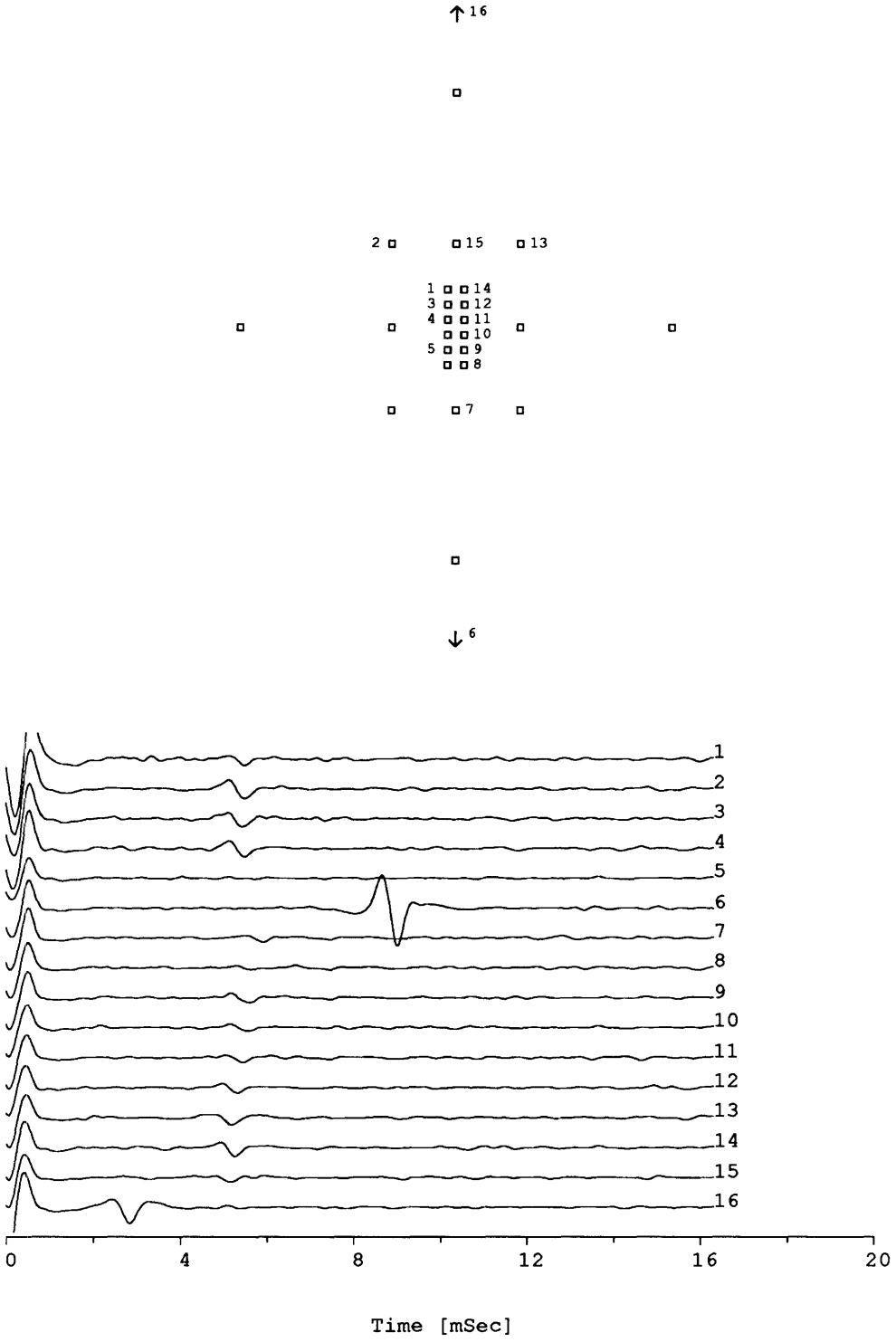

Figure 4-d8.1: A single beat under control conditions

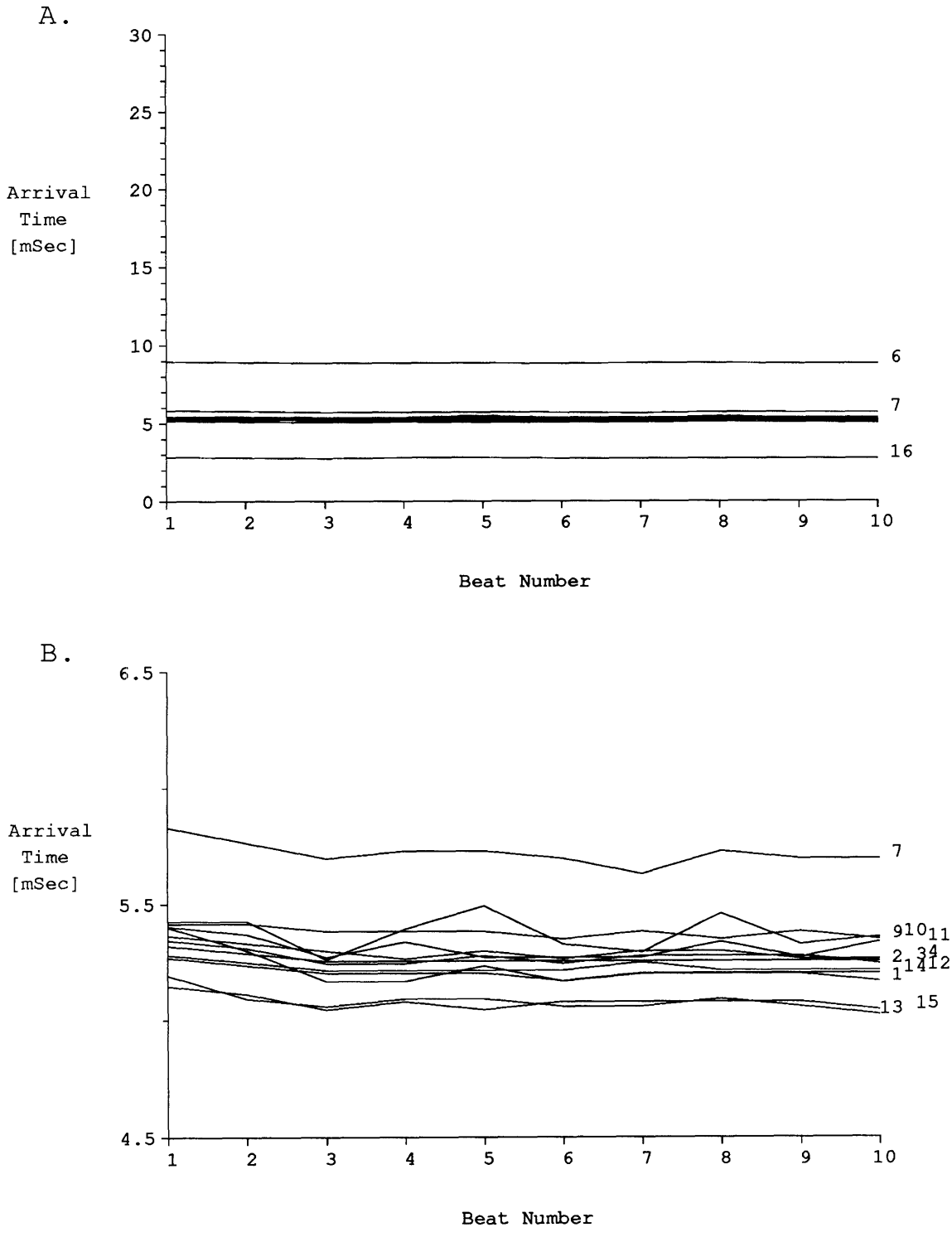

Figure 4-d8.2: Arrival times under control conditions in experiment d8

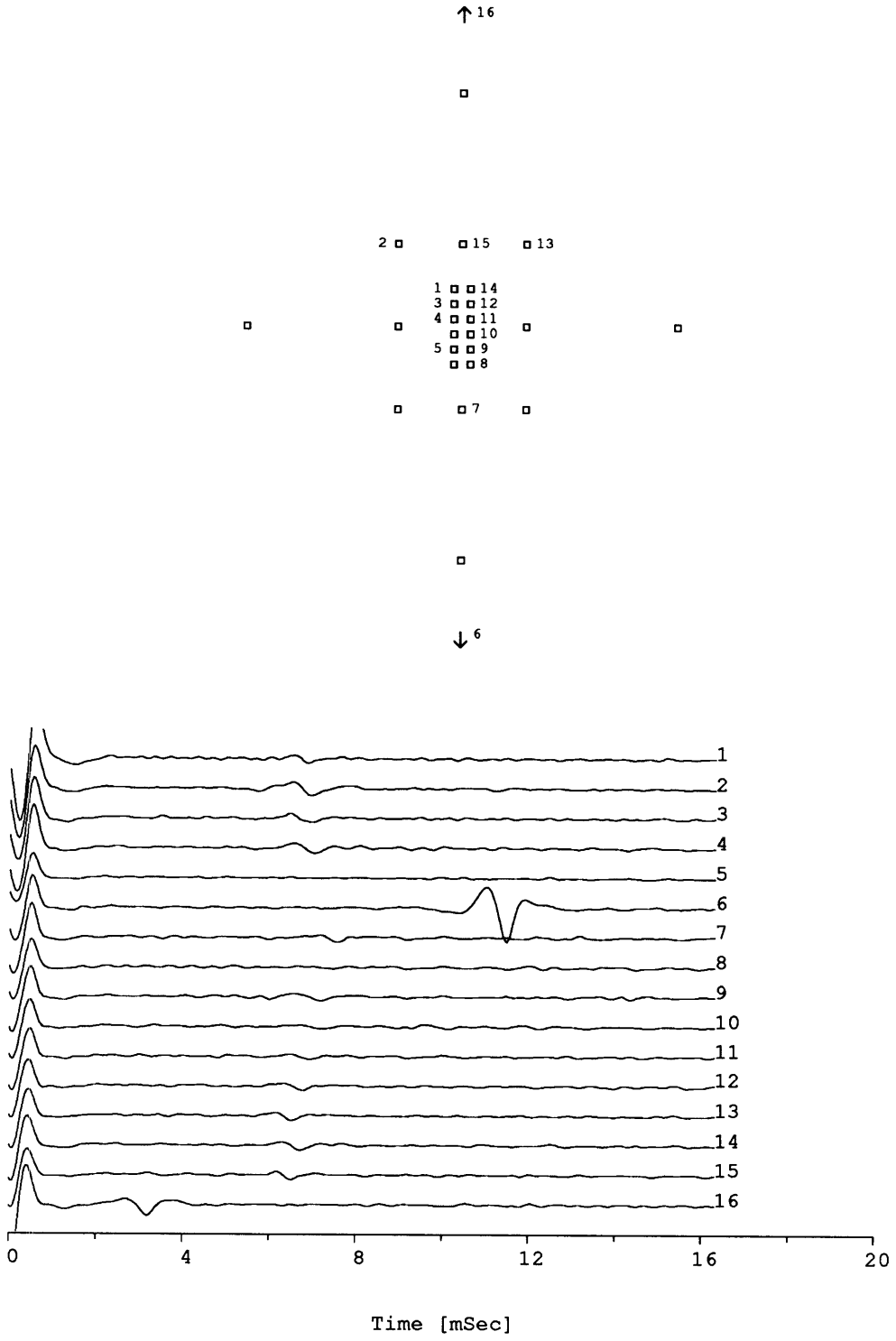

Figure 4-d8.3: A single beat under acidified conditions

slower during acidification than it was under control conditions in this preparation. The time taken for propagation from the stimulus electrode to electrode 16 was 3.22 mSec, corresponding to an apparent conduction velocity that was 89% of the velocity under control conditions. The arrival time at electrode 1 was 6.77 mSec, which corresponds to a 70% reduction of apparent conduction velocity in this region.

The activation arrival times at 5 minutes post-acidification for the last 10 beats of the series of 20 are shown in figure 4-d8.4. The beat of figure 4-d8.3 is the 1st beat in figure 4-d8.4.

Inspection of the arrival times under acidification revealed no obviously large delay times as seen in the experiments previously discussed. Several of the arrival time traces showed increased variability attributable to the reduction in signal to noise ratio. Examination of the delays between nearest neighbor electrodes revealed one which was out of proportion to the overall decrease in conduction velocity in this culture. The arrival time delay between electrodes 10 and 11 increased from 63 ± 20 to 150 ± 39 μSec in going from control to acidified conditions, corresponding to conduction velocities of 0.32 and 0.13 m/Sec. However, the SNR at these electrodes was low (mean 3.0 for electrode 10 under control conditions, decreasing to 1.8 under acidification; for electrode 11, means 2.4 and 2.7, respectively). The two-sided t-test for equality of means yielded a p-value of 0.12. Thus, while these results may suggest a disproportionately increased delay time under acidification, they are not statistically significant, possibly due to the poor signal to noise ratio in this experiment.

The time course of the difference in arrival times at this electrode pair during recovery from acidification is shown in figure 4-d8.5. The data from electrode pair (3, 4) are also shown for comparison. Unlike the previously shown experiments, no systematic decrease in arrival time differences is seen during recovery from acidification.

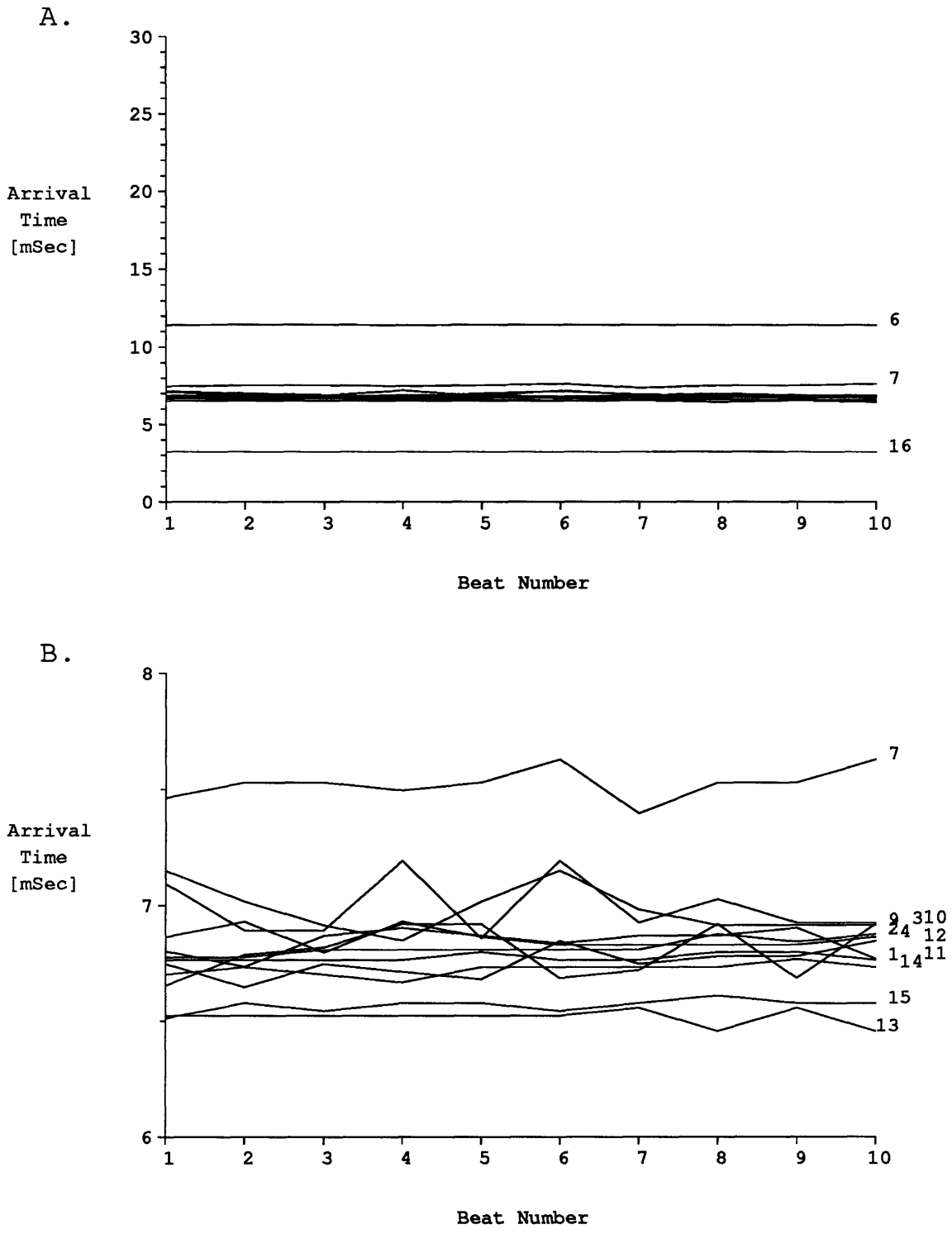

Figure 4-d8.4: Arrival times under acidified conditions in experiment d8

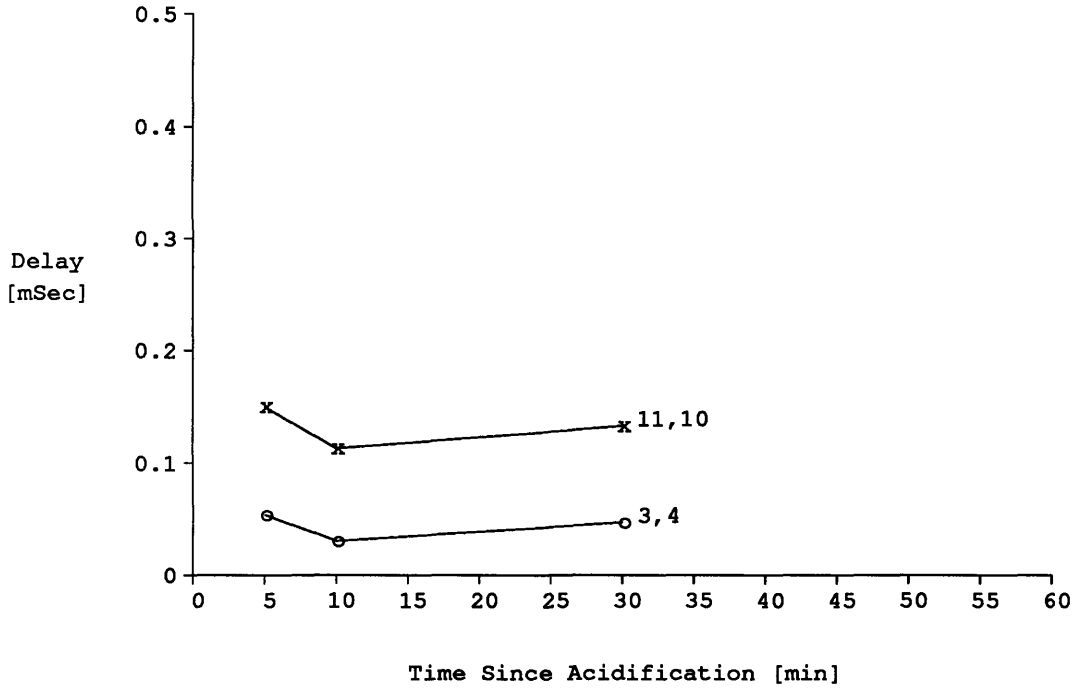

Figure 4-d8.5: Time-course of inter-electrode delays in experiment d8

4.5.5 Experiment d11

Figure 4-d11.1 shows the electrical activity under control conditions from another experiment, along with the relative locations of the recording electrodes. An equipment malfunction prevented the recording of activity from channels 1, 2, and 3, so those channels do not appear in these plots.

The stimulating electrode used in this experiment was located beyond the top of the diagram in figure 4-d11.1 (electrode 1 in figure 3-1). The first electrode to record an action potential after the stimulus was electrode 16, which was located 500 μm from the stimulating electrode in this experiment. The arrival time at electrode 16 was 3.06 mSec for this beat. The apparent average conduction velocity in this region of the preparation was thus about .16 m/Sec. Activity next arrived at electrode 15, which was 700 μm from electrode 16, at 6.61 mSec. The apparent conduction velocity in this part of the preparation was 0.20 m/Sec.

The beat shown in figure 4-d11.1 is the 6th in a series of 20 beats which were recorded under identical conditions at a stimulus rate of 3.3 Hz. The timing of the fiducial points for ten of these beats is shown in figure 4-d11.2. The arrival times for the beat of figure 4-d11.1 are plotted in figure 4-d11.2 as the ordinates of the 6th beat. The distance from electrode 14 to electrode 8 was 100 μm, and the mean difference in arrival times at these two electrodes was 191 μSec under control conditions, corresponding to an apparent average conduction velocity of about 0.52 m/Sec. There was a relatively even progression of activation from electrodes 14 to 12 to 10 and then to 8. Electrodes 13 and 11, which were located 85 μm from the center of the array, had activation arrival times which were later than the neighboring central electrodes 15 and 10, respectively. This indicates that the propagation of activity across the central region of the array was not in the form of a straight wavefront travelling parallel to the central axis. This might have

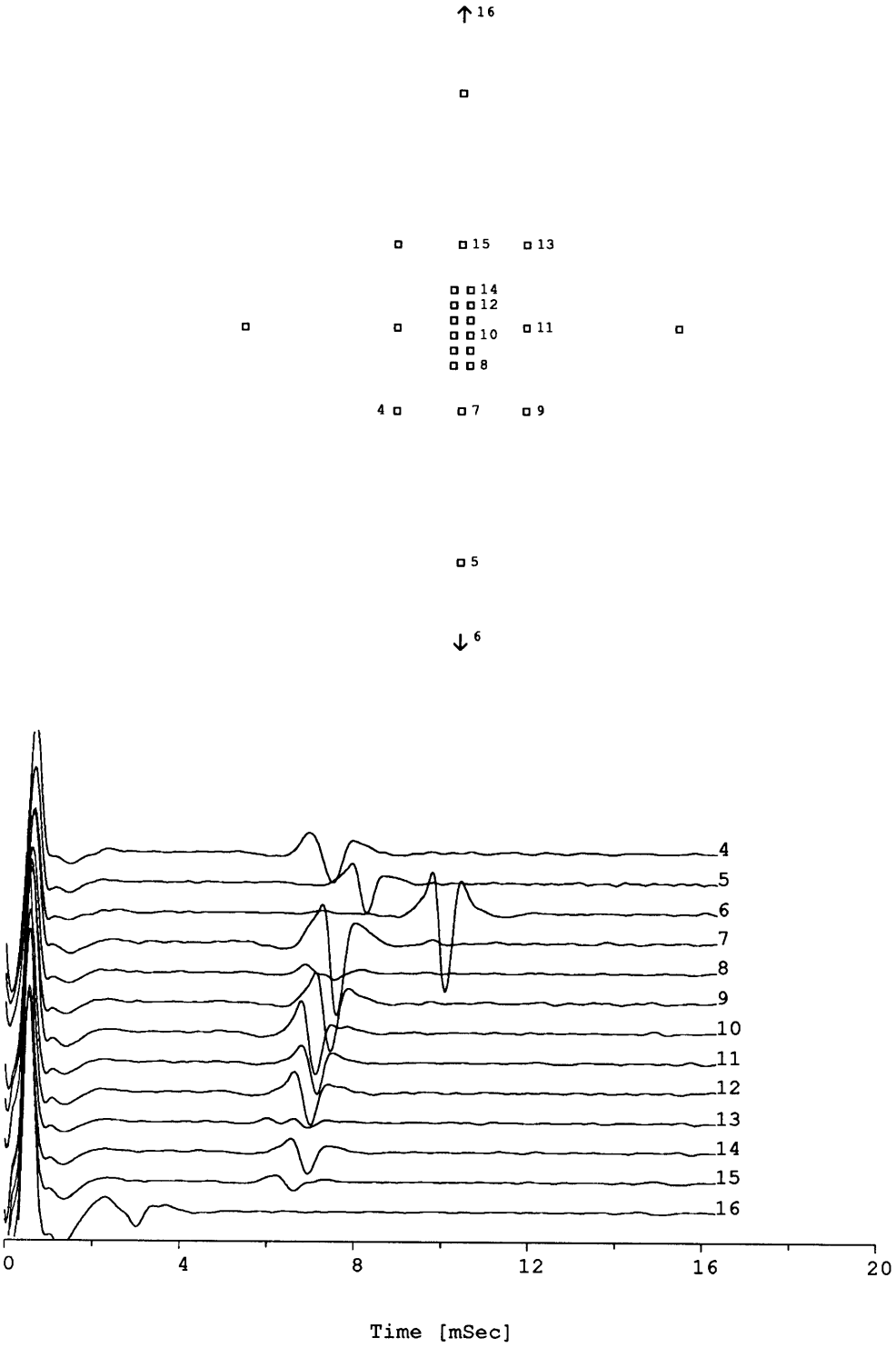

Figure 4-d11.1: A single beat under control conditions

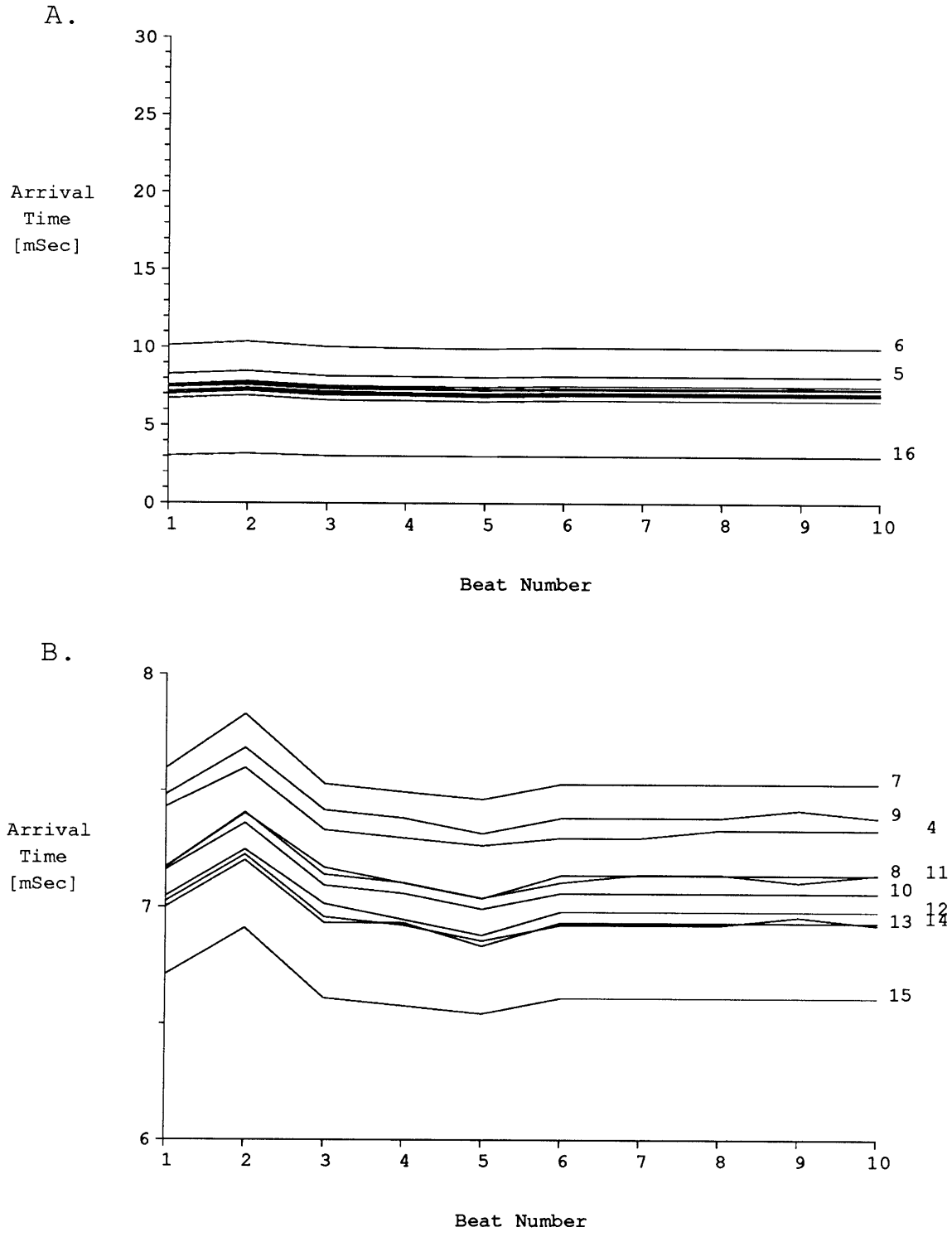

Figure 4-d11.2: Arrival times under control conditions in experiment d11

been the result of a straight wavefront travelling at some angle to the central axis. However, if this held true over the entire region, activation at electrode 7 would be expected to precede activation at electrode 9, which was not the case. An alternative hypothesis, which can explain the data, is that the wavefront propagated at different rates and directions in different locations. However, arrival time data from many more points would be needed to be able to determine the actual path of propagation under this hypothesis.

Figure 4-d11.3 shows the electrical activity at all of the recording electrodes in this preparation in response to a stimulus 3 minutes after cytoplasmic acidification by washout of ammonium chloride. The stimulus rate had to be increased to 3.8 Hz to prevent the culture from being paced by a fast endogenous pacemaker which emerged spontaneously. Conduction was slower during acidification than it was under control conditions in this preparation. Activation of the central region took place about 11 mSec following the stimulus, versus about 7 mSec under control conditions. The time taken for propagation from the stimulus electrode to electrode 16 was 4.82 mSec, corresponding to an apparent conduction velocity that was 63% of the velocity under control conditions. The mean difference in arrival times from electrode 14 to electrode 8 increased to 270 ± 24 μSec under these conditions, corresponding to an apparent average conduction velocity of about 0.37 m/Sec, or 70% of control.

Only 2 of the 20 stimuli applied at 3 minutes post-acidification initiated conducted action potentials. The activation arrival times for these two beats are shown in figure 4-d11.4. The beat of figure 4-d11.3 is the first conducted response in the series of figure 4-d11.4.

The pattern of activation at the recording electrodes during this series of beats was basically the same as it was under control conditions. Although the interelectrode delays

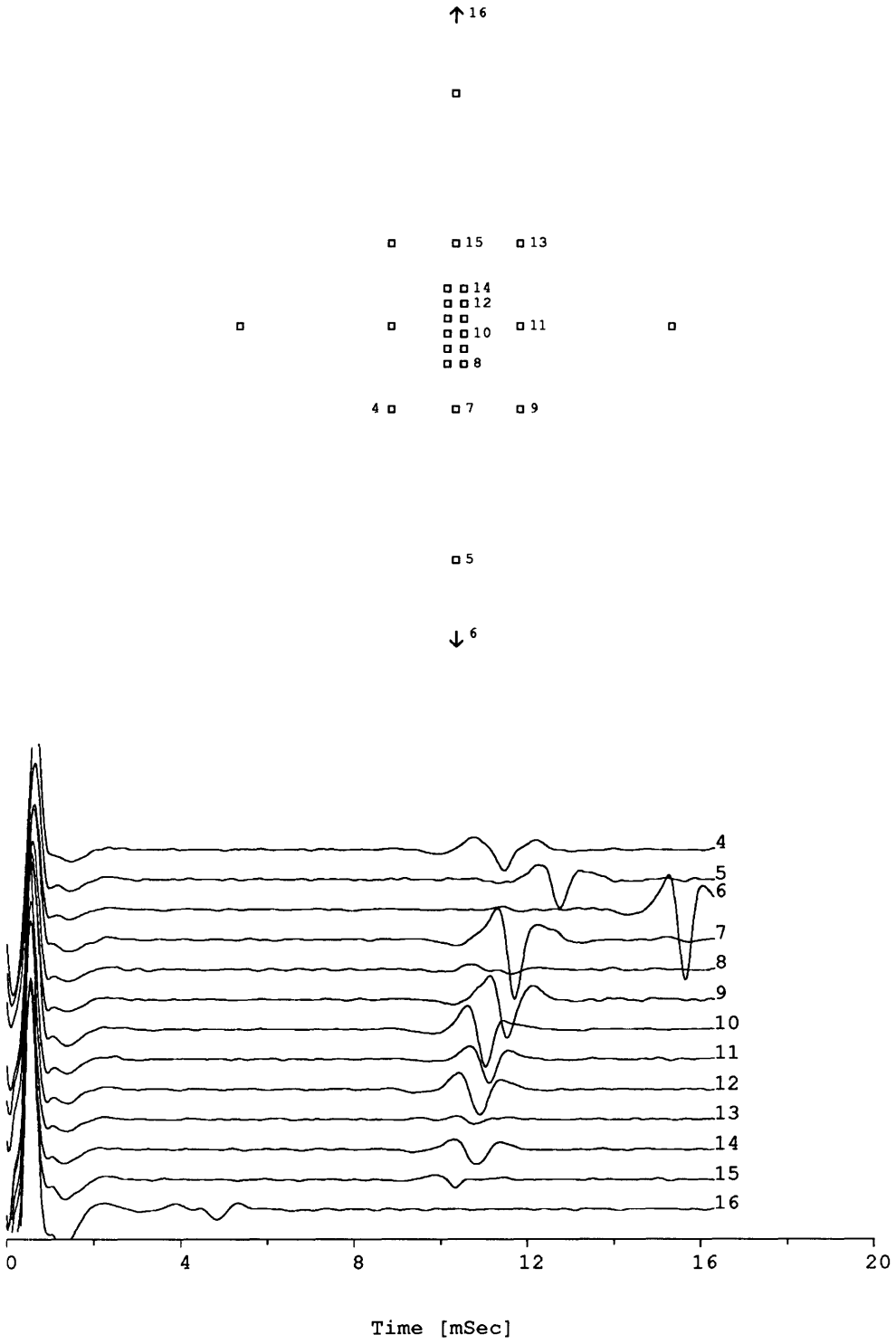

Figure 4-d11.3: A single beat under acidified conditions

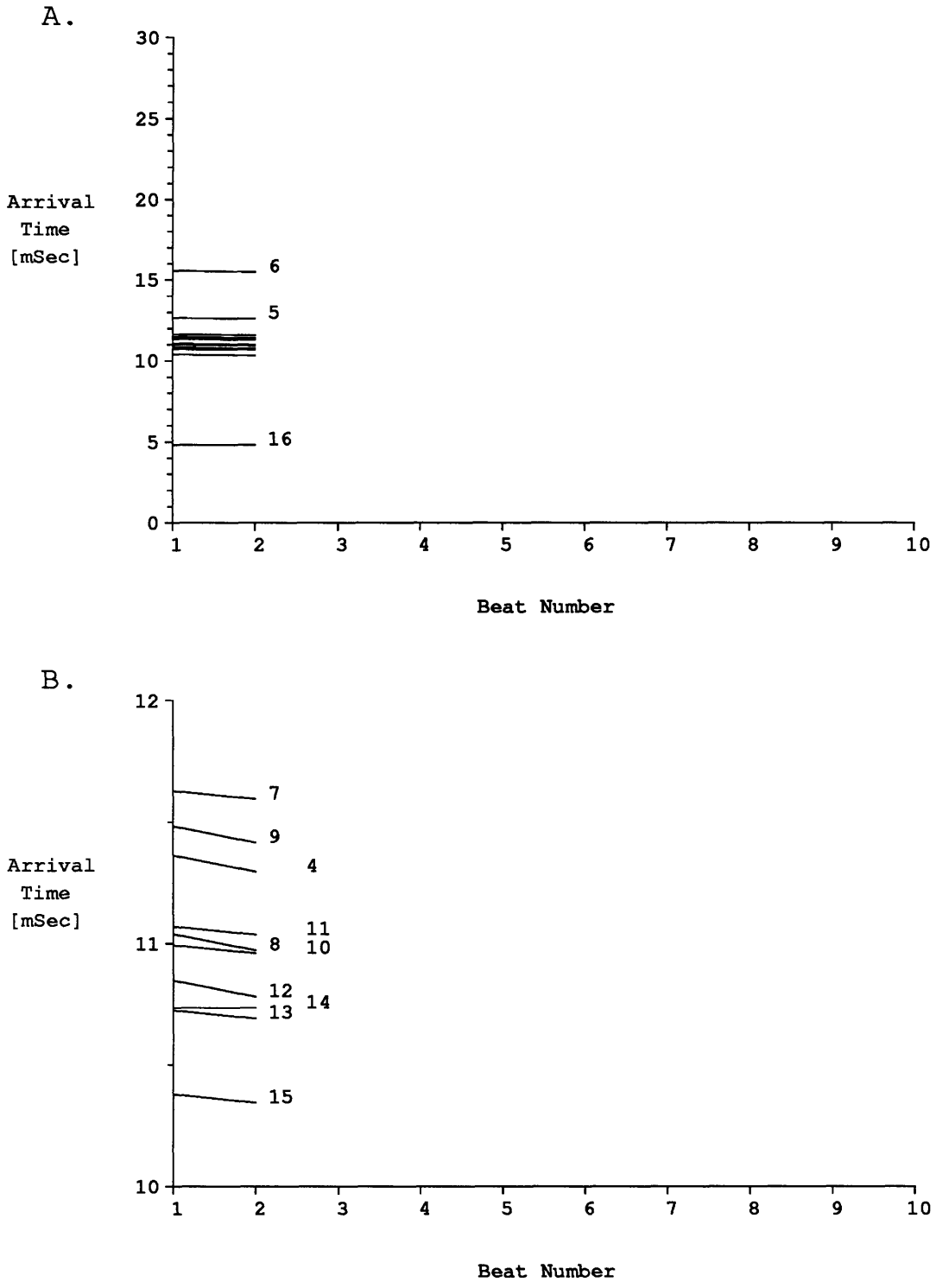

Figure 4-d11.4: Arrival times under acidified conditions in experiment d11

increased, they did so evenly, with no evidence of disproportionate delays at any location. For example, t-tests comparing the mean differences in arrival times at electrode pairs (12,14) and (10,12) before and after the interventions yielded p-values of 0.52 and 0.18, respectively. Although only two beats were conducted, the SNR remained high enough following the intervention that the variability in the arrival time estimates should be small.

The time course of the difference in arrival times at these electrode pairs during recovery from acidification is shown in figure 4-d11.5. No systematic trend is seen in these data during recovery from acidification.

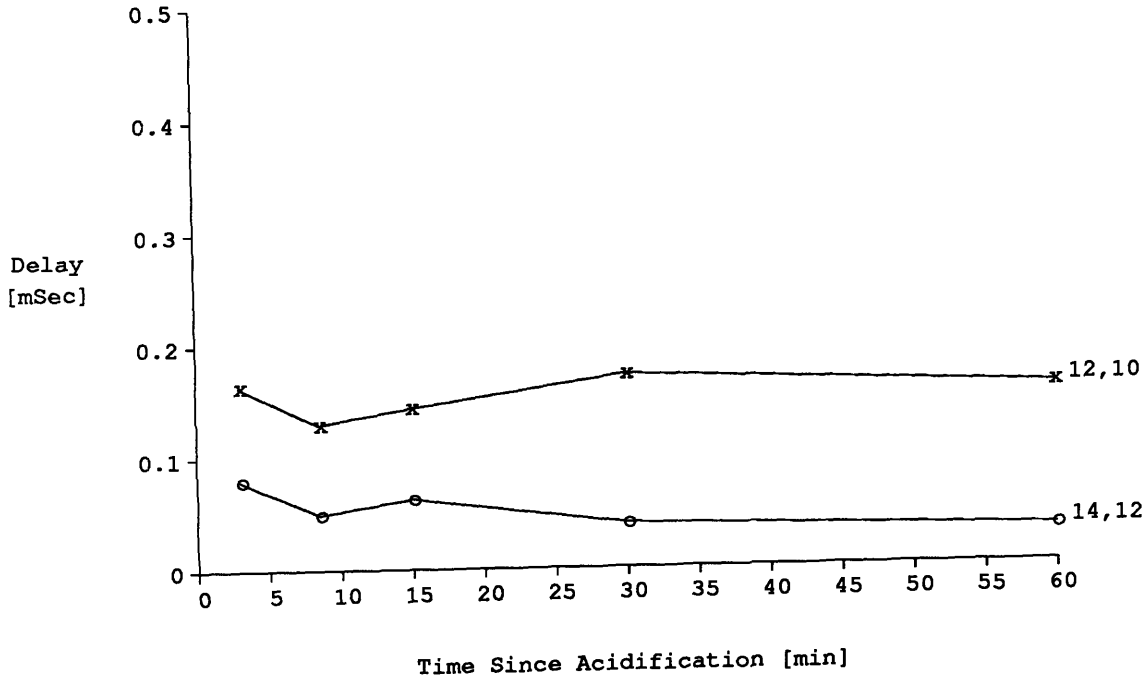

Figure 4-d11.5: Time-course of inter-electrode delays in experiment d11

4.5.6 Experiment d15

Figure 4-d15.1 shows the electrical activity under control conditions from experiment d15, along with the relative locations of the recording electrodes.

The stimulating electrode used in this experiment was located beyond the top of the diagram in figure 4-d15.1 (electrode 1 in figure 3-1). The first electrode to record an action potential after the stimulus was electrode 16, which was located 500 μm from the stimulating electrode in this experiment. The arrival time at electrode 16 was 3.89 mSec for this beat. The apparent average conduction velocity in this region of the preparation was .13 m/Sec. Activity was too small to be reliably detected at electrode 15. The next definite arrival of activity was at the central microelectrodes, with electrodes 14 and 1 seeing arrivals at 14.87 and 14.90 mSec, respectively. The apparent average conduction velocity in this part of the preparation was 0.069 m/Sec.

The beat shown in figure 4-d15.1 is the sixth in a series of 20 beats which were recorded under identical conditions at a stimulus rate of 3.4 Hz. The timing of the fiducial points for this series of beats is shown in figure 4-d15.2. The arrival times for the beat of figure 4-d15.1 are plotted in figure 4-d15.2 as the ordinates of the 2nd beat. The distance from electrode 14 to electrode 9 was 100 μm, and the mean difference in arrival times at these two electrodes was 310 ± 6 μSec under control conditions, corresponding to an apparent average conduction velocity of about 0.32 m/Sec. There was a fairly even progression of activation across the central region of microelectrodes.

Figure 4-d15.3 shows the electrical activity at all of the recording electrodes in this preparation in response to a stimulus 5 minutes after cytoplasmic acidification by washout of ammonium chloride. Conduction was slightly slower during acidification than it was under control conditions in this preparation. Activation of the central region began about 16.6 mSec following the stimulus, versus about 14.9 mSec under control

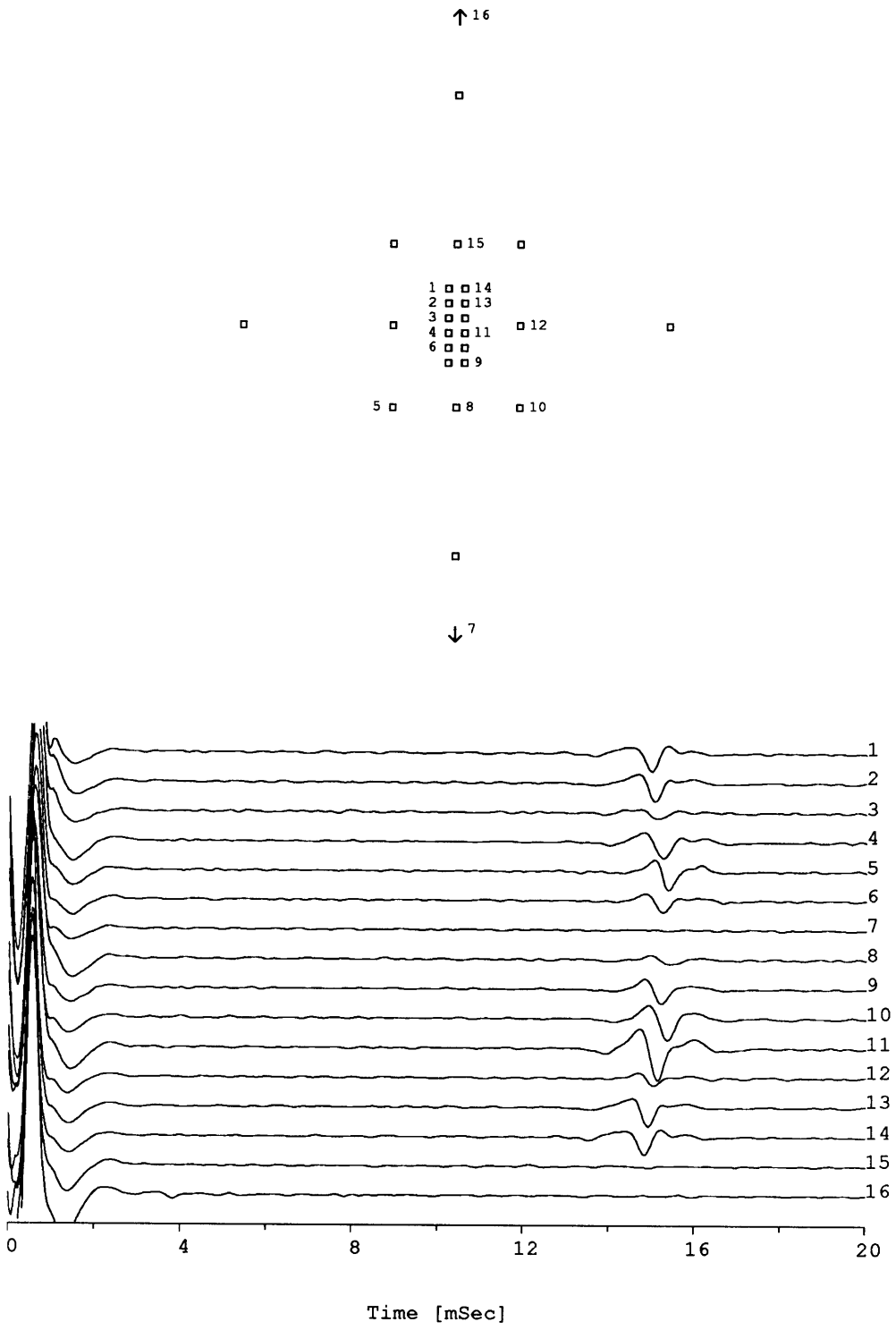

Figure 4-d15.1: A single beat under control conditions

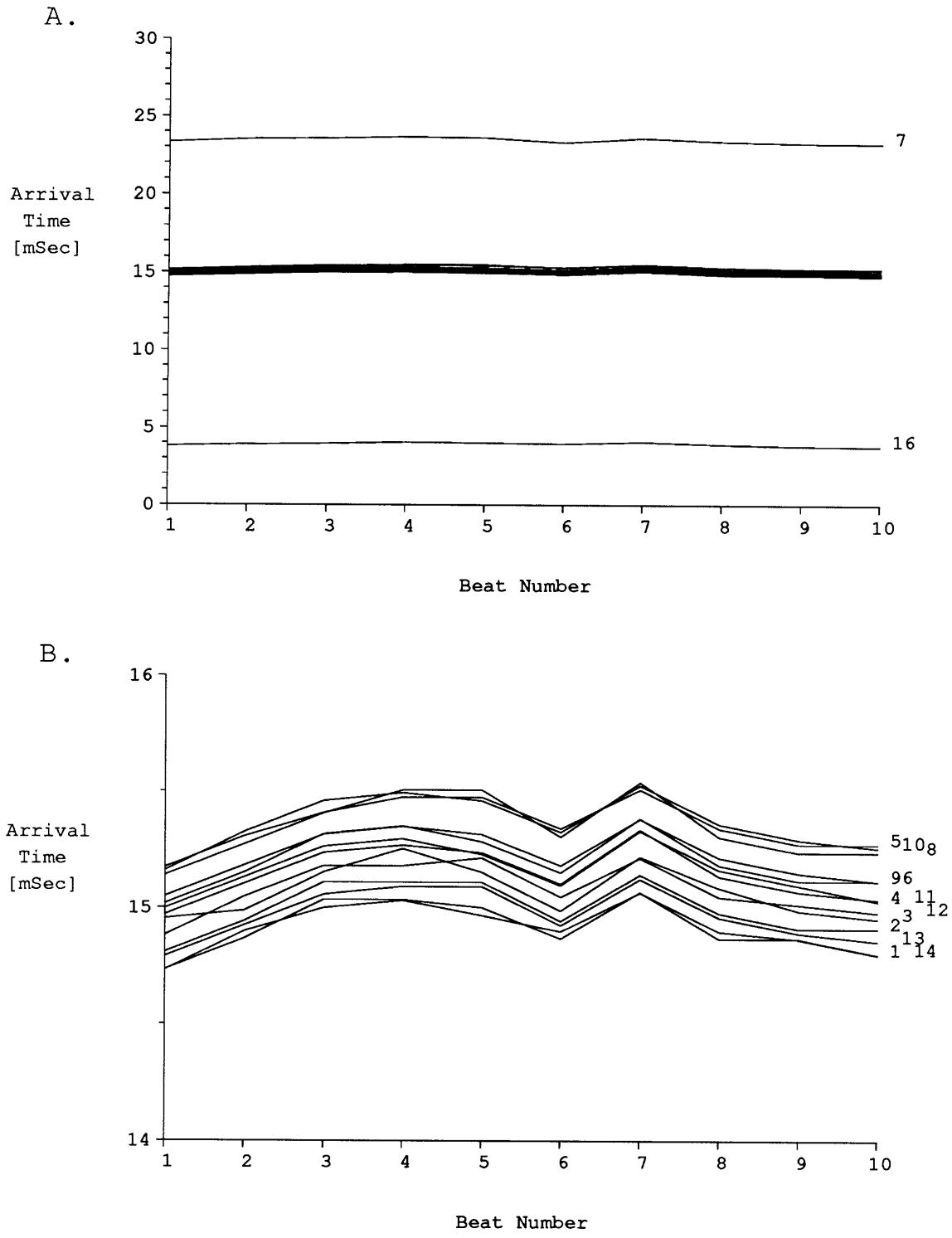

Figure 4-d15.2: Arrival times under control conditions in experiment d15

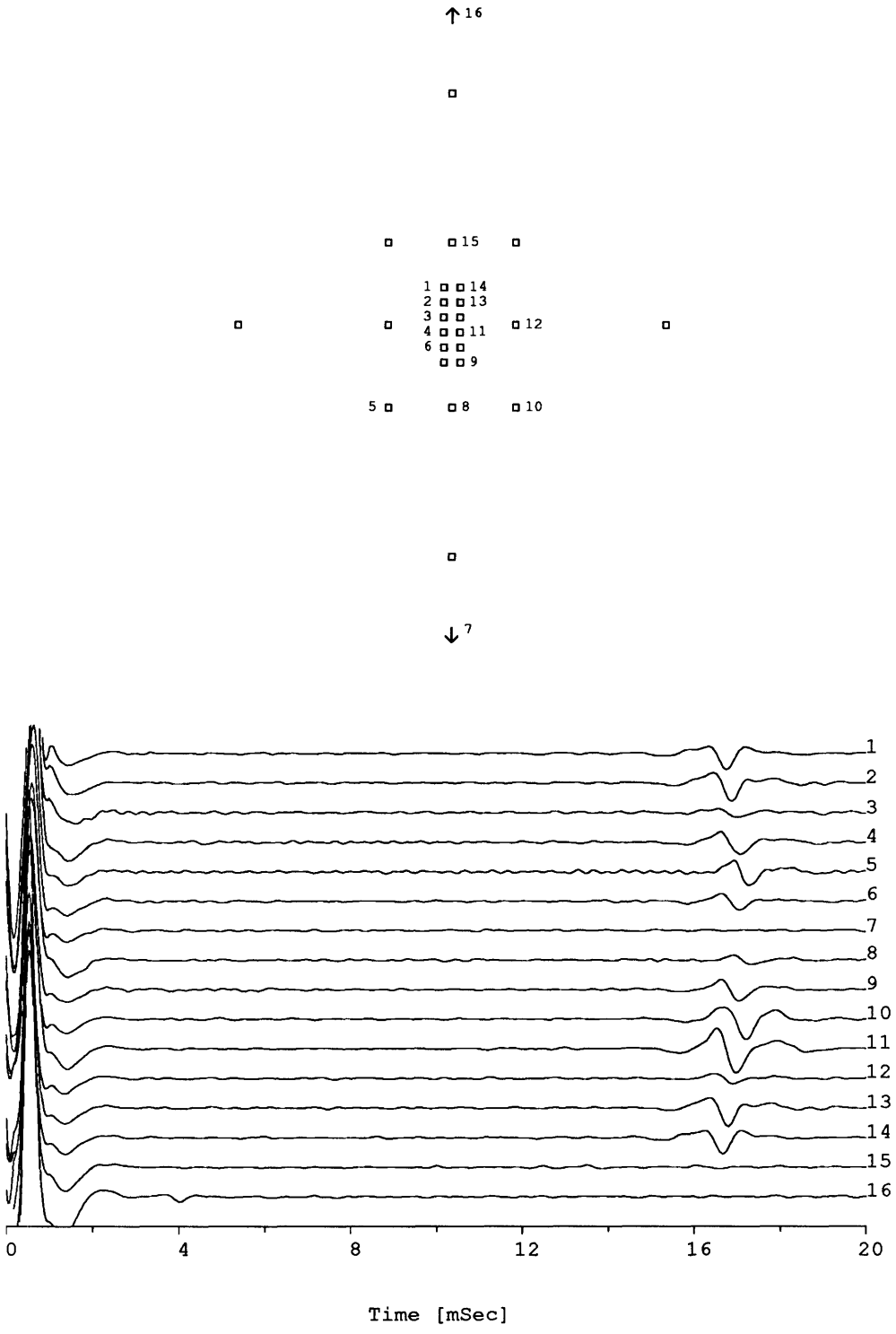

Figure 4-d15.3: A single beat under acidified conditions

conditions. The time taken for propagation from electrode 16 to electrode 14 was 12.61 mSec, corresponding to an apparent conduction velocity of 0.060 m/Sec, 87% of the velocity under control conditions.

The activation arrival times for ten beats at 5 minutes post-acidification are shown in figure 4-d15.4. The beat of figure 4-d15.3 is the 2nd beat in the series of figure 4-d15.4.

The pattern of activation at the recording electrodes during this series of beats was basically the same as it was under control conditions. The mean difference in arrival times across the central region between electrodes 14 and 9 was 310 ± 6 μSec, which was the same as the value under control conditions. However, there was slowing of conduction just beyond the central region. The arrival time at electrode 8, which occurred just before that at electrodes 5 and 10 under control conditions, was delayed so that it followed activation at these electrodes. The delay from electrode 9 to electrode 8 increased from 120 ± 11 μSec under control conditions to 290 ± 15 μSec during acidification (p=.0005). The corresponding conduction velocities were 0.5 and 0.21 m/Sec, respectively. This increase was out of proportion to the conduction velocity changes elsewhere in this preparation.

Figure 4-d15.5 shows the time course of the differences in arrival times at electrode pair (9, 8) during acidification and return to normal pH. For comparison, the arrival time differences at electrodes (11, 9) are also shown. The latter showed no appreciable change with recovery from acidification.

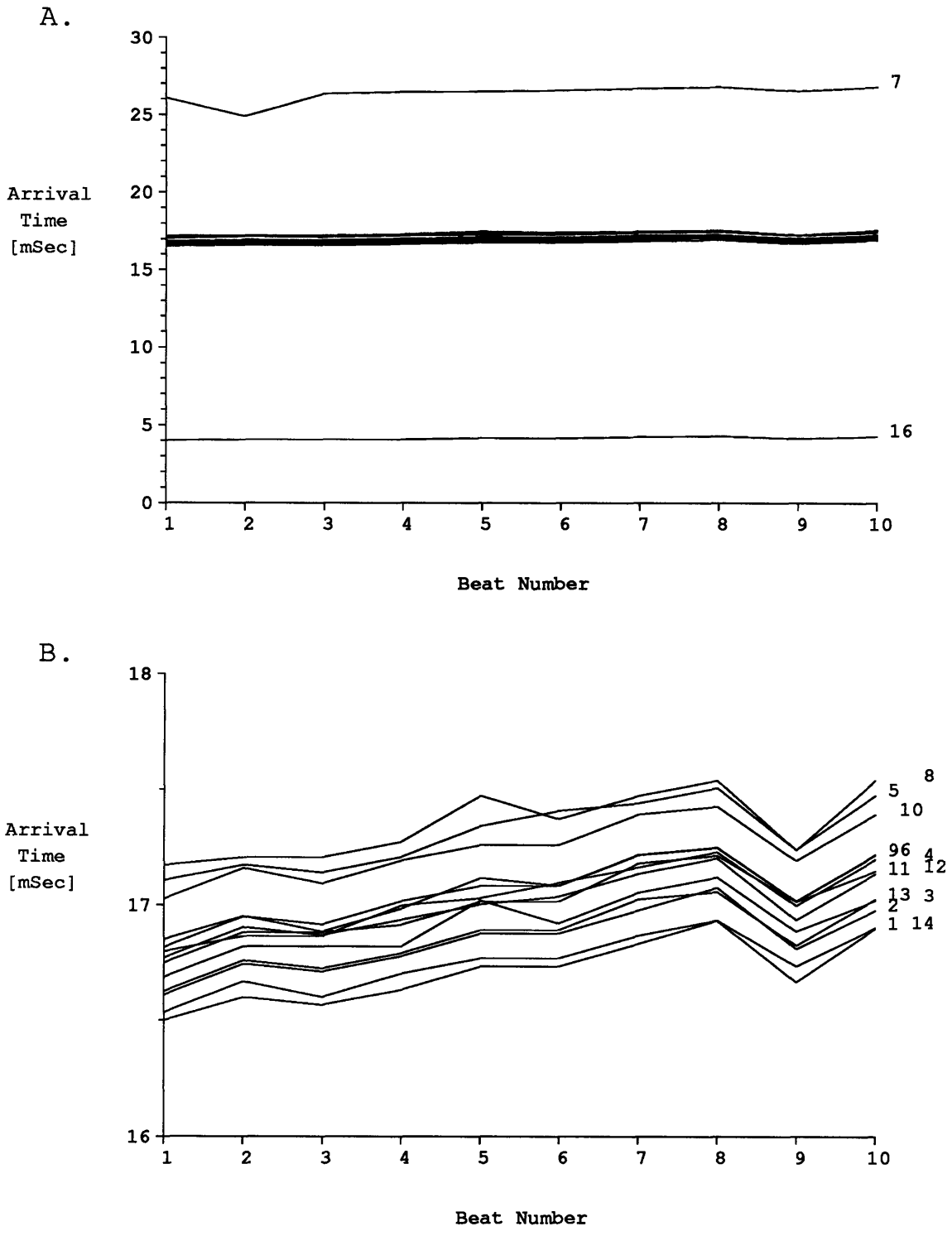

Figure 4-d15.4: Arrival times under acidified conditions in experiment d15

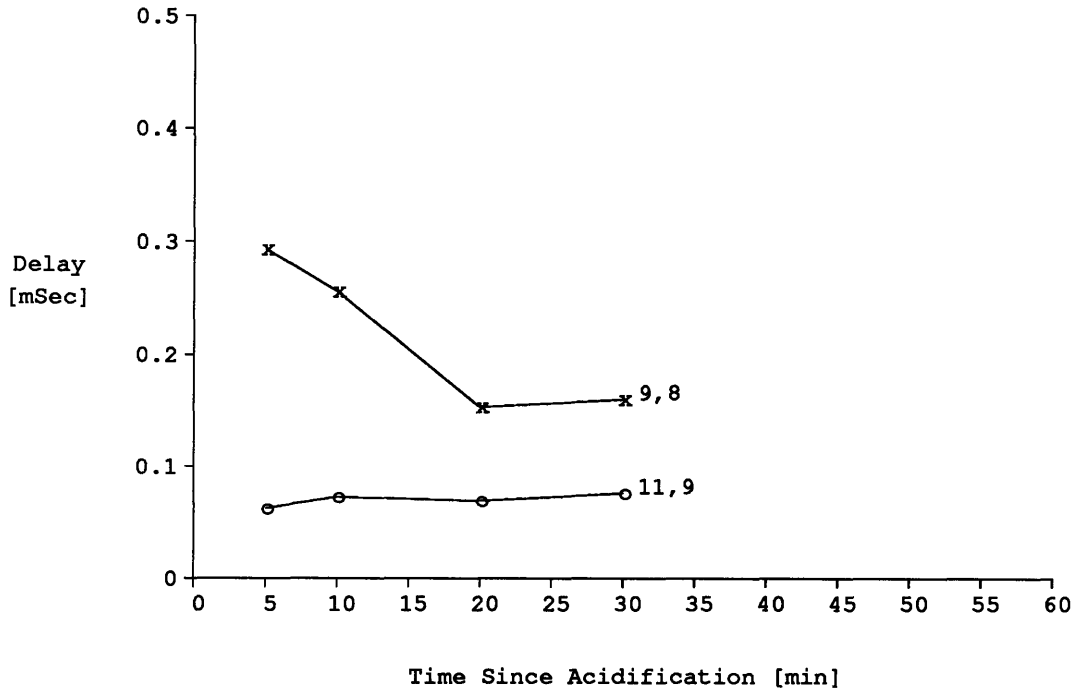

Figure 4-d15.5: Time-course of inter-electrode delays in experiment d15

4.5.7 Experiment d18

Figure 4-d18.1 shows the electrical activity under control conditions from experiment d18.

The stimulating electrode used in this experiment was located beyond the top of the diagram in figure 4-d18.1 (electrode 1 in figure 3-1). The first electrode to record an action potential after the stimulus was electrode 16, which was located 500 μm from the stimulating electrode in this experiment. The arrival time at electrode 16 was 2.82 mSec for this beat. The apparent average conduction velocity in this region of the preparation was thus about .18 m/Sec. Activity next arrived at electrode 2, which was approximately 1000 μm from electrode 16, at 5.71 mSec. The apparent conduction velocity in this part of the preparation was 0.35 m/Sec.

Ten stimuli were applied to this preparation under control conditions at a stimulus rate of 1.5 Hz. The timing of the fiducial points for these beats is shown in figure 4-d18.2. The arrival times for the beat of figure 4-d18.1 are plotted in figure 4-d18.2 as the ordinates of the 5th beat. The arrival times at the central microelectrodes in this preparation showed a smooth progression in proportion to the distances between electrodes. The mean difference in arrival times from electrode 15 to 11 was 300 ± 9 μSec, corresponding to an apparent conduction velocity in the central region of 0.33 m/Sec.

Figure 4-d18.3 shows the electrical activity at all of the recording electrodes in this preparation in response to a stimulus 6 minutes after cytoplasmic acidification by washout of ammonium chloride. Following acidification, the spontaneous beat rate of this preparation increased dramatically from 72 to 234 beats per minute. This required an increase in the rate of stimulation from 1.5 Hz to 4.0 Hz. However, not all of the

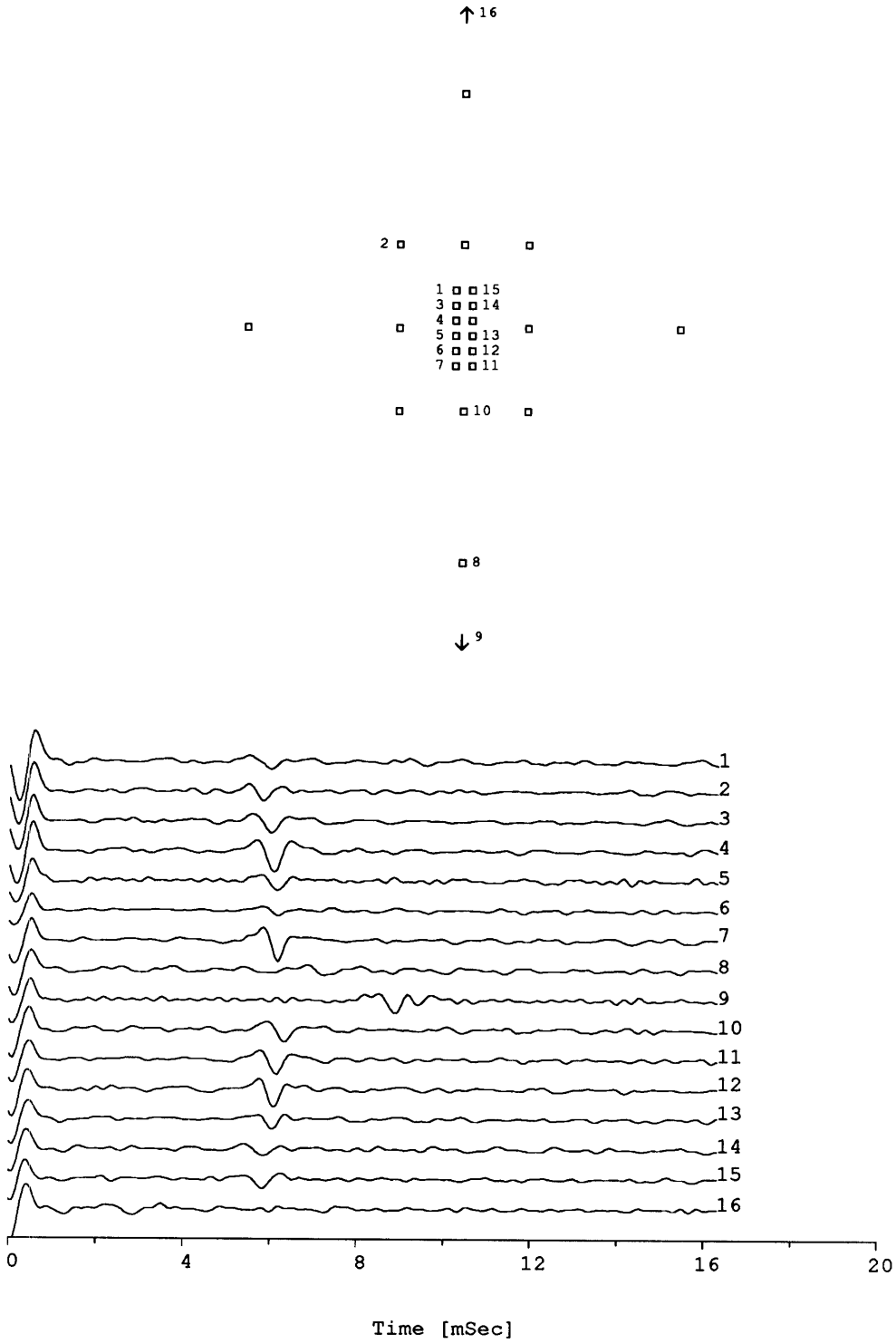

Figure 4-d18.1: A single beat under control conditions

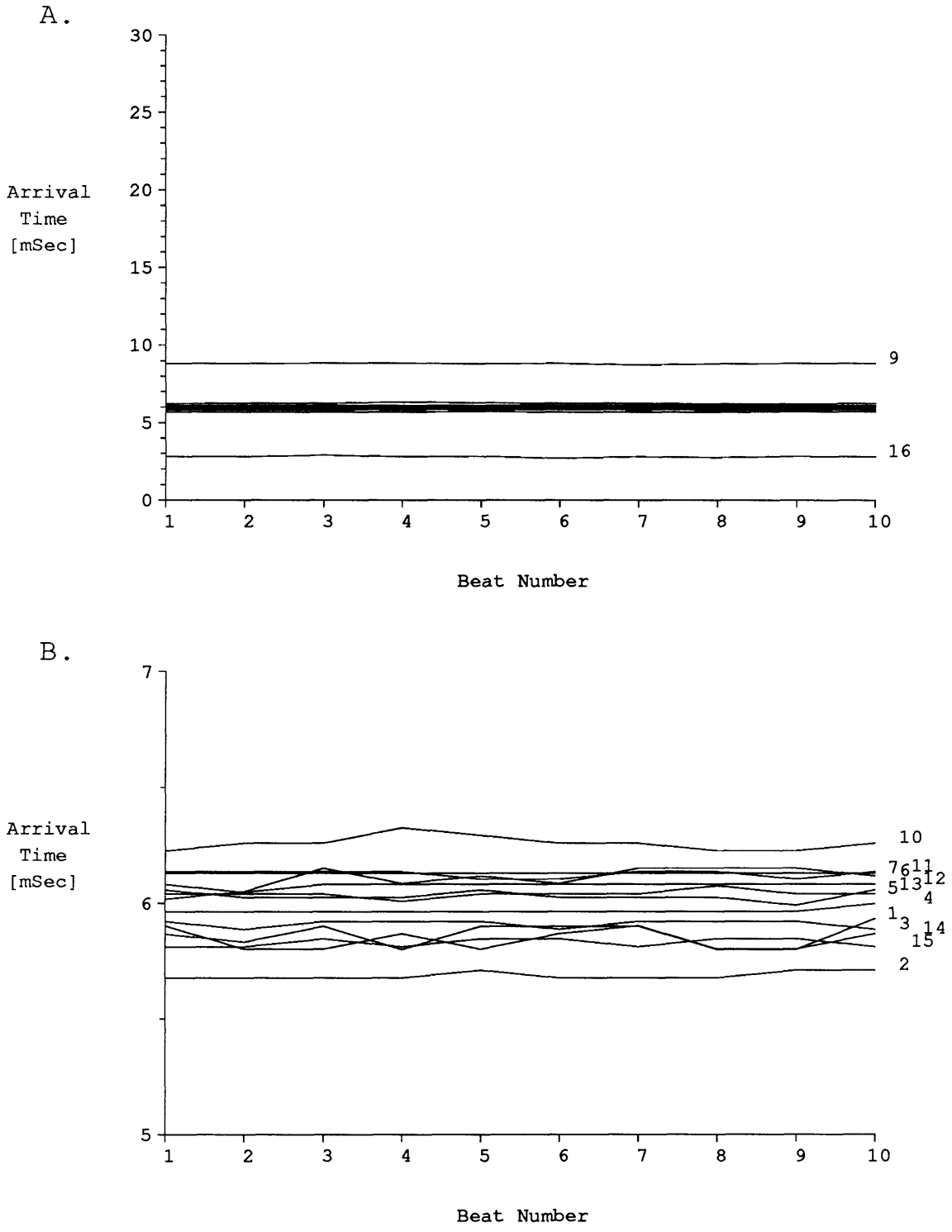

Figure 4-d18.2: Arrival times under control conditions in experiment d18

external stimuli were conducted at this stimulus rate. Conduction was slower during acidification than it was under control conditions in this preparation. The time taken for propagation from the stimulus electrode to electrode 16 was 5.46 mSec, corresponding to an apparent conduction velocity of 0.092 m/Sec, 52% of the velocity under control conditions. The arrival time at electrode 2 was 9.41 mSec, which corresponds to a reduction of apparent conduction velocity in this region to 0.25 m/Sec, 72% of its control value.

The activation arrival times at 6 minutes post-acidification are shown in figure 4-d18.4. The beat of figure 4-d18.3 is the 5th beat in the series of figure 4-d18.4.

Under acidified conditions, the mean difference in arrival times between electrodes 15 and 11 increased to 350 ± 13 μSec, corresponding to an average conduction velocity of 0.29 m/Sec in the central region, 86% of the control value. No disproportionate slowing of conduction was evident in the central region under these conditions. However, the mean difference in arrival times in the adjacent region from electrodes 2 to 1 increased from 180 ± 15 to 370 ± 29 μSec ($p=.0043$), corresponding to an apparent conduction velocity decrease to 49% of the control value.

Figure 4-d18.5 shows the time course of the differences in arrival times at electrode pair (2, 1) during acidification and return to normal pH. For comparison, the arrival time differences at similarly spaced electrodes (7, 10) are shown. While the former decreased toward the control value, the latter delay increased slightly during recovery from acidification.

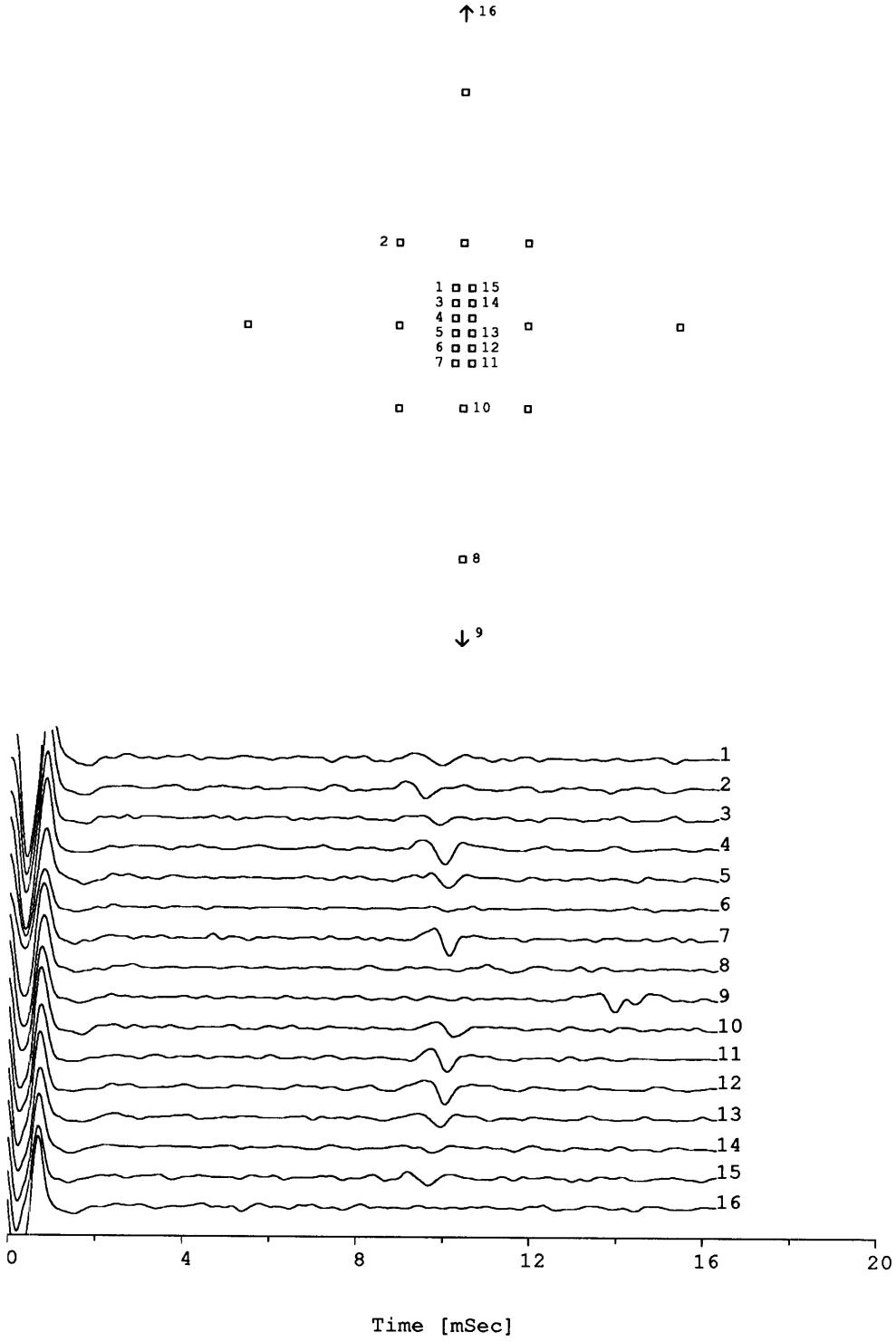

Figure 4-d18.3: A single beat under acidified conditions

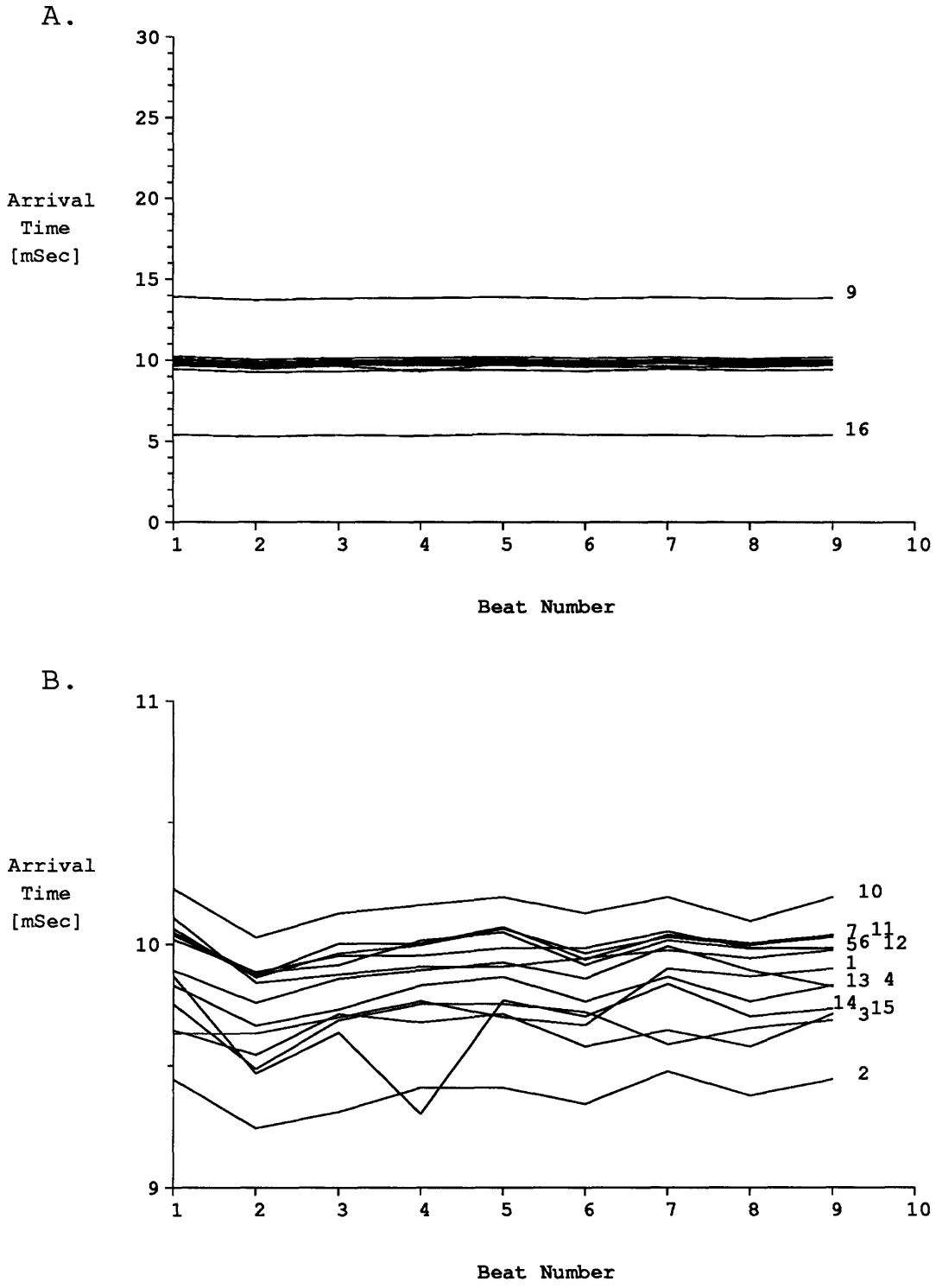

Figure 4-d18.4: Arrival times under acidified conditions in experiment d18

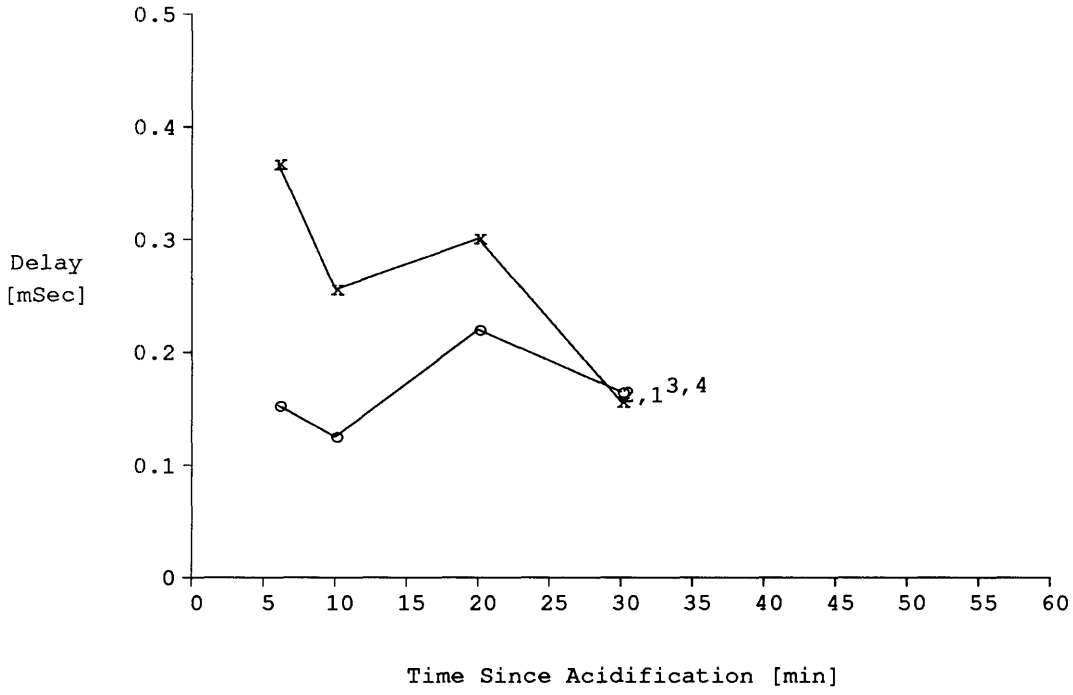

Figure 4-d18.5: Time-course of inter-electrode delays in experiment d18

4.5.8 Experiment j2

Figure 4-j2.1 shows the electrical activity during experiment j2 in response to a stimulus under control conditions. The stimulating electrode used is located beyond the bottom of this diagram (electrode 16 in figure 3-1).

The first electrode to record an action potential after the stimulus was electrode 7, which was 500 μm from the stimulating electrode. The arrival time at electrode 7 was 3.90 mSec for this beat, making the average conduction velocity 0.13 m/Sec. Activity next arrived at electrode 6, which was 500 μm from electrode 7, at 8.02 mSec, corresponding to an average conduction velocity of .12 m/Sec.

The beat shown in figure 4-j2.1 is the fourth in a series of beats which were recorded under control conditions at a stimulus rate of 3.3 Hz. The timing of the fiducial points is shown in figure 4-j2.2. The arrival times for the beat of figure 4-j2.1 are plotted in figure 4-j2.2 as the ordinates of the second beat. The arrival times at each electrode stayed fairly constant from beat to beat. The mean difference in arrival times between electrodes 8 and 12 was 310 ± 8 μSec; the apparent conduction velocity was thus 0.26 m/Sec. The activations at the central microelectrodes in this preparation occurred within this time-span with the exception of electrodes 2 and 14. The waveform on electrode 2 had low amplitude and was polyphasic with two downward deflections of similar slope separated by about 0.5 mSec. A consistent fiducial point could not be found for electrode 2. The arrival at electrode 14 occurred about 0.8 mSec later than at the other central microelectrodes. This was suspected to be due to the presence of a second, unintended recording surface somewhere along the shank of this electrode. This suspicion was supported by the behavior of this electrode during experiment j15, in which it recorded 2 deflections, one at about the same time as its neighbors, and one about a millisecond later. The behavior at electrode 2 may have been related to the problems at electrode 14,

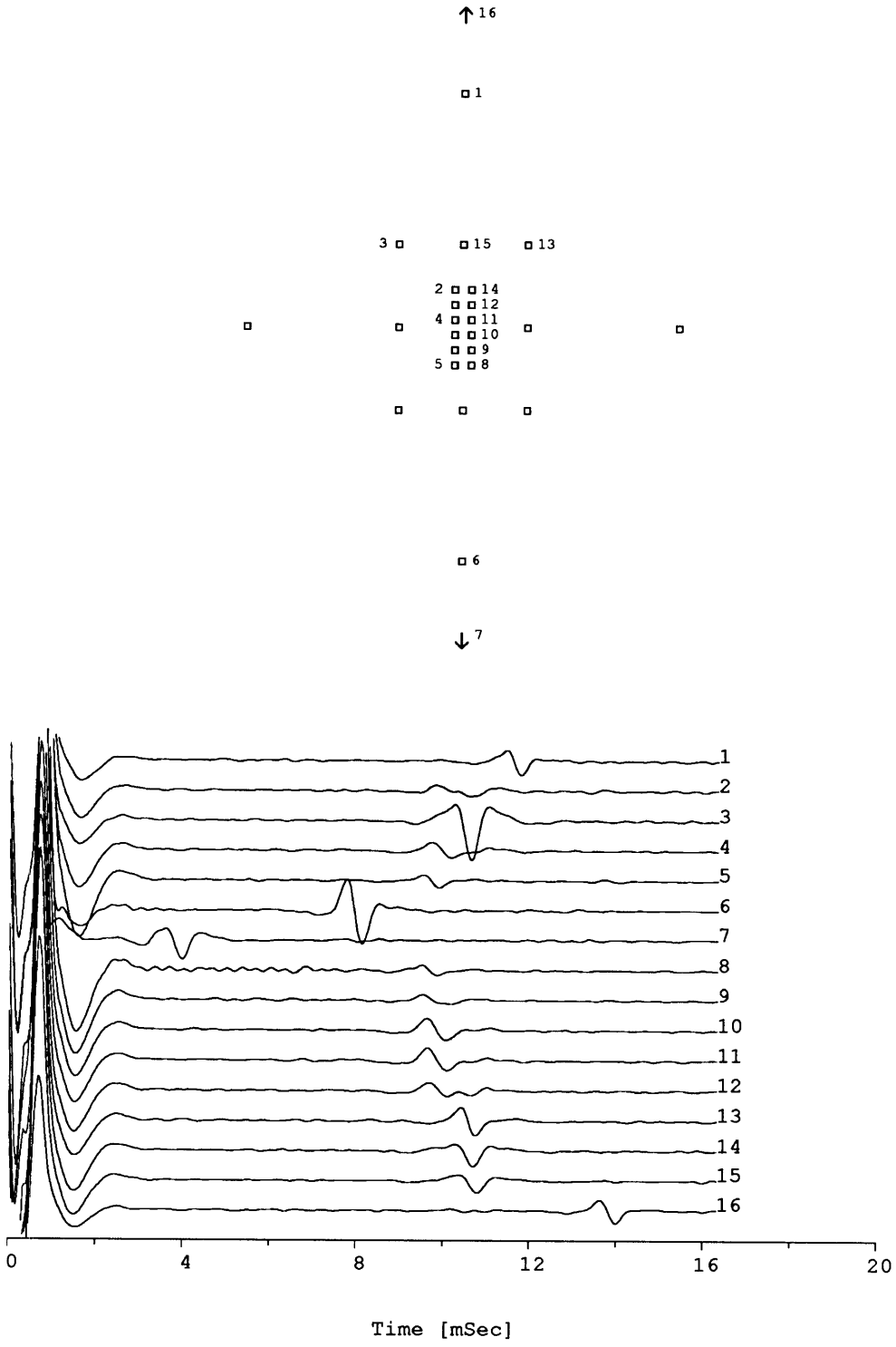

Figure 4-j2.1: A single beat under control conditions

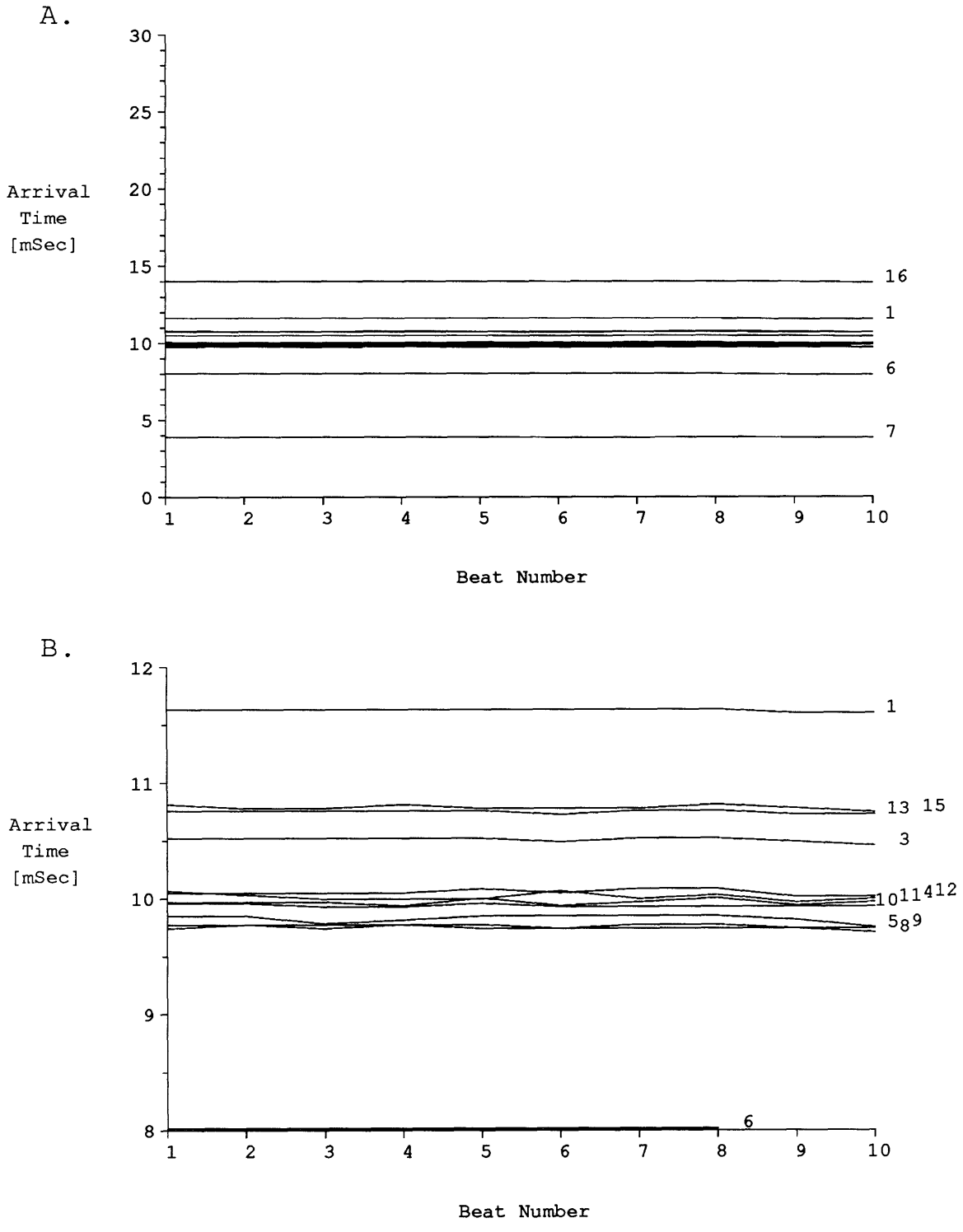

Figure 4-j2.2: Arrival times under control conditions in experiment j2

but this is unknown. A resistance check revealed no measurable conductance between electrodes 2 and 14. The signals on electrodes 2 and 14 were considered suspect and were not used in the subsequent analysis.

The mean delay time between electrodes 12 and 15 was 730 ± 7 μSec. This corresponded to a conduction velocity in this region of about 0.11 m/Sec, much slower than in the adjacent central region.

Figure 4-j2.3 shows the response to a stimulus 1.75 minutes after cytoplasmic acidification by washout of ammonium chloride. The conduction velocity under these conditions was slower than it was under control conditions. The time taken for propagation from the stimulus electrode to electrode 7 was 5.70 mSec, and activity reached electrode 6 at 12.32 mSec. The corresponding apparent conduction velocities were 0.087 and 0.075 m/Sec, respectively, about 65% of that under control conditions. No activity was recorded from electrode 16 since the recording interval ended before activation reached this location; this was also the case for electrode 1 on "late" beats (see below).

The activation arrival times for 10 beats under acidified conditions are shown in figure 4-j2.4. The beat of figure 4-j2.3 is the fourth beat in the series of figure 4-j2.4. The stimulus rate remained at 3.3 Hz. The conduction velocity in this series of beats varied from beat to beat far more than that of the control series. This variation was not random; rather, there was a regular alternation from beat to beat.† The difference in arrival times between the early beats and the late beats in this series was about 1 mSec. A similar beat-to-beat alternation has been noted previously in the same type of

† A failure of the synchronization scheme occurred during this experiment which caused the recording interval for the fifth beat to begin late and the sixth recording interval to be entirely out of synchronization with a stimulus. The arrival times for the fifth beat shown here were adjusted by matching the tail end of the stimulus artifact waveforms with those of the fourth beat.

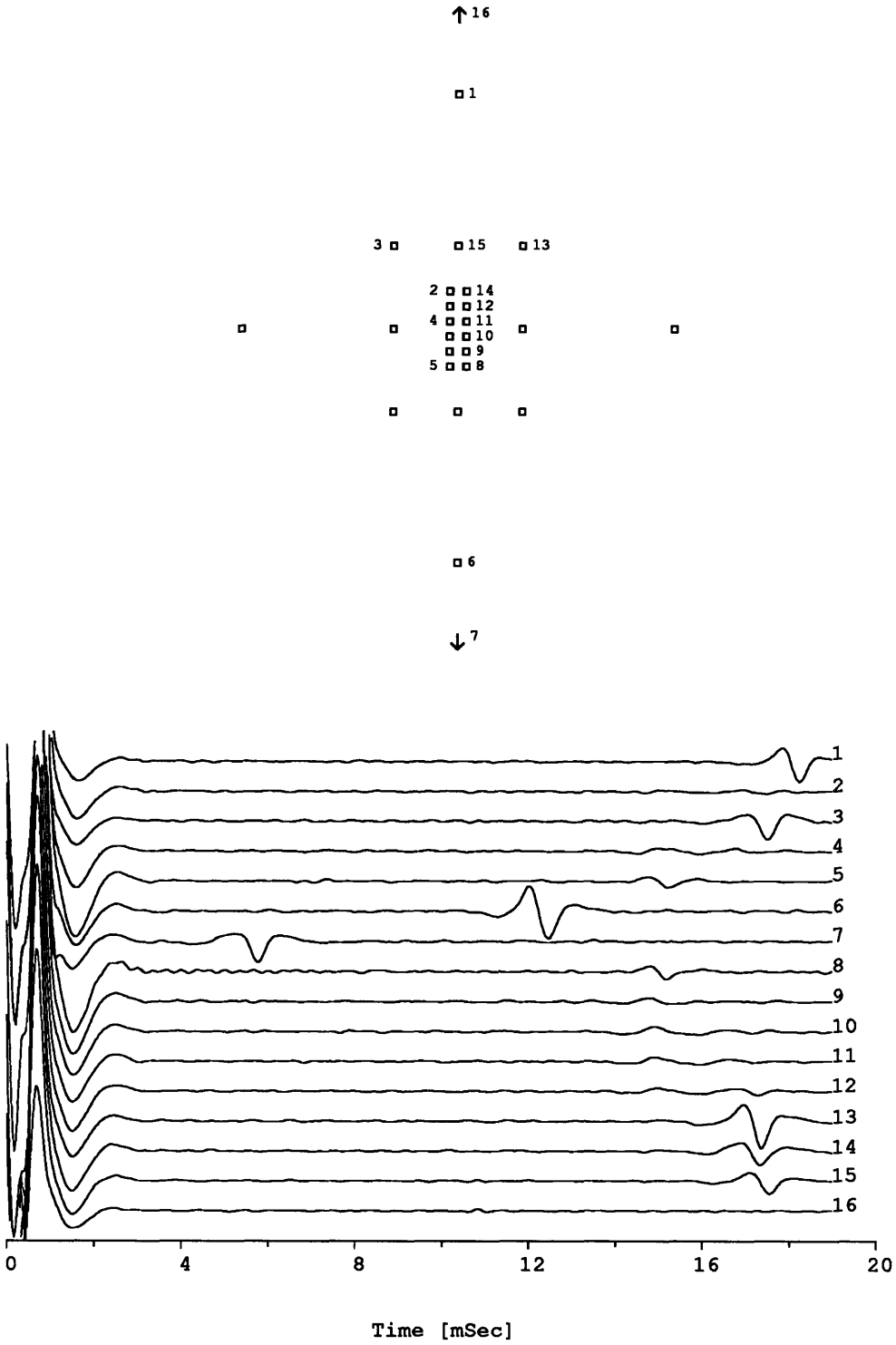

Figure 4-j2.3: A single beat under acidified conditions

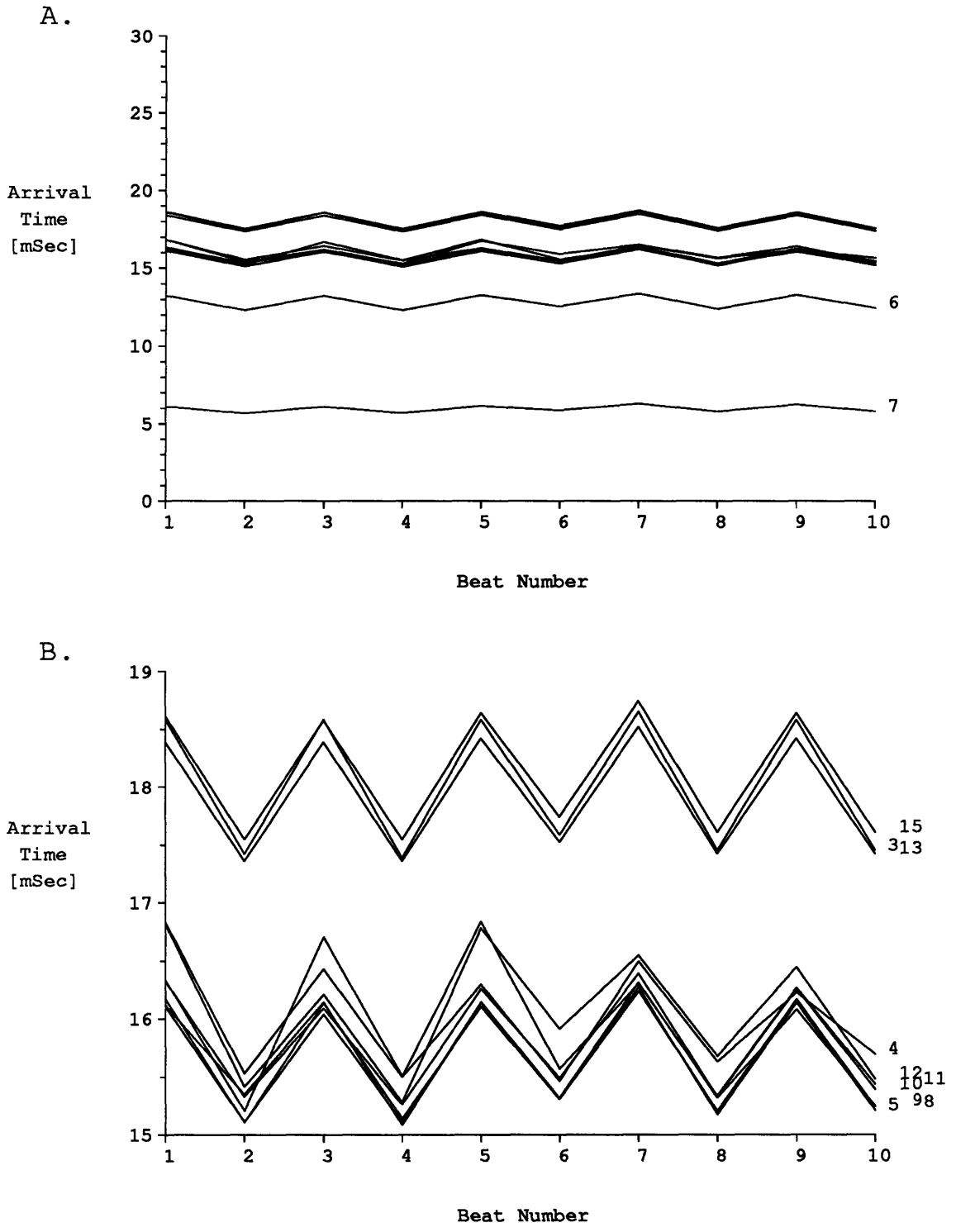

Figure 4-j2.4: Arrival times under acidified conditions in experiment j2

preparation under control conditions (Israel et al., 1984). At that time it was hypothesized that such a result might be due to the existence of a 2:1 conduction block in the conduction pathway; excitation would bypass the blocked area by propagating through a stable secondary pathway on alternate beats. Such an explanation might apply here as well.

The overall order of activation at the recording electrodes during this series of beats was basically the same as it was under control conditions. The mean difference in arrival time between electrodes 8 and 12 went from 310 ± 8 to 380 ± 60 μSec. These time delays correspond to apparent velocities of 0.26 and 0.21 m/Sec, respectively, a decrease to 81% of control. The mean delay time between electrodes 12 and 15 increased to 2070 ± 60 μSec under acidified conditions (p=.0000011). This corresponded to a conduction velocity in this region of about 0.039 m/Sec, a decrease to 35% of the control value.

Several more recordings of propagated activity were made from this preparation to monitor the course of arrival times as the NH_4Cl was washed out and the intracellular pH returned to normal. Recordings were made at 3, 5, 12, 22.5, and 30 minutes following acidification by removal of NH_4Cl. None of the subsequent recordings from this preparation showed the alternating conduction velocity that was noted above in the recordings taken at 1.75 minutes following acidification.

Figure 4-j2.5 shows the time course of the differences in arrival times at electrode pair (12, 15) during acidification and return to normal pH. For comparison, the arrival time differences at central electrodes (9, 10) are shown. By 12 minutes post-acidification, the delay between electrode pair (12, 15) had returned to the control value. The delay between the central electrode pair showed no major changes during the recovery from acidification.

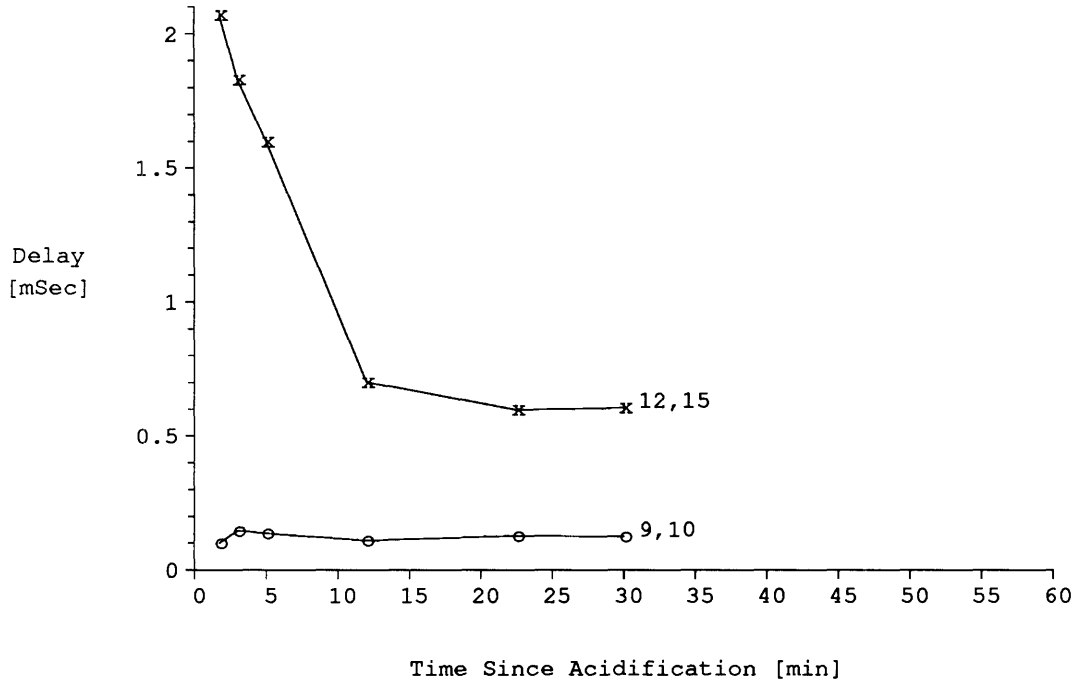

Figure 4-j2.5: Time-course of inter-electrode delays in experiment j2

4.5.8 Summary of experimental results

Figure 4-13 presents selected delay times from each of the experiments discussed above. In this figure, the delays have been normalized by dividing the delay time by the distance between electrodes, thus making the size of the bars comparable within and across experiments. For each experiment, two bars are presented, each showing the delay time at the pair of electrodes which is indicated in the label beneath the bar. The first electrode pair presented for each experiment was selected to represent disproportionate delays found in that experiment (if any); the second was selected to represent proportionate delays. The lower, shaded portion of each bar shows the delay time under control conditions. The upper, unshaded portion of each bar indicates the delay time at the same electrode pair at the first measurement after acidification. The error bars indicate the S.E.M. of each measurement.

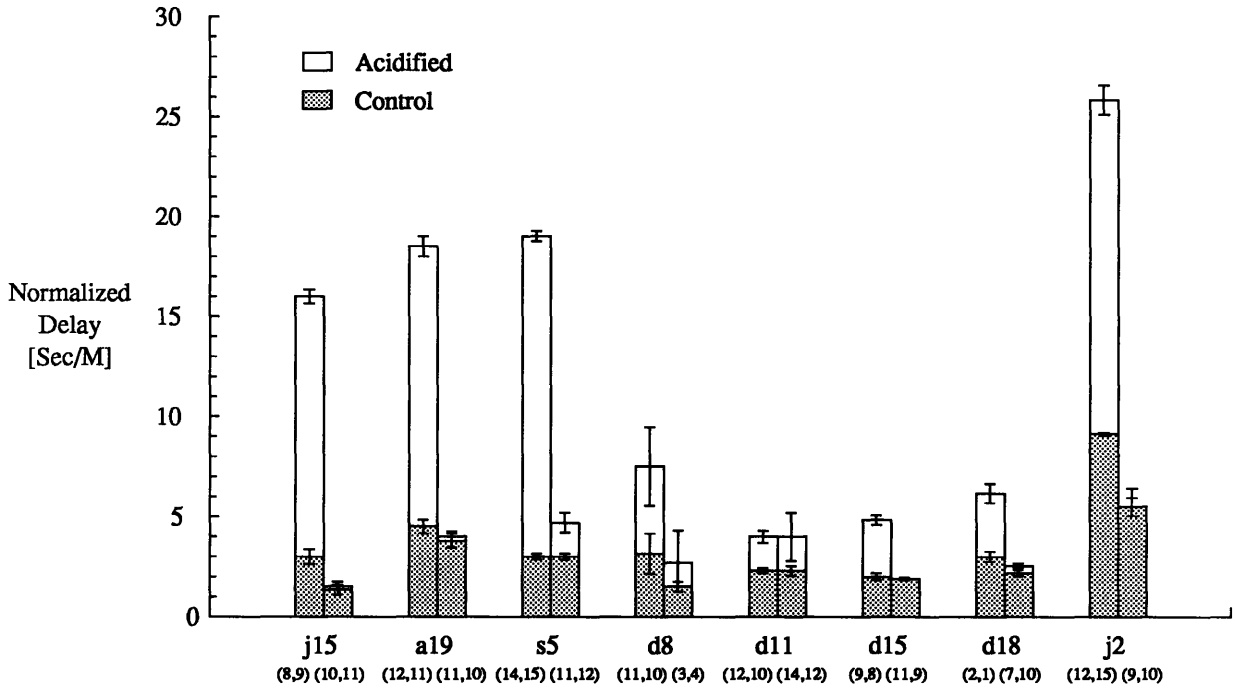

Figure 4-13: Summary of experimental results

Chapter 5: DISCUSSION

5.1 Experimental Results

The eight experiments presented in section 4.5 can be divided into four categories: those in which a large time delay occurred in the central region of microelectrodes (j15, a19), those in which a disproportionate time delay was found outside of the central region (s5, d15, j2), those in which the results suggest the presence of disproportionate slowing (d8, d18), and one in which only proportional slowing of conduction was observed (d11).

The experiments in which a large delay appeared between very closely spaced electrodes are best explained by the hypothesis of an intercellular junctional time delay. In experiment j15, for example, the delay in arrival of activation between electrodes 8 and 9, spaced on 20 μm centers, increased from 60 μSec under control conditions to 320 μSec following intracellular acidification. The delay between adjacent electrodes 4 and 3, which had the same spacing, increased similarly from 46 to 280 μSec. This result could be explained by the existence of a gap junction between two cells (one in contact with electrodes 8 and 4, and the other in contact with electrodes 9 and 3) if the junctional conductance were affected by the acidification. This result is not at all consistent with uniform slowing of conduction at all locations due to membrane effects.

Could an alternate explanation of this experimental result be that a longer pathway of propagation developed between the electrodes following acidification without any change in intercellular connections? Assume that electrode 8 recorded from cell "A" and that electrode 9 recorded from cell "B" as shown in figure 5-1. Electrode pair (8,9) exhibited a small difference in arrival times under control conditions and a large delay

A.

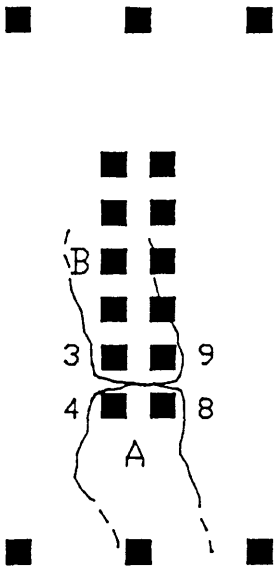

B.

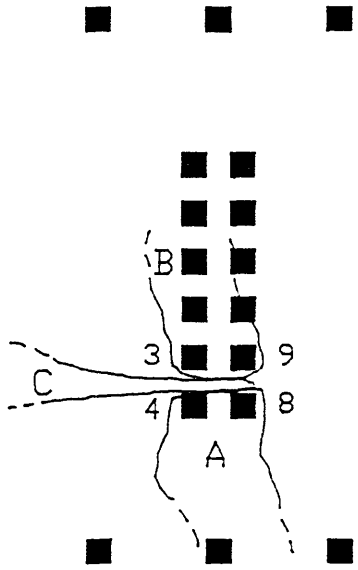

Figure 5-1: Hypothetical cell geometries for experiment j-15

following cytoplasmic acidification. The result under control conditions establishes that there was initially a fairly direct propagation pathway between cells A and B. Such a pathway might have involved either a single intercellular connection between A and B as shown in figure 5-1a, or multiple connections passing through at least one additional cell.

For the sake of argument, assume that the propagation path under control conditions passed through a third cell, "C", on its way from A to B as shown in figure 5-1b. The preparation was two-dimensional, so each cell had several neighbors to which it may have been connected. Also assume, for this hypothesis, that the NH_4Cl intervention did not affect propagation across intercellular junctions; instead, postulate that it rendered some cells inexcitable by, say, affecting the membrane properties. Propagation could still occur through the culture, because each cell in the path was connected to at least one other which was still excitable, but it was slower due to some combination of lower single-cell conduction velocity and increased path length. If it is postulated that cell C became inexcitable due to the intervention, the propagation time from A to B would increase in accordance with the length of the new, less direct pathway.

Now consider what happens if instead of passing through a third cell, propagation under control conditions proceeded directly from cell A to cell B through one intercellular junction, as depicted in figure 5-1a. This type of pathway should predominate when the distance between the two electrodes (and therefore between the cells that they are in contact with) is small, as it was in the case of electrodes 8 and 9 in experiment j15. Under the above hypothesis of lengthened pathways, the NH_4Cl intervention does not affect coupling at intercellular junctions, but affects propagation by making some cells inexcitable. In this case, the implication is that cell B has been made inexcitable (since we have assumed that propagation proceeded directly from cell A to cell B). However, the data from electrode 9 in experiment j15 show that cell B depolarized after a time delay of several hundred microseconds, establishing that it was

not inexcitable. Clearly this hypothesis is not viable if electrodes 8 and 9 were on either side of a single intercellular junction.

The hypothesis that the intervention results in lengthened propagation pathways leads to another prediction about the experimental results. Assume that the conduction pathway becomes lengthened because activity must travel around an inexcitable cell. After some time, the effects of the intervention wear off, and the original pathway is restored. The conduction time between electrodes under this hypothesis depends primarily upon the length of the pathway. A change from one path to another and then back to the original should result in discrete jumps in the conduction time from one value to another and then back to the first. In fact, the experimental data show evidence of gradually decreasing delays at different times after acidification. This can be seen for experiment j15 in figure 4-j15.5, in which the delay between electrodes 8 and 9 has an intermediate value at 5 minutes after acidification between its maximum at 3 minutes and its return to control level at 8 minutes.

The discussion of possible cell geometries made previously in the case of experiment j15 can be applied to the results of experiment a19. In this experiment, the delay time between electrodes 6 and 7 increased from 97 to 410 μSec in going from control to acidified conditions, and that between adjacent electrodes 12 and 11 increased from 90 to 370 μSec. These electrode pairs were space on 20 μm centers. This phenomenon could be explained by the introduction of delay at an intercellular junction between a cell in contact with electrodes 6 and 12, and a second cell in contact with electrodes 7 and 11. An alternate explanation of a tortuous pathway due to inexcitability of some cells would require that there be at least two intercellular junctions (at least one additional cell) in the path between the electrode pairs, and would imply that the path length be 3 to 4 times the interelectrode distance. For this experiment, no data are available concerning the time course of recovery from acidification, since recordings

were obtained at only one time following acidification.

In three experiments, disproportionate slowing developed outside of the central region of microelectrodes. In each of these cases, the slowing was observed between the central group of electrodes and the electrodes in the adjacent row that was 60 μm distant. In experiment s5, the delay between arrivals at electrodes 15 and 14 increased from 180 to 1140 μSec. The average conduction velocity measured across the central region was 0.24 m/Sec during acidification. Assuming that this was the actual microscopic conduction velocity after the intervention implies a path length of 270 μm between electrodes 14 and 15, which had an actual separation of 60 μm. If we instead assume that the reduction in average conduction velocity due to the intervention is entirely due to the development of longer pathways, i.e: that the microscopic conduction velocity remains the same as before the intervention, the implied path length in this experiment would be 380 μm. In experiment d15, the delay between arrivals at electrodes 9 and 8 increased from 120 to 290 μSec. The conduction velocity across this region under control conditions was 0.5 m/Sec. The average conduction velocity across the central region did not decrease following acidification in this experiment. If we therefore assume that 0.5 m/Sec was also the microscopic conduction velocity under acidified conditions, the implied path length is 150 μm. In experiment j2, a large time delay was observed between electrodes 12 and 15; the propagation time went from 730 to 2070 μSec. The propagation delay in this region was rather long under control conditions; it corresponded to a conduction velocity of 0.11 m/Sec, which was less than half of the velocity in the adjacent central region. This might indicate that the propagation path across this region under control conditions was not a direct one; however, the average conduction velocity was low in other large regions of this culture (0.12 m/Sec in the region between electrodes 7 and 6), so it is plausible that the low control velocity in the region between electrodes 12 and 15 was due to membrane rather than geometric factors. The average conduction velocity across the central region decreased to 81% of the control value

during acidification. Assuming a microscopic conduction velocity of 81% of the control value between electrodes 12 and 15 would imply a path length of 190 μm, about 3 times the interelectrode distance; assuming that the microscopic conduction velocity did not change following acidification would imply a path length of 230 μm, about 4 times the interelectrode distance.

Of the other experiments in which disproportionate delays were seen after the NH_4Cl intervention, experiments s5, d15, d18, and j2 all show a graded change in these delays during the recovery from acidification rather than assuming one of two values. As outlined before, these findings are not consistent with the explanation of a single pathway shift, but are consistent with the explanation of increased time delays due to a change in the degree of intercellular coupling.

The resistance of a gap junction depends upon the composition of the junction, i.e. the number of connexons it contains, and upon the state of the junction, i.e. how many connexons are "open", or alternately, how "open" all the connexons are. A frequently-used estimate of the resistance of a single open connexon is 10^{10} ohms. (Loewenstein, 1975) A closed connexon may be assumed to have a much higher resistance. Assuming a resistance of 10^{10} Ω for an open connexon, there would be 100 connexons per μm^2 of 1 Ω–cm^2 nexal membrane. This is much less than the maximum density of connexons that is possible, based on morphological studies that show connexons spaced on 10-12 nm centers in a hexagonal array (Caspar et al. 1977). Such spacing corresponds to a density of 8000 to 10000 connexons per μm^2. This number represents an approximate maximum, rather than a typical value; less dense spacings are also found. The packing density of connexons in the nexi of the cardiac cell-culture preparation has not been studied. Equally important for estimating the coupling resistance between cells is the area of the gap junctions; this is also unknown in the cardiac cell culture preparation. A priori, there is a wide range of possible resistances between adjacent cells in this preparation.

Can the data gathered in this experiment be used to estimate the intercellular resistances in the cardiac cell-culture preparation? Under normal conditions in this preparation, the coupling resistances are low enough to support action potential propagation at an average velocity comparable to that in intact heart. Simulations done by Diaz (1983) indicate that propagation can occur over a wide range of junctional resistivities; simulated propagation occurred with disk resistivities ranging from 0.1 to 3.0 Ω–cm^2. Higher values of disk resistivity may also have supported propagation in the model; the resistivity above which propagation failed was not stated. In the simulations, the junctional delay went from 46 μSec at a disk resistivity of 0.1 Ω–cm^2 to 200 μSec at a disk resistivity of 0.5 Ω–cm^2. The former delay is small on the scale of resolution of the measurements in these experiments, while the latter is appreciable. No central inter-electrode delays of magnitude 200 μSec were seen in these experiments under control conditions, suggesting that the typical junctional resistivity in the preparation was at the low end of this range. These simulation results also suggest that the junctional resistivity must have increased by a factor of about 5 to 10 to produce the observed increases in delay times.

The average conduction velocity in all experiments decreased following intracellular acidification. The amount of the decrease was different at different locations within a culture as well as from experiment to experiment. To compare experiments, we will consider the region between the stimulating electrode and the central recording electrodes. This distance was 1265 μm, long enough so that the propagation path must contain several intercellular junctions. Under control conditions, the time taken for activation to traverse this region was 5.2 mSec in experiment d8, compared to 14.4 mSec in experiment j15. Under acidified conditions, this time increased to 6.7 mSec in experiment d8, and to 24.0 mSec in experiment j15, increases of 1.5 and 9.6 mSec, respectively. The delays given here for acidified conditions should probably not be directly compared, even though each was the first post-acidification value obtained, since

the value for experiment j15 was recorded 3 minutes post-acidification, while the value for experiment d8 was recorded 5 minutes post-acidification. The propagation time for experiment j15 at 5 minutes post-acidification was 15.9 mSec, which corresponds to an increase from the control value by 1.5 mSec, coincidentally the same amount as in experiment d8.

If it is assumed that activity propagated along a straight line from the stimulating electrode to the central recording electrodes, the number of intercellular junctions traversed along this path can be estimated from the cell morphology data. As an upper bound, if all the cells in the path were aligned transversely, and all were at the lower bound of cell-width, there would be about 180 junctions in the path. For the lower bound, if all the cells were aligned longitudinally and all were at the upper bound of cell length, there would be only 6 junctions in the path. For a typical value, using the mean distance between boundaries along a straight line (section 4.2) would predict 57 junctions in the path.

To use these limited data to calculate a per-junction delay, it will be necessary to assume that all junctions produce an equal amount of delay. In the light of the above discussion of variability among junctions, this assumption is probably not true. Another simplifying assumption is that the junctions have sufficiently low resistance under control conditions that they introduce negligible delay, i.e., that the delay due to junctions is completely accounted for by the change in delay in going from control to acidified conditions. Given these assumptions, the junctional delay is then the overall delay divided by the number of junctions. For the shortest propagation delay increment of 1.5 mSec in experiment d8, assuming the smallest number of junctions in the path (6) yields a delay of 250 μSec per junction. Assuming an average number of junctions (57) yields a delay of 26 μSec per junction. For the longest propagation delay increment of 9.6 mSec in experiment j15, assuming an average number of junctions implies a junctional

delay of 168 μSec, while assuming the largest number of junctions (180) yields a junctional delay of 53 μSec per junction. For comparison, the measured delay between electrodes 8 and 9 in experiment j15, (which presumably represents a single junctional delay plus between 50 and 100 microseconds of non-junctional propagation time) at 3 minutes post-acidification, was 320 μSec. Thus, while these calculations are of necessity very rough, they do yield junctional delay times which are similar to those seen in the Diaz model (which ranged from 46 to 600 μSec).

The above discussion of changes in propagation times due to the presence of junctions assumes that the changes in velocity in these experiments were due only to junctional effects, i.e. that the NH_4Cl intervention had effects only on the junctional resistance. Ideally, an intervention used to study the effects of increasing junctional resistance would affect only this parameter. This was probably not the case with the ammonium chloride intervention. Evidence from other studies (see section 3.2.5) indicates that NH_4Cl may also have caused slight membrane depolarization. The membrane depolarization caused in other cardiac cells by this intervention was on the order of 5 to 10 mV. Such partial depolarization might contribute to lower conduction velocity (Cranefield, 1975). Furthermore, according to the Diaz model, decreasing intercellular coupling should lower the average conduction velocity by increasing intercellular delays but at the same time raise the microscopic conduction velocity. This effect of the intervention on the microscopic conduction velocity might tend to cancel any slowing caused by slight depolarization to some extent. Other experiments would be needed to separate these second-order effects.

5.2 Implications of the results

These experiments are consistent with the idea that, under conditions which decrease coupling between cells, propagation of the action potential in cardiac tissue can

change from the smooth, continuous mode modelled by classical cable theory to a halting, discontinuous mode with discrete delays between cells. Presumably, the limiting case of decreased intercellular coupling is complete failure of conduction from one cell to the next, if the junctional conductivity becomes too low to allow depolarization of the distal cell.

These phenomena could contribute to the development of conduction disturbances in the heart. Slow conduction and conduction block are the two most obvious consequences of decreased intercellular coupling. Both of these conduction disturbances, in turn, are thought to play a role in sustaining re-entry, which has been proposed in various forms to be the mechanism underlying a wide variety of arrhythmias.

Spach's group has examined the conditions under which the connectivity between cardiac cells might contribute to conduction disturbances (Spach et al., 1982b). Their study was carried out in isolated intact portions of canine atrial muscle, and was addressed to phenomena on a larger scale than that of individual intercellular junctions. Conduction was studied at locations of anatomical discontinuity that could easily be identified by eye, such as separate fascicles within a muscle, junction sites of separate muscle bundles, sites of branching in pectinate muscles, and junctions of pectinate muscle and crista terminalis. Intercellular connections are fewer at such sites owing to an increased presence of connective tissue septa and a lower density of gap junctions. Experimentally, it was found that conduction slowed in crossing these sites, and that there was a decreased safety factor for propagation of premature stimuli. When the extracellular $[K^+]$ was doubled (thus decreasing the take-off potential and hence the transmembrane current), unidirectional conduction block occurred at muscle branch points and bidirectional block occurred at muscle junctions. Thus, sites of decreased intercellular coupling in cardiac muscle on a macroscopic scale were found to be vulnerable to the development of conduction disturbances.

The findings in the present study suggest that such conduction disturbances may take place on a microscopic scale, at the level of individual intercellular connections. The presence of an anatomical discontinuity or a connective tissue septum appears not to be necessary for cardiac conduction to be discontinuous. Rather, the discontinuity may be a functional one, reversibly induced by a mechanism which causes decreased intercellular coupling at gap junctions. This is not to say that the presence of anatomical discontinuities is unimportant; other things being equal, it should be expected that functional decoupling should most strongly affect the locations at which the underlying intercellular connections are the most sparsely distributed. However, the evidence presented here does suggest that under pathological conditions which lead to decreased intercellular coupling, discontinuous propagation should be possible at any location in the heart.

It is a common clinical finding that following infarction of a region of myocardium, there is a greatly increased risk of arrhythmias, often fatal. Some of these arrhythmias are attributable to direct damage to regions of the cardiac conduction system by the infarction. However, most occur in cases in which there is no evidence of such damage. The explanation that is usually given for these arrhythmias is that the tissue at the edges of the infarcted region, which is still viable but ischemic, undergoes metabolic changes which lead to changes in membrane properties. For example, the resting potential decreases under these conditions, due to impairment of the Na^+ / K^+ pump. K^+ levels rise in the extracellular space. These changes cause inactivation of sodium channels which in turn decreases conduction velocity and results in calcium-channel mediated "slow response" action potentials. Release of catecholamines from local nerve endings may further enhance such slow response action potentials (Cranefield, 1975).

The loss of intercellular coupling in the vicinity of an infarct has been extensively considered as the mechanism of "healing over", which isolates damaged myocardium

from adjacent healthy tissue (De Mello, 1982b). In this context, coupling has more or less been considered to be all or none; the effects of partial uncoupling on conduction are not considered. De Mello has suggested that the arrhythmias following myocardial infarction might be related to increases in intracellular [H^+] and / or [Ca^{++}]. One of the metabolic changes that occurs during myocardial ischemia is intracellular acidosis (Neely et al., 1975). The results presented in this study suggest that intracellular acidosis may be expected to lead to degradation in conduction due to non-membrane factors. Thus, changes in intercellular coupling may have to be added to the list of pathogenic factors in post-infarction arrhythmias. Other experiments will be required to assess the relative importance of membrane and non-membrane factors in this situation.

Non-membrane factors may play a role in the arrhythmias induced by toxic doses of the cardiac glycosides (digitalis, digoxin, digitoxin, ouabain). These drugs are used primarily for the treatment of congestive heart failure because of their positive inotropic effect. This effect is thought to be due to inhibition of the membrane Na^+ / K^+ pump, resulting in increased intracellular [Na^+] and [Ca^{++}]. The difference between the therapeutic and toxic doses of these drugs is small, with toxic effects including a variety of sometimes fatal arrhythmias. These arrhythmias are generally explained on the basis of the membrane actions of the drugs, which include a reduction in resting potential and a decrease in conduction velocity. However, the non-membrane effects of these drugs on conduction may also contribute to their toxicity. Weingart (1977) found large increases in the longitudinal resistance of ventricular muscle preparations after 90 minutes of exposure to toxic doses of ouabain; these increases were said to be due to decreased intercellular coupling. Such decoupling might contribute to slow conduction and block, thereby creating favorable conditions for re-entrant arrhythmias.

The medical therapy of most arrhythmias is based on a model of the effects of various drugs on cardiac conduction. The actions of most anti-arrhythmic drugs are

explained on the basis of effects on membrane factors. For example, quinidine is used in the treatment of recurrent supraventricular and ventricular tachycardias and in the suppression of ectopic beats; it is sometimes administered to suppress ectopic activity following myocardial infarction after a lidocaine infusion is withdrawn. Quinidine depresses the maximum upstroke velocity of the cardiac action potential, and prolongs both the duration of the action potential and the effective refractory period. The mechanism of action is thought to be a dose-dependant block of the sodium channel (Rosen and Wit, 1983). Clinical and experimental evidence show that the toxic cardiac effects of quinidine, which include premature beats, tachycardia, complete AV block, severe myocardial depression, and fibrillation, occur more readily under ischemic conditions or if pH is unusually low. The potentiation of the effects of quinidine by low pH has been explained on the basis of alteration of the kinetics of the drug-receptor interaction by changes in the ionized fraction of drug due to changes in the pH (Grant et al., 1982). Note that the toxic effects of quinidine are consistent with mechanisms of conduction block and or re-entry. Thus, in addition to any modulation of the drug-receptor interaction by pH, degradation of conduction due to decreased intercellular coupling should be considered as a possible contributing factor in quinidine toxicity.

If cardiac conduction is indeed depressed in ischemia or other disease states by a direct effect on intercellular coupling, it is important to ask whether this effect can be altered by drugs or some other therapeutic intervention. This might take the form of an agent which alters intracellular pH, and thereby intercellular coupling; alternately, some substance might be found which acts on connexons directly. The discovery of such a substance could add a fundamentally different therapeutic model to the treatment of cardiac conduction disturbances.

5.3 Suggestions for further experiments

The results of these experiments suggest several other interesting experiments that could be done with the microelectrode array and cardiac cell culture techniques. One question that could be asked is to what extent different methods of reducing intercellular coupling cause discrete intercellular delays of the type seen using intracellular acidification by ammonium chloride. These might include other acidification techniques such as the application of CO_2 or changes in the pH of the extracellular fluid, and agents which raise the intracellular free Ca level, such as calcium ionophores. It would be particularly interesting to determine whether any of the various existing cardioactive drugs have such effects.

Another avenue of investigation would be to examine the effect of the incubation period of the culture on intercellular delays. Since these cultures begin as dissociated cells, younger cultures at some stage should be found to be less well-coupled than those incubated for 3 days. The evolution of coupling and its effect on conduction as the system is stressed may help to understand the behavior of damaged tissue, in which the degree of coupling and perhaps even the actual number of connexons could decrease over time.

Appendix A: Electrode impedance measurements

The impedance of the recording electrodes was measured using a two-channel spectrum analyzer (Hewlett-Packard 3582A) and the circuit shown in figure A-1. This circuit acts as a buffer for the spectrum analyzer, which has an input impedance of only 1 MΩ and therefore can not be used directly, since the impedances to be measured are of this order of magnitude. The electrode to be measured (Z_x) is connected in the feedback loop of an FET-input "electrometer" operational amplifier (Analog Devices AD515) having an input impedance of 10^{13} Ω shunted by 1.6 pF. A 1-kilohertz, 1-volt sine-wave is attenuated to 1 mV by the 1000:1 resistive divider and applied to one channel of the spectrum analyzer and, via the range switch, to one of the two input resistors connected to the inverting input of the operational amplifier. The non-inverting input of the amplifier is grounded; the amplifier maintains the inverting input at virtual ground. In the case of the high range, the input current is therefore 1 nA, and for the low range, 100 nA. By comparison, the input bias current required by the amplifier is negligible (0.0003 nA, worst case). Thus the current applied to the impedance under test is equal in magnitude and opposite in direction to the applied input current. The resulting voltage drop across the unknown impedance is passed through a single-pole, 2-Hz highpass RC filter and applied to the second channel of the spectrum analyzer. The filter removes low-frequency drift but has negligible effect at the 1 kHz measurement frequency. The spectrum analyzer is used in its transfer function mode, which computes the ratio between the voltage across the electrode and the current through it, yielding the magnitude and phase of the electrode impedance. Because the amplifier is used in an inverting configuration, the phase value must be corrected by 180°.

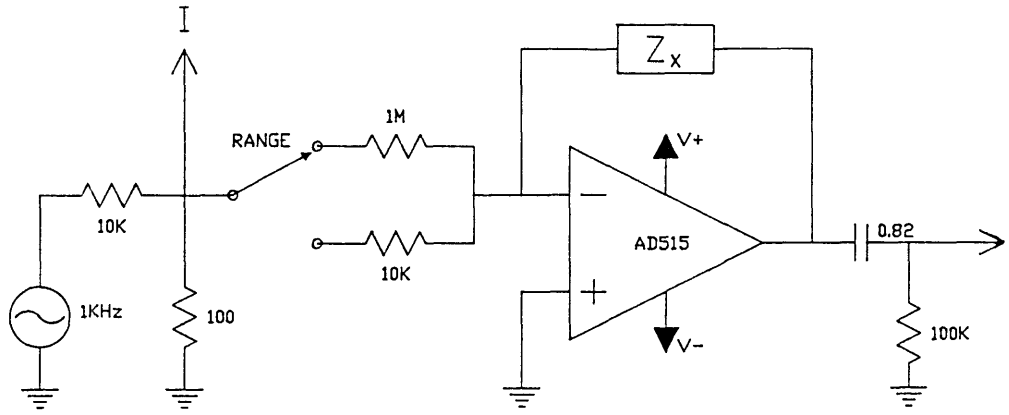

Figure A-1: Electrode impedance measurement buffer

Appendix B: The chick-embryo ventricle cell culture preparation

The chick-embryo ventricular myocyte cell culture preparation is undoubtedly simpler than intact cardiac tissue. The absence of geometric complexities caused by blood vessels and connective tissue septa, and the fact that intercellular connections can occur in only two dimensions should reduce the likelihood of tortuous propagation paths. On the other hand, the orientation of cells in this preparation is apparently random. The longitudinal and transverse axes that can be identified in intact muscle do not exist in this preparation, which means that the directional anisotropy that has been shown to have effects on the propagation of activity in intact cardiac muscle should also be absent. The lack of anisotropy was not important to the present study; however, it is a limitation of the tissue model which could make this preparation unsuitable for certain other types of studies of cardiac propagation.

As simplified as the preparation was, it was still far too complex to allow for a detailed, cell-by-cell model of its behavior. The number of cells on the microelectrode array during these experiments was between 10^5 and 10^6. Although the number of cells present in the region of the array bordered by the stimulating electrodes was two or three orders of magnitude smaller, around 10^3, there were still too many cells for a detailed model. Furthermore, the difficulties in ascertaining the actual geometry of the cell layer which were discussed in section 3.2.6 made such a model unattainable in these experiments.

There is potential for refinement of the tissue model used in these experiments. A primary goal should be simplification of the cell culture preparation by finding effective methods of patterning the cells. This would be beneficial because in a one-dimensional preparation there would be no question about the pathway of propagation; the possibility of tortuous pathways would be eliminated. During the course of this work, several

techniques were tried to restrict the growth of cells to a linear strip covering the recording electrodes. The first such method used a flexible template cut from a sheet of Silastic which had a slit of the desired dimensions cut through its center with a sharp blade. The template was positioned on top of the array before plating, to restrict the area with which cells could come into contact. This method achieved the desired result, but it was limited by the crudeness of the technique of cutting a slit through the Silastic by hand. The minimum width of the slit was around 1 mm, and its shape could not be very well controlled. In addition, the template was not held down to the surface of the array, so small motions tended to shear cells off the plate.

In a later variation on the same theme, rigid templates were fabricated from a 250-μm thick wafer of silicon by "micro-machining". The desired pattern of slits was photolithographed onto the surface of the wafer, and the slits were cut by etching the wafer in KOH at 80 °C. Templates with slit-widths of 200 and 400 μm were made, although narrower ones could easily be produced. Attempts to use these templates to pattern cells by laying the template on the surface of the microelectrode array invariably failed due to movement of the template during plating or incubation. Successful patterning was obtained when the template was fastened in place using a thin film of photoresist as adhesive. However, this prevented subsequent removal of the template. Interestingly, a tendency was noted for the cells to become longitudinally aligned with the sides of the slits in these templates. If it were desirable to control the orientation of cells in a preparation, it might be possible to do so by designing an array with ridges atop the surface. More preliminary experimentation would have to be done to evaluate the feasibility of this approach.

Another method of patterning that was tried was a modification of one that was used by Sachs to create linear strands of chick-embryo ventricular myocytes for electrophysiological studies (Sachs, 1976). The surface of a microelectrode array was

coated with a 1% agarose solution which was allowed to dry into a thin layer. The tip of a 27-gauge hypodermic needle was mounted on a specially-built holder that fixed it at the focal point of the 10X objective of a metallurgical microscope. The microelectrode array was fixed to the mechanical stage of the microscope, and the tip of the needle brought into contact with the agar. The stage was moved so that the needle scratched a fine trough in the surface of the agar, passing over the central recording electrodes. From the standpoint of patterning the cells, this method was better than the template methods. As described by Sachs, the cells did not adhere to the agar, but those which settled in the troughs formed thin, continuous strands. Unfortunately, the application of the method to microelectrode arrays presented major problems. More often than not, the array was damaged by the needle, either by scratching through the insulation or by completely breaking the substrate. However, the use of a tougher insulating layer, such as SiO_2/ Si_3N_4 discussed in Appendix D, and a cutting apparatus designed to apply a regulated pressure to the surface, could make this a practical method.

A variety of other agents can be used for the purpose of either promoting or inhibiting the adhesion of cells to surfaces in cell-culture. As is clear from the above discussion, the real problem is in creating the desired pattern. Perhaps some adhesion inhibitor can be found that can be applied to the entire surface of the array and then removed from selected areas without direct mechanical intervention, for example, by a laser beam. Such a method would offer great flexibility in the control of patterns of cell growth.

The interpretation of the results of extracellular recordings would be greatly enhanced if the location of intercellular boundaries were known. The difficulties encountered in attempting to do this were outlined in section 3.2.6. Some of the improvements suggested above, i.e: the use of a different (non-fluorescing) insulating material on the array, and the simplification of the preparation by restricting the region

of cell growth, might make this goal achievable with the fluorescent dyes described earlier. Having a very small number of cells would not only help in ascertaining geometry, but might allow a cell-by-cell simulation of propagation to be performed based on that geometry.

Appendix C: Recording apparatus -- circuit descriptions

C.1 Preamplifier

The recording electrodes were connected directly to the inputs of the preamplifiers, which were housed in an enclosure designed to attach directly to the electrode array in order to minimize the wiring lengths for the high-impedance nodes and to eliminate movable connections which might add noise to the input. All 20 channels were identical, and had the circuit shown in figure C-1. The amplifier used is the Burr-Brown OPA121, because of its low noise and high input impedance. The input impedance is $10^{13}\Omega$ shunted by 1 pF, and the noise performance is specified as 50 nV/$\sqrt{\text{Hz}}$ at 10 Hz and 10 nV/$\sqrt{\text{Hz}}$ at 1 kHz. It is connected in a gain-of-10, non-inverting, direct-coupled configuration. A higher gain can not be used at this stage due to the presence of variable offset potentials of up to several hundred millivolts on the recording electrodes. The connection to the reference electrode on the microelectrode array is common to all channels. The bandwidth of this amplifier at the chosen gain is 200 kHz. The R-C networks on the power supply leads are used to prevent interaction among adjacent channels via the power supply.

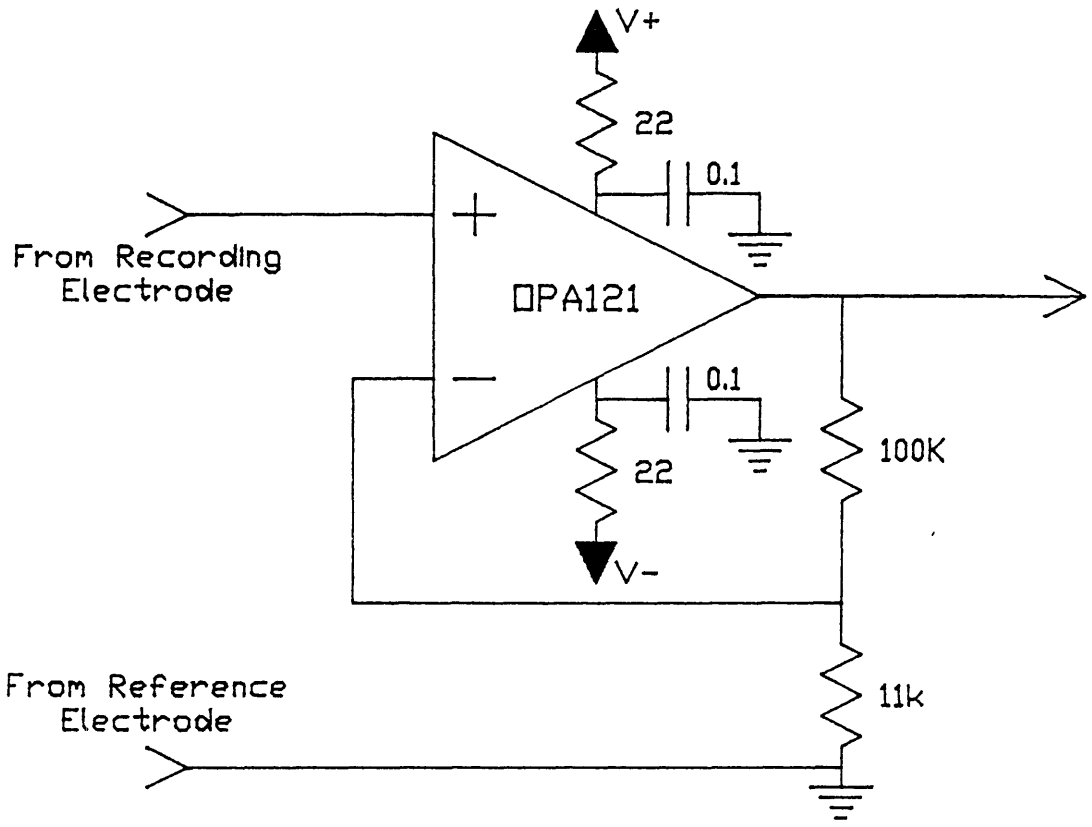

Figure C-1: Preamplifier

C.2 Second-stage amplifier and filter

The outputs of the preamplifier, described above, were connected to the second stage amplifier and filter circuit, shown in figure C-2. There were 16 identical channels. At the input is a single-pole highpass filter with a cutoff frequency of 0.31 Hz, to remove the DC offset and low-frequency drift introduced by the microelectrodes. The signal is then amplified by an LF356 FET-input operational amplifier (National Semiconductor) connected in a gain-of-100, non-inverting configuration. This is followed by an AF-100 active filter module (National Semiconductor) which is connected as a unity-gain, 3-pole Butterworth lowpass filter, with a cutoff frequency of 2000 Hz. All of the gain and frequency determining components for the second stage amplifier and filter are mounted on removable headers to allow easy reconfiguration. Bypass networks are used on all power supply leads to prevent interactions among the channels.

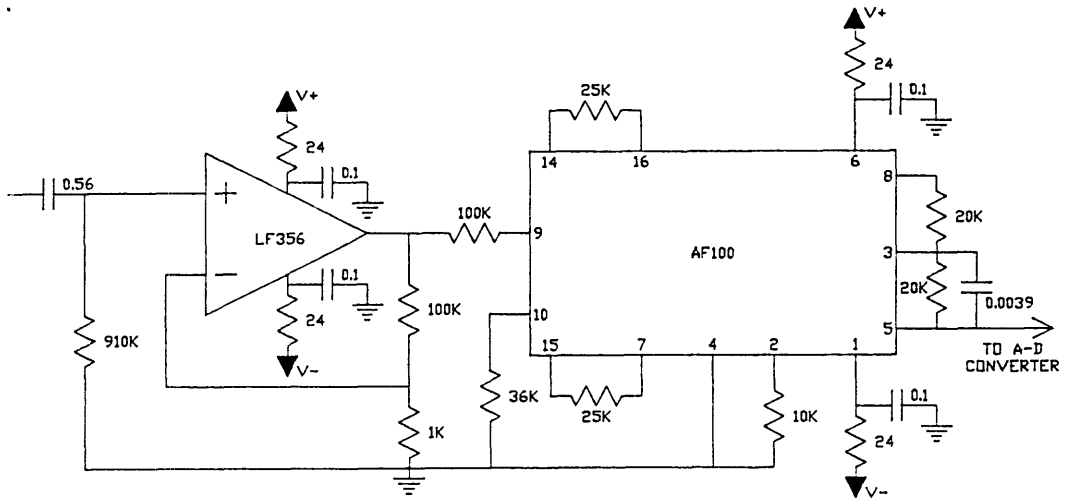

Figure C-2: Second stage amplifier and filter

C.3 Stimulus synchronizing circuit

The circuit shown in figure C-3 was used to clock the A-D converter and synchronize the sampling window to the stimulation of the cell culture. The heart of the circuit is a 16-bit binary counter implemented using 4 4-bit synchronous binary TTL counters (74LS163). The counter can be preset to any count up to 2^{15} by setting the corresponding logic levels at the counter load inputs (A,B,C,D). The counter circuit is clocked by a 192 kHz square wave obtained from a 6.144 MHz crystal oscillator module (Motorola) by using a 74LS393 divider to divide its output by 32. The 16th counter bit generates the 96 kHz clock train for the A-D converter by dividing the 192 kHz input clock by 2, thus ensuring that the initial state of the 96 kHz clock line is the same for each train of pulses. A second clock input, the "event clock", periodically enables the entire circuit to initiate sampling and stimulation of the cell culture; this event clock can be obtained from the digital output of the PDP-11/44, or from an adjustable astable multivibrator. When the event clock input goes low, it presets the 74LS163 counters to the assigned value and clears the LS109 flip-flop at the end of the counter chain. When the event clock input subsequently returns to the high state, the counters are enabled and counting starts, clocking the A-D converter and starting data acquisition. After the selected number of counts, the J input to the stimulus-trigger LS109 flip-flop goes high, causing the Q* output to go low on the next clock pulse and trigger the stimulus generator. Counting and sampling continue until the maximum count is reached, whereupon the holdoff flip-flop at the end of the counter chain changes state, forcing its Q* output low. This disables further counting by forcing the enable-P line on the first counter low, and clears the stimulus-trigger flip-flop in preparation for the next stimulus.

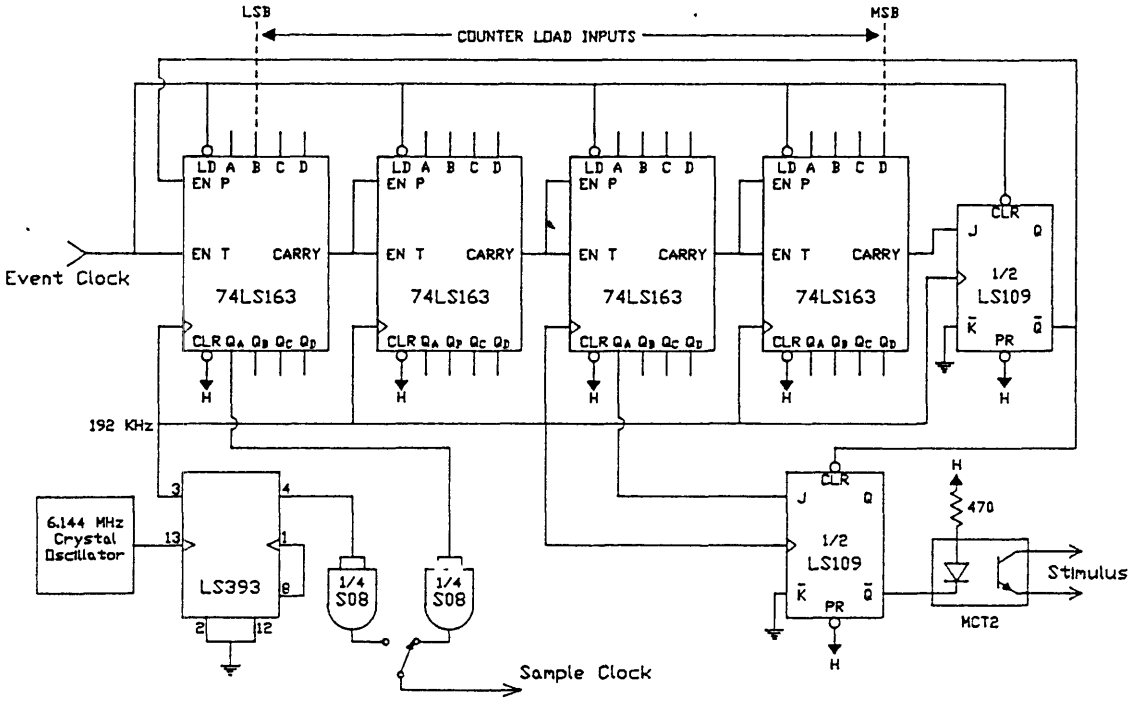

Figure C-3: Stimulus synchronizer

Appendix D: Technical considerations for microelectrode array design

Fundamental physical constraints and the practical considerations of fabrication technology limit the performance attainable from the microelectrode array. The need to record extracellular potentials with small electrodes to localize their origins must be balanced against the lower signal-to-noise ratios obtained with small electrodes and the increased difficulty of fabricating small structures.

The fundamental physical limit that affects microelectrode size is noise generation. The microelectrode resistance (the real part of the complex impedance) determines the amplitude of the Johnson noise generated by the electrode (Gesteland et al., 1959). The Johnson noise V_n generated by a resistive element over a bandwidth Δf is

$$V_n = \sqrt{4kTR\,\Delta f} \qquad \text{(D.1)}$$

where k is Boltzmann's constant, T is absolute temperature, and R is the resistance (real part of the microelectrode impedance). For the 10 x 10 μm platinized gold microelectrodes described here, the mean impedance at 1 kHz in normal saline was 620 kΩ, phase angle -53°. The resistive part of this impedance is 370 kΩ. For comparison with the measured noise shown in figure 4-1, the Johnson noise of such a resistance over a 60 Hz bandwidth would be 0.6 μV, or -124 dBV. (The noise in figure 4-1 was generated by an electrode with an impedance of 600 kΩ, phase -65°, at a frequency of 1 kHz.) The measured noise of this electrode at frequencies around 1 kHz was greater than the expected Johnson noise by about 6 dB; thus, it appears that other noise generation mechanisms were contributing significantly. Although not shown here, it was found that the impedance of the microelectrodes on the array was a function of frequency, being higher at low frequencies and lower at high frequencies. This behavior of metal microelectrodes has been well-described elsewhere (Gesteland et al., 1959, Geddes, 1972). As seen in figures 4-1 and 4-2, electrode noise decreased as the frequency increased, which would be expected because of the lower electrode impedances at higher

frequencies.

Besides noise generation, another factor that constrains the electrode size is the shunt impedance to ground Z_s of the path which connects the electrode to the recording equipment. This impedance and the electrode impedance Z_e together form a voltage divider which attenuates the signal by a factor

$$\frac{Z_s}{Z_e + Z_s} \tag{D.2}$$

The attenuation is frequency-dependant since both Z_s and Z_e are functions of frequency. The ideal case is to have

$$Z_s \gg Z_e \tag{D.3}$$

for all frequencies of interest. Z_s should be made as high as possible; note that a low Z_e helps to minimize this problem as well as noise generation. In the case of the microelectrode array, Z_s has a resistive component R_s due to the conductivity of photoresist, and a capacitive component C_s whose magnitude is determined by the dielectric constant of the photoresist and the area of the conducting path:

$$R_s = \frac{\rho d}{A} \quad , \quad C_s = \frac{\varepsilon A}{d} \tag{D.4}$$

where ρ is the resistivity of the insulating material, ε is its dielectric constant, d is its thickness, and A is the area of the conducting lead from the microelectrode to the edge of the culture dish. In order to keep Z_s large, the insulating layer should have a high resistivity and a low dielectric constant, and should be made as thick as possible. The length and width of the connecting leads should be minimized.

These goals were pursued in the design of the microelectrode array. The connecting lead width in the present design was 10 μm from the bonding pad to near the center of the array, where it was made 5 μm for short distances. This was based on earlier experience which showed that 5 μm lines of long lengths could not be reliably fabricated

using the wet-etching technique that was being used at the time, but that 10 μm lines could be made. However, during actual attempts at production of this design, it was found that the yield of even 10 μm lines was too low using the chemical etching method, prompting the switch to the present sputter-etching process. Much less undercutting is observed with this technique, which raises the possibility that 5 μm (or even smaller) lines might be feasible for the entire length of the connecting leads. The lower limit on line-widths is effectively set by the limitations of the fabrication process and the photolithography, since the conductivity of the gold is very high. For example, a gold conductor 10 mm long, 1 μm wide, and 0.4 μm thick would have a series resistance of 610 Ω, which is negligible in comparison to the electrode impedance.

The thickness of the insulating layer of KTI 732 photoresist used in the present design was 1.6 μm. This is thicker than is typically used when photolithography rather than insulation is the primary objective, and is near the upper end of the range of thicknesses recommended by the manufacturer. Since photo-patterning of this layer was required in this design to produce the holes for the electrodes, it was not feasible to use greater thicknesses. Photoresist is not intended for use as an insulator, and its resistivity and dielectric constant are not specified by the manufacturer.

In the early stages of this work, test electrodes were fabricated without contact holes in the insulation in order to evaluate the photoresist as an insulator. Impedance measurements on these devices yielded a shunt impedance of $4.4 \times 10^4 \pm 1.2 \times 10^3$ Ω–cm^2 for a 1.6 μm thick layer of KTI 732 photoresist. The area of the electrode shanks on the microelectrode array ranged from about 1.0×10^{-3} cm^2 for electrode 17 to 1.5×10^{-3} cm^2 for electrode 32; these areas are only approximate because of variability in the hand-assembly of the arrays. Thus, the shunt impedance of the microelectrodes ranged from about 29 to 44 MΩ. Given the average electrode impedance of about 620 kΩ, shunt impedances of this magnitude would cause a 1.5 to 2% attenuation of the input signal

(eq. D.2).

There are many possible ways to improve upon the present design of the microelectrode array. The most significant of these would be to use a more durable insulating material over the electrode metal. The photoresist used to insulate the arrays is not meant to be used in the saline cell-culture environment. After a variable number of uses it began to crack and eventually peel off the surface, thus rendering the device useless. (It is not possible to apply a new layer of photoresist after an array has been assembled.) The easiest improvement to make would be to use polyimide as the insulator instead of photoresist. Polyimide is a synthetic resin that is widely used as a passivating material in the microelectronics industry. It has well-characterized insulating properties and is available in photo-patternable formulations. Our preliminary tests of this material show that it is bio-compatible with the chick-embryo ventricular myocyte preparation and that it apparently withstands the saline environment for longer periods than the currently used photoresist. A sputtered layer of silicon dioxide / silicon nitride is another possible insulator. Such layers are also used for passivation of microelectronics, and have well-characterized insulating properties. Such a layer would probably be far more durable than any organic insulator, polyimide included. However, it is also much more difficult to make, since it requires a multiple-step process to apply and pattern.

A far more ambitious improvement to the microelectrode array would be to make an array incorporating active amplifying devices. In this type of design, the surface upon which cells are cultured is essentially a circuit fabricated using microelectronics technology. Each electrode could be the gate of a metal-oxide semiconductor field effect transistor (MOSFET), for example. These devices provide an essentially-infinite input impedance and a very low output impedance; this would allow smaller electrode areas while eliminating the detrimental effects of the shunt impedance on the signal and reducing the problem of interference from external sources. With active circuitry on the

microelectrode array it would be possible to multiplex the outputs of many electrode sites onto a small number of output leads. The major constraint on the number of electrodes that can be made on a passive array is not the size of the electrodes themselves, but rather the size of the connecting leads and bonding areas needed to connect them to the outside world. With circuitry on the array to switch between electrodes, many more sites could be monitored with a given number of connections to the outside. The design and fabrication of an array of this type has been discussed by Wheaton (Wheaton, 1982) and McNeil (McNeil, 1985). Further development will be necessary before such devices can be used for experiments.

Improvements in the method of assembling microelectrode arrays would also be useful. The current procedure is labor-intensive and tedious, requiring 15 to 20 hours of work on each array. A better method would require no assembly at all; the glass wafer containing the array would be mounted in a re-usable holder which would have mating contacts and provide the wall of the culture dish. A less elegant but still useful improvement would be to redesign the circuit board which holds the microelectrode array to include gold-plated leads which would mate directly with an edge-connector on the input of the pre-amplifier. The array could then be connected to the circuit board using a wire-bonder that holds and automatically feeds the gold wire, which would be much faster than the manual method used. The gluing of gold wires into connector pins would also be eliminated.

References

Barry, W.H., J. Pober, J.D. Marsh, S.R. Frankel, and T.W. Smith, "Effects of graded hypoxia on contraction of cultured chick embryo ventricular cells. ," *Am. J. Physiol.* **239**, pp.H651-657 (1980).

Beeler, G.W. and H. Reuter, "Reconstruction of the action potential of ventricular myocardial fibres.," *J. Physiol. London* **286**, pp.177-210 (1977).

Bement, S.L., K.D. Wise, D.J. Anderson, K. Najafi, and K.L. Drake, "Solid-State Electrodes for Multichannel Multiplexed Intracortical Neuronal Recording," *IEEE Trans. Biomed. Eng.* **BME-33**, pp.230-241 (1986).

Berger, W.K., "Correlation between the Ultrastructure and Function of Intercellular Contacts," pp. 63-88 in *Electrical Phenomena in the Heart*, ed. W.C. De Mello, Academic Press, New York (1972).

Burt, J.M., J.S. Frank, and M.W. Berns, "Permeability and Structural Studies of Heart Cell Gap Junctions under Normal and altered Ionic Conditions," *J. Membr. Biol.* **68**, pp.227-238 (1982).

Caspar, D.L.C., D.A. Goodenough, L. Makowski, and W.C. Phillips, "Gap junction structures. I. Correlated electron microscopy and X-ray diffraction ," *J. Cell Biol.* **1977**, pp.605-628 (1977).

Clapham, D.E., A. Shrier, and R. DeHaan, "Junctional Resistance and Action Potential Delay between Embryonic Heart Cell Aggregates," *J. Gen. Physio.* **75**, pp.633-654 (1980).

Clark, E.B., N. Hu, J.L. Dummett, G.K.Vandekieft, C. Olson, and R. Tomanek, "Ventricular function and morphology in chick embryo from stages 18 to 29," *Am. J. Physiol.* **250**, pp.H407-H413 (1986).

Cranefield, P.F., *Conduction of the Cardiac Impulse,* Futura, Mount Kisco, N.Y. (1975).

Crochiere, R.E., "A General Program to Perform Sampling Rate Conversion of Data by Rational Ratios," pp. 8.2-1-8.2-7 in *Programs for Digital Signal Processing*, IEEE Press, New York (1979).

Dahl, G. and G. Isenberg, "Decoupling of Heart Muscle Cells: Correlation with Increased Cytoplasmic Calcium Activity and with Changes of Nexus Ultrastructure," *J. Membr. Biol.* **53**, pp.63-75 (1980).

DeHaan, R.L. and R. Hirakow, "Synchronization of pulsation rates in isolated cardiac myocytes," *Exp. Cell. Res.* **70**, pp.214-226 (1972).

DeMello, W.C., "Intercellular Communication in Cardiac Muscle," *Circ Res* **51**, pp.1-9 (1982a).

DeMello, W.C., "Cell-to-Cell Communication in Heart and other Tissues," *Prog Biophys Molec Biol* **39**, pp.147-182 (1982b).

Deitmer, J.W. and D. Ellis, "Interactions between the regulation of the intracellular pH and sodium activity of sheep cardiac Purkinje fibres.," *J. Physiol.* **304**, pp.471-488 (1980).

Deleze, J., "Calcium ions and the healing-over of heart fibers.," pp. 147-148 in *Electrophysiology of the Heart*, ed. G. Marchetti, Pergamon Press, London (1965).

Diaz, P.J., Y. Rudy, and R. Plonsey , "A Model Study of the Effect of the Intercalated Discs on Discontinuous Propagation in Cardiac Muscle," *Adv. Exp. Med. and Biol.* **161**, pp.79-89 (1982).

Diaz, P.J., Y. Rudy, and R. Plonsey , "Intercalated Discs as a Cause for Discontinuous Propagation in Cardiac Muscle: A Theoretical Simulation," *Ann. Biomed. Eng.* **11**, pp.177-189 (1983).

Diaz, P.J., "The Effect of the Intercalated Disc on Propagation in Cardiac Muscle: A Theoretical Study," *Doctoral dissertation*, Case Western Reserve University (1983).

Edell, D.J., "A Peripheral Nerve Information Transducer for Amputees: Long-Term Multichannel Recordings from Rabbit Peripheral Nerves," *IEEE Trans. Biomed. Eng.* **BME-33**, pp.203-214 (1986).

Fange, R., H. Persson, and S. Thesleff, "Electrophysiologic and Pharmacological Observations on Trypsin-Disintegrated Embryonic Chick Hearts Cultured in Vitro.," *Acta Physiol. Scand.* **38**, pp.173-183 (1956).

Geddes, L.A., in *Electrodes and the Measurement of Bioelectric Events*, Wiley, New York (1972).

Gesteland, R.C., B. Howland, J.Y. Lettvin, and W.H. Pitts, "Comments on Microelectrodes," *Proc. IRE* **47**, pp.1856-1862 (1959).

Grant, A.O., J.L. Trantham, K.K. Brown, and H.C. Strauss, "Guinea Pig Ventricular Myocardium," *Circ. Res.* **50**, pp.210-217 (1982).

Gross, G.W., E. Rieske, G.W. Kreutzberg, and A. Meyer, "A new fixed array multimicroelectrode system designed for long term monitoring of extracellular single unit neuronal activity in vitro.," *Neurosci. Lett* **6**, pp.101-105 (1977).

Gross, G.W., "Simultaneous Single Unit Recording in vitro with a Photoetched Laser Deinsulated Gold Multimicroelectrode Surface," *IEEE Trans. Biomed. Eng.* **BME-26**, pp.273-279 (1979).

Gross, G.W., A.N. Williams, and J.H. Lucas, "Recording of spontaneous activity with photoetched microelectrode surfaces from mouse spinal neurons in culture," *J. Neurosci. Meth.* **5**, pp.13-22 (1982).

Hakansson, C.H., "Action Potentials Recorded Intra- and Extra-cellularly from the Isolated Frog Muscle Fibre in Ringer's Solution and in Air," *Acta Phys. Scand.* **39**, pp.291-312 (1957).

Hamburger, V. and H.L. Hamilton, "A series of normal stages in the development of the chick embryo.," *J. Morphol.* **88**, pp.49-92 (1951).

Heppner, D.B. and R. Plonsey , "Simulation of Electrical Interaction of Cardiac Cells," *Biophysical Journal* **10**, pp.1057-1075 (1970).

Hertzberg, E.L. and N.B. Gilula, "Isolation and characterization of gap junctions from

rat liver.," *J. Biol. Chem.* **254**, pp.2138-2147 (1979).

Hogg, B.M., C.M. Goss, and K.S. Cole, "Potentials in embryo rat heart muscle cultures," *Proc. Soc. Exp. Biol. Med.* **32**, pp.304-307 (1934).

Hyde, A., B. Blondel, A. Matter, J. Cheneval, B. Filloux , and L. Girardier, "Homo and Heterocellular Junctions in Cell Cultures: An Electrophysiological and Morphological Study," *Prog. Brain Res.* **31**, pp.283-311 (1969).

Israel, D.A., W.M. Barry, D.J. Edell, and R.G. Mark, "An Array of Microelectrodes to Stimulate and Record from Cardiac Cells in Culture," *Am. J. Physiol 247 (Heart Circ. Physiol. 16)*, pp.H669-H674 (1984).

Ito, S. and W.R. Loewenstein, "Ionic communication between early embryonic cells," *Dev. Biol.* **19**, pp.228-243 (1969).

Jobling, D.T., J.G. Smith, and H.V. Wheal, "Active microelectrode array to record from the mammalian central nervous system in vitro," *Med. and Biol. Eng. and Comput.* **19**, pp.553-560 (1981).

Jongsma, H.J. and H.E. van Rijn , "Electrotonic Spread of Current in Monolayer Cultures of Neonatal Rat Heart Cells," *J. Membr. Biol.* **9**, pp.341-360 (1972).

Jongsma, H.J., M.A. Masson-Pevet, and L. Tsjernina , "The Development of Coupling between Beating Heart Cells in Tissue Culture," *Proc. Phys. Soc* **334**, pp.59P-60P (1982).

Joyner, R.W., "Effects of the Discrete Pattern of Electrical Coupling on Propagation through an Electrical Syncytium," *Circ. Res* **50**, pp.192-200 (1982).

Kanno, Y. and W.R. Loewenstein, "Intercellular Diffusion," *Science* **143**, pp.959-960 (1964).

Kim, D. and T.W. Smith, "Altered Transsarcolemmal Ca Fluxes and Contractile State during Intracellular and Extracellular acid-base changes in Cultured Chick Heart Cells," *Am. J. Physiol.* (In press).

Kim, S.J., M. Kim, and W.J.Heetderks, "Laser-Induced Fabrication of a Transsubstrate Microelectrode Array and its Neurophysiological Performance," *IEEE Trans. Biomed. Eng.* **BME-32**, pp.497-502 (1985).

Krakau, C.E.T., "On the Decrement Function of an Action Potential in a Volume Conductor," *Experientia* **15**, pp.352-353 (1959).

Kuperstein, M. and D.A. Whittingtion, "A Practical 24 Channel Microelectrode for Neural Recording in Vivo," *IEEE Trans. Biomed. Eng.* **BME-28**, pp.288-293 (1981).

Kurachi, Y., "The Effects of Intracellular Protons on the Electrical Activity of Single Ventricular Cells," *Pflugers Arch.* **394**, pp.264-270 (1982).

Lieberman, M. and A. Paes de Carvalho, "The Spread of Excitation in the Embryonic Chick Heart," *J. Gen. Physiol.* **49**, pp.365-379 (1965).

Loewenstein, W.R., "Permeable junctions," *Cold Spring Harbor Symp Quant. Biol* **40**,

pp.49-63 (1975).

Loewenstein, W.R., "Junctional Intercellular Communication: The Cell-to-Cell Membrane Channel," *Physiological Reviews* **61**, pp.829-913 (1981).

Lompre, A.M., J. Pogglioli, and G. Vassort, "Maintenance of fast Na^+ channels during primary culture of embryonic chick heart cells.," *J. Mol. Cell. Cardiol.* **11**, pp.813-825 (1979).

McLean, M.J. and N. Sperelakis, "Rapid loss of sensitivity to Tetrodotoxin by Chick ventricular myocardial cells after separation from the heart," *Exp. Cell Res.* **86**, pp.251-364 (1974).

McNeil, V.M., "Fabrication of a MOSFET Cardiac Cell Culture Array," *S.B. Thesis*, Massachusetts Institute of Technology (1985).

Neely, J.R., J.T. Whitmer, and M.J. Rovetto, "Effect of coronary flow on glycolytic flux and intracellular pH in isolated rat hearts," *Circ Res* **37**, pp.733-741 (1975).

No, R. Lorente de, "A Study of Nerve Physiology: Analysis of the Distribution of the Action Currents of Nerve in Volume Conductors (Chapter 16)," *Studies from The Rockefeller Institute for Medical Research* **132**, pp.384-477 (1947).

Noble, D., in *The Initiation of the Heartbeat*, Oxford University Press, Oxford (1979).

Noble, D., "The Surprising Heart: A Review of Recent Progress in Cardiac Electrophysiology ," *J. Physiol* **353**, pp.1-50 (1984).

Oetken, G., T.W. Parks, and H.W. Schussler, "A Computer Program for Digital Interpolator Design," pp. 8.1-1-8.1-6 in *Programs for Digital Signal Processing*, IEEE Press, New York (1979).

Oppenheim, A.V. and R.W. Schafer, pp. 26-30 in *Digital Signal Processing*, Prentice-Hall Inc., Englewood Cliffs (1975).

Pickard, R.S. and T.R. Welberry, "Printed Circuit Microelectrodes and their Application to the Honeybee Brain," *J. Exp. Biol.* **64**, pp.39-44 (1976).

Pickard, R.S., "Printed Circuit Microelectrodes," *Trends in Neurosciences* **2**, pp.259-261 (1979).

Pine, J., "Recording action potentials from cultured neurons with extracellular microcircuit electrodes," *J. Neurosci. Meth.* **2**, pp.19-31 (1980).

Plonsey, R. and R.C. Barr, "Effect of Junctional Resistance on Source-Strength in a Linear Cable," *Ann. Biomed. Eng.* **13**, pp.95-100 (1985).

Pollack, G.H. and L.L. Huntsman, "Intercellular Pathways in the Heart: Direct Evidence for Low Resistance Channels," *Experientia* **29**, pp.1501-1503 (1973).

Purdy, J.E., M. Lieberman , A. Roggeveen , and R. Kirk, "Synthetic Strands of Cardiac Muscle: Formation and Ultrastructure," *J. Cell Biol.* **55**, pp.563-578 (1972).

Reber, W.R. and R. Weingart, "Ungulate cardiac Purkinje fibres: The influence of

intracellular pH on the electrical cell-to-cell coupling," *J. Physiol.* **328**, pp.87-104 (1982).

Robinson, R.B. and M.J. Legato, "Maintained Differentiation in Rat Cardiac Monolayer Cultures: Tetrodotoxin Sensitivity and Ultrastructure," *J. Mol. and Cell. Cardiol.* **12**, pp.493-498 (1980).

Rose, B. and W.R. Loewenstein, "Permeability of a cell junction and the local cytoplasmic free ionized calcium concentration. A study with Aequorin.," *J. Membr. Biol.* **28**, pp.87-119 (1976).

Rosen, M.R. and A.L. Wit, "Electropharmacology of antiarrhythmic drugs," *Am. Heart J.* **106**, pp.829-839 (1983).

Sachs, F., "Electrophysiological Properties of Tissue Cultured Heart Cells Grown in a Linear Array," *J. Membrane Biol.* **28**, pp.373-399 (1976).

Schwarzmann, G., H. Weigandt, B. Rose, A. Zimmerman, D. Ben-Haim, and W.R. Loewenstein, "Diameter of the cell-to-cell junctional channels as probed with neutral molecules," *Science* **213**, pp.551-553 (1981).

Shtark, M.B., A.S. Ratushnyak, L.V. Voskresenskaya, and S.N. Olenev, "A Multielectrode Perfusion Chamber for Tissue Culture Research," *Bull. Exp. Biol. Med.* **78**, pp.1090-1092 (1974).

Sjostrand, F.S. and E. Andersson, "Electron Microscopy of the Intercalated Discs of Cardiac Muscle Tissue," *Experientia* **10**, pp.369-370 (1954).

Sommer, J.R. and E.A. Johnson, "Ultrastructure of cardiac muscle," pp. 113-186 in *Handbook of Physiology, sec 2: The Cardiovascular System*, ed. R.M. Berne, American Physiological Society, Bethesda (1979).

Sommer, J.R. and P.C. Dolber, "Cardiac Muscle: Ultrastructure of Its Cells and Bundles," pp. 1-27 in *Normal and Abnormal Conduction in the Heart*, ed. M. Lieberman, Futura, Mt. Kisco (1982).

Spach, M.S., R. Barr, G. Serwer, E. Johnson, and J. Kootsey , "Collision of Excitation Waves in the Dog Purkinje System: Extracellular Identification," *Circ. Res.* **29**, pp.499-511 (1971).

Spach, M.S., R. Barr, G. Serwer, J. Kootsey , and E. Johnson, "Extracellular Potentials Related to Intracellular Action Potentials in the Dog Purkinje System," *Circ. Res.* **30**, pp.505-519 (1972).

Spach, M.S., R. Barr, E. Johnson, and J. Kootsey , "Cardiac Extracellular Potentials: Analysis of Complex Wave Forms about the Purkinje Networks in Dogs," *Circ. Res.* **33**, pp.465-473 (1973).

Spach, M.S., W.T. Miller, D.B. Geselowitz, R.C. Barr, J.M. Kootsey, and E.A. Johnson , "The Discontinuous Nature of Propagation in Normal Canine Cardiac Muscle," *Circ. Res.* **48**, pp.39-54 (1981).

Spach, M.S., "The Role of Cell-to-Cell Coupling in Cardiac Conduction Disturbances," *Adv. Exp. Med. Biol.* **161**, pp.61-77 (1982).

Spach, M.S., J.M. Kootsey, and J.D. Sloan, "Active Modulation of Electrical Coupling between Cardiac Cells of the Dog," *Circ. Res.* **51**, pp.347-362 (1982a).

Spach, M.S., W.T. Miller, P.C. Dolber, J.M. Kootsey , J.R. Sommer, and C.E. Mosher , "The Functional Role of Structural Complexities in the Propagation of Depolarization in the Atrium of the Dog," *Circ. Res.* **50**, pp.175-191 (1982b).

Spach, M.S., "The Discontinuous Nature of Electrical Propagation in Cardiac Muscle," *Ann Biomed. Eng.* **11**, pp.209-261 (1983).

Spach, M.S. and J.M. Kootsey, "Relating the Sodium Current and Conductance to the Shape of Transmembrane and Extracellular Potentials by Simulation: Effects of Propagation Boundaries," *IEEE Transactions on Biomedical Engineering* **BME-32**, pp.743-755 (1985).

Sperelakis, N. and D. Lehmkuhl, "Insensitivity of cultured chick heart cells to autonomic agents and tetrodotoxin ," *Am. J. Physiol.* **209(4)**, pp.693-698 (1965).

Sperelakis, N. and K. Shigenobu, "Changes in Membrane Properties of Chick Embryonic Hearts during Development ," *J. Gen. Physiol.* **60**, pp.430-453 (1972).

Sperelakis, N. and M.J. McLean, "Electical Properties of Cultured Heart Cells," pp. 645-666 in *Recent Advances in Studies on Cardiac Structure and Metabolism* , University Park Press, Baltimore (1978).

Spray, D.C., R.L. White, A. Campos de Carvalho, A.L. Harris, and M.V.L. Bennett, "Gating of gap junction channels," *Biophys. J.* **45**, pp.219-230 (1984).

Spray, D.C., R.L. White, F. Mazet, and M.V.L. Bennett, "Regulation of gap junctional conductance," *Am. J. Physiol* **248**, pp.H753-H764 (1985).

Thomas, C.A., P.A. Springer, G.E. Loeb, and Y. Berwald-Netter, "A Miniature Microelectrode Array to Monitor the Bioelectric Activity of Cultured Cells," *Exp. Cell Res.* **74**, pp.61-66 (L.M. Okun).

Thomas, R.C., "Intracellular pH of snail neurones measured with a new pH-sensitive glass microelectrode.," *J. Physiol.* **238**, pp.159-180 (1974).

Turin, L. and A.E. Warner, "Carbon dioxide reversibly abolishes ionic communication between cells of early amphibian embryo.," *Nature* **270**, pp.56-57 (1977).

Weidmann, S., "The electrical constants of Purkinje fibres," *J. Physiol. London* **118**, pp.348-360 (1952).

Weidmann, S., "The diffusion of radiopotassium across intercalated disks of mammalian cardiac muscle," *J. Physiol.* **187**, pp.323-342 (1966).

Weingart, R., "The Actions of Ouabain on Intercellular Coupling and Conduction Velocity in Mammalian Ventricular Muscle," *J. Physiol.* **264**, pp.341-365 (1977).

Wheaton, P.M., "Development of Microelectronic Arrays for Cell Culture Research," *S.M. Thesis*, Massachusetts Institute of Technology (1982).

White, R.L., D.C. Spray, A.C. Campos de Carvalho, B.A. Wittenberg, and M.V.L.

Bennett, "Some physiological and pharmacological properties of cardiac myocytes dissociated from adult rat.," *Am. J. Physiol.* **249** (in press).

Williams, E.M. Vaughan, "Relation of Extracellular to Intracellular Potential Records from Single Cardiac Muscle Fibres," *Nature* **183**, pp.1341-1342 (1959).

Wise, K.D., J.B. Angell, and A. Starr, "An Integrated-Circuit Approach to Extracellular Microelectrodes," *IEEE Trans. Biomed. Eng.* **BME-17**, pp.238-247 (1970).

Wise, K.D. and J.B. Angell, "A Low-Capacitance Multielectrode Probe for Use in Extracellular Neurophysiology," *IEEE Trans. Biomed. Eng.* **BME-22**, pp.212-219 (1975).

Wit, A.L. and P.F. Cranefield, "Reentrant Excitation as a cause of Cardiac Arrhythmias," *Am. J. Physiol.: Heart Circ. Physiol.* **4(1)**, pp.H1-H17 (1978).

Woodbury, J.W., "Cellular electrophysiology of the heart," pp. 237-286 in *Handbook of Physiology. Section 2* (1962).

Yeh, B.K. and B.F. Hoffman, "The Ionic Basis of Electrical Activity in Embryonic Cardiac Muscle," *J. Gen. Physiol.* **52**, pp.666-680 (1968).